Molecular Tweezers in Nitroaromatic Sensing

Inauguraldissertation

zur

Erlangung der Würde eines Doktors der Philosophie

vorgelegt der

Philosophisch-Naturwissenschaftlichen Fakultät

der Universität Basel

von

Lukas Emanuel Jundt

aus **Bottmingen (BL), Schweiz**

Basel, 2016

Genehmigt von der Philosophisch-Naturwissenschaftlichen Fakultät

auf Antrag von

Prof. Dr. Marcel Mayor

Prof. Dr. Oliver Wenger

Basel, den 21.06.2016

Prof. Dr. Jörg Schibler

Dekan

Acknowledgments

First and foremost, I thank Prof. Dr. Marcel Mayor, not only for giving me the opportunity to work in his group but also for help and guidance.

I thank Prof. Dr. Oliver Wenger for agreeing to be co-referee.

Special thanks go to Dr. Jürgen Rotzler, for his support and contributions to extents impossible to be listed here, but I'm sure he knows.

I thank Emma Louise Dunphy (†) for the same.

Equally special thanks go to Dr. Loïc Le Pleux for valuable advice in conceptual questions.

A very big thank you goes to the people who proofread this thesis: Yves Aeschi, Dr. Michel Rickhaus, Dr. Michal Juríček and Linda Bannwart.

I thank Dr. Daniel Häussinger, Dr. Heiko Gsellinger, Kaspar Zimmermann and Thomas Müntener for their help in my titration measurements.

I also thank Prof. Dr. O. Anatole von Lilienfeld for his input concerning data analysis.

Special thanks go to Markus Hauri, Andreas Koller, Alois Schäuble, Markus Ast and the whole Werkstatt in general as well as to Roy Lips.

I thank all the current and past members of the Mayor Group. Extra thanks go to my lab mates from OC 4.

I especially want to thank the following people I worked with and/or met in Basel:

Michel (fear of a blank planet! ~~Dark side of the moon~~! Mantra III !!! And your general enthusiasm. And btw, dinosaurs can learn as well!!), Sylvie (humour and watter bottles! I will miss your everyday (ir)rationality. And everything in between.), Yves (music, reason and bad language. But, more importantly, trust and havoc.) Lolo (brains and manners. The amines do not stand a chance!) and Dr. Patrick Burch (PhysChem and libraries, but not only.)

Abstract

Apart from their destructive force, nitroaromatic compounds also are toxic and harmful to humans and the environment. While a number of plants, bacteria and fungi produce nitroaromatic compounds, the largest part of these compounds found in the environment stem from industrial uses. Although nitroaromatic compounds can be detected in a laboratory, the corresponding equipment may be too delicate and/or not mobile enough to be used in the field where smaller devices are more suitable. Sensor-systems relying on the interaction or reaction of nitroaromatics with other molecules are of interest (notable for hand-held devices) because of ease of detection, simple material handling and short response time. Molecular tweezers constitute a promising class of molecules that could be able of molecular recognition of trace quantities of nitroaromatic compounds. In this thesis, the synthesis of different designed molecular tweezers is presented as well as their sensing properties in the presence of a guest, as determined from ^{1}H-NMR titrations. The results are then interpreted in relation to molecular structure, with the aid of computational calculations.

Chapter 1: section 1.1 gives a general overview over explosives and nitroaromatic compounds; section 1.2 shortly describes supramolecular chemistry in the context of miniaturization of technology. In section 1.3 non-covalent and π-π interactions between aromatic molecules and the effects involved are discussed, with emphasis on electrostatics. Sections 1.1 – 1.3 are combined in section 1.4 where, after a short overview over other nitroaromatic sensing methods, examples of molecular recognition of nitroaromatic compounds are presented. The examples in section 1.4 include fluorescent conjugated polymers and polycyclic aromatic hydrocarbons, which are then related to molecular tweezers. Molecular tweezers and their structural features are introduced, before several molecular tweezers that were developed for the detection of nitroaromatic compounds are shown and discussed. Sections 1.5 – 1.7 explain how the sensing performances of the molecules synthesized in this work were determined. Section 1.5 explains the association model used; this model is then applied to explain the formula used for the determination of the association constants from ^{1}H-NMR

titration shifts through nonlinear regression. Nonlinear regression is shortly discussed in section 1.6. In section 1.7 it is shown how the determined association constant values were analyzed and the corresponding statistical values and procedures are introduced and explained.

Chapter 2: in section 2.1 the details of the project are introduced and the molecular design is illustrated. Section 2.2 describes the synthesis of a xanthone-based molecular tweezers; its titration experiments are shown and discussed. The results lead to section 2.3, which describes the synthesis and the guest-sensing performance of two anthracene-based sensor molecules with different electron-densities. The findings are related to section 2.2, and the structural similarities between both sensor-classes are used in the synthesis (and titration experiments) shown in chapter 2.4. In sections 2.5 and 2.6 further structural features of molecular tweezers are investigated. While the sensor molecule in section 2.5 is relatively rigid, the tweezers in section 2.6 are designed to potentially adjust to various guest-molecules. In both sections the synthesis of the respective molecules is described and titration experiments are shown and analyzed. In section 2.7 selected self-association studies from the molecules introduced in sections 2.2 – 2.6 are shown and interpreted in order to evaluate the influence of self-association of these molecular tweezers on their guest-binding performance. This influence is investigated using two different overall-binding models. In section 2.8 the results from sections 2.2 – 2.6 are interpreted by aid of computational calculations. The optimized geometries and other properties of all the molecular tweezers synthesized in sections 2.2 – 2.6 are used after calculation to discuss the titration results, in terms of molecular structure but also in terms of non-covalent binding forces. Section 2.9 describes concepts and synthetic steps towards two classes of molecular tweezers with different sensing-principles than in sections 2.2 – 2.6.

Chapter 3 gives a summary of the work and an outlook.

Chapter 4 provides the experimental details of the compounds described in this thesis and the corresponding titration experiments.

Table of Contents

III

1. Introduction

1.1 Explosives and Nitroaromatic Compounds

Right now, there are over a hundred military and civilian explosives used.[1] Numerous authors have classified explosives according to their chemical nature, their performance and their use. With respect to their chemical nature, explosives can be divided in two categories:[2]

- Explosive substances (e.g. TNT)

- Explosive mixtures (e.g. Black Powder).

The functional groups that lend the substances their explosive properties can be divided into eight classes or explosophores:[2]

1. $-NO_2$ and $-ONO_2$ in organic and inorganic substances

2. $-N=N-$ and $-N=N=N-$ in organic and inorganic azides and diazo compounds

3. $-NX_2$, with X=halogen

4. $-N=C$ in fulminates

5. $-OClO_2$ and $-OClO_3$ in organic and inorganic chlorates and perchlorates

6. $-O-O-$ and $-O-O-O-$ in organic and inorganic peroxides and ozonides

7. $-C{\equiv}C-$ in acetylene and metal acetylides

8. M-C metal bonded with carbon in some organometallic compounds.

Table 1 gives an overview of todays most used explosives.[3]
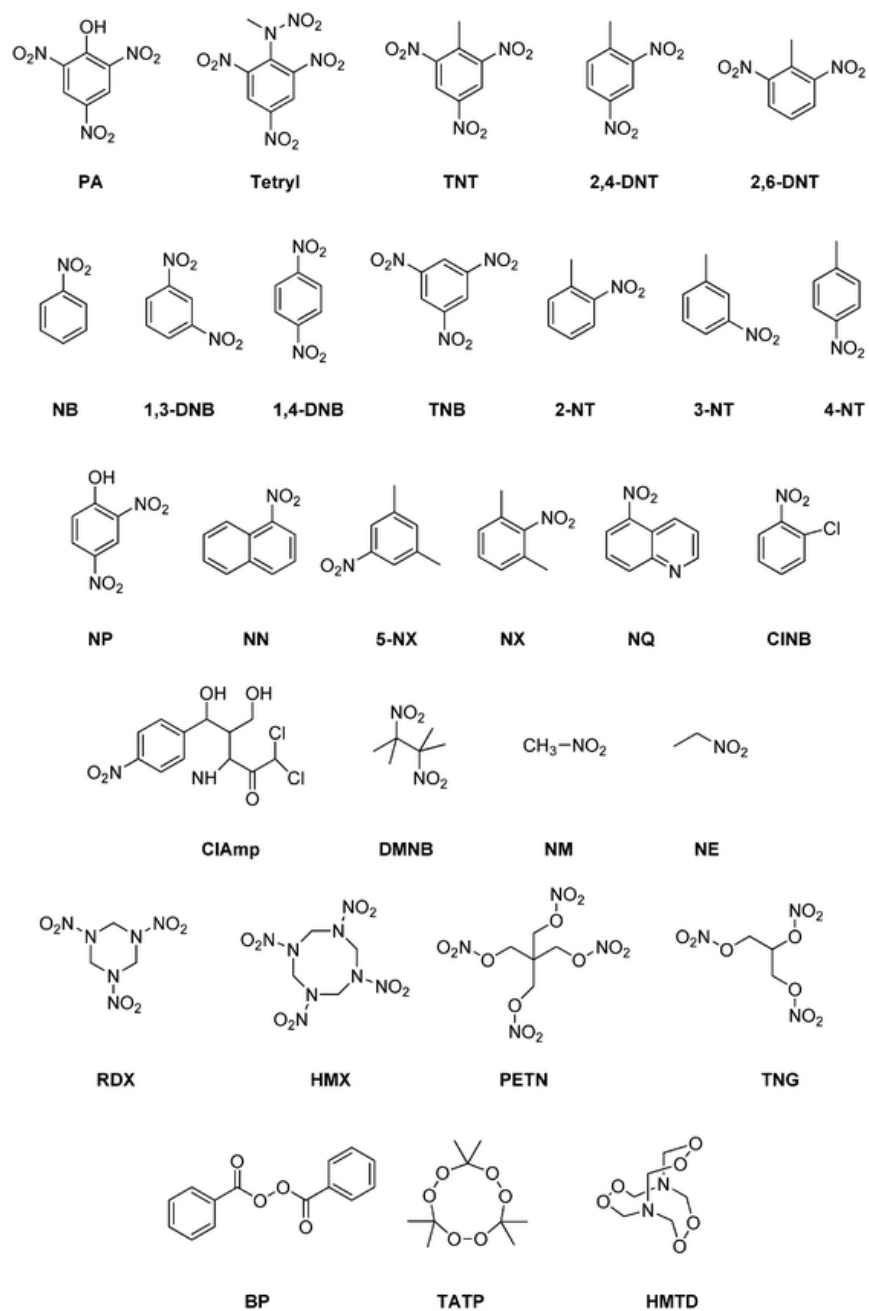
Table 1. *Overview over the most common explosives.*[3]

Class 1 compounds constitute the most abundantly present group of explosives, be it for civilian or military purposes.[4] TNT is not only one of the most abundantly used explosives today but is also used in the production of other explosives, such as TNB or hexanitrobenzene.[5] Nitroaromatic compounds are also used in the production of numerous industrial and consumer products, for example pesticides, pharmaceuticals,

2

rubbers and dyes.[4, 6-9] Although nitroaromatic compounds have been detected as natural products in plants, fungi and bacteria, the majority of these compounds found in the environment are manufactured.[10] Aside from the uses described above, nitroaromatic compounds are also released uncontrolled and accidentally. In 2002, around 5.1 tons of nitrobenzene and 1.1 tons of 2,4-dinitrotoluene were released into the environment in the USA alone.[11] In China, over 100 tons of nitroaromatics ended up in the Songhua River in 2005 after an aniline production factory exploded.[12] Also, contaminations from up to 50 years ago, caused by the agricultural use of nitroaromatic products, are discovered worldwide regularly.[4, 11] The mutagenicity and toxicity of these compounds is well documented.[13, 14] In short, additionally to their destructive force, nitroaromatic compounds are also toxic and harmful to the environment and humans. Therefore there is clearly a need to detect trace amounts and residues of such chemicals in numerous contexts. Nitroaromatic compounds can be detected and found in a laboratory setting, but when measurements in the field have to be taken devices of smaller proportions are preferable.[15]

1.2 Miniaturization

Machines and devices are assembled from single components where each element carries out a specified function. Their combination gives rise to a more complex function that defines the nature of the device.[16] The same concept can be applied on a molecular level to perform specific functions in or with molecular assemblies; through an external stimulus, molecular devices can undergo and display changes by altering the relative positions of their components.[17, 18] Apart from basic research, the miniaturization of such functions to the molecular level is also important for the growth and the development of nanotechnology.[19, 20] Whereas the first electronic computer weighed 30 tons, had to be repaired every 5.6 hours on average and contained 18 000 valves, modern processors have more than 40 million transistors, usually doing their job perfectly for several months.[21] The constant miniaturization of components is inseparable from the impressive leaps in information technology. The transition of technology to the molecular level is also expected to provide new applications and technologies in medicine, the

development of new materials, renewable energy sources and enable progress in environmental concerns.[20]

The miniaturization of components can be approached from two directions, top-down and bottom-up. The top-down approach can be likened to removing bulk material until the required smaller structure is obtained.[22]

Top-down processes include hard-template methods (filling porous templates with materials to obtain nanoparticles), microfluidic methods (solidifying emulsion droplets from a microfluidic reactor with micrometer-sized channels to fabricate nanoparticles), particle stretching (heating, stretching and dissolution of a film containing the particles of interest) and lithographic processes.[23]

The bottom-up approach can be compared to building a house from bricks. The molecular structures are assembled in single steps from atoms or molecules.[21] The bottom-up addition of molecules into larger structures emerged in the late 1970s and is closely linked to terms like "supramolecular chemistry" and "self-assembly".[16, 22]

Supramolecular chemistry enables scientists to assemble molecules through noncovalent interactions.[24,25] Its origins are traced to Emil Fischer's lock-and-key concept, Alfred Werner's coordination chemistry and Paul Ehrlich's receptor idea.[16] The field is very interdisciplinary and covers fields such as π-conjugated chromophores, supramolecular polymers, self-organization of metal containing molecules, fibrillary gels and the assembly of π-conjugated amphiphiles.[26-30] The main focus is on molecular assemblies and/or multicomponent systems with new emerging properties.[31] The underlying forces and interactions cover not so much the "traditional" chemical bonds (covalent, ionic, metallic) but rather van der Waals forces, hydrogen bonding and electrostatic interactions.[32] In biological systems, chemistry is dominated by self-organization of molecules through these non-covalent interactions.[33, 34] Supramolecular chemistry and its concepts are currently used in the construction of a multitude of compounds aiming at applications in energy transfer, molecular mechanical machines and multistate systems.[16] This work revolves around the synthesis and interactions of aromatic compounds.

1.3 Aromatic Interactions

1.3.1 Overview

Functional properties of molecules are based on their organization and their interactions. There are several models and forces that describe and govern the interactions between aromatic moieties. The latter are summarized under the term π-stacking. Multiple possible points of contact, variable geometries of interaction and a rather big range of involved functional groups leave the picture less clear than interactions like H-bonding that are well understood (table 2, pictures 2 and 3). The substituents attached to aromatic molecules greatly influence charge density in the molecule, where it is differentiated between electron-donating and electron-accepting substituents.[35]

Charge-transfer (CT) interactions can be the main driving force behind the stacking of aromatic donor (D) and acceptor (A) molecules (table 2).[24, 36]
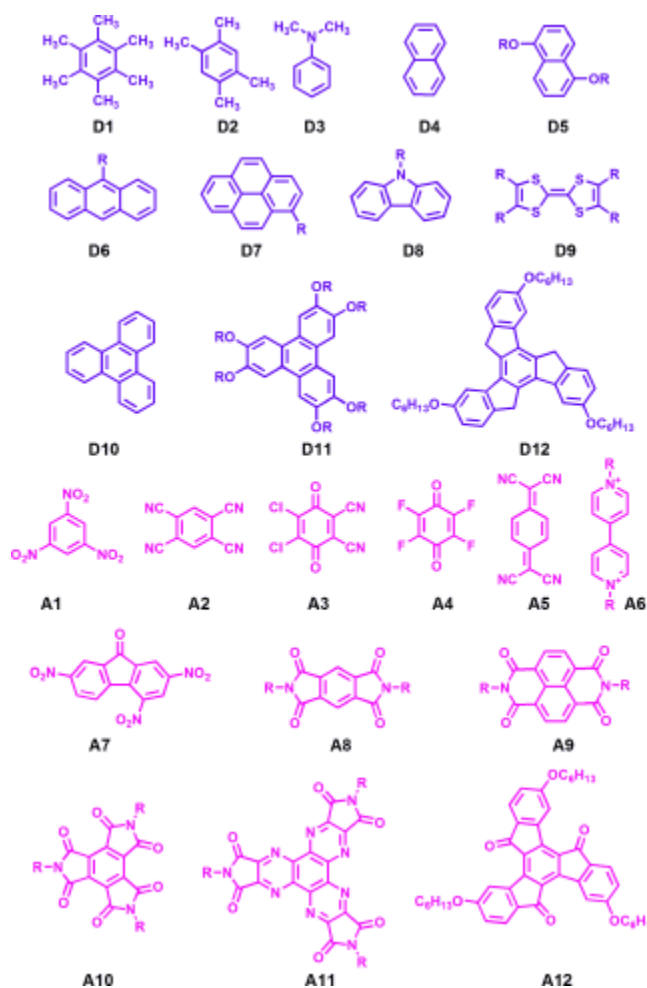
Table 2. *Examples of electron-rich (**D**) and electron-poor (**A**) π-systems.*[24]

For example, the mixing of aniline and *m*- or *p*-nitrobenzene yields in highly colored solutions which is attributed to the formation of charge transfer complexes, where the chemical structures of the chemicals are still intact.[38, 39] The Mulliken theory can be used to describe such complexes:

$$\Psi_N = a\Psi_0(D,A) + b\Psi_1(D^+ - A^-) \tag{1}$$

Formula 1 describes the wave function Ψ_N of a 1:1 complex as a hybrid of Ψ_0 and Ψ_1. Ψ_0 is a nonbonding wave function and Ψ_1 represents a dative bond wave function congruent

to the transfer of an electron from D (donor) to A (acceptor) with formation of a weak covalent bond, i.e. intermolecular electron-pair bond. Transition from ground state ($a \approx 1, b \approx 0$) to an excited state ($a \approx 0, b \approx 1$) constitutes the CT absorption band. [24, 35, 36, 37]

In other words, CT bands are formed upon the electronic transition from the highest occupied molecular orbital (HOMO) of the donor to the lowest unoccupied molecular orbital (LUMO) of the acceptor. Several pairs in scheme 2 have been used in the assembly of supramolecular structures.[24, 40-43]

However, CT bands are much more the result of intermolecular interactions and not necessarily related to the mechanism of the latter. There are a number of effects to be considered in non-covalent interactions between molecules:

a) electrostatic interactions; in 1990, Hunter and Sanders proposed a model for aromatic interaction based on orientation. The aromatic ring is treated as a positively charged σ-framework between two regions or clouds of negatively charged π-electron density (picture 2). Picture 3 gives the summarized findings of Hunter and Sanders.[35, 44]
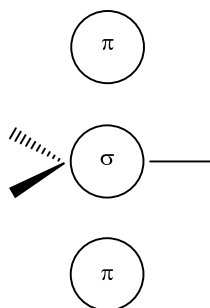
Picture 2. sp^2-hybridized atom in an aromatic system.[35]
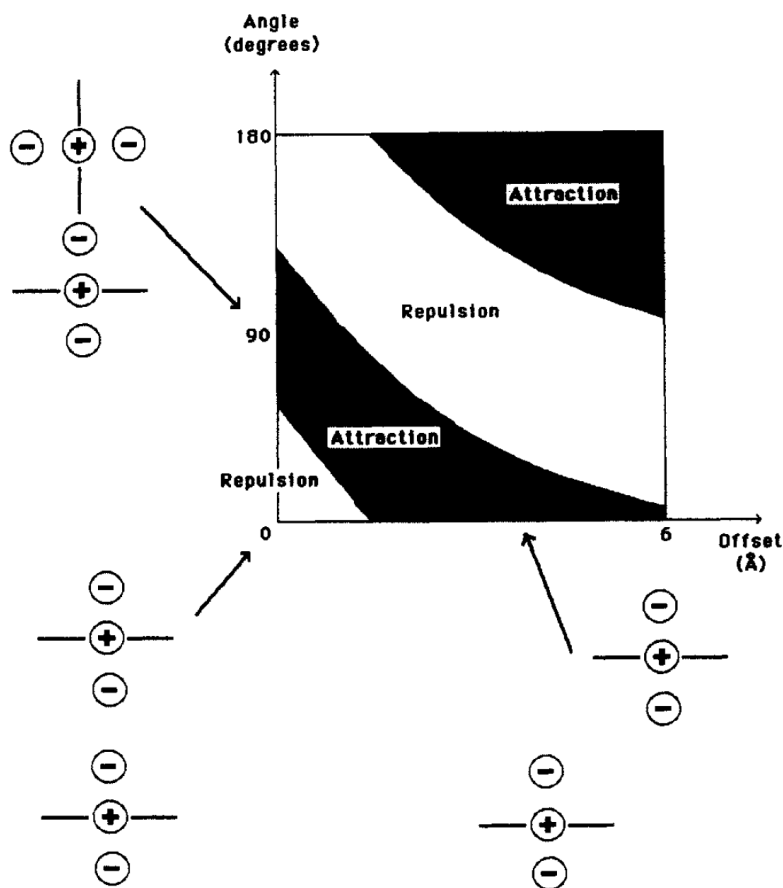
Picture 3. *Electrostatic interactions between π-charges as a function of orientation according to Hunter and Sanders.[44]*

The schematic representation in picture 2 and its translation in picture 3 allow for the description of an additional feature of aromatic rings, the quadrupole moment. A quadrupole moment can be regarded as two dipoles that are oriented such that the net dipole moment is zero; quadrupole moments are not exclusive to aromatic compounds, but they are a measure of the charge distribution within a molecule relative to a particular molecular axis, for example the C_6 rotational axis of benzene: sp^2 carbons are more electronegative than protons, and under the symmetry of a benzene ring the six C-H bond dipoles give rise to a quadrupole moment, where (as in the model of Hunter and Sanders) the π-electron clouds on both faces of the aromatic ring are negatively charged and the σ-framework is positively charged (pictures 2 and 3).

Polarization of the aromatic ring by a heteroatom or a substituent can affect the stacking. Electron donating substituents increase π-electron repulsion by increasing the electron density of the ring and thereby the quadrupole moment which carries a negative charge above both aromatic faces and a partial positive charge at the periphery. Electron withdrawing substituents cause the opposite. Heteroatoms can be electron rich, electron deficient or neutral. Consequentially, in polarized π-systems, like polarizations are repulsive und unlike polarizations are attractive. In unpolarized π-systems, interactions are dominated by π-electron repulsion. An electron-deficient π-system would decrease the repulsion, thereby stabilizing the interaction (picture 4).[35, 45]
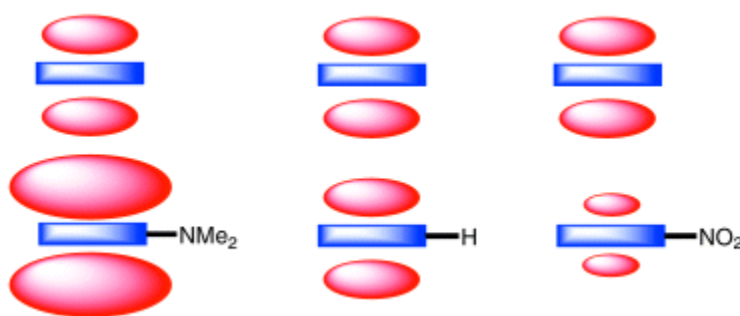
Picture 4. *Basic sketch of the influence of substituents on stacking interactions.[35]*

b) van der Waals dispersion forces, the attraction between molecules arising from the instantaneous charge fluctuations on each; because aromatic moieties possess large planar surfaces van der Waals contact is maximized in stacked arrangements. Although it is known that the strength of dispersive van der Waals interactions depends on molecule size and weight, the degree to which they contribute to π-stacking interactions is debated in the literature.[35, 46-50]

c) induction energy between the static molecular charge distribution of one molecule with the induced charge distribution of the other. Evidence so far suggests that they are less important but merely stabilize favorable interactions.[35]

d) charge transfer (CT) as described above, the mixing of a ground state with an excited charge separate state leading to stabilization, as described above; CT is not always observable in aromatic stacking events. At least in theoretical calculations the

contribution of CT to the stability of the ground state of molecular complexes is rather small.[35]

1.3.2 Electrostatics in π-π interactions

In a quantitative approach, Cozzi and Siegel measured the rotational barrier of the phenyl rings in substituted 1,8-diarylnaphthalenes via dynamic NMR (picture 5).[51] The activation energy of the isomerism delivers a solid estimate for the strength of the aromatic interaction between the stacked phenyl rings in their ground state.
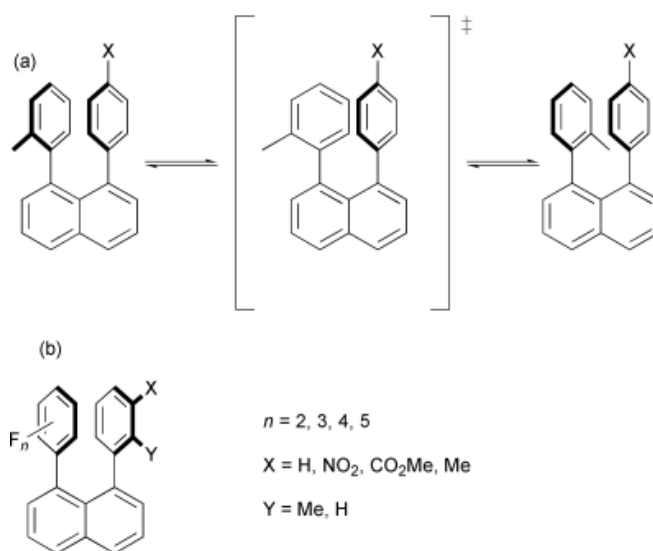
Picture 5. *a) Equilibrium system employed by Cozzi and Siegel. b) Fluorination of the 1,8-diarylnaphthalenes changed the trends in stacking energy.*[35, 53]

A linear relationship was found when plotting the results against Hammett constants, pointing towards electrostatic effects being the most important in this system; there was no spectroscopic evidence of charge transfer interaction. However, the increase of the rotational barrier by going from electron donating to electron withdrawing groups allowed for the conclusion that between the phenyl rings, polar π-interaction is significant. In the case where both aromatic rings were substituted, a linear relationship between rotational

barrier and the sum of the Hammett constants was established. Donor-acceptor interactions would dominate if a CT interaction was dominant, followed by acceptor-acceptor and finally donor-donor interactions. But in this study acceptor-acceptor interactions were found to be the most favorable, followed by donor-acceptor and donor-donor interactions (table 3). The reason for the observed trend is very likely that electron withdrawing groups reduce the repulsion between π- electron density of the phenyl rings when they are in a stacked conformation.[51, 52]

Substituent	$\Delta G^{\ddagger}/\mathrm{kJ\ mol^{-1}}$
OMe	58.2
Me	60.2
H	61.5
Cl	64.9
CO_2Me	70.7
NO_2	72.4

Table 3. *Rotational barriers in substituted 1,8-diarylnaphthalenes.*[51]

The electrostatic model was tested by reversing the charge distribution in the quadrupole of the aromatic rings. Therefore several fluorinated compounds were investigated. The rotational barrier increased with progressive fluorination of one of the phenyl rings because the electronegative fluorines decreased the mutual repulsion by removing electron density from the π-systems. In the perfluorinated ring it was even observed that the reversed quadrupole moment reversed the original trend of the rotational barriers as a function of further substituents. Therefore, in this system, electrostatics is suggested to be more important.[53]
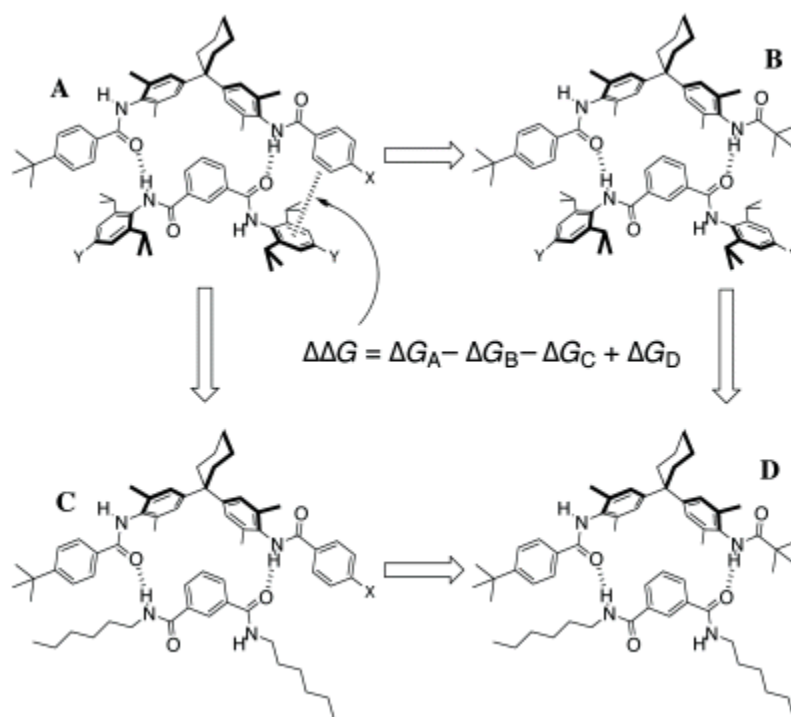
In order to measure edge-to-face interactions, Wilcox *et al.* designed a molecular torsion balance based on conformational isomerism (picture 6).[54, 55]
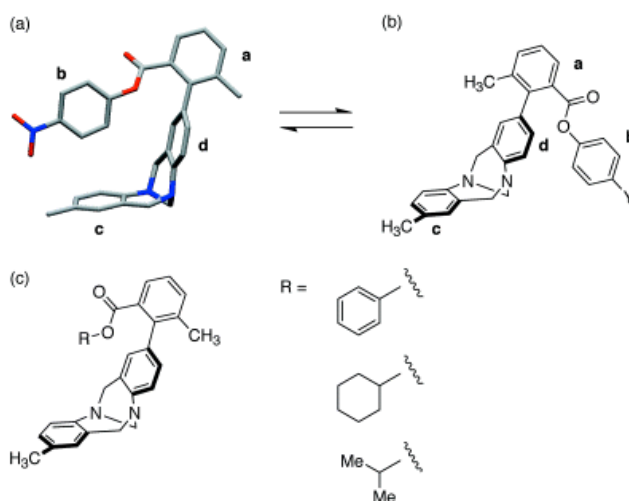
Picture 6. *Wilcox' torsion balance to quantify edge-to-face interactions. (a) is the crystal structure of the folded conformation. A range of functional groups was used to measure their interaction with the face of an aromatic ring (c).*[35, 54, 55]

The edge of ring **b** is situated over the face of ring **c** in the folded conformation. In contrast, the rings **b** and **c** are remote in open conformation. The interaction between the two rings was measured through deviations from the 1:1 ratio of states. Although rings **b** and **d** interact the relative populations are not perturbed. At room temperature, the molecule rotates between the two conformations. For Y=H the folded conformation is predominant; whereas the methoxy group has no discernible effect on the equilibrium, it is slightly shifted when Y=methyl. Y=I, CN or NO_2 further enhance the preference for the folded state, showing the importance of electrostatic effects in edge-to-face interactions.[54] On the other hand, for R=phenyl, cyclohexyl and isopropyl in each case the affinities to the face of ring **c** are similar. Several electron withdrawing and donating groups were used to replace the methyl group in ring **c** (NH_2, OH, CH_3, I, Br, CN, NO_2) but the folding energies of isopropyl and phenyl esters were -2.0±0.4 and -1.3±0.4 kJ mol^{-1} respectively.[55] These results suggest that London dispersion forces are much more important in edge-to-face interactions than electrostatic forces; however, the fact that the populations of the two conformations are not affected by solvent changes also suggests that these systems are not fully understood yet.[54, 55]

The approach of Hunter *et al.* towards measuring edge-to-face interactions was along similar lines. They designed a chemical double mutant cycle constructed from H-bonded molecular zippers (picture 7).[56, 57]

Picture 7. *Chemical double mutant cycle for the measurement of edge-to-face aromatic interactions,* $\Delta\Delta G(\pi\text{-}\pi).$[35, 57]

After measuring the association constants of a number of complexes by ^{1}H-NMR they determined that the edge-to-face interaction of the unfunctionalised aromatic rings was -1.4±0.8 kJ in chloroform. The edge-to-face conformation of the aromatic rings was confirmed by X-ray crystal structure.[56] Then substituent effects were investigated through functionalizing the edge and face rings with electron donating and electron withdrawing groups (table 4).[57] The aromatic interactions were quantified by measuring the association constants for all the complexes in picture 7 and constructing the depicted cycle. Going from complex **A** to complex **B** removes the aromatic interaction of interest but also removes secondary interactions between the aromatic ring and the core of the complex and alters the strength of the adjacent H-bond. The latter two are measured directly by carrying out the same mutations by going from complex **C** to complex **D**. The strength of indicated aromatic interaction can then be calculated using the formula in picture 7.

Substituent Y	Substituent X		
	NO_2	H	NMe_2
NO_2	+1.2	−0.2	−1.4
H	−3.4	−1.4	−1.1
NMe_2	−4.6	−1.8	−0.9

Table 4. *Aromatic edge-to-face interactions (kJ mol^{-1}) in zipper molecules in CDCl$_3$ at 295 K.*[57]

The values were found to correlate with Hammett substituent parameters for X and Y:

$$\Delta\Delta G\ (\pi - \pi) = 5.2\sigma_X\sigma_Y - 1.9\sigma_X + 1.4\sigma_Y - 1.5 \qquad (2)$$

Hunter *et al*. treated the last three terms as an electrostatic interaction between the positively charged CH groups on the edge ring and the negatively charged π-electron density on the face ring. When X and Y have opposite effects the first term is attractive which stands for an electrostatic interaction between the overall dipoles induced by the polarizing effects of the substituents.[57]

1.4 Nitroaromatic Sensing

Current nitroaromatic sensing methodologies can be largely split between optical and non-optical protocols. Non-optical instrumentations include metal detectors, canine teams and rather sophisticated spectrometric and instrumental methods. Metal detectors are of course not able of directly sensing the presence of explosive but only the casings containing the latter. However, considering the fact that most explosive devices have plastic shells nowadays, this approach seems rather limited.[58] To date canine teams (sniffer dogs) are the most secure way to detect nitroaromatic vapors. They perform very precisely and reliably, with their olfactory system being roughly four times bigger than in humans. Their ability to differentiate between target compounds is utilized in airports and

in the field. However, their training takes some time and they require an assigned handler for optimal performance; testing and validation exercises for a variety of scenarios have to be designed. Plus, the dogs can operate only a limited amount of time per day and tire after 30-120 min, calling for two or more dogs per location.[59]

Concerning instrumental detection of traces of compounds, there is a large array of methods that have been proposed and/or used, for example plasma-desorption mass spectrometry,[60] gas chromatography-electron capture detection,[61] surface-enhanced Raman spectroscopy,[62] mass spectrometry,[63] X-ray imaging,[64] thermal neutron analysis,[65] electrochemical procedures and ion-mobility spectroscopy.[66, 67] Despite the advantages these methods may offer, their drawbacks include vulnerability towards false positives due to environmental contaminants, false-negatives due to certain interfering compounds and their at best limited portability which reduces their employment in the field.[58, 68] D. S. Moore wrote an excellent review concerning instrumentation for the detection of high explosives.[69]

On the other hand, sensor-systems and devices that are based on interactions or reactions of nitroaromatics with other molecules are promising for hand-held devices because of their rapid response time, ease of detection in the form of color change or fluorescence output and simple material handling.[58, 68]

On a molecular level, several concepts and molecules have been introduced for the detection of nitroaromatic and other electron-poor aromatic compounds, some of which are introduced in this section.

1.4.1 Fluorescent Conjugated Polymers

One of the reasons why fluorescent conjugated polymers have been widely investigated is their capacity to amplify signals. This is a consequence of their exciton/excited state transport features including mixing of electronic states and/or through space dipolar couplings. In other words, these polymers are capable of signal gain as a consequence of their interactions with target compounds/analytes. The electron-poor nature of

nitroaromatic compounds makes them ideal candidates for fluorescence quenching processes through photo-induced electron transfer.[68] There are numerous criteria that decide on the performance of polymer films, such as the permeability of the film and the strength of interaction between the fluorescent polymer and the analyte. Swager *et al.* showed that the incorporation of a bulky pentiptycene moiety increases the polymers response towards explosives vapours by expanding the polymers permeability (picture 8). Also, the incorporation of the sterically demanding pentiptycene into the polymer prevents backbone π-stacking, excimer formation and self-quenching, which all would result in lower quantum yields and are commonly encountered drawbacks in fluorescent polymers. Swager *et al.* prepared polymers **1** and **2** and measured the sensing capabilities of the respective polymer films with TNT, 2,4-DNT and benzoquinone in fluorescence quenching assays.[70, 71]
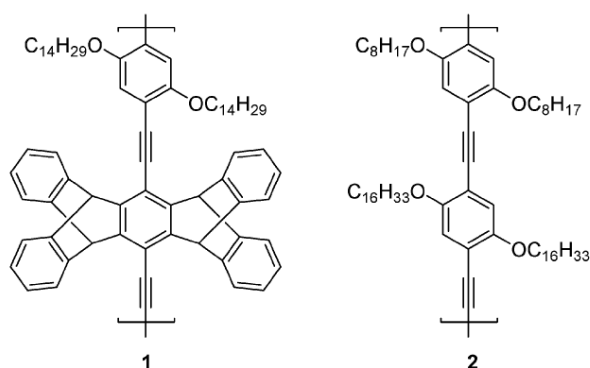
Picture 8. *Structures of polymers* **1** *and* **2**.[70, 71]

 The efficiency of fluorescence quenching proved to be dependent on the thickness of the film and the exposure time to TNT and 2,4-DNT vapors. A film thickness of 25 Å and exposure time of 60 seconds led to 100% quenching for 2,4-DNT and 75% quenching for TNT in films made from polymer **1**. When incorporated into handheld sensing prototypes, TNT vapors could be detected in femtograms per mL of air.[71]

In one of several extensions of the previous work (also by Swager *et al.*), polymer **3** not only has bulkier side chains than **1** but the substituents are less electron donating as well. Polymer **4** has identical substituent features like polymer **1** but the pentypticene is

even more bulky, with a naphthalene moiety replacing the benzene moiety of **1** on one side of the molecule (picture 9).[72]
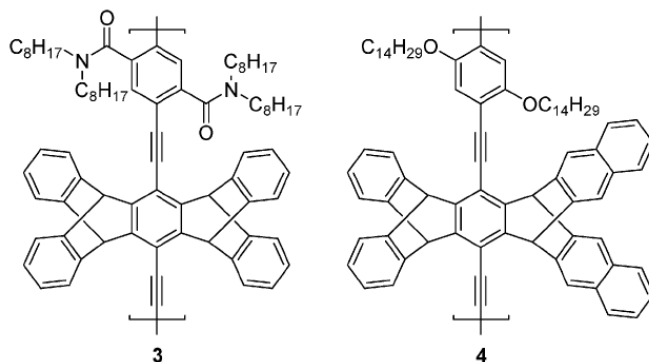
Picture 9. *Structures of pentypticene-containing polymers **3** and **4**.*[72]

Polymers **3** and **4** were applied in in 200 Å thick films. The hypothesis was that analytes that diffuse better or faster into the film should distribute throughout the bulk and the film should therefore show higher fluorescence quenching. Nitroaromatics showed very slow diffusion compared to other analytes. Furthermore, due to the electron withdrawing properties of amides, quenching efficiencies for polymer **3** were lower than for polymer **4**. In other words, the amide groups in **3** render it less electron donating than polymer **4**. Also, polymer **3** interacted less with the nitroaromatic analytes, which further diminishes fluorescence quenching.[72] Polyacetylene **5** was used for the fluorescent detection of TNT in multiphoton excitation experiments. The obtained emission band at 460 nm was quenched upon the addition of TNT (picture 10).[73]
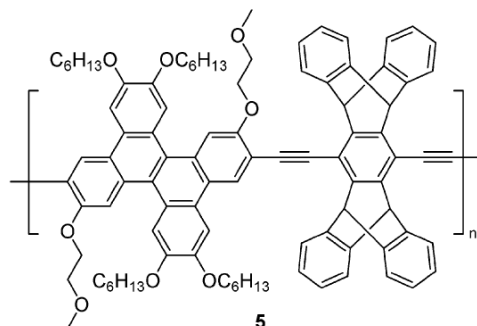
Picture 10. *Structure of polymer **5**.*[73]

17

Aside from Swager and coworkers, Zhang and Liu independently from on another conducted research along similar lines. Zhang *et al.* described the quenching properties of TNT with quinoxaline-containing polymers **6** and **7** both in solution and in films (picture 11).[74]
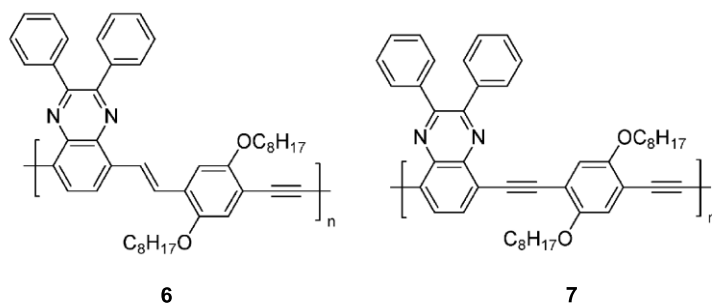
Picture 11. *Structures of quinoxaline-based polymers* **6** *and* **7**.[74]

Polymers **6** and **7** show emission lines at 500 nm and 620 nm respectively in chloroform solution which are quenched with the addition of TNT. When using films instead of solution the same effect was observed. Quenching was more efficient in the case of polymer **7**, which the authors attributed to the fact that the more planar backbone of **7** allows for easier exciton migration in comparison to polymer **6**.[74]

Liu and coworkers developed polymer **8** which displayed emission bands at 427 nm and 453 nm in chloroform solution that were considerably quenched when 2,4-DNT was present (picture 12). They prepared two types of films which showed different amount of quenching upon exposure to 2,4-DNT vapours. This was accounted for by the fact that depending on mode of fabrication, a unique porous structure with a big surface area was observed.[75]

8
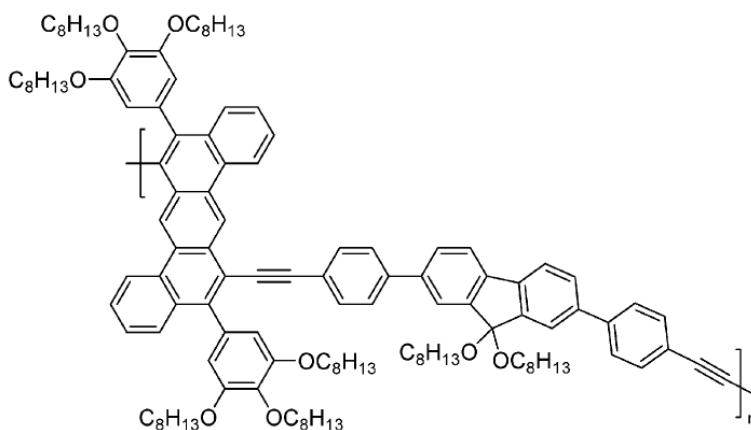
Picutre 12. *Structure of polymer* **8**.[75]

Poly(phenylene vinylenes) constitute another class of fluorescent conjugated polymers that have been applied for the detection of nitroaromatics (picture 13).[68, 75] For example, polymers **9** and **10** were deposited as film on glass plates where they exhibited intense fluorescence bands at 574 nm and 488 nm respectively.
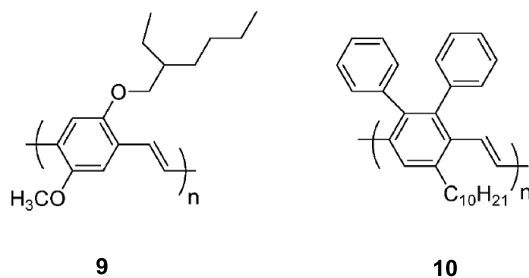
9　　　　　**10**

Picture 13. *Structure of poly(phenylene vinylene) polymers* **9** *and* **10**.[75]

In the presence of TNT vapours, **9** displayed quenching efficiencies up to 90% which was the highest value measured in the study. The superior performance of polymer **9** over polymer **10** was attributed to the donor moieties of polymer **9** which are not present in polymer **10**. These donor moieties enable strong polar interactions of the polymeric film with the electron poor aromatic subunit of TNT. Apart from TNT, other nitroaromatics were used as well, such as 2,4-DNT, 2,6-DNT and 4-NT. As mentioned before, the most

19

promising results were achieved with the combination of polymer **9** with TNT (90% quenching after 1000 seconds of exposure).[75]

Vinylic polymer **11** contains an iptycene backbone to prevent self-quenching through interaction among the chains (picture 14). As a direct consequence, films of polymer **11** also exhibit enhanced permeability towards analytes, as seen in numerous polymers that were developed by Swager and coworkers and partly shown above. **11** showed, with a quantum yield of 0.76, an intense emission band at 477 nm that was quenched through the addition of TNT.[76]
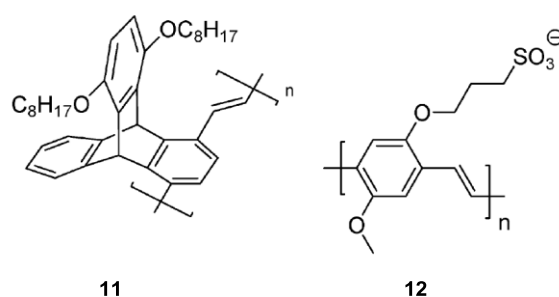
Picture 14. *Structures of polymers* **11** *and* **12**.[76, 77]

Polymer **12** constitutes an exception in so far as that it is water soluble (picture 14). Although it showed strong emission in aqueous solution that could be easily quenched with methyl viologen, quenching performances were orders of magnitude lower with nitroaromatic analytes such as TNT or 2,6-DNT. Although nitroaromatics are lacking electrons they are still neutral and therefore can't compete with the strong association between the positively charged quencher methyl viologen and the negatively charged polymer **12**. However, in the presence of a surfactant, in this case dodecyltrimethylammonium bromide DTA, the opposite was true. DTA turns the environment around the polymer **12** hydrophobic and in an aqueous solution with **12** and DTA the intense emission of **12** was severely quenched upon the addition of TNT and 2,6-DNT. For 2,6-DNT vapors the same held true for polymer films of **12**.[77]

Polymer **13** is a semiconductor and was used for the detection of TNT and 2,4-DNT vapors (picture 15). It displayed an intense emission band at 500 nm that was quenched with vapors from the aforementioned nitroaromatics. A number of different devices were also built for the fabrication of solid sensors with amplified signaling. Polymer **13** was

applied to different supports in different coating techniques. The films were then excited with a 4 ns nitrogen laser leading to the generation of multimode lasing action and amplified emission. The latter could be quenched with TNT and 2,4-DNT with a sensitivity 30 times larger than observed before. Since the devices showed no reaction towards benzene and naphthalene, it was concluded that the observed sensitivity is caused by the strong binding of the analytes to the electron rich polymer **13**.[78]
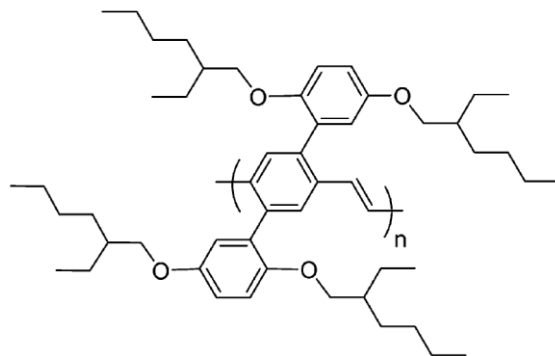
13

Picture 15. *Structure of semiconduncting polymer* **13**.[78]

1.4.2 Polycyclic aromatic hydrocarbons

Polycyclic aromatic hydrocarbons are hydrocarbons that are composed of multiple, sometimes fused, aromatic rings. Because of the availability of a large number of compounds, their comparably high quantum yields and because their (photo-) physical properties are mostly well known they are perfect candidates for the sensing of charged and neutral molecules. Their electron density can be addressed rather easily i.e. their electron donating or withdrawing features can be tuned and compared; smaller molecular sensors are mostly soluble in common solvents.[68]

Focsaneanu and Scaiano used ethanol solutions of pyrene in emission quenching assays to sense nitro explosives. Upon excitation at 355 nm the solutions showed two emission bands at 400 nm (from the singlet excited state monomer) and at 470 nm (from excimers). While electron-rich compounds were not able to substantially alter the emissions, both bands were quenched through the addition of electron- poor derivatives

such as 1,4-NB, 1,3-DNB, 5-NX, NB, NM or NE. The ratio of excimer intensity and monomer emission in dependency of the quencher concentration allowed for the differentiation between nitro compounds.[79]

Calix[4]arene-based receptor **14** contains pyrene-moieties as well. It was employed both in fluorimetric and colorimetric experiments to detect nitroaromatics (picture 16). In acetonitrile both emission bands (375 nm for the monomer and 450 nm for the excimer at an excitation wavelength of 343 nm) could be significantly quenched with TNB and TNT. Upon the addition of 2,6-DNT, 1,3-DNB and NB only mediocre quenching was observed. Molecule **14** emerged also to be convenient for the colorimetric detection of TNB and TNT. Displaying the typical absorption bands between 320-360 nm, the colorless chloroform solutions of receptor **14** turned yellow and reddish-orange upon the addition of TNT or TNB, respectively.[80]

14
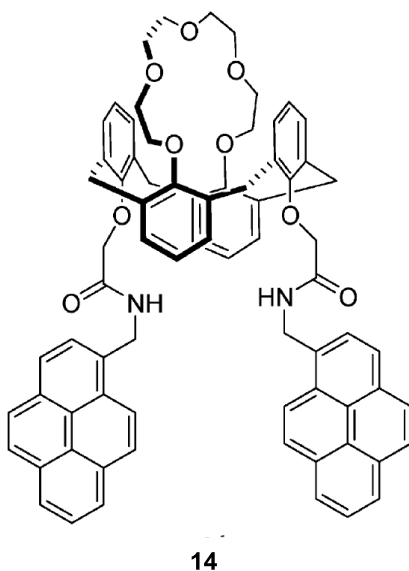
Picture 16. *Structure of calix[4]arene-based receptor* **14**.[80]

Pyrenebutyric acid **15** (picture 17) was used as fluorophore in cellulose triacetate

membranes that were plasticized with isodecyl diphenylphosphate.[81]
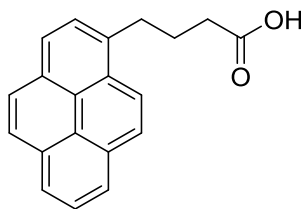
15

Picture 17. *Pyrenebutyric acid* **15**.[81]

The membrane extracted TNT, 2,4-DNT and RDX from water for the quenching of the emission band of acid **15** around 412 nm (excitation: 354 nm). TNT and 2,4-DNT were detected with a limit of 2 ppm and RDX showed a detection limit of 10 ppm. The performance of the membrane towards the analytes corresponded well with the octanol-water partition coefficients of nitrated compounds.

Binaphthyl-based receptor **16** was functionalized with donor-acceptor substituted *trans*-stilbenes (picture 18). Possessing considerably higher quantum yields in films than in solution, drop-casted films on 3:1 v/v toluene-chloroform mixtures emitted an intense band at 510 nm. The band was quenched 91% in intensity after 10 minute exposure to 2,4-DNT vapours and 72% using TNT under the same conditions. The difference in quenching is partly due to the higher vapour pressure of 2,4-DNT. The quenching itself was attributed to a PET-process from binaphthyl **16** to the nitro analytes.[82]
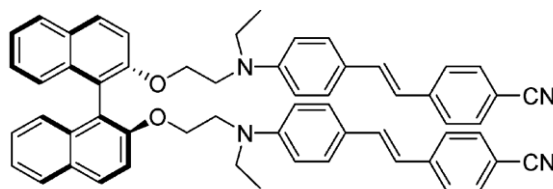
16

Picture 18. *Structure of binaphthyl-derivative* **16**.[82]

The rather bulky 1,4-diarylpentiptycenes **17-21** were developed by Anzenbacher Jr. and

23

his coworkers (picture 19). In dichloromethane, molecule **21** emits at 450 nm which could be quenched by the stepwise addition of NB, 2,4-DNT and TNT. In the same solvent, receptors **17**-**20** give identical results. When incorporated in polyurethane films, molecules **20** and **21** displayed sensitivity towards 2,4-DNT and TNT vapors; the latter were able to quench the fluorescence of the receptors.[83]
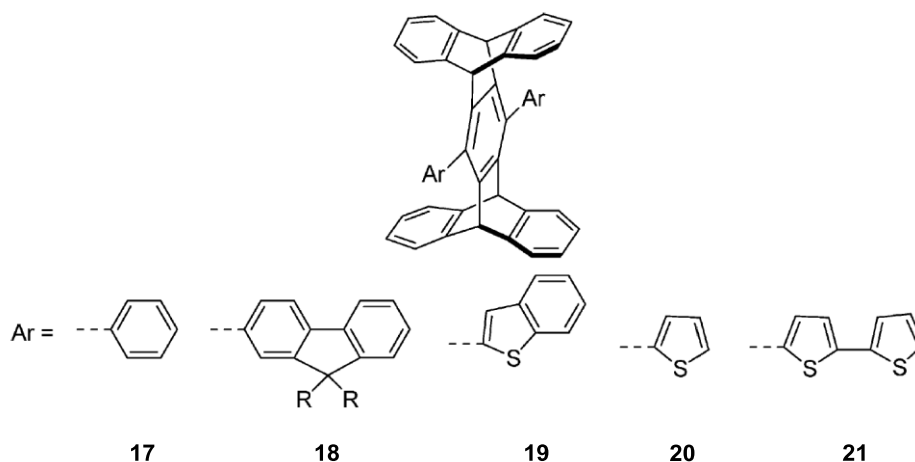
Picture 19. *Structure of pentypticenes* **17**-**21**.[83]

Dendrimers have been suggested and tested as potential sensors for nitrated explosives as well. Meredith *et al*. studied the photophysical properties of the fluorene-based dendrimers **22** and **23** for the detection of explosives (picture 20). In THF both molecules **22** and **23** were spectroscopically identical. Their emission bands at 393 nm (with a quantum yield of 90%) could be quenched by adding 1,4-DNB, 2,4-DNT and 4-NT, where quenching was more efficient for the three-dimensional structure **23**. This was attributed to the possibility for one analyte to quench multiple identical chromophores, leading to an amplification effect. The quenching itself was ascribed to PET processes from excited fluorine chromophores to analytes.[84]
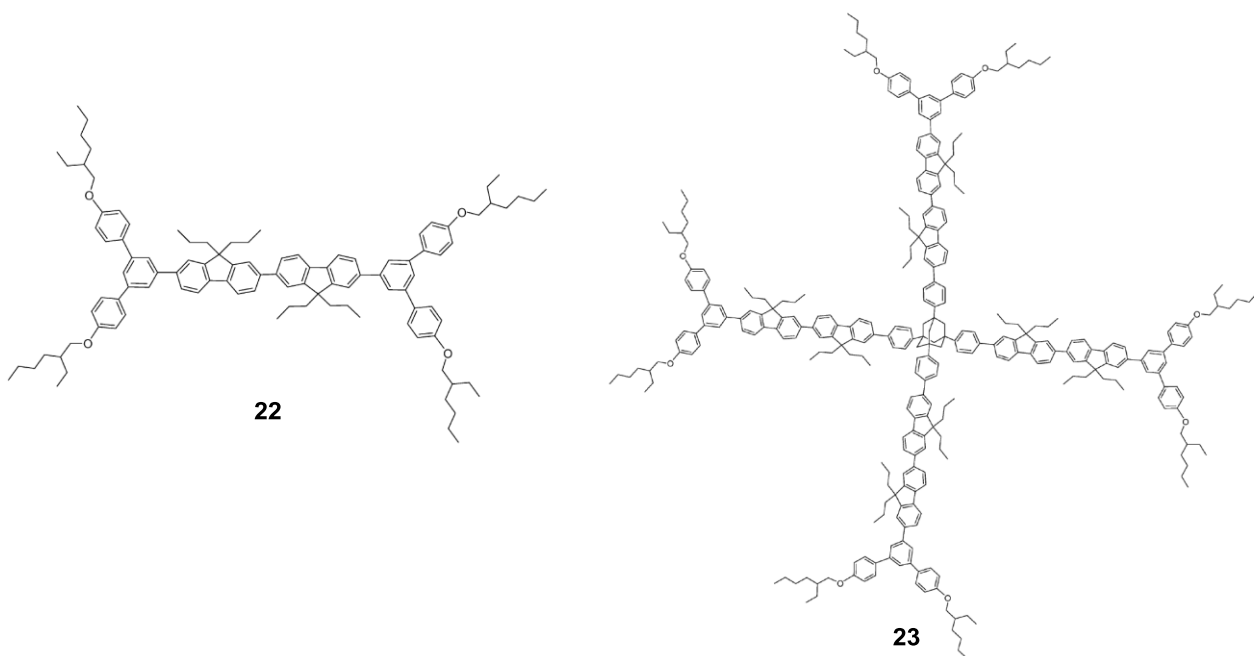
Picture 20. *Structure of fluorine-based dendrimers* **22** *and* **23.**[84]

Apart from aromatic hydrocarbons, heterocycles have been used for detection of explosives as well. With carbazole trimer **24** porous films consisting of embroiled fibril networks were prepared (picture 21). The fibrils had a diameter of roughly 30 nm and were several microns in length. The fibrils emitted at 438 nm.
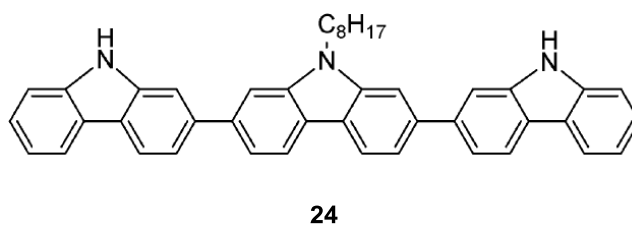
Picture 21. *Structure of carbazole trimer* **24.**[85]

The porosity of the films is tunable and they possess a large surface area to volume ratio. Their extended intermolecular π-π electronic interaction leads to long-range exciton diffusion. Hence, the fluorescent quenching of nitroaromatics is rather efficient. TNT vapors quenched 70% of the fluorescence intensity after 60 seconds of exposure

and 2,4-DNT quenched 50% after 10 seconds. The quenching process is based on PET processes between carbazole **24** and the analytes. Moreover, the fluorescence of the fibrils could be restored by heating the films for 10 minutes at 50 °C under vacuum.[85]

Benzothiophene **25** is planar (picture 22) and was employed to prepare 1D nanobelts and 3D "super –nanoflowers" (pictures 23 and 24) by means of π-π stacking and van der Waals interactions.[86]
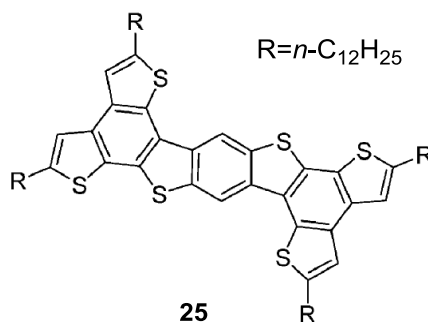
Picture 22. *Structure of benzothiophene* **25**.[86]

The nanobelts were self-assembled by drop casting a solution of **25** in 1,4-dioxane (picture 23).
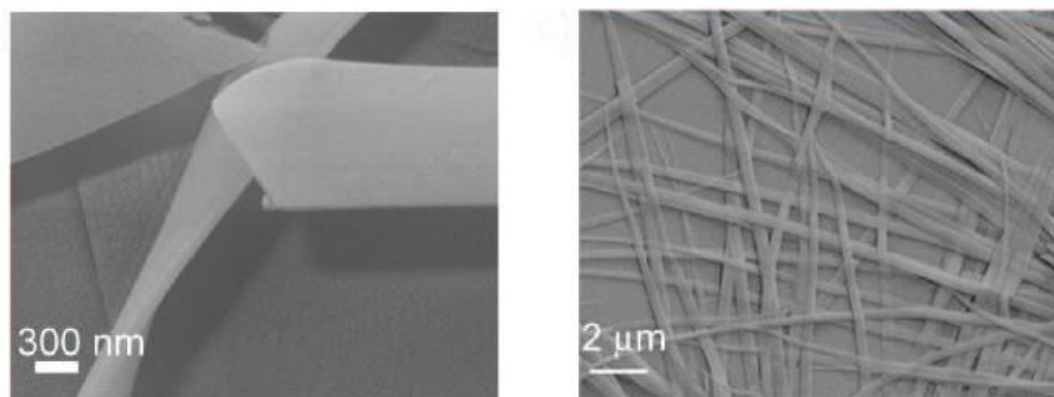
Picture 23. *SEM images of nanobelt assembled from* **25**.[86]

When in place of 1,4-dioxane THF and n-decane were used under the same conditions, two 3D flower shaped supernanostructures were obtained, A and B (picture 24).
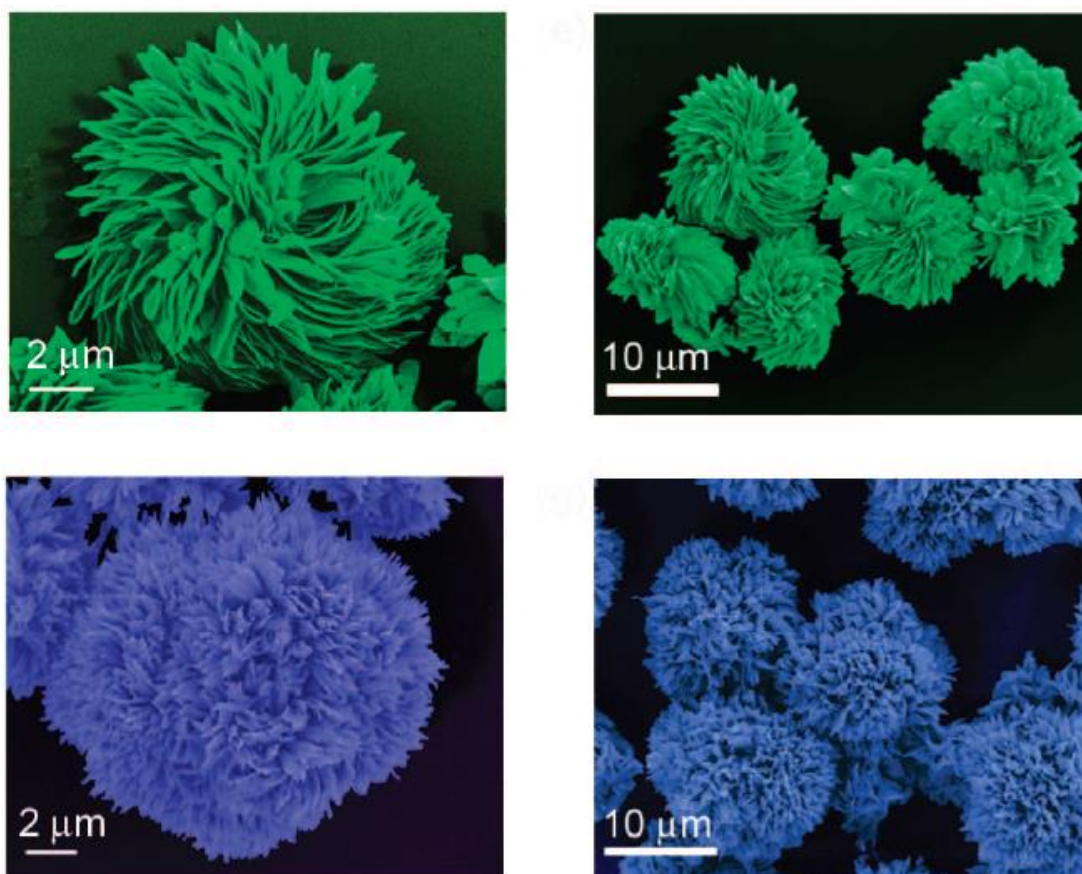
Picture 24. *Pictures of nanoflowers A (above) and B (below) assembled from* **25**.[86]

The films of A and B showed intense emission between 450 nm and 480 nm. Exposing films of A or B to 2,4-DNT vapors led to quenching of the emission intensity by 50% after 330 seconds (A) or 30 seconds (B). On the other side, the same result only arose after an exposure time of 22000 seconds for the 1D nanobelt. These huge differences in response time were explained by the larger surface area and the morphology that is more porous for A and B than for the nanobelt. The sensing mechanism is ascribed to electron transfer processes between the electron poor analyte and the electron rich nanostructures.[86]

Water-soluble porphyrin **26** showed two emission bands at 702 nm and 645 nm

(excitation wavelength: 413 nm) in buffered aqueous solution at pH 7 (picture 26). Upon the addition of TNT, the formation of a non-emissive complex between TNT and porphyrin **26** was observed.[87]
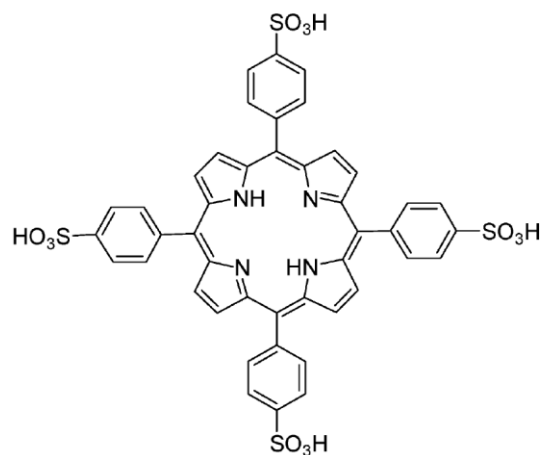
26

Picture 26. *Structure of water-soluble porphyrin* **26**.[87]

The authors determined a detection limit of 200 ppb for TNT by means of emission quenching experiments. The same group also used structurally related porphyrin **27** for identical purposes (picture 27). In aqueous solution at pH 7 an absorption band in the Soret region appeared at 413 nm. Not only was extinction coefficient of the band reduced when TNT was added but also a broad shoulder appeared around 424 nm. Upon the excitation of the aqueous solutions at 413 nm, porphyrin **27** displayed two emissions around 636 nm and 706 nm. Both bands were moderately quenchable by incrementally adding TNT.[88]
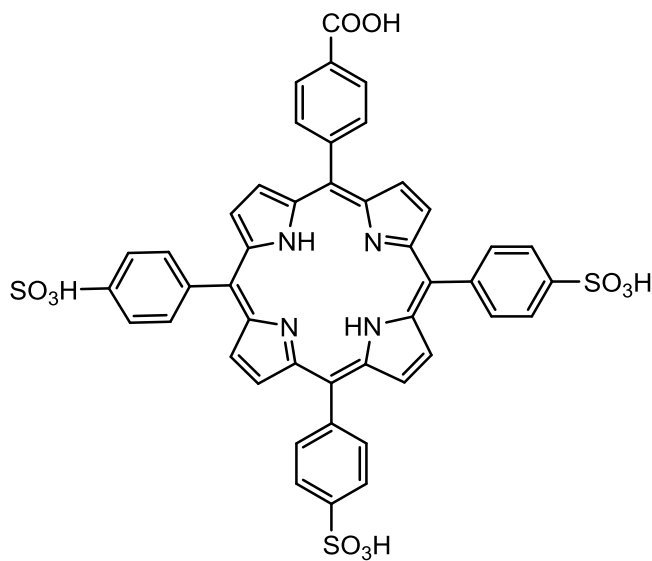
27

Picture 27. *Structure of water-soluble porphyrin* **27**.[88]

Siloles possess the distinct characteristic of becoming efficient emitters upon the formation of aggregates, which is hardly ever seen in more traditional chromophores.[67] For example, silole **28**, in THF-water 1:9 v/v solution, produced an intense emission band at 500 nm (excitation wavelength: 370 nm) due to formation of exceptionally fluorescent aggregates (picture 28). The band could be quenched when PA was added.[89]
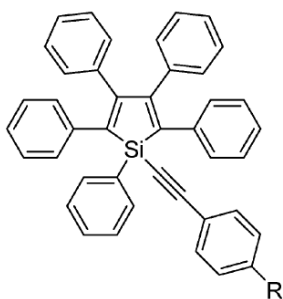
28, R=-NH$_2$
29, R=-OH

Picture 28. *Structure of siloles* **28** *and* **29**.[89]

29

The same was true for silole **29** (picture 28). Both receptors **28** and **29** showed selectivity towards PA, quenching experiments with 2,4-DNT were only moderately successful. The receptors showed a detection limit towards PA of ca. 0.1 ppm. The observed quenching was attributed to the cracking of siloles **28** and **29** caused by the coordination to PA.[89]

Montméat *et al.* developed a portable device based on fluorescent films of the π-conjugated phenylene-ethylene-diimine **30** (picture 29). After the deposition of the films on glass substrates they acted as waveguides for the detection of ultra-trace amounts of 2,4-DNT and TNT. The device was used in ambient air and on objects stained with the explosives. The diamine moiety exhibits a large electron density that lends it great affinity towards the electron poor analytes. In the presence of 2,4-DNT or TNT, the fluorescence of the film (around 480 nm) dropped by 80% (10 min exposure) and 40% (also 10 min exposure), respectively. Films of **30** showed detection limits of 9 ppb for 2,4-DNT and 0.75 ppb for TNT. Remarkably, humidity or interfering compounds did not diminish the performance of the devices.[90]

30
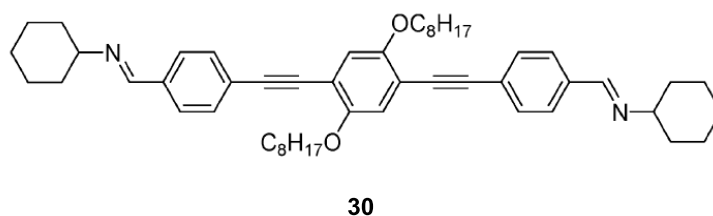
Picture 29. *Structure of diimine* **30**.[90]

Phenyl derivatives **31** – **35** emitted between 400-440 nm in hexane-ethyl acetate 91:9 v/v solutions (picture 30). Adding 2,4-DNT, TNT and NB quenched the emissions each. The quenching was ascribed to PET processes between the excited receptor and the respective derivative **31** – **35** due to the formation of 1:1 complexes. The largest quenching effect was observed for molecule **31** with 2,4-DNT.[91]
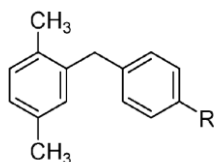
31 R=-H
32 R=-CH₃
33 R=-OC(O)CH3 ³
34 R=-OCH3
35 R=-OH

Picture 30. *Structures of phenyl derivatives* **31**-**35***.*[91]

1.4.3 Molecular Tweezers

Strictly speaking, structure **14** belongs to a class of sensors that was introduced by Whitlock in 1978, the molecular tweezers. The underlying concept is to strengthen binding of aromatic guests with a host through formation of a π-system "sandwich" through use of a cooperative effect between the two aromatic clips in the host (picture 31).[92]
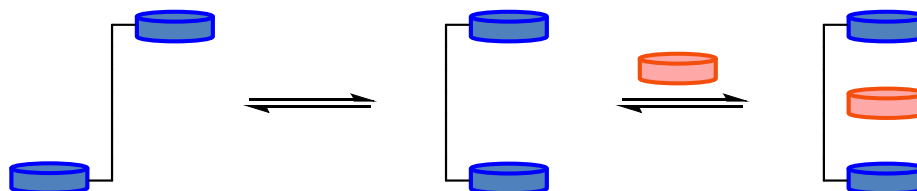
Picture 31. *Supramolecular interaction principle between aromatic tweezers host (blue) and aromatic guest (red), as described Whitlock.*[92]

Conceptually, tweezers as depicted in picture 31 consist of two parts. The part of the molecule that binds guests, the pincers (blue cylinders in picture 31), and the backbone or spacer the pincers are attached to (black lines in picture 31). The exact structure of the binding units depends on the chemical nature of the intended guests. The structure of the spacer is restricted by the three criteria identified that can enhance the binding features of molecular tweezers; (1) the prevention of self-association through the

presence of a suitable spacer or backbone either by steric constraints or reducing intramolecular binding affinity in contrast to the guest, (2) a spacer/backbone that defines the distance between the pincers or the clips of the tweezer and (3) a spacer that restricts the conformation between the pincers. When these criteria are compared to the definitions given in chapter 1.2, it is clear that these structures may be accessed in a bottom- up approach through molecular design. Although the interplay between the design criteria and their implementation in actual molecules is far from being resolved, it has been shown that the presence of a second host molecule can greatly enhance binding strength towards aromatic guests.[92, 93]

Prominent examples of molecular tweezers based on these principles were developed by Zimmerman and coworkers (picture 32).
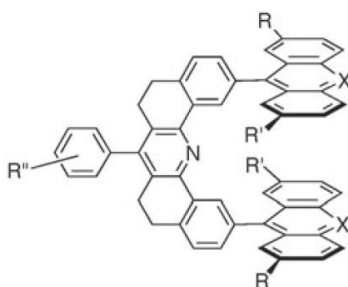
36 X=N, X'=N
37 X=CH, X'=N
38 X=X'=CH

Picture 32. *Structure of Zimmermans tweezers* **36**-**38**.[94]

The conformation in tweezers **36-38** is mobile; the gap between the two pincers can be adjusted for binding an aromatic guest. In this series the nature of the aromatic backbone is minor (i.e. the part of the molecule defining the distance between the acridine and/or anthracene pincers); this was shown through increasing affinity towards 2,4,5,7-tetranitrofluorenone by substituting the acridines in molecule **36** (K_a=900 M^{-1} in CDCl$_3$) with one (**37**, K_a=2800 M^{-1} in CDCl$_3$) or two (**38**, K_a=20 000 M^{-1} in CDCl$_3$) anthracenes. Zimmerman *et al.* also demonstrated in a string of similar experiments the

importance of a rigid spacer and the general effect of a tweezers-like structure compared to the corresponding single chromophore.[94]

The question how much more stable a sandwiched π-complex could be compared to its singly stacked counterpart cannot be answered absolutely. The influencing factors are largely inherent to the molecule under consideration.[94, 95] Breslow stated that a good host molecule avoids conformational change with unfavorable entropy upon binding; therefore preorganization of the host is an important factor.[96] The pincers attached to the backbone constitute the second big parameter; because they are the active binding component of the tweezers-structures, their chemical nature determines the strength of any interaction to a good degree.[94, 95]

Apart from the examples mentioned above (**14** and **36**-**38**), several molecular tweezers for the sensing of nitroaromatic compounds were developed.

Otsuki *et al.* reported molecular tweezers **39** that are structurally based on the molecules introduced by Zimmerman (picture 33). Like tweezers **38**, molecule **39** has anthracene binding units. But whereas in tweezers **38** they share a single bond with the spacer, in molecule **39** the anthracenes are attached in benzylic fashion to the dihydroxyanthraquinone backbone. Compared to molecules **36** and **37**, the resulting elevated degrees of freedom of the anthracene host units are reflected in the binding affinity of tweezers **39** towards aromatic guests. Its association constant towards 2,4,5,7-tetranitrofluorenone (K_a=2.17±0.02*10^3 M^{-1} in CDCl$_3$) is higher than in molecule **36** (two acridine pincers) but lower than in molecule **37** (one acridine and one anthracene pincer).[97] This is a good example of the interdependence between the influence of the spacer and the pincers with regards to preorganization and binding strength of such molecules.
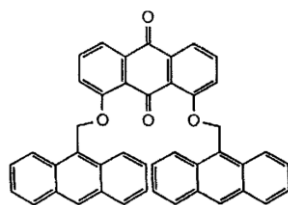
39

Picture 33. *Structure of molecular tweezers* **39**.[97]

Molecule **40** consists of 1,2-diaminocyclohexane as spacer with two usnic acid units as pincers (picture 34).[98]
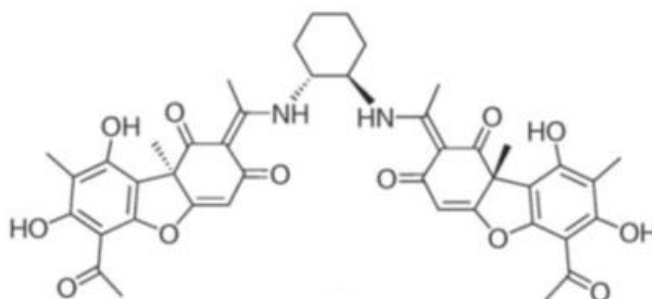
40

Picture 34. *Structure of usnic acid-based tweezers* **40**.[98]

Complexation of TNF between the two acid units was observed (K_a=72 M^{-1} in CD$_2$Cl$_2$). A strong color change was observed upon titration (picture 35) with the guest.
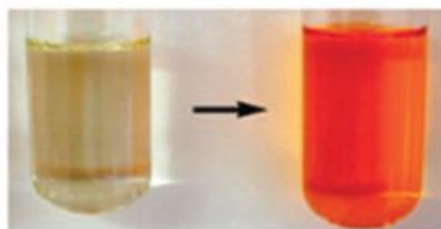
Picture 35. *Color change upon complexation of tweezers* **40** *with TNF.*[98]

This is attributed to the formation of a charge transfer complex between tweezers **40** and TNF.[98]

Chiral tweezers **41** comprises a rigid bile acid spacer and pyrene pincers/sidewalls.
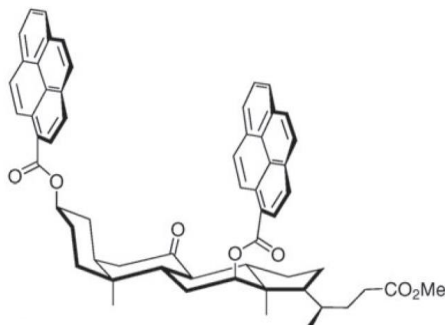
41

Picture 36. *Structure of rigid tweezers* **41**.[99]

The resulting structure **41** is able to bind several electron-deficient aromatic guests, including polyaromatic compounds (K_a=220 M^{-1} with TNF in CDCl$_3$).[99]

Sessler and coworkers devised a tweezers molecule which can be driven to self-associate as well as binding to guests (picture 37).[100]

42
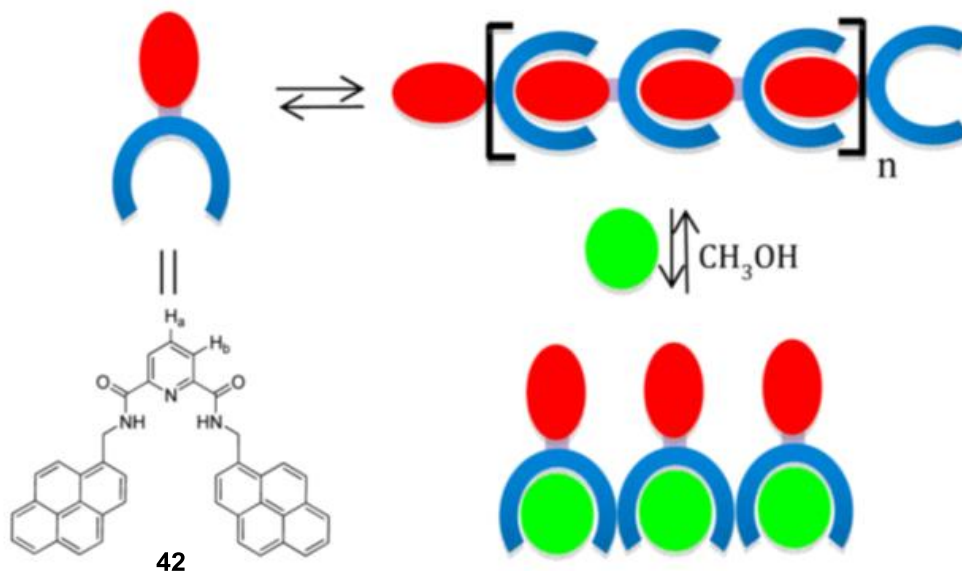
Picture 37. *Depiction of oligomeric structures formed by tweezers* **42** *and deaggregation through addition of TNB or TNT.* [100]

Molecule **42** self-associates into oligomeric species in the absence of suitable guests in solution through intermolecular amide-pyridine-, pyrene-pyridine- and pyrene-pyrene-interactions. Upon the addition of electron-deficient guests, aggregates of **42** disassembled and formed 1:1 complexes with the guests. The reported association constants determined by ^{1}H-NMR ranged from K_a=7.32*10^4 M^{-1} (TNB in CDCl$_3$) to K_a=7.69*10^2 M^{-1} (TNT in CDCl$_3$). Addition of methanol to the solutions led to regeneration of the aggregates observed in the absence of guests, which the authors supposed is due to the solvation of TNB by methanol. The extended arrays of the aggregates are characterized not only by NH-H hydrogen bonds but also by intermolecular pyrene-pyridine and pyrene-pyrene contacts.[100]

Molecule **43**, introduced by Klärner and his group, is much more rigid and only one example of the numerous similar structures whose complexation behavior towards aromatic guests was investigated by him and his group (picture 38).[101-106]
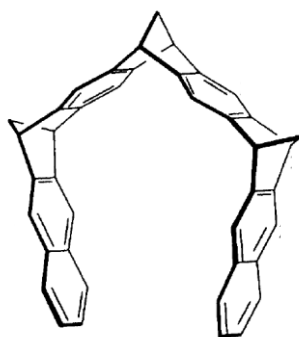
43

Picture 38. *Structure of* Klärner-*type tweezers* **43**. [101]

The rigidity of this class of tweezers renders them much more susceptible to the chemical nature of the guests. Congruously, association constants of tweezers **43** with electron-deficient guests change from K_a=10 M^{-1} (1,2-DNB in CDCl$_3$) and K_a=56 M^{-1} (1,4-DNB in CDCl$_3$) to K_a>10^5 M^{-1} (1,2,4,5-TBN in CDCl$_3$).[101]

Glycoluril-based tweezers and hosts have been attracting much attention which is traced back to the work of Nolte *et al.* Straightforward synthetic protocols allowing great functional variety and interesting preorganizational features make glycoluril an interesting building block.[95, 107]

Molecule **44** is a representative example (picture 39). The acetylated *o*-xylylene sidewalls form a deep cavity together with the spacer. Molecule **44** selectively recognizes 4-nitrophenol (K_a=10 000 M^{-1} in THF/MeOH 9:1). Also, low detection limits were demonstrated in fluorescence quenching experiments.[108]
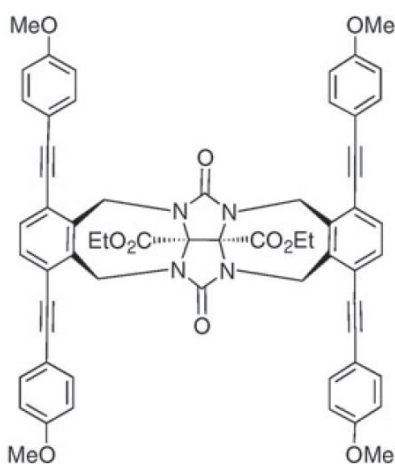
44

Picture 39. *Glycoluril-based tweezers **44**.*[108]

The many possibilities to access molecular tweezers through molecular design have, apart from nitroaromatic sensing, already resulted in numerous new findings and potential applications.[109] Partly because of the multitude of ways in which the initially macroscopic phenomenon of pinching objects can be recreated on the molecular level and partly because the individual contribution of each molecular interaction involved in the resulting binding phenomenon is not necessarily fully unraveled, the interplay between topology, chemical features and binding affinity between tweezers and guests obscures potential design criteria at the moment.[95, 110] This work investigates the influence of the gap size in the tweezers on their binding affinity towards electron-deficient guests.

1.5 Association Constants in the 1:1 System [111, 112]

When the concentration of species in a solution is proportional to their activity, the association constant (K_a) for 1:1 host-guest equilibriums is defined as

$$K_a = \frac{[HG]}{[H][G]} \tag{3}$$

with [H] being the host concentration, [G] the guest concentration, and [HG] the concentration of the host-guest complex.

The mathematical model used to determine K_a relies on the fact that the observed physical change (Y) and the concentration of the complex [HG] are correlated. In case the equilibrium is fast on the NMR-timescale, the observed NMR shifts are the result of the contribution of the individual components and can be described the following way in the case of NMR:

$$Y = Y_H f_H + Y_G f_G + Y_{HG} f_{HG} \tag{4}$$

By combining equations (3) and (4) and by acknowledging that

$$\tag{5}$$
$$[H]_0 = [H] + [HG]$$

And

$$[G]_0 = [G] + [HG] \tag{6}$$

the following equation is obtained:

$$f_{HG} = \frac{K_a[G]}{1 + K_a[G]} \tag{7}$$

Equation (7) is a description of the general binding isotherm for 1:1 binding systems as a relation between f_{HG} and the free-guest concentration [G]. [G] cannot be determined directly, therefore different approaches are required.

Because $f_{HG} = [HG]/[G]_0$, equation (7) can be rewritten as

$$[HG] = [H]_0 K_a[G]/(1 + K_a[G]) \tag{8}$$

After insertion of equation (8) into equation (6) and rearranging, the quadratic equation (9) is obtained

$$[G]^2 - [G]\left([G]_0 - [H]_0 - \frac{1}{K_a}\right) - \frac{[G]_0}{K_a} = 0 \tag{9}$$

which has only one real solution:

$$\tag{10}$$

$$[G] = \frac{1}{2}\left([G]_0 - [H]_0 - \frac{1}{K_a}\right) - \sqrt{\left([G]_0 - [H]_0 - \frac{1}{K_a}\right)^2 + 4\frac{[G]_0}{K_a}}$$

Another possibility is to isolate equations (3) and (4) for [H] and [G] separately and insert them into equation (1) which, after expanding the right-hand denominator, can be rearranged into the following equation:

$$\tag{11}$$

$$[HG]^2 - [HG]\left([G]_0 + [H]_0 + \frac{1}{K_a}\right) - [H]_0[G]_0 = 0$$

The corresponding solution takes the following form:

$$[HG] = \frac{1}{2}\left([G]_0 + [H]_0 + \frac{1}{K_a}\right) - \sqrt{\left([G]_0 + [H]_0 + \frac{1}{K_a}\right)^2 + 4[H]_0[G]_0} \tag{12}$$

Furthermore, if we assume that

$$\Delta Y = Y_{\Delta HG}\left(\frac{[HG]}{[H]_0}\right) \tag{13}$$

by combining equations (12) and (13) the following equation is obtained

$$\Delta Y = \frac{Y_{\Delta_{\mathrm{HG}}}}{[\mathrm{H}]_0} \left\{ \frac{1}{2} \left(\left([\mathrm{G}]_0 + [\mathrm{H}]_0 + \frac{1}{K_a} \right) - \sqrt{\left([\mathrm{G}]_0 + [\mathrm{H}]_0 + \frac{1}{K_a} \right)^2 + 4[\mathrm{H}]_0[\mathrm{G}]_0} \right) \right\} \quad (14)$$

In our case, the exchange between host and guest is fast on the NMR time scale, so the observed NMR resonance is the average between the bound and the unbound species. Therefore, equation (12) can be applied because it is dependent on the relative mole fractions of the species of interest. If the NMR resonance of the unbound host is δ_H, the resonance of unbound guest is δ_G and the resonance of the host-guest complex δ_{HG}, the change in the resonance for the host-guest complex can be defined as $\delta_{\Delta HG} = \delta_H - \delta_{HG}$. If we additionally define that δ_0 = NMR resonance of the host at the start of the titration (before guest is added), the observable change in NMR resonance can be expressed as $\Delta\delta = \delta_{measured} - \delta_0$. Consequently equation (12) becomes

$$\Delta \delta = \frac{\delta_{\Delta_{\mathrm{HG}}}}{[\mathrm{H}]_0} \left\{ \frac{1}{2} \left(\left([\mathrm{G}]_0 + [\mathrm{H}]_0 + \frac{1}{K_a} \right) - \sqrt{\left([\mathrm{G}]_0 + [\mathrm{H}]_0 + \frac{1}{K_a} \right)^2 + 4[\mathrm{H}]_0[\mathrm{G}]_0} \right) \right\} \quad (15)$$

Equation (15) is the formula that was used to analyze the NMR titration experiments to find the association constants K_a via nonlinear regression with OriginPro 8.5.1.[113] The NMR titrations are described in the next section.

1.6 Nonlinear Regression

Older (linear regression) methods like Lineweaver-Burke, Benesi-Hildebrand, Hanse-Woolf or Scathard transformation were developed and used when computer power did not or hardly exist. Although still in use to some degree, fundamental difficulties are associated with the use of these methods: (1) with the data stemming from nonlinear processes, the experimental error is falsified through the violation of some of the fundamental suppositions behind linear regression. (2) These transformations use objectionable shortcuts such as $[\mathrm{G}]_0 \approx [\mathrm{G}]$ or assumptions that the final observed physical change in an experiment (Y_{final}) is identical with the change from the fully

formed complex Y_{HG}. With regard to the power modern computers have and the availability of numerous programs that can be employed for the task, using formula (15) is the method of choice, presuming no systematic and/or experimental error.[111, 112, 116]

In nonlinear regression, a nonlinear model f (here equation (15)) with parameters θ (K_a and $\delta_{\Delta HG}$) can be fitted to N data values y_n ($\Delta\delta$), measured with errors σ_n for every position x_n ($[G]_0$), through minimization of

$$\chi^2 = \sum_{n=1}^{N} \left(\frac{y_n - f(x_n; \theta)}{\sigma_n} \right)^2 \tag{16}$$

This process is called chi-square minimization. The estimation of parameters θ is carried out iteratively. The process aims at the minimization of the deviation between the measured and the calculated data. In principle, starting with some initial values, a value for χ^2 is computed for each iteration and the parameter values are adjusted accordingly to reduce χ^2. When the change in χ^2 is small enough (in OriginPro 8.5.1 and this work: $1*10^{-9}$) between two successive iterations, the fitting procedure has converged and estimations of best-fit values for parameters θ (K_a and $\delta_{\Delta HG}$) are established. Variation of initial parameter values is an easy way to rule out the presence of a local minimum.[114, 115, 117]

After a successful fitting process the resulting results need to be analyzed. OriginPro 8.5.1 not only delivers the desired estimated (i.e. fitted) values of the parameters but also a number of other statistical test values and calculations that allow to evaluate the quality of the fit and the reliability of the parameter estimates. In order to facilitate the discussion of the results in the later chapters, data analysis and the statistics of OriginPro 8.5.1 will be discussed in the following sections.

1.7 Data Analysis[111-118]

1.7.1 Goodness of Fit

Often, problems with the fit can be detected visually. Therefore, it is important to examine the graph of the fit superimposed on the data points. It has been called "inappropriate" to use the results of a nonlinear fit without the aforementioned superposition.[116] Additionally, a number of statistical tests and methods can be applied to quantify the goodness of fit.

A residual plot shows the difference between the measured and the calculated data as a function of guest concentration $[G]_0$. Ideally, the residuals account for experimental error only, that is, the data is appropriately represented by the formula. Thus, a trend in this plot would suggest a bad fit. In other words, the residual plot should show a random distribution of negative and positive residuals. When the used formula is inappropriate, clustering of the positive and negative residuals is observed, which is indicative of systematic differences between the data and the predicted values from the curve. Residual plots were easily obtained for this work because they were part of the OriginPro 8.5.1 output file.

The runs test (Wald-Wolfowitz Test) is a simple but robust way to determine whether the regression curve deviates systematically from the data. A run can be defined as a consecutive series of points where the residuals have the same sign. For randomly distributed data points on both sides of the regression curve, the expected number of runs can be calculated. If N is the total amount of data points with N_a points above the curve and N_b points below, the expected number of runs equals $[(2N_aN_b)/(N_a+N_b)]+1$. If fewer than expected runs are found, how can be ascertained if it is coincidence or if it is due to an inept regression model causing the curve to systematically deviate from the data? The answer to this question lies in the P value. In principle, P values measures the randomness of the distribution of the residuals. It quantifies the probability of obtaining the amount of runs observed under the condition that the data follows the selected model. In this work for each fitting process the number of runs is given and the

upper and lower limit of runs that statistically allow to assume the distribution of the residuals to be random.

The R^2 value is the coefficient of determination. It is used to account for the degree to which the variance of the "*dependent*" variable is explained by the "*independent*" variable. The sum of the square of the residuals and the sum of the squares of the regression are needed for its calculation. The former describes the error between the estimated and the actual data, the latter shows how far the estimated values differ from the overall mean:

$$R^2 = 1 - \frac{\Sigma(y - y_{fit})^2}{\Sigma(y - y_{mean})^2} \tag{17}$$

R^2 values range between 0 and 1. For example, an R^2 value of 0.997 means that 99.7% of the variation of the dependent variable is caused or explained by the variation of the independent one. The traditional R^2 value, however, has the drawback that its value is dependent on the number of parameters. The more parameters are contained in the formula, the higher the value of R^2, independently from the contribution of the parameters to the model. The *adjusted R^2* value, $\overline{R^2}$, corrects this bias by adjusting the number of parameters in relation to the number of data points. It is usually smaller than the regular R^2 value:

$$\overline{R}^2 = 1 - \frac{\Sigma(y - y_{fit})^2 \big/ (n - K)}{\Sigma(y - y_{mean})^2 \big/ (n - 1)} \tag{18}$$

with n being the number of data points and K the number of parameters fit by the regression; the expression $(n - K)$ gives the number of degrees of freedom of the sum-of-squares of the residuals from the regression line.

43

1.7.2 Chi-Square χ^2 and Reduced Chi-Square χ^2_{red}

Reduced chi-square χ^2_{red} is best described by first describing with chi-square χ^2. In linear regression χ^2 is a measure of how well the observed data is consistent with the theoretical (calculated) data as also defined in equation (16). χ^2 is expected to be of order n if the fit is good. A value that is much greater than n is indicative of a poor fit. However, χ^2 can only be used if the theoretical values and the standard deviation are known, which is not often the case, even more so in the nonlinear case (see next section).

The difference between the reduced chi-square χ^2_{red} and chi-square χ^2 is that while the latter is referenced to the standard deviation, the former is referenced to the degrees of freedom $(n - K)$:

$$\chi^2_{red} = \frac{\chi^2}{n-K} \tag{19}$$

In theory, χ^2_{red} has the expected value of 1, where a value much bigger than 1 indicates a wrong model and a value smaller than 1 overparametrization.

In OriginPro 8.5.1, χ^2 is defined differently. Whereas during the fitting process χ^2 is used as defined in equation (16), the value listed as χ^2_{red} in the fit statistics table of the software corresponds to what is usually denominated the mean square error (MSE). MSE is calculated from the residual sum of squares (the nominator term in equation (16)) and the degrees of freedom:

$$MSE = \frac{\sum(y-y_{fit})^2}{n-K} \tag{20}$$

In order to facilitate the discussion of results in this work, the nomenclature employed in OriginPro 8.5.1 is followed. It is therefore defined that for the remainder of this work

$$\chi^2_{red} = \frac{\sum(y-y_{fit})^2}{n-K} \tag{21}$$

Hence, regarding the determination of the goodness of fit, the closer the value of χ^2_{red} is to 0, the better the fit, signifying that the random error component of the model is small and that the fit is more useful for prediction purposes.

1.7.3 F- Value

The *F* value in the OriginPro 8.5.1 ANOVA table describes the ratio between the two mean square values, namely, the mean square of the regression and the mean square error. It indicates whether the applied model any explains the dependent variable in any way or whether the observed measurements are random. More exactly, the *F*-test aims at verifying the hypothesis that the variables in the model do not significantly differ from 0 (null hypothesis). Mathematically, it is very close to the $\bar{R}^2$ value explained above:

$$F = \frac{\sum(y-y_{fit})^2 \big/ (n-K)}{\sum(y-y_{mean})^2 \big/ (n-1)} \tag{22}$$

Although mathematically *F* and $\bar{R}^2$ are very similar, the interpretations of the respective values are different. While $\bar{R}^2$ measures how well the model explains the variance of the dependent variable, *F* shows whether the model explains the dependent variable at all. Yet, with the null hypothesis possessing less parameters than the model in question, the latter almost certainly fits the data better (lower sum-of-squares) than the former. Therefore, from the *F*-value a *P* value is calculated. It answers this question: what is the probability to obtain data where the ratio between the sum-of-squares is as large as or larger than in this experiment if the null hypothesis (i.e. the simpler model) is correct? It is important to note that *F* does not allow to decide if one of the models is correct. It only allows to decide whether or not to reject the simpler null hypothesis.

1.7.4 Estimation of uncertainties

After acquiring data the question always remains how accurate and reliable the results are. This task has two components, the experimental repeatability uncertainty and the fitting process (data analysis) uncertainty.

In order to obtain an estimation of uncertainty regarding the repeatability of the experimental data it was proposed to repeat the experiment and analyzing the data in (near-)identical manner six to eight times. This is not always feasible for economic reasons or time constraints; three experimental cycles are recommended.[118]

However, an unfortunate feature of nonlinear regressions is that no straightforward way exists to calculate or estimate the uncertainty in the fitting process. The majority of programs report the 95% confidence interval or an error estimate on the fitted data. Motulsky and Ransnas state: "In non-linear functions, errors are neither additive nor symmetrical, and exact confidence limits cannot be calculated. The reported standard error values are based on linearizing assumptions and will always underestimate the true uncertainty of any non-linear equation […]."[116] These asymptotic standard errors assume, among other things, that the physical property *Y* is the only source of experimental error. Because uncertainties in the concentrations can be notable the biggest experimental error resides in the $[G]_0/[H]_0$ ratio, which is the *x*-estimate. Also, the asymptotic standard error is calculated under the assumption that the ± errors are the same, i.e. that the confidence interval is symmetrical around the parameter, which is probably not true for most cases.[117] Despite these drawbacks asymptotic standard errors as reported in OriginPro 8.5.1 are still precise enough to qualitatively evaluate the results of the fit. Hence they will be used in this work to judge the estimates for the parameters θ (K_a and $\delta_{\Delta_{HG}}$). The fitted curves will be displayed with the 95% confidence bands in order to visualize the quality of the fitting procedure with regards to the original data. The uncertainty of $\Delta\delta$ (*y*-estimate) will be addressed by the specified measurement uncertainty of the instrument and will also be displayed in the corresponding graphs. Because asymptotic standard errors usually underestimate the uncertainty in non-linear procedures, large errors can indicate poor precision during measurements, wrong choice of model or may even hint at non-occurrence of the process under investigation, according to context.[117]

Appendix A: Abbreviations

1,2-DNB: 1,2-dinitrobenzene

1,3-DNB: 1,3-dinitrobenzene

1,4-DNB: 1,4-dinitrobenzene

2,6-DNT: 2,6-dinitrotoluene

2,4-DNT: 2,4-dinitrotoluene

NB: Nitrobenzene

NE: Nitroethane

NM: Nitromethane

4-NT: 4-nitrotoluene

5-NX: 5-nitro-*m*-xylene

PA: Picric acid

PET: photo-induced electron transfer

RDX: Hexahydro-1,3,5-trinitro-1,3,5-triazin

TNB: 2,4,6-trinitrobenzene

TNT: 2,4,6-trinitrotoluene

Appendix B: Symbols

[H] concentration of host

[G] concentration of guest

$[H]_0$ total concentration of host

$[G]_0$ total concentration of guest

[HG] concentration of host-guest complex

Y measured physical property (i.e. δ in NMR)

Y_H measured physical property of pure host

Y_G measured physical property of pure guest

Y_{HG} measured physical property of host- guest complex

f_H mole fraction of host

f_G mole fraction of guest

f_{HG} mole fraction of host-guest complex

ΔY $Y-Y_H$

$Y_{\Delta_{HG}}$ YH -YHG $\Delta\delta$ difference between NMR resonance of pure host and observed NMR resonance

$\delta_{\Delta_{HG}}$ difference in NMR resonances of the saturated host-guest complex and pure host
$\delta_{measured}$ measured NMR resonance of unsaturated host-guest complex

Bibliography

(1) Singh, K. A. nanOpinion May 2009,.

(2) Agrawal, J. P.; Hodgson, R. D. *Organic chemistry of explosives*; John Wiley & Sons Ltd: Chichester, England ; Hoboken, NJ, 2007.

(3) Salinas, Y.; Martínez-Máñez, R.; Marcos, M. D.; Sancenón, F.; Costero, A. M.; Parra, M.; Gil, S. *Chem. Soc. Rev.* **2012**, *41* (3), 1261.

(4) Ju, K.-S.; Parales, R. E. *Microbiology and Molecular Biology Reviews* **2010**, *74* (2), 250.

(5) *Explosive effects and applications*, 1. softcover printing, [Nachdr. d. Ausg.] New York, 1998.; Zukas, J. A., Ed.; High pressure shock compression of condensed matter; Springer: New York, 2003.

(6) Dalpozzo, R.; Bartoli, G. *Current Organic Chemistry* **2005**, *9* (2), 163.

(7) Schmidt, M.; Teitge, M.; Castillo, M. E.; Brandt, T.; Dobner, B.; Langner, A. *Archiv der Pharmazie* **2008**, *341* (10), 624.

(8) *The chemistry of anilines. Pt. 1: [...]*; Rappoport, Z., Ed.; Wiley: Chichester, 2007.

(9) Ware, G. W. *The pesticide book*, 4th Ed.; Thomson: Fresno, 1994.

(10) Winkler, R.; Hertweck, C. *ChemBioChem* **2007**, *8* (9), 973.

(11) White, P. A.; Claxton, L. D. *Mutation Research/Reviews in Mutation Research* **2004**, *567* (2-3), 227.

(12) Li, D.; Yang, M.; Li, Z.; Qi, R.; He, J.; Liu, H. *FEMS Microbiology Ecology* **2008**, *65* (3), 494.

(13) Spain, J. C. *Annual Review of Microbiology* **1995**, *49* (1), 523.

(14) Lotufo, G. R.; Blackburn, W.; Marlborough, S. J.; Fleeger, J. W. *Ecotoxicology and Environmental Safety* **2010**, *73* (7), 1720.

(15) Shanmugaraju, S.; Mukherjee, P. S. *Chemistry - A European Journal* **2015**, *21* (18), 6656.

(16) Balzani, V.; Credi, A.; Venturi, M. *Chemistry - A European Journal* **2002**, *8* (24), 5524.

(17) Ungaro, R.; Dalcanale, E. *Supramolecular Science: Where It Is and Where It Is Going*; Springer Netherlands : Imprint : Springer: Dordrecht, 1999.

(18) Balzani, V.; Credi, A.; Raymo, F. M.; Stoddart, J. F. *Angewandte Chemie* **2000**, *39* (19), 3348.

(19) Ball, P. *Nature* **2000**, *406*, 118.

(20) *Sci. Am.* **2001**, *285*.

(21) McCartney, S. *ENIAC, the triumphs and tragedies of the world's first computer*; Walker: New York, 1999.

(22) Iqbal, P.; Preece, J. A.; Mendes, P. M. In *Supramolecular Chemistry*; Gale, P. A., Steed, J. W., Eds.; John Wiley & Sons, Ltd: Chichester, UK, 2012.

(23) Merkel, T. J.; Herlihy, K. P.; Nunes, J.; Orgel, R. M.; Rolland, J. P.; DeSimone, J. M. *Langmuir* **2010**, *26* (16), 13086.

(24) Das, A.; Ghosh, S. *Angewandte Chemie International Edition* **2014**, *53* (8), 2038.

(25) Castellano, R. K.; Rebek, J. *Journal of the American Chemical Society* **1998**, *120* (15), 3657.

(26) Chen, Z.; Lohr, A.; Saha-Möller, C. R.; Würthner, F. *Chem. Soc. Rev.* **2009**, *38* (2), 564.

(27) De Greef, T. F. A.; Smulders, M. M. J.; Wolffs, M.; Schenning, A. P. H. J.; Sijbesma, R. P.; Meijer, E. W. *Chemical Reviews* **2009**, *109* (11), 5687.

(28) Cook, T. R.; Zheng, Y.-R.; Stang, P. J. *Chemical Reviews* **2013**, *113* (1), 734.

(29) Steed, J. W. *Chem. Commun.* **2011**, *47* (5), 1379.

(30) Ryu, J.-H.; Hong, D.-J.; Lee, M. *Chem. Commun.* **2008**, No. 9, 1043.

(31) Lehn, J.-M. *Angewandte Chemie International Edition in English* **1990**, *29* (11), 1304.

(32) Steed, J. W.; Atwood, J. L. *Supramolecular chemistry*; Wiley: Chichester, UK, 2009.

(33) Goodsell, D. S. *Our molecular nature the body's motors, machines, and messages*; Copernicus: New York, 1996.

(34) Davis, J. T. *Angewandte Chemie International Edition* **2004**, *43* (6), 668.

(35) Hunter, C. A.; Lawson, K. R.; Perkins, J.; Urch, C. J. *Journal of the Chemical Society, Perkin Transactions 2* **2001**, No. 5, 651.

(36) Mulliken, R. S. *Journal of the American Chemical Society* **1950**, *72* (1), 600.

(37) Klán, P.; Wirz, J. *Photochemistry of organic compounds: from concepts to practice*; Wiley: Chichester, West Sussex, U.K, 2009.

(38) Landauer, J.; McConnell, H. *Journal of the American Chemical Society* **1952**, *74* (5), 1221.

(39) Lawrey, D. M. G.; McConnell, H. *Journal of the American Chemical Society* **1952**, *74* (24), 6175.

(40) Foster, R. *Organic charge-transfer complexes*; Organic chemistry; a series of monographs; Academic Press: London, New York, 1969.

(41) Nielsen, M. B.; Lomholt, C.; Becher, J. *Chemical Society Reviews* **2000**, *29* (3), 153.

(42) Ma, X.; Tian, H. *Chem. Soc. Rev.* **2010**, *39* (1), 70.

(43) Van Dongen, S. F. M.; Cantekin, S.; Elemans, J. A. A. W.; Rowan, A. E.; Nolte, R. J. M. *Chem. Soc. Rev.* **2014**, *43* (1), 99.

(44) Hunter, C. A.; Sanders, J. K. M. *Journal of the American Chemical Society* **1990**, *112* (14), 5525.

(45) Martinez, C. R.; Iverson, B. L. *Chemical Science* **2012**, *3* (7), 2191.

(46) Hwang, J.; Dial, B. E.; Li, P.; Kozik, M. E.; Smith, M. D.; Shimizu, K. D. *Chem. Sci.* **2015**, *6* (7), 4358.

(47) Sinnokrot, M. O.; Sherrill, C. D. *The Journal of Physical Chemistry A* **2004**, *108* (46), 10200.

(48) Jaffe, R. L.; Smith, G. D. *The Journal of Chemical Physics* **1996**, *105* (7), 2780.

(49) Hunter, C. A. *Angewandte Chemie International Edition* **2004**, *43* (40), 5310.

(50) Wagner, C.; Fournier, N.; Ruiz, V. G.; Li, C.; Müllen, K.; Rohlfing, M.; Tkatchenko, A.; Temirov, R.; Tautz, F. S. *Nature Communications* **2014**, *5*, 5568.

(51) Cozzi, F.; Cinquini, M.; Annunziata, R.; Dwyer, T.; Siegel, J. S. *Journal of the American Chemical Society* **1992**, *114* (14), 5729.

(52) Cozzi, F.; Cinquini, M.; Annuziata, R.; Siegel, J. S. *Journal of the American Chemical Society* **1993**, *115* (12), 5330.

(53) Cozzi, F.; Ponzini, F.; Annunziata, R.; Cinquini, M.; Siegel, J. S. *Angewandte Chemie International Edition in English* **1995**, *34* (9), 1019.

(54) Paliwal, S.; Geib, S.; Wilcox, C. S. *Journal of the American Chemical Society* **1994**, *116* (10), 4497.

(55) Kim, E.; Paliwal, S.; Wilcox, C. S. *Journal of the American Chemical Society* **1998**, *120* (43), 11192.

(56) Adams, H.; Carver, F. J.; Hunter, C. A.; Morales, J. C.; Seward, E. M. *Angewandte Chemie International Edition in English* **1996**, *35* (1314), 1542.

(57) Carver, F. J.; Hunter, C. A.; Carver, F. J.; Seward, E. M. *Chemical Communications* **1998**, No. 7, 775.

(58) Germain, M. E.; Knapp, M. J. *Chemical Society Reviews* **2009**, *38* (9), 2543.

(59) Yinon, J. *Analytical Chemistry* **2003**, *75* (5), 98 A.

(60) Håkansson, K.; Coorey, R. V.; Zubarev, R. A.; Talrose, V. L.; Håkansson, P. *Journal of Mass Spectrometry* **2000**, *35* (3), 337.

(61) Walsh, M. *Talanta* **2001**, *54* (3), 427.

(62) Sylvia, J. M.; Janni, J. A.; Klein, J. D.; Spencer, K. M. *Analytical Chemistry* **2000**, *72* (23), 5834.

(63) Mathurin, J. C.; Faye, T.; Brunot, A.; Tabet, J. C.; Wells, G.; Fuché, C. *Analytical Chemistry* **2000**, *72* (20), 5055.

(64) Hallowell, S. *Talanta* **2001**, *54* (3), 447.

(65) Vourvopoulos, G. *Talanta* **2001**, *54* (3), 459.

(66) Krausa, M.; Schorb, K. *Journal of Electroanalytical Chemistry* **1999**, *461* (1-2), 10.

(67) Wallis, E.; Griffin, T. M.; Popkie, Jr., N.; Eagan, M. A.; McAtee, R. F.; Vrazel, D.; McKinly, J. Gardner, P. J., Ed.; 2005; pp 54–64.

(68) Salinas, Y.; Martínez-Máñez, R.; Marcos, M. D.; Sancenón, F.; Costero, A. M.; Parra, M.; Gil, S. *Chem. Soc. Rev.* **2012**, *41* (3), 1261.

(69) Moore, D. S. *Review of Scientific Instruments* **2004**, *75* (8), 2499.

(70) Zhou, Q.; Swager, T. M. *Journal of the American Chemical Society* **1995**, *117* (26), 7017.

(71) Yang, J.-S.; Swager, T. M. *Journal of the American Chemical Society* **1998**, *120* (21), 5321.

(72) Yang, J.-S.; Swager, T. M. *Journal of the American Chemical Society* **1998**, *120* (46), 11864.

(73) Yamaguchi, S.; Swager, T. M. *Journal of the American Chemical Society* **2001**, *123* (48), 12087.

(74) Chen, S.; Zhang, Q.; Zhang, J.; Gu, J.; Zhang, L. *Sensors and Actuators B: Chemical* **2010**, *149* (1), 155.

(75) Long, Y.; Chen, H.; Yang, Y.; Wang, H.; Yang, Y.; Li, N.; Li, K.; Pei, J.; Liu, F. *Macromolecules* **2009**, *42* (17), 6501.

(76) Narayanan, A.; Varnavski, O. P.; Swager, T. M.; Goodson, T. *Journal of Physical Chemistry C* **2008**, *112* (4), 881.

(77) Chen, L.; McBranch, D.; Wang, R.; Whitten, D. *Chemical Physics Letters* **2000**, *330* (1-2), 27.

(78) Rose, A.; Zhu, Z.; Madigan, C. F.; Swager, T. M.; Bulović, V. *Nature* **2005**, *434* (7035), 876.

(79) Focsaneanu, K.-S.; Scaiano, J. C. *Photochemical & Photobiological Sciences* **2005**, *4* (10), 817.

(80) Lee, Y. H.; Liu, H.; Lee, J. Y.; Kim, S. H.; Kim, S. K.; Sessler, J. L.; Kim, Y.; Kim, J. S. *Chemistry - A European Journal* **2010**, *16* (20), 5895.

(81) Jian, C.; Seitz, W. R. *Analytica Chimica Acta* **1990**, *237*, 265.

(82) Vijayakumar, C.; Tobin, G.; Schmitt, W.; Kim, M.-J.; Takeuchi, M. *Chemical Communications* **2010**, *46* (6), 874.

(83) Zyryanov, G. V.; Palacios, M. A.; Anzenbacher, P. *Organic Letters* **2008**, *10* (17), 3681.

(84) Cavaye, H.; Shaw, P. E.; Wang, X.; Burn, P. L.; Lo, S.-C.; Meredith, P. *Macromolecules* **2010**, *43* (24), 10253.

(85) Zhang, C.; Che, Y.; Yang, X.; Bunes, B. R.; Zang, L. *Chemical Communications* **2010**, *46* (30), 5560.

(86) Wang, L.; Zhou, Y.; Yan, J.; Wang, J.; Pei, J.; Cao, Y. *Langmuir* **2009**, *25* (3), 1306.

(87) Rahman, M.; Harmon, H. J. *Spectrochimica Acta Part A: Molecular and Biomolecular Spectroscopy* **2006**, *65* (3-4), 901.

(88) Hikal, W. M.; Harmon, H. J. *Journal of Hazardous Materials* **2008**, *154* (1-3), 826.

(89) Li, Z.; Dong, Y. Q.; Lam, J. W. Y.; Sun, J.; Qin, A.; Häußler, M.; Dong, Y. P.; Sung, H. H. Y.; Williams, I. D.; Kwok, H. S.; Tang, B. Z. *Advanced Functional Materials* **2009**, *19* (6), 905.

(90) Caron, T.; Guillemot, M.; Montméat, P.; Veignal, F.; Perraut, F.; Prené, P.; Serein-Spirau, F. *Talanta* **2010**, *81* (1-2), 543.

(91) Cartmill, L.; Sereda, G. A. *J. Undergrad. Chem. Res.* **2007**, *6* (2), 63.

(92) Chen, C. W.; Whitlock, H. W. *Journal of the American Chemical Society* **1978**, *100* (15), 4921.

(93) Harmata, M. *Accounts of Chemical Research* **2004**, *37* (11), 862.

(94) Zimmerman, S. C. In *Bioorganic Chemistry Frontiers*; Dugas, H., Ed.; Springer Berlin Heidelberg: Berlin, Heidelberg, 1991; Vol. 2, pp 33–71.

(95) Hardouin–Lerouge, M.; Hudhomme, P.; Sallé, M. *Chem. Soc. Rev.* **2011**, *40* (1), 30.

(96) Breslow, R. *Israel Journal of Chemistry* **1979**, *18* (3-4), 187.

(97) Otsuki, J.; Chiang, L. C.; Lee, S. H.; Araki, K.; Seno, M. *Supramolecular Chemistry* **1993**, *2* (1), 25.

(98) Legouin, B.; Uriac, P.; Tomasi, S.; Toupet, L.; Bondon, A.; van de Weghe, P. *Organic Letters* **2009**, *11* (3), 745.

(99) D'Souz, L. J.; Maitra, U. *The Journal of Organic Chemistry* **1996**, *61* (26), 9494.

(100) Kim, S. K.; Lim, J. M.; Pradhan, T.; Jung, H. S.; Lynch, V. M.; Kim, J. S.; Kim, D.; Sessler, J. L. *Journal of the American Chemical Society* **2014**, *136* (1), 495.

(101) Klärner, F.-G.; Lobert, M.; Naatz, U.; Bandmann, H.; Boese, R. *Chemistry - A European Journal* **2003**, *9* (20), 5036.

(102) Klärner, F.-G.; Kahlert, B. *Accounts of Chemical Research* **2003**, *36* (12), 919.

(103) Klärner, F.-G.; Panitzky, J.; Bläser, D.; Boese, R. *Tetrahedron* **2001**, *57* (17), 3673.

(104) Klärner, F.-G.; Kahlert, B.; Boese, R.; Bläser, D.; Juris, A.; Marchioni, F. *Chemistry - A European Journal* **2005**, *11* (11), 3363.

(105) Marchioni, F.; Juris, A.; Lobert, M.; Seelbach, U. P.; Kahlert, B.; Klärner, F.-G. *New Journal of Chemistry* **2005**, *29* (6), 780.

(106) Fukuhara, G.; Madenci, S.; Polkowska, J.; Bastkowski, F.; Klärner, F.-G.; Origane, Y.; Kaneda, M.; Mori, T.; Wada, T.; Inoue, Y. *Chemistry - A European Journal* **2007**, *13* (9), 2473.

(107) Rowan, A. E.; Elemans, J. A. A. W.; Nolte, R. J. M. *Accounts of Chemical Research* **1999**, *32* (12), 995.

(108) She, N.; Gao, M.; Cao, L.; Wu, A.; Isaacs, L. *Organic Letters* **2009**, *11* (12), 2603.

(109) Leblond, J.; Petitjean, A. *ChemPhysChem* **2011**, *12* (6), 1043.

(110) Hunter, C. A. *Angewandte Chemie International Edition* **2004**, *43* (40), 5310.

(111) Thordarson, P. *Chem. Soc. Rev.* **2011**, *40* (3), 1305.

(112) Thordarson, P. In *Supramolecular Chemistry*; Gale, P. A., Steed, J. W., Eds.; John Wiley & Sons, Ltd: Chichester, UK, 2012.

(113) OriginLab (2011), *OriginPro 8.5.1*, Northampton, MA.

(114) *Numerical recipes: the art of scientific computing*, 3rd ed.; Press, W. H., Ed.; Cambridge University Press: Cambridge, UK ; New York, 2007.

(115) http://www.originlab.com/doc/Origin-Help/NLFit-Algorithm.

(116) Ransnas, L. A., Motulsky, H. J. **1987**, *FASEB J.* (1 (5)), 365.

(117) Christopoulos, A., Motulsky, H. J. In *Fitting Models to Biological Data using Linear and Nonlinear Regression*; GraphPad Software Inc.: San Diego, CA, 2003.

(118) Hibbert, D. B.; Gooding, J. J. *Data analysis for chemistry: an introductory guide for students and laboratory scientists*; Oxford University Press: Oxford ; New York, 2006.

2. Molecular Sensors for the Detection of Nitroaromatic Compounds

2.1 Concept and Molecular Design

Nitroaromatic compounds are electron-deficient due to the electron-withdrawing $-NO_2$ substituents. Accordingly, they may form donor-acceptor (D-A) pi-stacking complexes with more electron-rich receptor molecules (picture 1).[1, 2] In these complexes electron-density transfer from the electron-rich donor to the electron-deficient nitroaromatic acceptor should occur.[3] The impact of the change in electron-density was followed by observing ^{1}H-NMR shifts and the association constants of the receptors with the electron-deficient guests were determined.
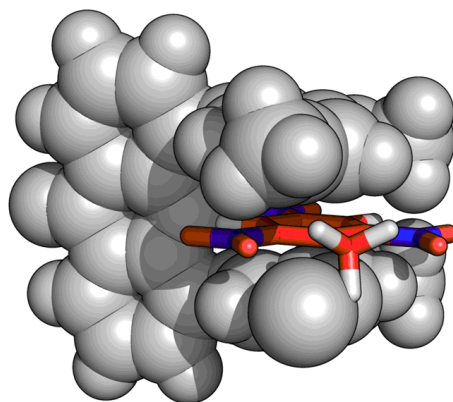
Picture 1. *Model of complex between TNT and sensor* **1c***.*

Essentially, the sensor molecules in this work are designed to act like tweezers. They consist of two main building blocks (picture 2). The first building block (in blue in picture 2) serves as rigid backbone. The second building block (orange in picture 2) can be thought of as clips or pincers which hold the nitroaromatic analyte. Together with the rigid backbone, these rods form the tweezers.

Concerning the rigid backbone, in picture 2 anthracene is shown but there are other possibilities, as will be seen later. The main requirement is rigidity because this part of the molecule defines the distance between both clips. The gap (i.e. the distance between the pincers and their position) has to be well-defined, because the strength of π-π interactions depends on both the distance between the participating species and their relative orientation.[4] In addition to being rigid, the backbone also has to be

modifiable. Chromophores such as xanthone, anthracene or anthraquinone may fulfill both criteria.[5, 6, 7]
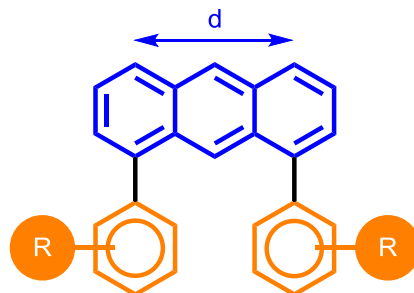
Picture 2. *Molecular design of the sensor molecules. The rigid backbone (in blue, here: anthracene) defines the size of the gap while the aromatic pincers (in orange) constitute the pincers of the molecular tweezers which should interact with the nitroaromatic guests.*

The second building block consists of aryl substituents. They are used as the clips of tweezers in the target compounds but also to tune electronic properties of the target compounds (picture 2). The size of the chromophore backbone and/or the position in which the clips are attached define the cavity size. The substituents of aromatic clips are responsible for the electron density of the clips, which should help the formation of D-A stacks with the electron-deficient nitroaromatic molecules as shown in picture 1.[8]

Because several chromophores with different chemical and electronic properties were used, the exact synthetic strategies are presented in the corresponding sections.

2.2 Synthesis of Xanthone- Based Sensors

2.2.1 Synthetic Strategy

The first chromophore backbone used is xanthone (picture 3), which is a dye and thus the binding event might be observed spectroscopically. It was chosen due to its rigid

structure and because it offers higher stability towards oxidation than anthracene which can be oxidized in the 9,10-positions to the corresponding anthraquinone.[9]

1a: R = OMe, R' = H
1b: R = R' = OMe
1c: R = R' = H
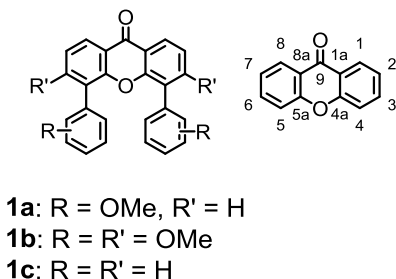
Picture 3. *Left: General structure of the targeted sensor. Right: structure and numbering of xanthone.*

The synthetic strategy is shown in scheme 1.

In pathway A the intention is to functionalize the commercially available xanthone **2** such that it serves as an independent building block where different aryl-clips can be introduced. A literature-known lithiation-iodination reaction at the 4- and 5-position of the xanthone is planned to introduce the iodine substituents, resulting in 4,5-diiodoxanthone **5**.[10] For the last step in the assembly of target compounds **1a** and **1c**, the insertion of the aryl-clips, a Suzuki-coupling is envisaged, turning molecule **5** into the desired target compounds **1a** and **1c**. A wide range of boronic acids and their esters are commercially available, and their general functional group tolerant reaction conditions make Suzuki couplings the ideal candidate for the introduction of the aryl-clips.[11]

58
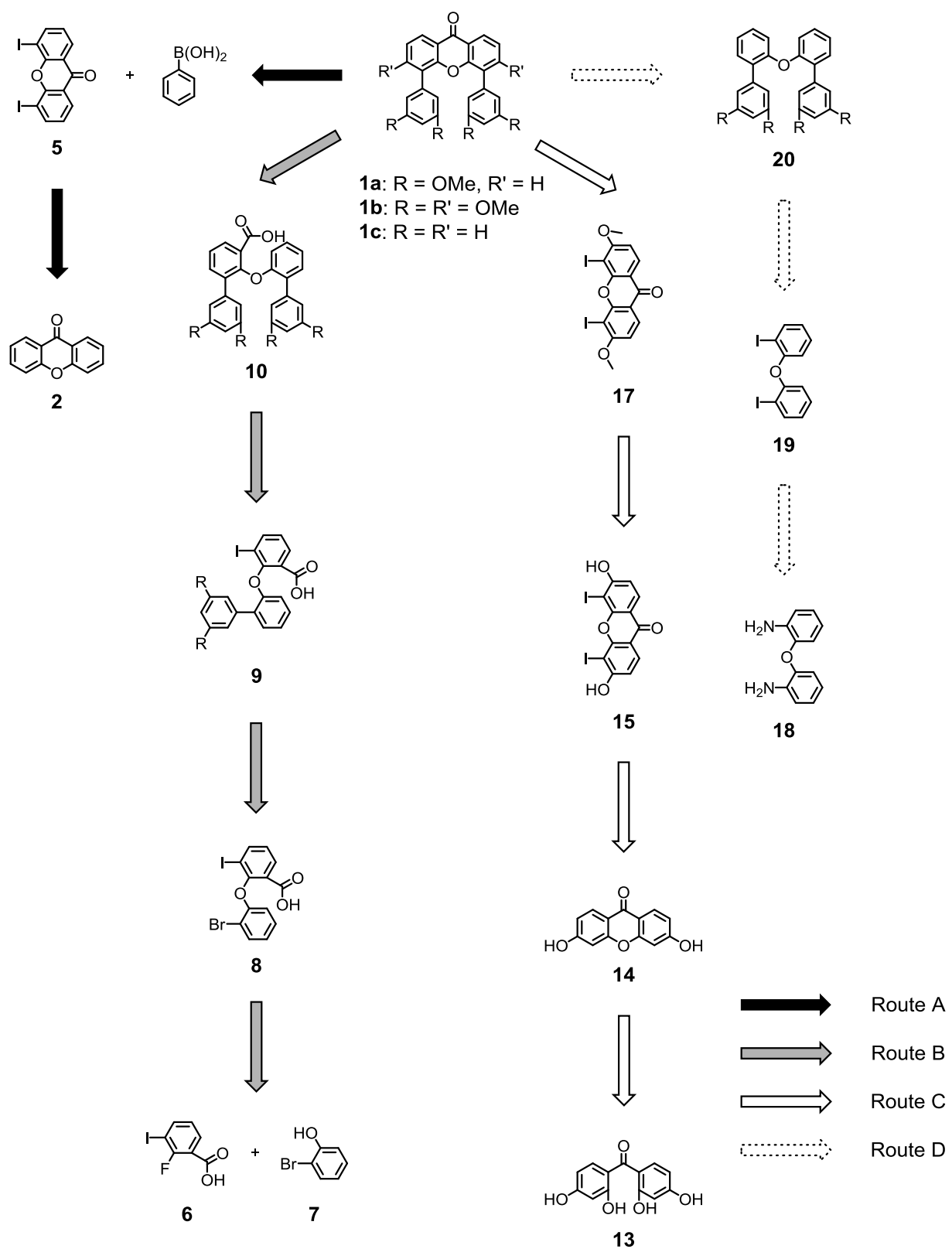
**Scheme 1**. *Retrosynthetic analysis of xanthone-based sensor 1.*

Pathway B: building block **8** is planned to be assembled in a nucleophilic aromatic substitution from benzoic acid **6** and phenol **7**. Protection of benzoic acid **6** by means of the corresponding methyl ester up to structure **10** must be considered. Because the bromine and iodine substituent in acid **8** show different reactivity in coupling reactions, molecule **8** should allow for the stepwise introduction of the phenyl moieties to molecule **10** via iodo-substituted species **9** in two consecutive Suzuki-couplings. The target molecules **1a** and **1c** are then thought to be finalized by establishing the xanthone-backbone in an intramolecular Friedel-Crafts acylation. Because intermediate **8** contains both a bromide and an iodide moiety, pathway B potentially offers the possibility to modularly synthesize target structures with two differently substituted phenyl-pincers.

In Route C the xanthone core is adressed first: dihydroxyxanthone **14** is intended to be synthesized in an intramolecular condensation reaction from benzophenone **13**.[12] Additionally, in building-up the backbone in one step the hydroxyl groups in xanthone **14** also allow further potential functionalization of the sensor molecule. A literature-known iodination protocol is intended to iodinate the xanthone-core in the 4- and 5-positions, leading to xanthone **15**.[13] Methylation with dimethyl sulfate under alkaline conditions is envisaged to furnish the electron rich xanthone **17**. The target compound is then envisaged to be assembled by the introduction of phenyl-substituents in the 4- and 5-positions in a twofold Suzuki-coupling.

Route D is similar to route B. In both cases the chromophore backbone is finished in the last step, after the introduction of the aryl clips. Therefore 2,2'-oxydianiline **18** is set to undergo a Sandmeyer reaction to yield 2,2'-oxybis(iodobenzene) **19**. For the subsequent introduction of the clips a double Suzuki-coupling is planned, resulting in molecule **20**. A Pd-catalyzed C-H activation carbonylation reaction under CO-atmosphere is planned to furnish the target molecules **1a** and **1c** by closing the xanthone backbone.[14]

2.2.2 Synthesis

Following route A, the initial goal was to synthesize xanthone **5**. Following a literature-known procedure the carbonylic C=O double bond of the xanthone needed to be protected first to minimize side-reactions.[10] The iodination procedure involved ^{t}BuLi which, due to the presence of highly nucleophilic species, could cause several side-reactions, such as the attack at the carbonylic C-9 atom of xanthone **2**. In the literature cited the carbonyl group of xanthone **2** was protected as its corresponding dimethyl ketal **4** in a two-step procedure. However, the procedure turned out to be unreliable for two reasons. (1) Dichloroxanthene **3** degraded within minutes when exposed to air, turning from light yellow to red. (2) The yield of step b) in scheme 2 decreased in the presence small traces of SOCl$_2$ left in the remaining crude of molecule **3**. Even under reduced pressure SOCl$_2$ was difficult to remove.
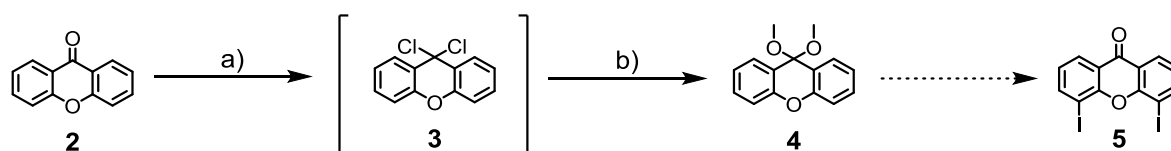

a) DMF, SOCl$_2$, reflux, 4h b) NaOMe, THF, 0°C to rt, 2h, 20-90% (2 steps)

Scheme 2. *Initial route towards 4,5-diiodoxanthone* **5**.

In the search of a more reliable way of ketal formation of xanthone **2** several protocols of were attempted initially but proved to be unsuccessful (scheme 3 below).
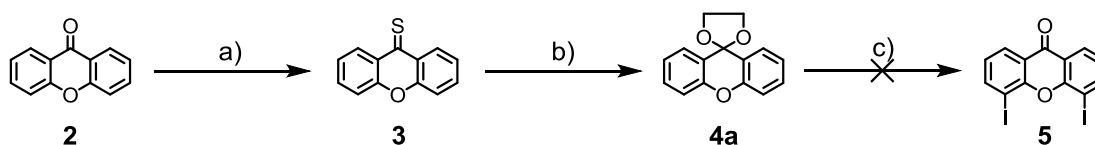
a) Lawesson's Reagent, Toluene, reflux, 1 h, 75% b) Ethylene glycol, AgOCOCF$_3$, MeCN, NEt$_3$, rt, 15 min, 65% c) ^{t}BuLi, ^{t}BuOK, I$_2$, THF, -78°C

Lawesson's Reagent:
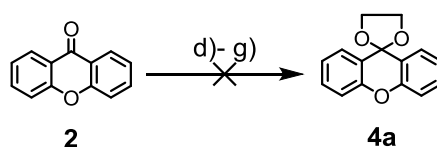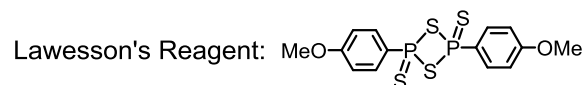
d) ethylene glycol, *p*-TsOH, toluene, reflux, overnight e) ethylene glycol, H$_2$SO$_4$, 160°C, overnight
f) ethylene glycol, SO$_3$H-SiO$_2$, MeCN, rt, 24h g) ethylene glycol, SO$_3$H-SiO$_2$, MeCN, reflux, 24h

Scheme 3. *Above: protection of xanthone* **2** *and attempted iodination towards 4,5-diiodoxanthone* **5**.
Below: preliminary attempts of formation of ketal **4**.

Finally a literature known procedure was applied.[15] Lawesson's reagent can be used for the thionation of carbonyl compounds. In solution it forms a dithiophosphine ylide and the mechanism of the reaction with carbonyl compounds is similar to the Wittig reaction.[16] Thioxanthone **3** was obtained in 75% yield by refluxing xanthone **2** in toluene with a stoichiometric amount of Lawesson's reagent for 1h and purifying compound **3** by column chromatography. The strong affinity of divalent sulfur for silver(I) ions was used in the subsequent reaction to turn thioxanthone **3** into the corresponding ketal **4a**.[15] The end of the reaction between xanthone **3** and silver(I)triflate (AgOCOCF$_3$) in the presence of propargyl alcohol was signaled by the end of Ag$_2$S formation upon the addition of NEt$_3$ (65% yield). Purification was carried out through flash chromatography. The following intended iodination as described by Cordopatis and coworkers to obtain 4,5-diiodoxanthone **5** was not successful.[10] They reported that a 1:1 mixture of ^{t}BuLi/^{t}BuOK and subsequent quenching with I$_2$ yielded xanthone **5**. This could not be reproduced in spite of several attempts.

Route B is based on the formation of the biaryl ether moiety of the final xantone which is then supposed to be functionalized with the tweezers moieties before the condensation to the xanthone is accomplished.

2-fluoro-3-iodobenzoic acid **6** was obtained in 45% yield after treating 1-fluoro-2-iodobenzene with LDA at -78°C for 2h in THF and quenching the reaction mixture with solid CO_2.[17] The product was purified by repeated precipitation from H_2O and then dried under reduced pressure. It seems noteworthy that the yield of the reaction could be improved significantly by switching from commercial sources to freshly prepared LDA.
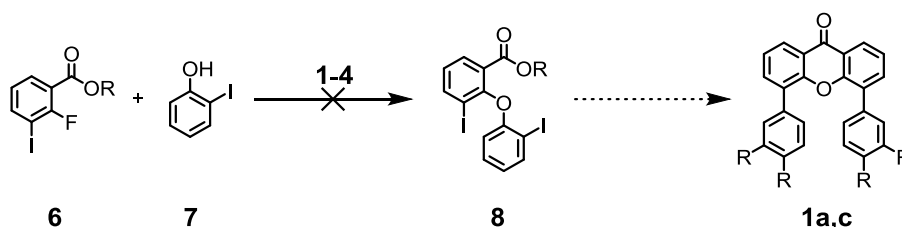
Entry	-R	Base	[eq. Base]	Solvent	T [°C]
1	-H	K_2CO_3	2	THF	70
2	-H	NaH	2	THF	70
3	-H	K_2CO_3	2	Toluene	110
4	-H	NaH	2	Toluene	110

Scheme 4. *Conditions applied towards diaryl ether* **8**.

In an attempted nucleophilic aromatic substitution heating a solution of benzoic acid **6** and 2-iodophenol **7** with 2 eq. of K_2CO_3 in THF resulted in no observable reaction (scheme 4). Stirring only the phenol **7** with K_2CO_3 in THF before adding the benzoic acid did not result in any product formation either. The same held true when replacing K_2CO_3 with NaH and changing the solvent from THF to toluene. To prevent slow reaction due to repulsion or coulombic effects in the benzene ring through deprotonation of the acid moiety in the benzoic acid **6** it was protected in form of its ester **6a** (scheme 5).
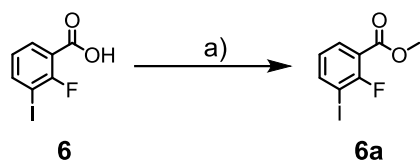
a) SOCl$_2$, MeOH, reflux, 3h, quant.

Scheme 5. *Esterification of 2-fluoro-3-iodobenzoic acid.*

Nucleophilic aromatic substitution of ester **6a** did not result in any conversion to the desired product (scheme 6). This might be for steric reasons because of the iodine in the 2-position of phenol **7**.
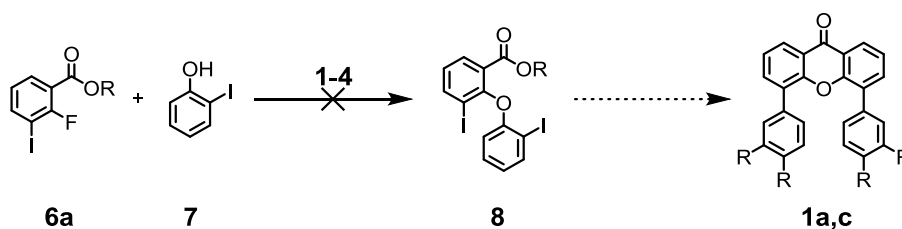
Entry	-R	Base	[eq. Base]	Solvent	T [°C]
1	-Me	K$_2$CO$_3$	2	THF	70
2	-Me	NaH	1.1	THF	70
3	-Me	K$_2$CO$_3$	2	Toluene	110
4	-Me	NaH	1.1	Toluene	110

Scheme 6. *Conditions applied towards diaryl ether **8**.*
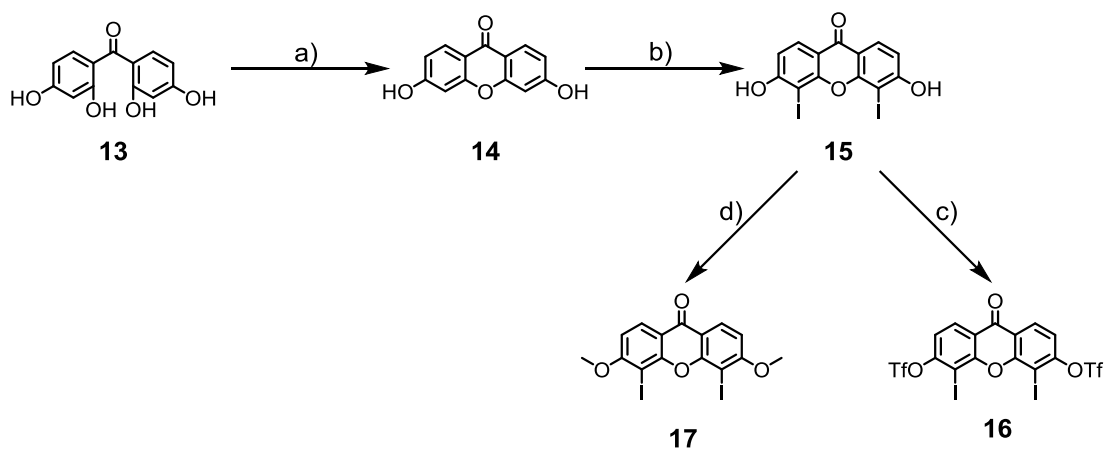
a) 220°C, 24h, 85% b) HIO$_3$, I$_2$, EtOH, reflux, 63% c) *N*-phenylbis(trifluoromethanesulfonimide), Ethyldiisopropylamine, CH$_2$Cl$_2$, rt, 6h, 73% d) Dimethyl sulfate, K$_2$CO$_3$, acetone, reflux, overnight, 90%

Scheme 7. *Synthesis of xanthones* **17** *and* **16**.

Route C relies on the assembly and functionalization of the xanthone, followed by the tweezers-formation through the introduction of the phenylic moieties as described before. 3,3'-dihydroxy-4,4'-diiodo-9H-xanthone **15** was synthesized in a two-step procedure (scheme 7). The first step was an intramolecular condensation reaction. 2,2',4,4'-tetrahydroxybenzophenone **13** was suspended in H$_2$O and heated to 180°C in a pressure tube for 2 days. This resulted in the formation of 3,3'-dihydroxyxanthone **14** with about 90% yield.[18] For larger batches, at least up to a 10 g scale, the reaction was carried out by heating benzophenone **13** in a furnace at 220°C overnight with comparable yields.[12] In both procedures xanthone **14** was purified by suspending the crude H$_2$O at 60°C. Benzophenone **13** and potential side products were soluble in H$_2$O at that temperature, whereas xanthone **14** was not. Xanthone **14** was then iodinated with I$_2$ and HIO$_3$ in ethanol at 80°C to give 3,3'-dihydroxy-4,4'-diiodoxanthone.[15] The two hydroxyl substituents in the 3- and 6-position of xanthone **15** were first transformed into triflates resulting in xanthone **16** with the aim of defunctionalization to obtain 4,5-diiodoxanthon **5**. A substitution reaction of molecule **15** with trifluoromethanesulfonic anhydride and pyridine was unsuccessful. Then again, the S$_N$2 reaction of 3,3'-dihydroxy-4,4'-diiodoxanthone with N-Phenylbis(trifluoromethanesulphonimide and diisopropylethylamine furnished xanthone **16** in 73%.[19]

65

However, methoxy groups are generally electron donors in aromatic systems; therefore it was decided to turn the hydroxyl groups in xanthone **15** into the corresponding methoxy moieties; the advantage would be that the chromophore is even more electron rich which should increase the desired charge-transfer complex formation ratio with nitroaromatic molecules.[19, 20] The substitution reaction of dihydroxyxanthone **15** with dimethyl sulphate and K_2CO_3 in boiling acetone overnight afforded 3,3'-dimethoxy-4,4'diiodoxanthone **17** in 90% yield. Another benefit of the methoxy groups is the increased solubility of the xanthone-system.

The next step was to introduce the clips into xanthone **17**. Considering its structure and substitution pattern several potential hurdles stand out, similar to those described by Whiting *et al.* in the synthesis of hindered 5,6-diarylacenaphthenes.[21] The two methoxy substituents in the 3- and 6-positions, ortho to the iodine moieties, are donating electrons into the chromophore, thereby deactivating the system towards oxidative addition with Pd-catalysts in Suzuki cross-couplings. The methoxy moieties ortho to the reactive center (the iodines in the 4- and 5-positions) can add electrostatic repulsion towards potential reaction partners. Also, the van der Waals radius of each of the iodine atoms in xanthone **17** is between 2.1 Å and 2.2 Å which is only slightly smaller than half the (calculated) distance between the 2- and the 2'-carbon atoms of the chromophore (cf picture 4).[22]
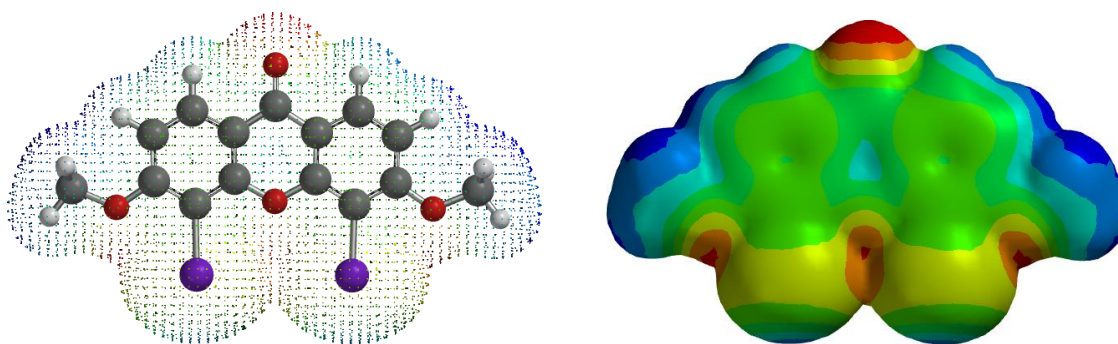
Picture 4. *Right: calculated electrostatic potential of the van der Waals surface of diiodoxanthone* **17** *(MM2/B3LYP/6-31G*). Left: overlay of the molecule and the semi-transparent map (MM2/B3LYP/6-31G*).*

The deactivating factor of the methoxy moieties can be addressed by the choice of catalyst.[23] The most common catalyst is $Pd(PPh_3)_4$, but a variety of different palladium/phosphine complexes can be used and prepared. The reactivity of a catalyst depends on the stoichiometry of phosphine to palladium as well as the bulkiness and the donating ability of its phosphine ligands. More bulky ligands make more reactive catalysts because formation of coordinatively unsaturated species is facilitated. The reactivity of catalysts is also enhanced if the ligands display stronger electron donation towards the active palladium(0) metal center.[24]

In order to introduce the benzene moieties in a Suzuki coupling several catalysts were tested in order to find a starting point for further optimization. THF has been used as solvent throughout because xanthone **17** showed by far the best solubility in this solvent, exceeding solubilities in DMF, DMSO, Toluene, CH_2Cl_2 and Dioxane. THF was used in 10:1 mixture with H_2O because the latter facilitates the formation of the active borates.
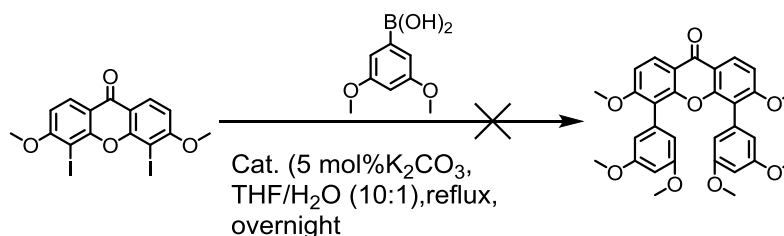
Catalysts: $Pd(PPh_3)_4$, $Pd(dppf)Cl_2$, $Pd_2(dba)_3$, $Pd_2(dba)/ P(^tBu)_3$, $Pd(P(OH)_2^tBu_2)Cl_2$

Scheme 8. *Catalyst screening in the Suzuki-coupling towards sensor* **1b**.

In all cases the reactions were carried out in flame-dried glassware in degassed solvents under Ar atmosphere. Even under prolonged reaction times up to 24 h no reaction was observed in any of the conditions employed. This seemed conceivable in the case of $Pd(PPh_3)_4$. Even though xanthone **17** is substituted with electron donating methoxy moieties, the iodines as leaving groups were hypothesized to compensate in reactivity, even more under the light that the PPh_3 ligand is rather bulky. $Pd(dppf)Cl_2$ has a large P-M-P angle and was initially designed for sp^3- coupling reactions.[25] Due to its rather big

67

bite angle the dppf ligand is also known to be useful in slow Suzuki reactions.[26] Pd$_2$(dba)$_3$ was used as a control experiment, because of the advantages of ligandless catalysts. They eliminate side-reactions involving phosphine (phosphonium salt formation, phosphine-bound aryls) and have a potentially high catalytic efficiency and therefore reaction times are shorter.[27,28] On the other hand, the Pd$_2$(dba)$_3$/P(^{t}Bu)$_3$ system contains bulky and electron-rich P(^{t}Bu)$_3$ ligands. It has shown efficiency in the coupling of chloroarenes and slowly reacting electron-rich arenes.[23] Usually in Suzuki-couplings with chlorides the oxidative addition is the rate determining step.[29] If the oxidative addition has occurred and the reaction is very slow, at least partial dehalogenation should be observed, which was not the case. This leads to the conclusion that the catalysts did not undergo oxidative addition. The one notable exception was Pd(P(OH)$_2$^{t}Bu$_2$)Cl$_2$ (POPd) where partial dehalogenation was observed in GC-MS. POPd is a palladium- phosphinous acid complex which upon deprotonation with a base (in this case K$_2$CO$_3$) becomes a very electron-rich anionic compound; this should facilitate the oxidative addition to the aryl-halide, xanthone **17** in this case .[30] Although the catalyst seems to undergo oxidative addition to the xanthone **17**, the reaction did not proceed from there. Dehalogenation mostly occurs when alcohols are used as solvents, which was not the case here.[31, 32] The question remains why the reaction was so slow that even after the oxidative addition of the catalyst it did not continue. The methoxy moieties attached to the chromophore are electron-donating, as is the ether bridge between the two phenyl rings of the chromophore.[33] On the other hand, the carbonyl group of the xanthone is rather activating, and literature suggest that similarly electron-rich aryl iodides can react in Suzuki cross-couplings.[34] In view of the structure of xanthone **17** and the distance between the two targeted iodines including their van der Waals radius steric reasons are the most probable explanation for the low reactivity of molecule **17**.
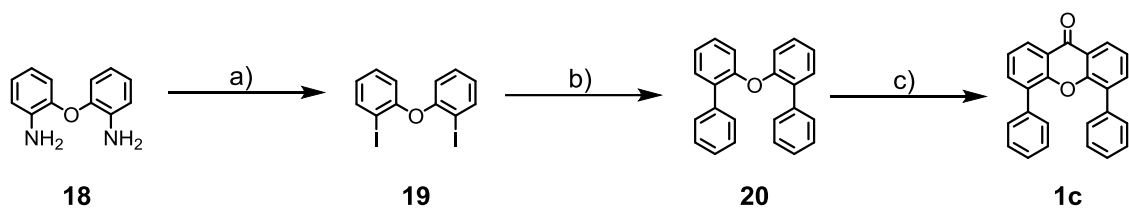
a) NaNO$_2$, KI, pTsOH, MeCN, H$_2$O, 0°C to 90°C, 3h, 55% b) PhBPin, K$_2$CO$_3$, Pd(PPh$_3$)$_4$, Methanol/H$_2$O (3:1),89°C, overnight, 67% c) CO (1 atm), K$_2$S$_2$O$_8$, Pd(OAc)$_2$, TFA, 50°C, 3h, 41%

Scheme 9. *Synthesis of sensor* **1c***.*

As introducing the phenyl moieties towards the end of the reaction sequence was unsuccessful the strategy in route D was to assemble the direct precursor **20** to product **1** first and conduct carbonylation to the xanthone core only in the last step (schemes 1 and 9). 2,2'-oxybis(iodobenzene) **19** was synthesized from 2,2'-oxydianiline **18** in a Sandmeyer-reaction in 55% yield by adding an aqueous solution of 5.0 eq KI and 4 eq NaNO$_2$ at 0°C to a suspension of dianiline **18** and pTsOH in MeCN and stirring the resulting solution at 90°C for 3h. The introduction of the phenyl moieties was carried out in a Suzuki-reaction. The aromatic framework of diiodide **19** has a mildly increased electron-density because of the oxy-bridge between the two rings but in return has two iodide moieties as reactive centers which should facilitate the reaction. In contrast to diiodoxanthone **16** diiodide **19** is not rigid but can rotate around the oxy-bridge; therefore the steric constraints encountered in the coupling of xanthone **19** should not be encountered in this case. Because preliminary results indicated poor results with boronic acid, it was replaced with its easily accessible pinacol ester counterparts (scheme 10).
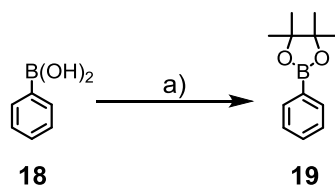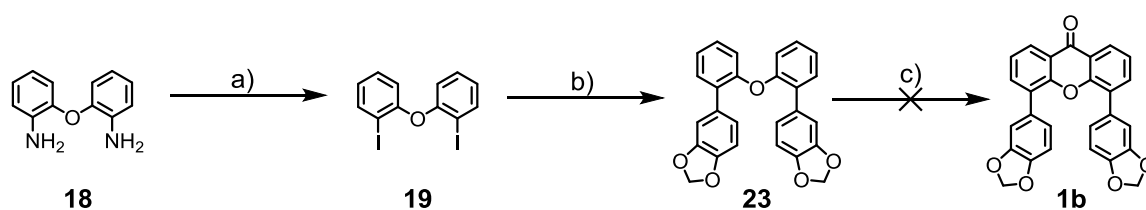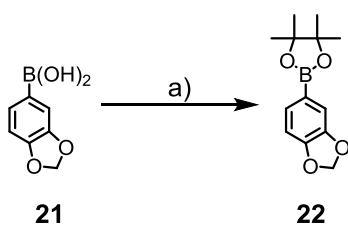

a) Pinacol, acetone, rt, overnight, quant.

Scheme 10. *Transformation of phenylboronic acid* **18** *to phenylboronic acid pinacol ester* **19***.*

The coupling was carried out under the conditions given in scheme 9 and resulted 2,2'-oxydi-1,1'-biphenyl **20** in a yield of 67%. Finally the xanthone core was approached in a double C-H activation/carbonylation reaction in trifluoroacetic acid (TFA) under a CO atmosphere after a literature known procedure.[14] The mechanism is still somewhat unclear and the reaction conditions were optimized for the synthesis of xanthones. Therefore the conditions were chosen as described in the literature (cf. scheme 9). This yielded target compound **1c** as a white solid in 41% yield, after purification with column chromatography. Interestingly, when dry TFA was used the reaction yield decreased to around 10%.

Synthesis of xanthone **1b** started the same way as in the case for **1a** (scheme 11).

a) NaNO$_2$, KI, pTsOH, MeCN, H$_2$O, 0°C to 90°C, 3h, 55% b) **22**, K$_2$CO$_3$, Pd(PPh$_3$)$_4$, Methanol/H$_2$O (3:1),90°C, overnight, 50% c) CO (1 atm), K$_2$S$_2$O$_8$, Pd(OAc)$_2$, TFA, 50°C, 3h, 41%

a) Pinacol, Acetone, rt, overnight, quant.

Scheme 11. *Synthesis towards sensor* **1c**.

The introduction of the methoxylated tweezers moieties proceeded as before in a Suzuki coupling between diiodide **19** and the corresponding pinacolate boron ester. However, the oxidative carbonylation was unsuccessful and only a mixture of products was obtained. Proton NMR spectra revealed that a mixture of aldehydes was formed. In the synthesis of **1a** both steps of the oxidative carbonylation are directed to take place in *ortho*-position to the ether bridge between the two biphenylic systems. Both these systems can be considered to act as electron-abundant substituents to each other via

the ether linkage. The substitution pattern of the attached aryl clips consists of two methoxy-substituents on each phenyl ring. This total of four Lewis basic moieties can be expected to have a stronger directing effect than a shared mutual phenoxy-substituent on a neighbored ring, accounting for the observed formation of a mixture of aldehydes.

2.2.3 Titration Experiments

All titrations until chap. 2.6 were carried out in $CDCl_3$ at 1mM sensor **1c** concentration. Further details of the titration experiments are described in the experimental part of this work.

Picture 5 shows sensor **1c** and the numbering used in the discussion.
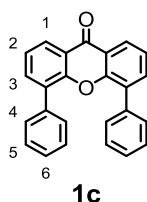
Picture 5. *Structure and numbering of sensor* **1c**

The sensor was titrated with 1,3-dinitrobenzene (DNB) and benzonitrile. 1,3-dinitrobenzene was used as a model compound. Like TNT it is electron-deficient and toxic, but it is much less explosive. Benzonitrile was used to examine the response of the sensor towards other electron-deficient species. Association constants were determined for various protons in molecule **1c**. Picture 6 shows the ^{1}H-NMR spectrum of **1c** with proton assignments according to picture 5.
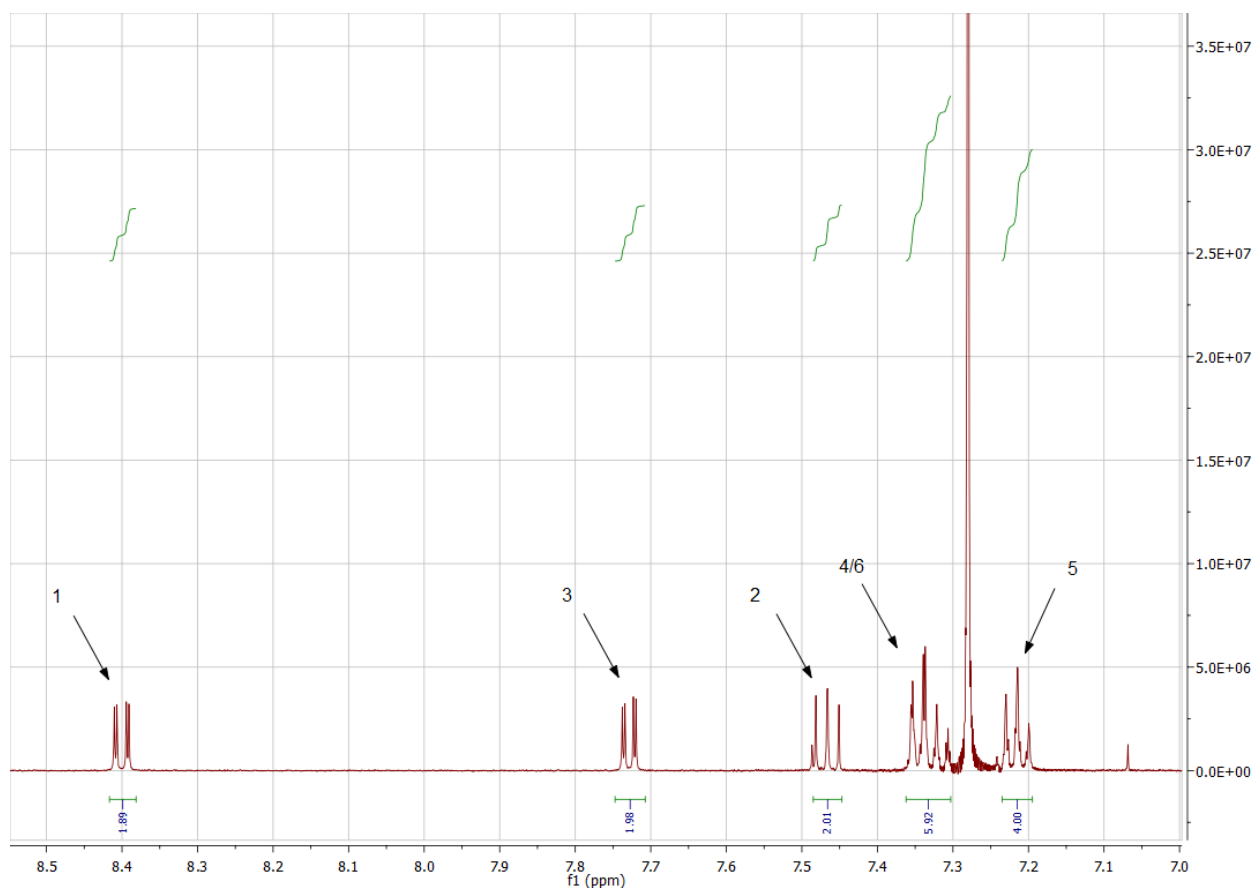
Picture 6. *¹H-NMR spectrum of sensor* **1c** *with proton assignments.*

Table 1 gives an overview of the measured association constants according to the assigned protons and the goodness of fit tests described in the introduction of this work.

Proton	K_a [M⁻¹]	Observed runs	Upper and lower limit of runs	$\overline{R}^2$	χ^2_{red}
1	22.8±0.43	11	13, 4	0.997	$4.03*10^{-8}$
2	23.9±1.26	8	13, 4	0.997	$2.27*10^{-9}$
3	22.8±1.3	11	13, 4	0.997	$1.84*10^{-9}$
4+6	20.7±1.2	8	13, 4	0.997	$2.22*10^{-9}$
5	17.4±2.36	8	13, 4	0.986	$6.11*10^{-9}$

Table 1. *Summary of the fitting procedures of sensor* **1c** *with DNB.*

As discussed in the introduction, determination of goodness of fit and the estimation of uncertainties are not trivial tasks. The inset of picture 7 shows the fitted curve of the ^{1}H-NMR shifts of proton 2 in the titration with DNB. No substantial clustering of positive or negative points is observed, indicating no systematic differences between the data and the predicted curve. The corresponding runs test shows no statistically significant deviation, because 9 runs are observed and the upper and lower limit of runs are 4 and 13 according to critical values table. With $\overline{R}^2$ = 0.997, the largest part of the variance of the measured proton shifts seems to be explained by the variation of [DNB] in the titration solution. As far as the random error of the fit is concerned, χ^2_{red} = 2.27*10[-9] indicates good prediction properties.
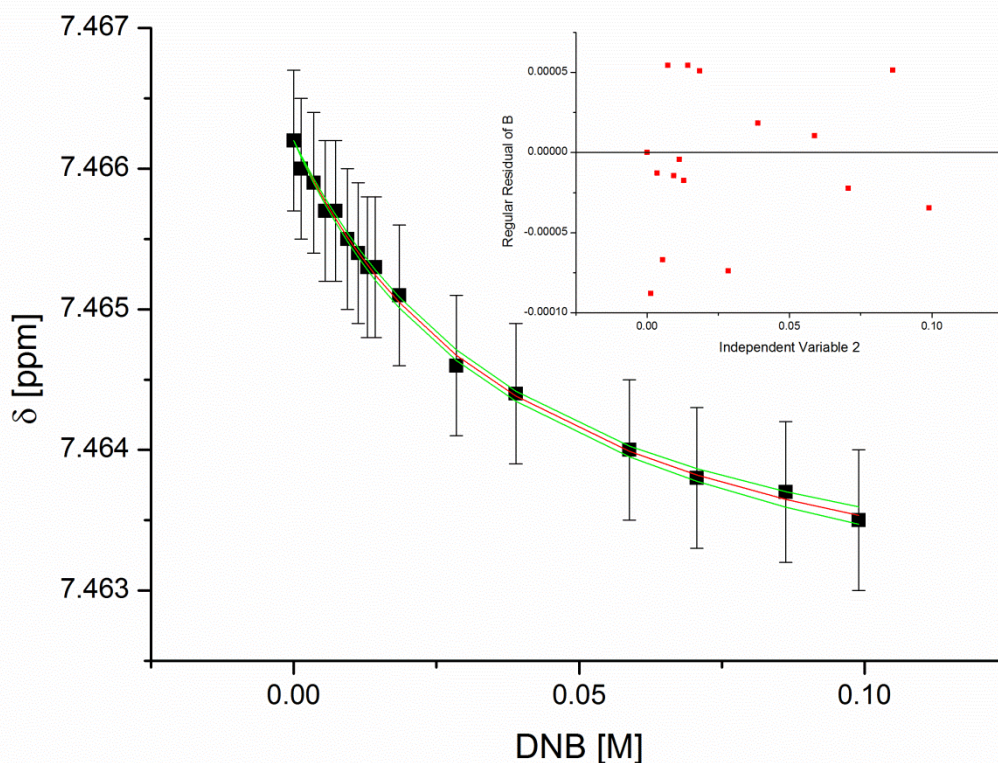
Picture 7. *Fitted curve (red) and corresponding 95% confidence intervals (green) of proton 2 in the titration with DNB. The error bars in the y-direction correspond to the measurement uncertainty of the spectrometer. The inset shows the residual plot of the fitted curve from which the runs test was performed.*

For all the protons, the association constant is in the range of 17-24 M^{-1}, roughly. Because protons 4 and 6 could not be differentiated in the spectrum due to overlap its

value has to be regarded and treated as mean value. The F values are not given in the tables in this work because their value given in the output is 0 for all the regressions shown. Considering the sum of these values for each fit it is safe to say that the fits are good.

The uncertainties given for the estimated K_a values in table 1 are possibly not entirely correct, as explained in the introduction. Usually when operating under linearizing assumptions, as is the case in OriginPro 8.5.1, the values of the uncertainties are underestimated. Furthermore, it is very likely that the real uncertainties are not symmetric because the parameters used in equation (15) are not independent from each other.[35, 36] Additionally, the biggest source of error may lie in the x-axis and not in the y-axis. Hence the significance of error bars in any dimension would be very restricted and would not allow any inference because the errors are not additive in nonlinear regression. Instead, confidence intervals at 95% level for the fit are given in the fitting graphs. They are also approximate. This should be ignorable because no further formal calculations are made with these values. They are precise enough to decide whether the parameters are determined with reasonable precision.[36] For sensor **1c**, even if all the uncertainties would be twice as big as indicated in table 1, the overall effect on the estimated K_a values would be limited and the values would not appear as uncertain or imprecise. The confidence intervals depicted in picture 7 confirm these findings. The difference between the fitted data and the upper and the lower limits for every point is comparable to the range of measurement uncertainty of the ^{1}H NMR spectrometer. The confidence interval shown above gets wider towards higher DNB concentrations. But this is to be expected because at higher values errors gain more weight.[37] The K_a values in table 1 can therefore be considered solid.

When DNB was replaced with benzonitrile in the titrations, no measurable effect could be found. Earlier experiments looked promising but could not be reproduced after elimination of potential error sources. The proton shifts that may have been induced by benzonitrile were lower than the measurement error of the spectrometer for every proton in sensor **1c**, even when 100+ equivalents were employed. The respective fits were much more a measure of the randomness of instrumental measurement errors than

anything else and the fitting program did not converge, i.e. no calculation of K_a was obtained.

Interpreting the values from the titrations with DNB it is safe to say that sensing occurs to a certain degree. It cannot be said in which mode DNB stacks with xanthone **1c**. The results imply that no real preference exists between stacking to the backbone or the clips. Averaging all the measured association constants in sensor **1c** suggest a $K_a = 21.5 \pm 1.31$ M^{-1}. The fact that benzonitrile did not discernibly trigger any sensor response might be due to its lower electron-deficiency compared to DNB or a less favourable difference in HOMO-LUMO gap between benzonitrile and **1c**. It is also possible to say that sensor **1c** is able to differentiate between DNB and benzonitrile.

With regards to the general design of the envisioned TNT sensor molecules (picture 2) it is appropriate to replace the xanthone core with a different chromophore. Although structurally similar, anthracene might not only offer a different gap size between the aryl clips but potentially also different π-stacking and complexation features. The comparison between sensors with different chromophore backbones could therefore offer further insight into the binding behavior of nitroaromatics in molecular tweezers.

2.3 Synthesis of Anthracene-Based Sensors

2.3.1 Synthetic Strategy

A retrosynthesis of anthracene-based sensors is given in scheme 12.

1d: R = H
1e: R = -OCH$_2$O-

Route A

Route B
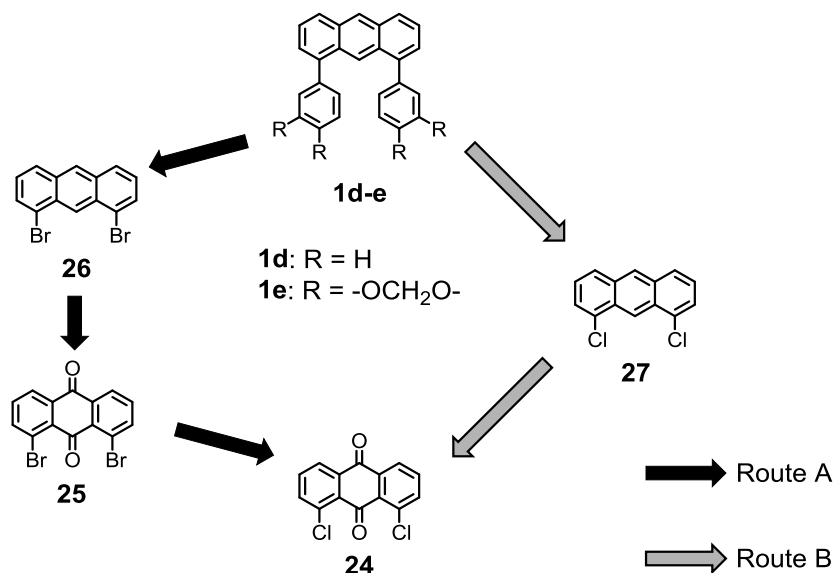
Scheme 12. *Retrosynthetic analysis of sensors* **1d** *and* **1e**.

A wide range of substituted anthracenes and potential precursors are commercially available. The main synthetic advantage anthracene holds over xanthone in this case is that its basic structure is already present in precursors. Therofore to both retrosynthetic routes presented the same starting compound is attributed, 1,8-dichloroanthraquinone **24**. In both routes the general proceeding is to reduce anthraquinone **24** into an anthracene and then couple the latter in a Suzuki reaction to the final molecule(s). Because Suzuki reactions generally work better/faster on bromines than on chlorines, the difference between the two suggested routes is that Route A aims at conducting this last step with bromine and Route B with chlorine. Route A starts by exchanging the chlorine moieties of anthraquinone **24** with bromines in a halogen exchange reaction. This can potentially be achieved either by reacting **24** with a strong base such as ^{t}BuLi and quenching the intermediate with Br$_2$ or in a Cu-promoted substitution reaction. The main drawback of the first method is that in this case the nucleophilic species would probably also cause a multitude of byproducts, not only rendering purification tedious but

mainly reducing the yield of intended 1,8-dibromoanthraquinone **25**. Therefore a Cu-promoted substitution with excess KBr is envisaged.[38] For the following reduction of anthraquinone **25** to the corresponding anthracene **26** it is considered to reduce molecule **25** with $NaBH_4$ followed by HCl as described by Harvey *et al.*[39] As discussed above, the last step, the introduction of the clips, is intended to be performed in a double Suzuki reaction. Route B is resolved to be started with the reduction of 1,8-dichloroanthraquinone **24** in aqueous ammonia and excess zinc powder to yield in 1,8-dichloroanthracene **27**.[40] For the second (and last) step of Route B a double Suzuki reaction is envisaged, analogous to route A.

2.3.2 Synthesis

The first step following route A was the Cu-promoted bromination of 1,8-dichloroanthraquinone **24** in presence of H_3PO_4 and KBr in nitrobenzene at reflux temperature. No full conversion was observed and the reaction stopped at about 60% after 36h. And although the product **25** can be isolated and purified through crystallization from $MeOH/CHCl_3$ (1:1), considerable loss of product has to be accepted in this case.[39] There is still the possibility to ignore this second drawback and continue with the crude material because 1,8-dibromoanthracene **26** should react considerably faster in Pd-catalyzed cross coupling reactions than 1,8-dichloroanthracene **27**.

The reduction of 1,8-dichloroanthraquinone **24** to 1,8-dichloroanthracene **27** was accomplished by slowly adding Zn-powder into a solution of anthraquinone **24** in 28% NH_3 (aq.) and H_2O at 0°C (scheme 13). After the addition the red slurry was allowed to reach room temperature before being heated to 80°C for 4h. The direct heating from 0°C to 80°C diminished the yield of the reaction. The product was isolated by extraction with CH_2Cl_2 and purified through recrystallization from 12 M HCl/*i*-PrOH (1:11), yielding 1,8-dichloroanthracene **27** in 55%.[40] The subsequent introduction of the aryl clips to form the target compounds was tackled from two directions. Pd-catalyzed Suzuki cross-couplings offer general tolerance of a variety of functional groups and mild reaction conditions. On the other hand a Kumada-coupling with phenyl magnesium bromide, $[Ni(acac)_2]_3$ and triphenylphosphine has been used for the synthesis of similar compounds.[40] The

advantage of Suzuki reactions in this case could include more benign reaction conditions due to the absence of the highly reactive Grignard reagents and for the same reasons better functional group tolerance in the synthesis of potential future molecules. Pd(amphos)Cl$_2$ is known to perform well as a catalyst in cross-couplings involving aryl chlorides.[41]
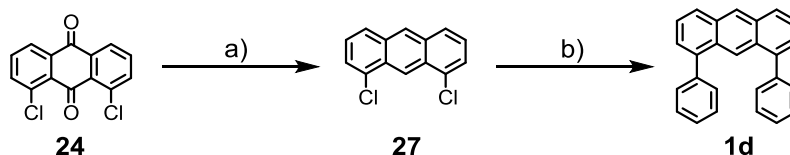
a) 28% NH$_3$ (aq.), Zn, H$_2$O, 0°C to 80°C, 4 h, 55% b) Phenylboronic acid, Pd(amphos)Cl$_2$, K$_2$CO$_3$, Toluene/H$_2$O (10:1), 2 h, 63%

Scheme 13. *Synthesis of sensor* **1d**.

It was therefore tried first for the Suzuki coupling between 1,8-dichloroanthracene **27** and phenylboronic acid, also in light of the eventual coupling of more electron rich arylboronic acids later on. The combination of the aforementioned catalyst with K$_2$CO$_3$ as base in Toluene/H$_2$O was used in our group before for the Suzuki coupling of chlorides.[42] In the case of anthracene **27** and phenylboronic acid, these conditions delivered diphenylanthracene **1d** in 63% yield after heating the reaction mixture for 2 hours. The purification of diphenylanthracene **1d** was challenging insofar as after subjecting the crude to flash chromatography multiple runs by GPC were necessary to purify the compound. The synthesis of anthracene **1e** was identical to molecule **1d** (scheme 14).
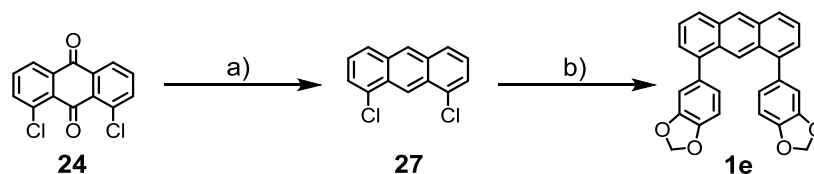
a) 28% NH$_3$ (aq.), Zn, H$_2$O, 0°C to 80°C, 4 h, 55% b) Phenylboronic acid, Pd(amphos)Cl$_2$, K$_2$CO$_3$, Toluene/H$_2$O (10:1), overnight, 40%

Scheme 14. *Synthesis of sensor* **1e**.

78

2.3.3 Titrations Experiments
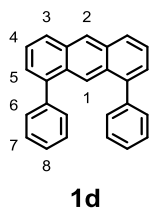
**Picture 8**. *Structure and numbering of sensor* **1d**.
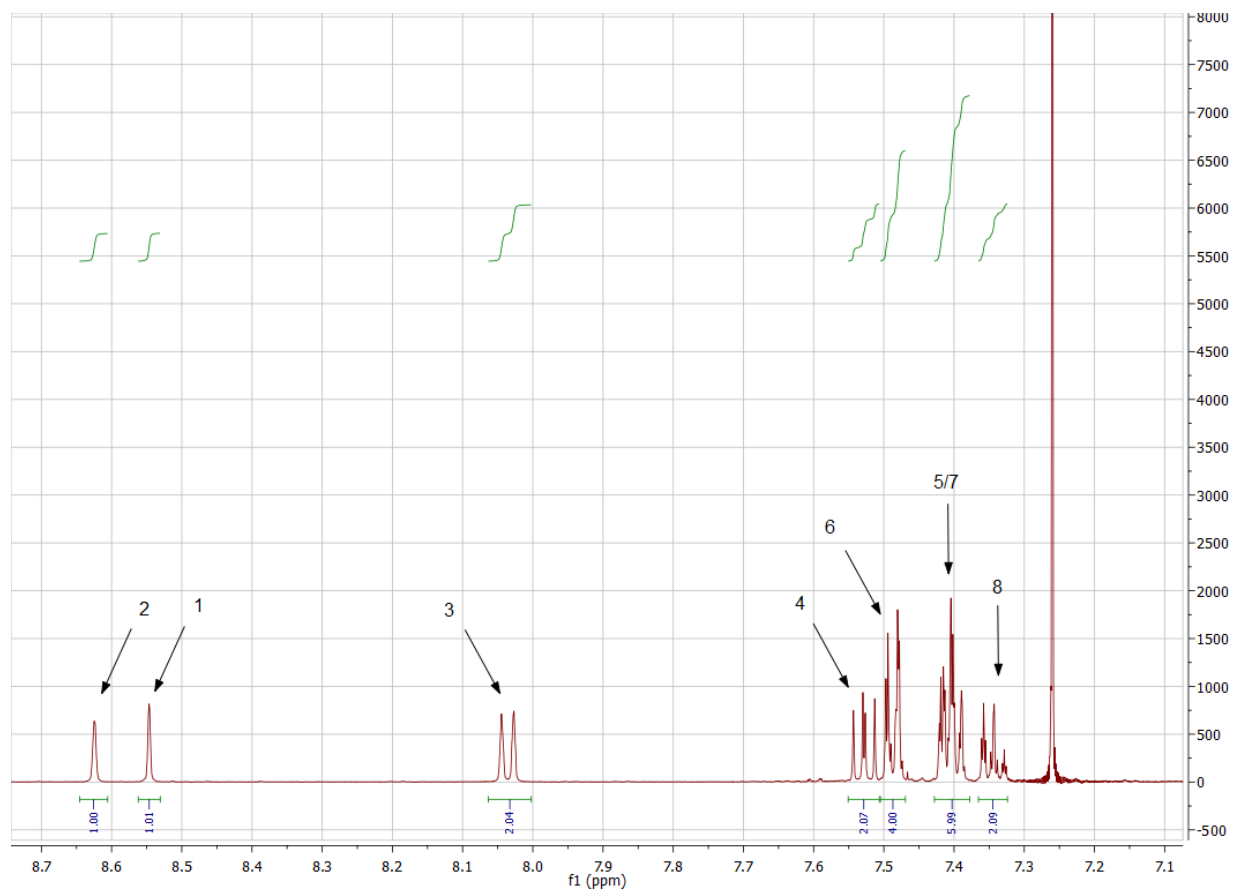
Picture 9. *^{1}H-NMR spectrum of sensor* **1d** *with proton assignments.*

Table 2 gives the results of the titration of molecule **1d** with DNB.

Proton	K_a [M^{-1}]	Observed runs	Upper and lower limit of runs	$\overline{R}^2$	χ^2_{red}
1	0.44±0.10	7	4, 13	0.998	6.00*10^{-6}
3	0.39±0.13	6	3, 12	0.997	3.44*10^{-6}
4	0.31±0.09	10	4, 13	0.997	9.40*10^{-7}
6	0.48±0.07	9	4, 13	0.999	4.22*10^{-7}
8	0.15±0.07	9	4, 13	0.998	2.42*10^{-7}

Table 2. *Summary of the fitting procedures of sensor* **1d** *with DNB.*

Following the argumentation for sensor **1c**, it is safe to say that the fits are reasonably good for all the given protons. Values for protons 5 and 7 are omitted because their peaks in the ^{1}H-NMR spectrum overlap at low concentrations and separate at higher concentrations, making it impossible to reliably assign their shifts. The uncertainties of the constants are rather large, pointing at less well determined constants which is confirmed by looking at the confidence intervals. The effect of DNB towards the sensor is small with an averaged association constant K_a = 0.35±0.09 M^{-1}, therefore it is not surprising that the inherent measurement variances become a large source of error.[37]
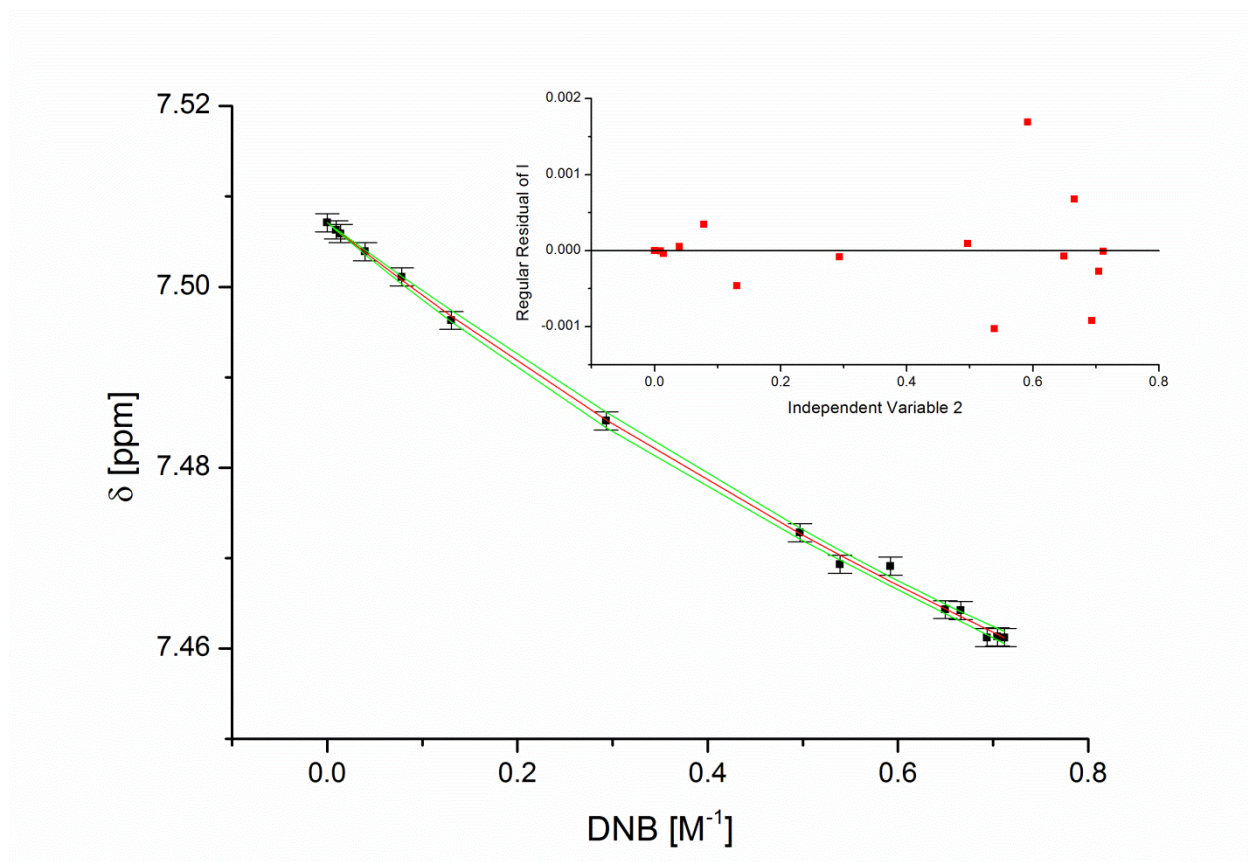
Picture 10. *Fitted curve (red) and corresponding 95% confidence intervals (green) of proton 6 in the titration with DNB. The error bars in the y-direction correspond to the measurement uncertainty of the spectrometer. The inset shows the residual plot of the fitted curve from which the runs test was performed.*

It must be pointed out though that although uncertainties are rather large, the values as they are presented in table 2 still give a good idea of the magnitude of the effect. Even though all constants are within the same order of magnitude, the constants with the least small values were found for protons 1 and 6. Of course this does not prove that π-stack sandwich formation between DNB and the aryl rods is favored, but it confirms they are influenced by the presence of DNB.Titrations with sensor **1e** could shed some light on the complexation behavior of DNB towards a comparable sensor with more electron-abundant aryl clips.

Again, titrations with benzonitrile did not yield results. The changes in proton shifts for all protons were treated smaller than the uncertainty of the measurements of the NMR

spectrometer. The only conclusion that can be drawn is that benzonitrile did not stack with the sensor, as was the case for sensor **1c**.

Pictures 11 and 12 show the numbering of molecule **1e** and the ^{1}H-NMR spectrum of sensor **1e**; table 3 shows the summarized findings of titration of sensor **1e** with DNB.
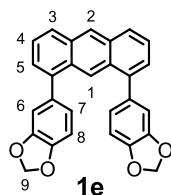
Picture 11. *Structure and numbering of sensor* **1e**.
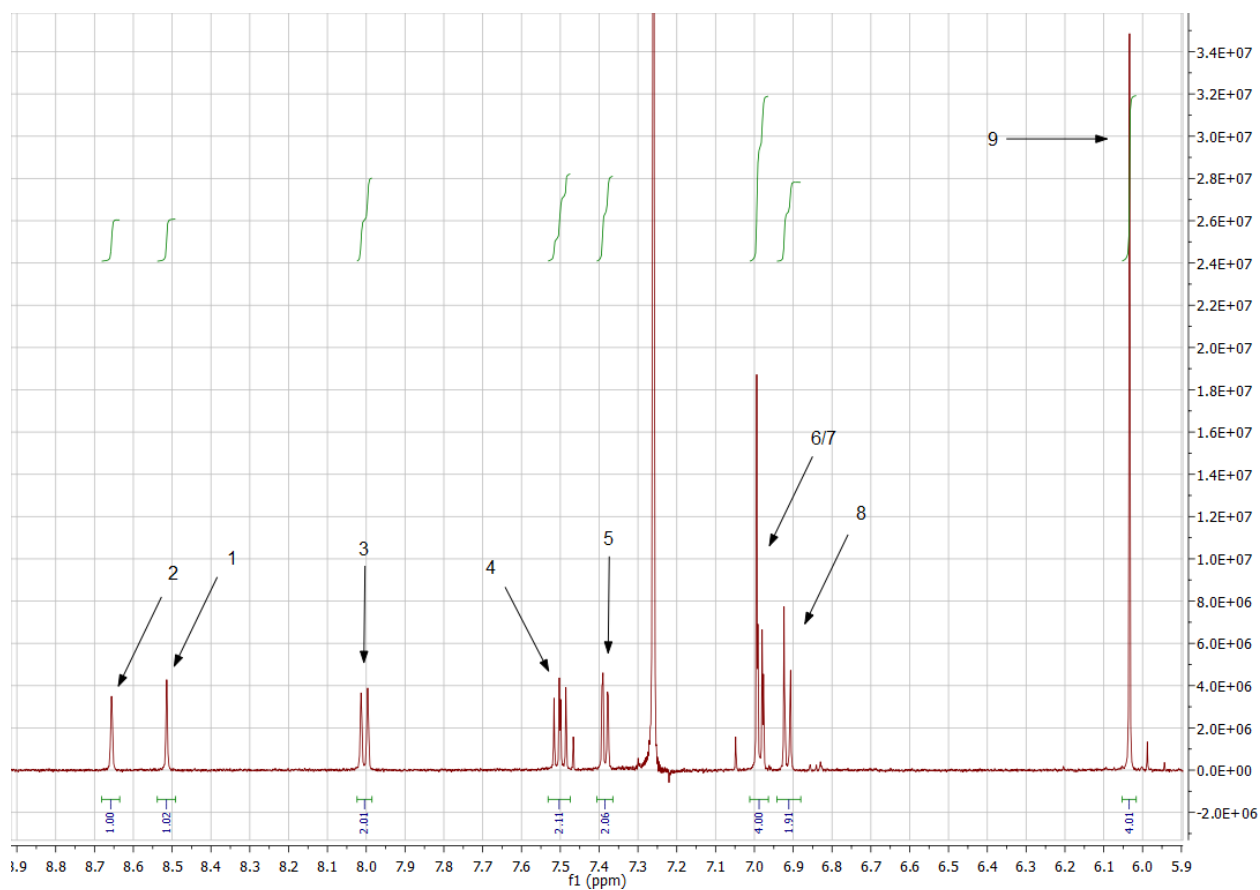
Picture 12. *^{1}H-NMR spectrum of sensor* **1e** *with proton assignments.*

82

Proton	K_a [M^{-1}]	Observed runs	Upper and lower limit of runs	$\overline{R}^2$	χ^2_{red}
1	0.47±0.19	11	4, 13	0.995	2.81*10^{-6}
3	0.49±0.19	8	4, 13	0.995	1.13*10^{-6}
4	0.47±018	8	4, 13	0.989	1.36*10^{-6}
5	0.48±0.18	10	4, 13	0.989	2.15*10^{-6}
8	0.42±0.06	11	4, 13	0.999	1.44*10^{-6}
9	0.30±0.17	8	3, --	0.987	7.14*10^{-7}

Table 3. *Summary of the fitting procedures of sensor* **1e** *with DNB.*
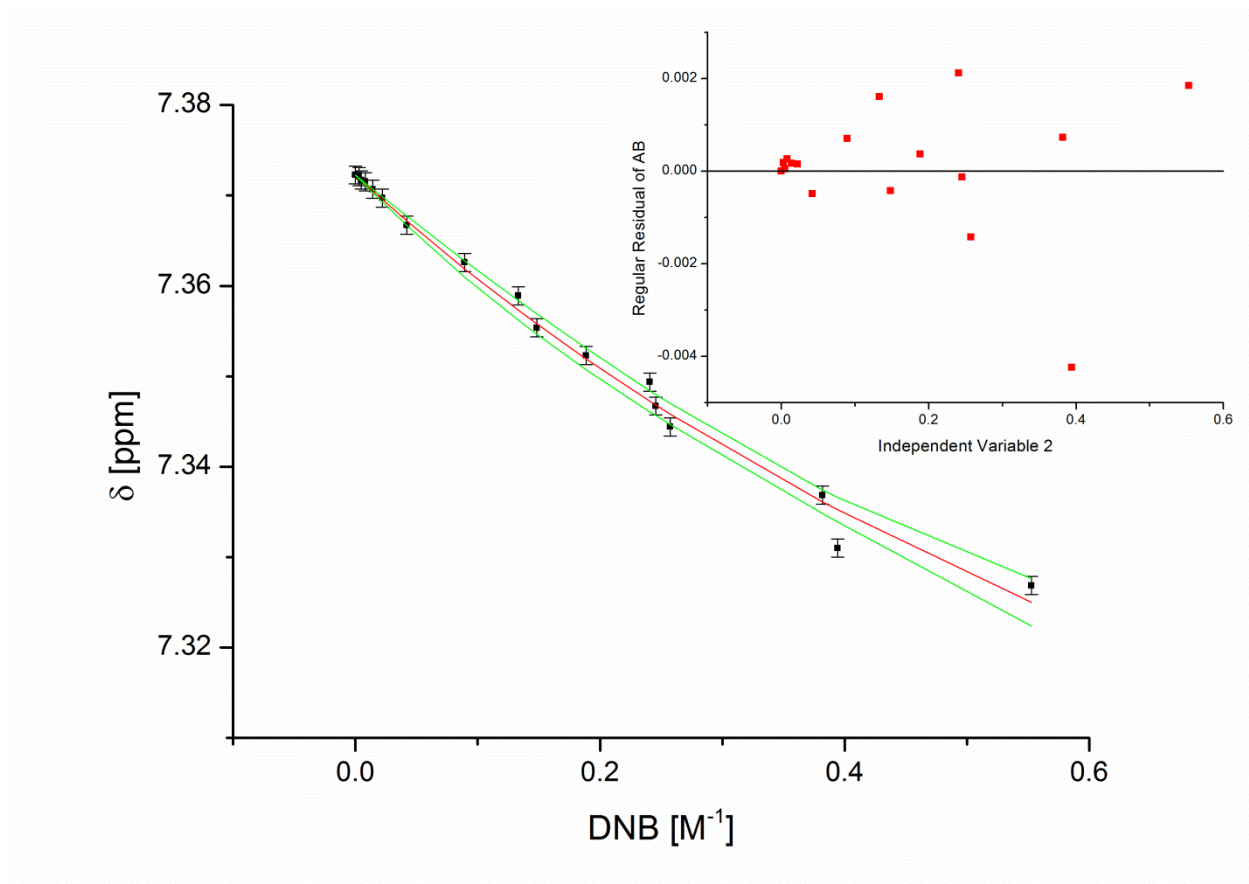
Picture 13. *Fitted curve (red) and corresponding 95% confidence intervals (green) of proton 5 in the titration with DNB. The error bars in the y-direction correspond to the measurement uncertainty of the spectrometer. The inset shows the residual plot of the fitted curve from which the runs test was performed.*

Even though the aryl clips of sensor **1e** are more electron-dense than in molecule **1d** their effect on the sensing performance is negligible, with the averaged K_a = 0.43±018 M^{-1}. Runs, $\overline{R^2}$ and χ^2_{red} allow to conclude satisfying Goodness-of-Fit in all cases. All the association constants are still below 1 and the corresponding uncertainties are rather large. Therefore it is safe to say that for anthracene-based sensors **1d** and **1e** the electron-abundace of the aryl clips does not influence the sensing performance towards DNB and complexation is clearly not favored. Hence it was decided to explore the influence of the distance between the aryl clips in coming sensors.

No further experiments with benzonitrile were conducted due to the negligible stacking interactions with sensors **1c** and **1d**.

2.4 Acetylenic Linkers

Another way to address gap size is to change the clip moiety. Bonds formed with acetylene can be floppy and can distort from the expected 180° angle by over 20°.[43] In sensor **1f** it is tried whether this could be used to build to let the gap size adjusts itself to the nitroaromatic guest according to need. It was decided to use anthraquinone as backbone. Anthraquinone is structurally more similar to xanthone (the sensor based on which showed the best results so far) than to anthracene and sensor **1f** can be assembled from commercially available precursors in one step.

The synthesis of anthraquinone-based receptor **1f** is shown in scheme **15**.

24   **1f**
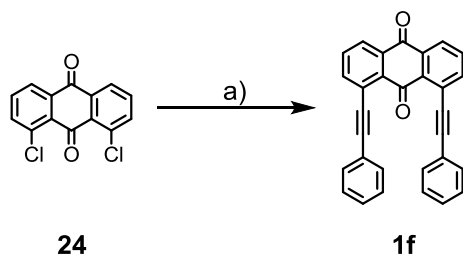
a) Phenylacetylene, Pd(CNCH$_3$)$_2$Cl$_2$, XPhos, Cs$_2$CO$_3$, Toluene, 110°C, 4 h, 30%

Scheme 15. *Synthesis of sensor* **1f**.

The Sonogashira coupling on chlorides was performed in a with the strongly electron-donating Pd(amphos)Cl$_2$ with CuI and freshly distilled excess triethylamine. The resulting sensor molecule **1f** may be a little less electron dense than the corresponding anthracene-analogue, but if the guest molecule is complexed between the two aryl clips, the latter will be approximately perpendicular to the backbone, thereby minimizing π-conjugation between the two moieties and consequently the influence of the chromophore.[44] It was decided to introduce phenylacetylene as clips to have a model compound. The reaction given in scheme **15** yielded sensor **1f** in 30% It was purified by flash chromatography.

2.4.1 Titration Experiments

Pictures 14 and 15 show the numbering of molecule **1f** and the ^{1}H-NMR spectrum of sensor **1f**.
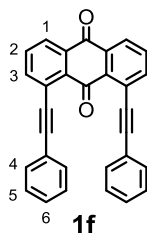
Picture 14. *Structure and numbering of sensor* **1f**.

85
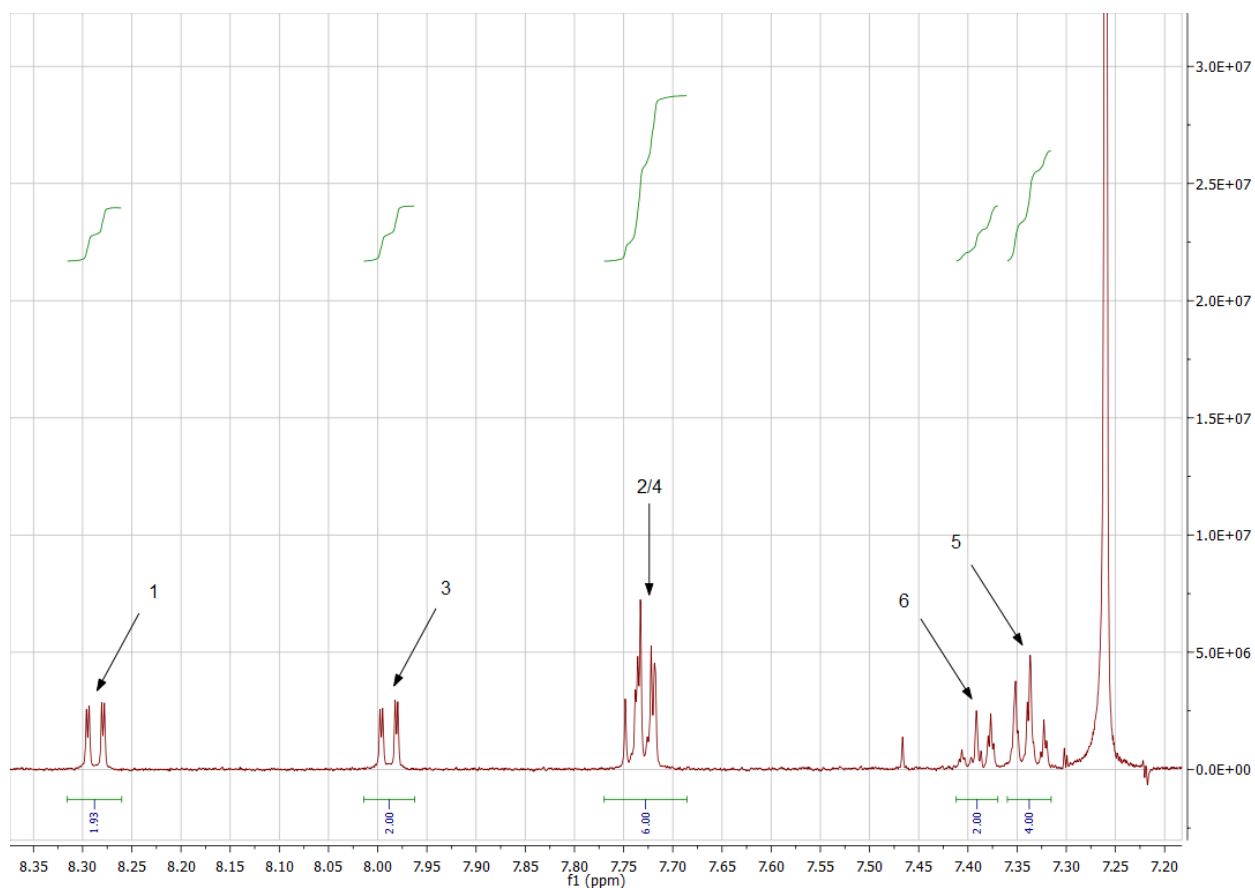
Picture 15. *¹H-NMR spectrum of sensor* **1f** *with proton assignments.*

Table 4 gives the results of the titration of molecule **1f** with DNB.

Proton	K_a [M^{-1}]	Observed runs	Upper and lower limit of runs	$\overline{R}^2$	χ^2_{red}
1	0.10±0.05	8	7, 18	0.998	4.10*10^{-8}
2	0.30±0.06	6	6, 16	0.998	2.84*10^{-8}
5	0.32±0.06	11	5, 15	0.998	4.20*10^{-8}
6	0.28±0.06	11	5, 15	0.998	1.96*10^{-8}

Table 4. *Summary of the fitting procedures of sensor* **1f** *with DNB.*
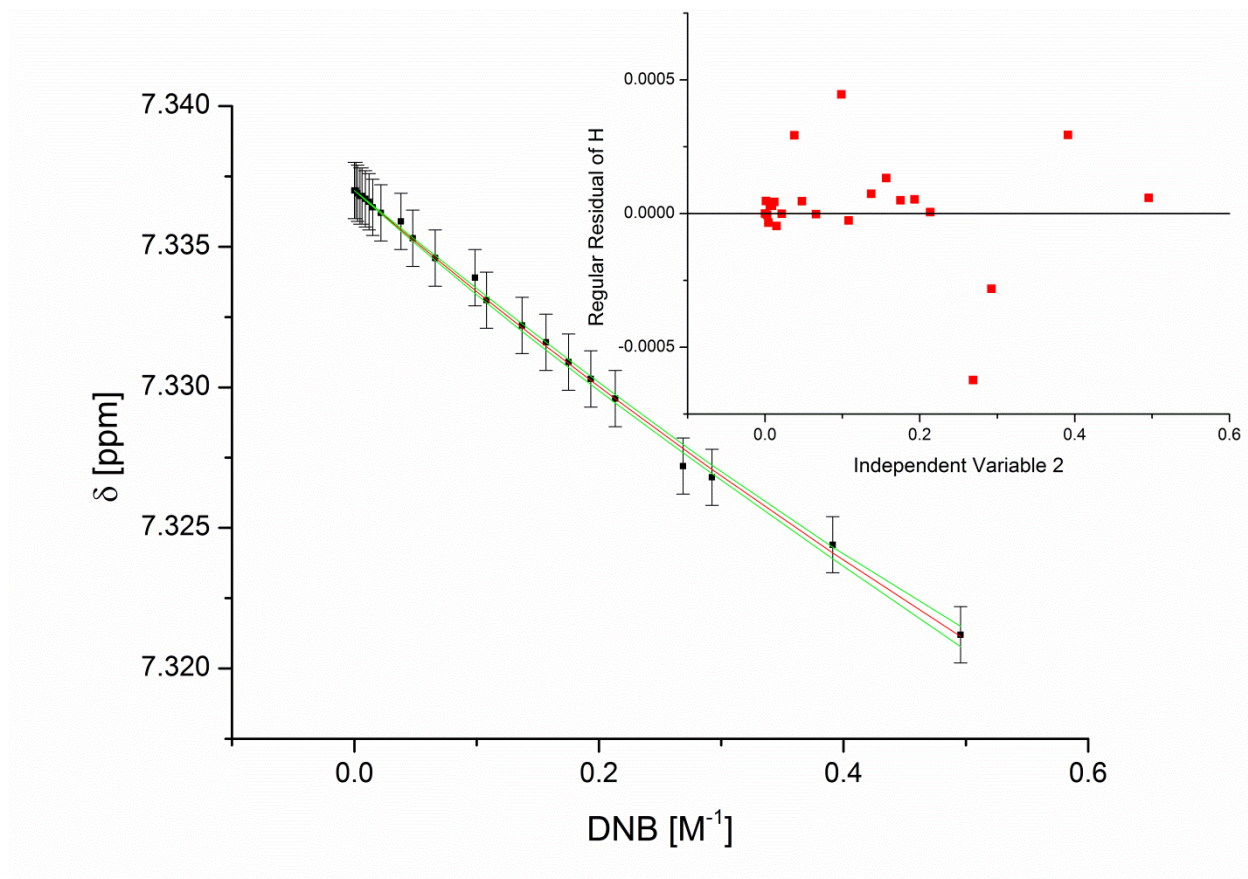
Picture 16. *Fitted curve (red) and corresponding 95% confidence intervals (green) of proton 5 in the titration with DNB. The error bars in the y-direction correspond to the measurement uncertainty of the spectrometer. The inset shows the residual plot of the fitted curve from which the runs test was performed.*

The association constants in table 4 give an average value of K_a = 0.25±0.06. For protons 3 and 4 no values could be determined because the calculated uncertainties of the K_a values were of the size of the value itself. Again the fitted curves are solid and the parameters well-defined. The uncertainty of the association constant of proton 1 is relatively large, but this is most likely again because as good as no sensing effect was measured and the measurement uncertainty of the spectrometer, even if it is small, becomes more dominant (picture 16). The best-fit association constants for the titration of sensor **1f** with DNB are of the same order of magnitude as for anthracene-based sensors **1d** and **1e**. The beneficial influence of the floppy acetylene-bonds could not be confirmed.

87

2.5 7H-dibenzo[c,h]xanthene-Based Sensors

Another way of expanding the distance between the aryl rods is to use a different backbone chromophore. Since distances in xanthone, anthracene and anthraquinone are small, a change of backbone was suitable. In order to not expand the gap too much it seemed reasonable to fuse additional rings in the 4,5- and the 3,6-positions of xanthone. When applying this to xanthone **1c**, the gap increases from 4.8 Å in **1c** to 6.8 Å in dibenzoxanthone **1g**.

2.5.1 Synthetic Strategy
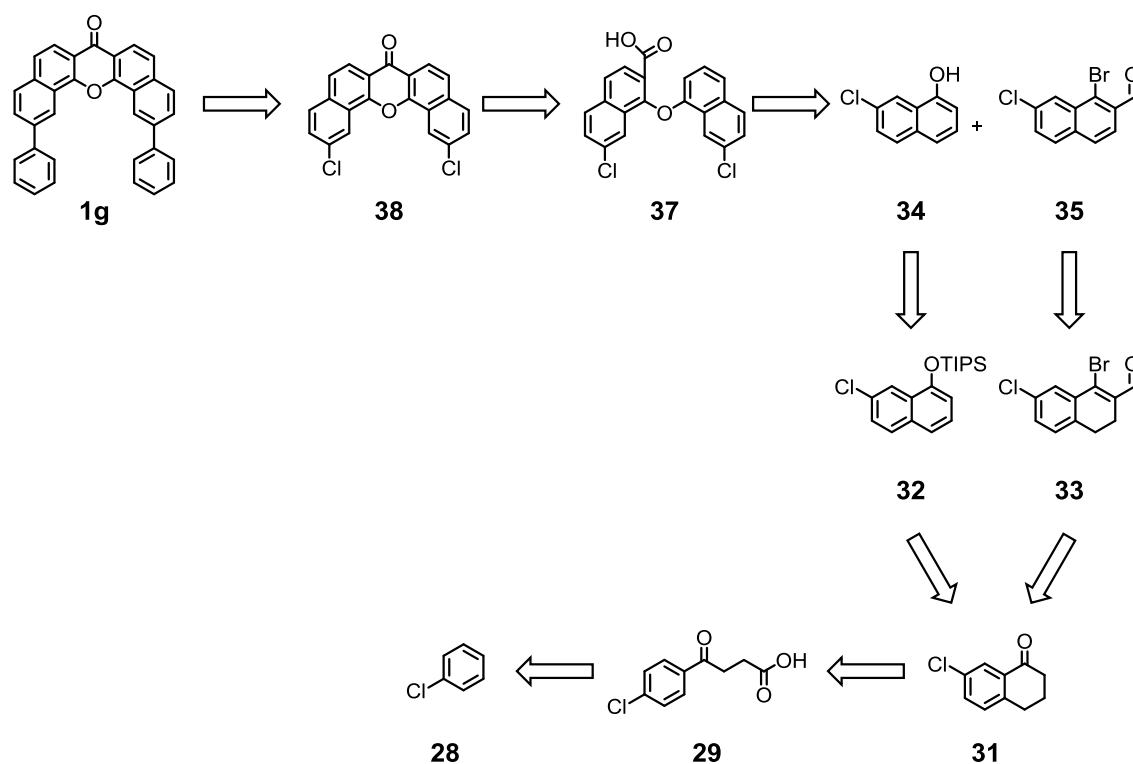
Scheme 16. *Synthetic strategy towards sensor* **1g**.

The synthetic strategy is based on tetralone- and naphthalene intermediates, in this case tetralone **31** and naphthalenes **34** and **35**. Tetralone **31** is envisaged to be synthesized in a Haworth synthesis.[45] Starting from chlorobenzene **28**, **28** is to be reacted in a Friedel-Crafts reaction to give carboxylic acid **29**. A Wolff-Kishner-type reduction of the latter followed by intramolecular Friedel-Crafts acylation is expected to

result in tetralone **31**.[46] Tetralone **31** can account for both naphthalene key intermediates **34** and **35**. Converting molecule **31** to its TIPS-protected enol ether and subsequent aromatization with DDQ is proposed to result in napththalene **32**. Alkaline deprotection of the TIPS-group is expected to yield in hydroxynaphthalene **34**. Naphthaldehyde **35** is proposed to be synthesized also from tetralone **31** in two steps. A Vilsmeyer-Haack-Arnold bromoformylation is expected to result in molecule **33,** the following aromatization of aldehyde **33** with DDQ is planned to provide naphthaldehyde **35**.[47] The intended Ullmann-coupling between the two naphthalenes **34** and **35** with the subsequent oxidation with hydrogen peroxide of the aldehyde moiety is envisaged to result in naphthoic acid **37**. Acid-promoted intramolecular Friedel-Crafts reaction of acid **36** in H_2SO_4 is planned to establish the xanthone-moiety, finalizing the direct precursor dibenzoxanthone **38**. A double Suzuki cross-coupling is proposed to introduce the two phenyl tweezers, resulting in target compound 2,12-diphenyl-7H-dibenzo[c,h]xanthen-7-one **1g**.

2.5.2 Synthesis

Scheme 17 depicts the Haworth-synthesis of 7-chloro-1-tetralone **31**. [45]
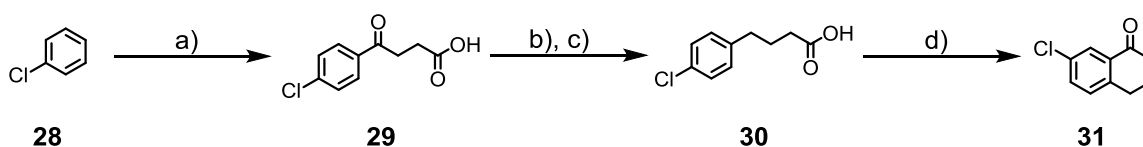
a) Succinic anhydride, Toluene, reflux, overnight, 74% b) N_2H_4*H_2O, KOH, TEG, 180°C, 5 h
c) HCl, H_2O, rt, overnight 67% (2 steps) d) Polyphosphoric acid, 15 min., 90°C, 95%

Scheme 17. *Haworth-synthesis of 7-chloro-1-tetralone* **31**.

The sequence starts with Friedel-Crafts-reaction of chlorobenzene with succinic anhydride, promoted by $AlCl_3$. After quenching the reaction mixture with 6M HCl at 0°C and subsequent extraction the product was precipitated with concentrated HCl. Acid **29** was obtained in 74% yield after drying under reduced pressure. Wolff-Kishner conditions in triethylene glycol with subsequent acidic precipitation overnight gave tetralone-

precursor **30** in 67% after the crude product was precipitated once again from acidic conditions and dried.[46] In the last step in the Haworth-reaction, acid **30** was cyclized into 7-chloro-1-tetralone **31** through an intramolecular Friedel-Crafts reaction in polyphosphoric acid.[48] Interestingly the reaction showed only very modest results when performed in H_2SO_4, methanesulfonic acid or even phosphoric acid, where little to no reaction was observed at the same temperature. It is possible that polyphosphoric acid not only acts as solvent, but also is a better drying agent than the other acids mentioned. 7-chloro-1-tetralone was isolated and purified in nearly quantitative amount by diluting the reaction mixture with H_2O and extracting it with MTBE. After repeatedly washing the assembled organic phases the solvent was removed and the product **31** dried under reduced pressure.

Scheme **18** shows the synthesis of 7-chloronaphthalen-1-ol **34** and 1-bromo-7-chloro-2-naphthaldehyde **35** from tetralone **31**.
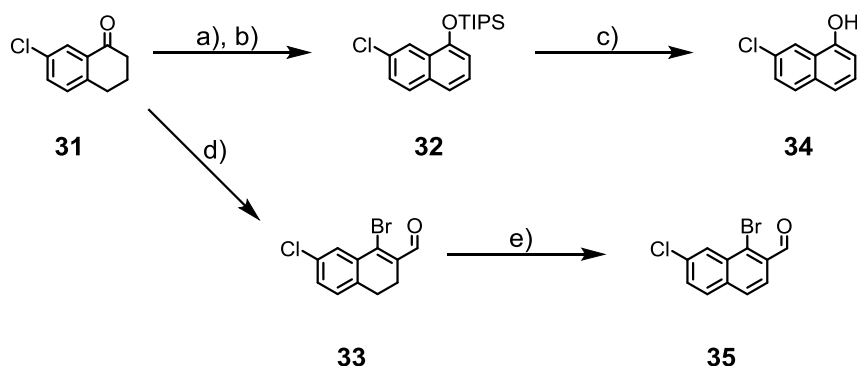
a) TIPSOTf, NEt$_3$, CH$_2$Cl$_2$, rt, 2 h b) DDQ, Dioxane, 80°C, 1 h, 80% (2 steps) c) NaOH, MeOH/H$_2$O, NMP, 60°C, 3 h, 74% d) PBr$_3$, DMF, CHCl$_3$, reflux, 5 h, 40% e) DDQ, Toluene, reflux, 3 d, 65%

Scheme 18. *Synthesis of naphthalenes **34** and **35**.*

Starting with 7-chloronaphthalen-1-ol **31**, it was first turned into its corresponding triisopropylsilane (TIPS) protected enolate by adding NEt$_3$ into a solution of **31** and TIPSOTf in CH$_2$Cl$_2$, in analogy to Niculescu *et al.*[49] After quenching the reaction mixture in ice-water and separation of the organic layer the solvent was removed and the crude

product was aromatized by treating it with DDQ in dioxane for 1h at 80°C. After purification by column chromatography ((7-chloronaphthalen-1-yl)oxy)triisopropylsilane **32** was obtained in 80% yield after two steps. Alkaline removal of the TIPS group in MeOH/H_2O (1:1 v:v%) afforded 7-chloronaphthalen-1-ol **34** in 74% yield.[49] Purification of **34** was again achieved by column chromatography.

Starting again from tetralone **31**, 1-bromo-7-chloro-3,4-dihydronaphthalene-2-carbaldehyde **33** was obtained by a Vilsmeier-Haack-Arnold reaction. After stirring PBr$_3$ and DMF in chloroform, tetralone **31** was slowly added into the solution and the mixture was refluxed for another 4h. After quenching the reaction with H_2O and extraction with CH_2Cl_2, the combined organic phases were washed and the solvent removed. The crude product **33** was used without further purification in the next reaction, the aromatization to 1-bromo-7-chloro-2-naphthaldehyde **35** in toluene with DDQ. The reaction was rather slow, taking 3 days at reflux temperature.[50] After filtration of the reaction mixture to remove insoluble components the solvent was removed from the filtrate and napthaldehyde **35** was obtained in 65 % yield after purification by flash chromatography.

a: K_2CO_3, CuO, DMSO, 190°C, 3 h
b: K_2CO_3, CuO_2, DMSO, 190°C, 3 h
c: Pd(OAc)$_2$, K_3PO_4, tBu-XPhos, THF, 85°C, overnight
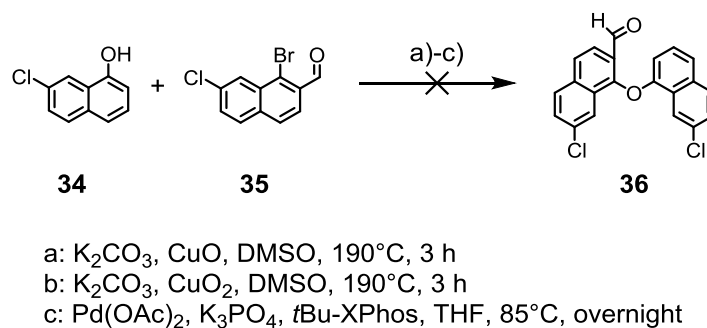
Scheme 19. *Preliminary attempts towards precursor* **36**.

With both of the naphthalene intermediates in hand the next step was the building up of the backbone of sensor **1g**. Initially, it was planned to assemble the dibenzobackbone **36** in a reaction sequence starting with an Ullmann coupling, followed by an intramolecular Friedel-Crafts reaction. However, preliminary attempts were not encouraging (cf. scheme 19).

Instead, by adopting a procedure for similar compounds, the condensation of 7-chloronaphthalen-1-ol **34** with acetone in molten pTsOH at 125°C delivered dimethylxanthene **39**, which is structurally similar to the originally intended xanthone **38** scheme 20). [51] Although the boiling point of acetone is at 56°C and the reaction was heated to 125°C, the reaction time indicated in scheme 20 was necessary to observe full conversion of naphthalene **34**. It seems save to postulate that the driving force behind this condensation is the loss of 2 equivalents of water, with one equivalent stemming from the naphthalene and the other from the acetone. The large excess of protons in the very acidic reaction should readily promote the generation of $-OH_2^+$ in both cases, were the elevated reaction temperature ensures the removal of moisture and (generated) water from the reaction mixture. The 45% yield of the reaction was unsatisfactory and might have been due to losses in the purification procedure. After cooling the reaction, diluting it with water and extracting the crude with toluene the solvent was removed. The crude was purified twice by column chromatography and then subjected to GPC. In analogy with the procedures used for the anthracene backbone, the conditions for the subsequent double Suzuki coupling were chosen accordingly, giving sensor **1h** in 30% yield.
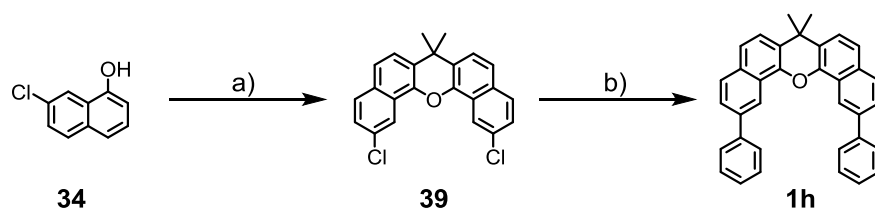
a) Acetone, p-TsOH, 125°C, 1.5 h, 45% b) Phenylboronic acid, Pd(amphos)Cl$_2$, Cs$_2$CO$_3$, Toluene/H$_2$O (10:1), 110°C, 6h, 30%

Scheme 20. *Final assembly of sensor* **1h**.

2.5.3 Titration Experiments
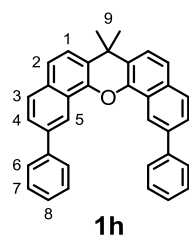
Picture 17. *Structure and numbering of sensor* **1h**.
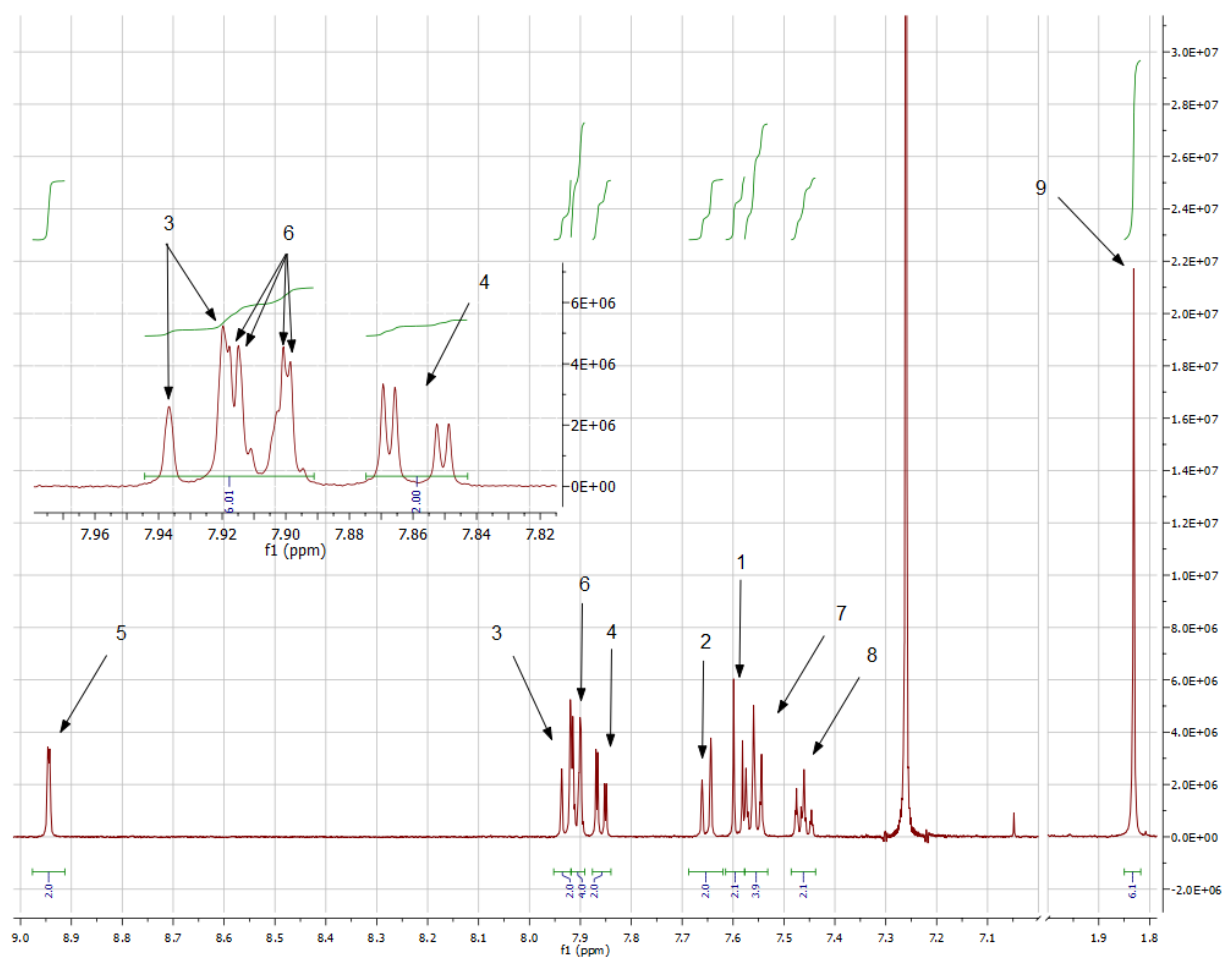
Picture 18. *^{1}H-NMR spectrum of sensor* **1h** *with proton assignments. The inlay on the left shows the assignments of protons 3,4 and 6 for clarity.*

Proton	K_a [M^{-1}]	Observed runs	Upper and lower limit of runs	$\overline{R}^2$	χ^2_{red}
1	0.53±0.24	3	2, --	0.995	5.01*10^{-7}
2	0.59±0.05	6	2, 9	0.999	1.66*10^{-8}
5	0.90±0.05	9	3, 10	0.999	5.32*10^{-7}
6	1.75±0.46	5	2, --	0.995	6.53*10^{-7}
7	0.45±0.16	6	2, --	0.985	1.03*10^{-6}
8	0.07±0.05	7	3, 11	0.997	1.58*10^{-7}
9	0.89±0.02	9	3, --	0.999	1.53*10^{-8}

Table 5. *Summary of the fitting procedures of sensor* **1h** *with DNB.*

Pictures 17 and 18 show the numbering of molecule **1h** and the ^{1}H-NMR spectrum of sensor **1h**. Table 5 gives the summarized results of the titration of molecule **1h** with DNB.
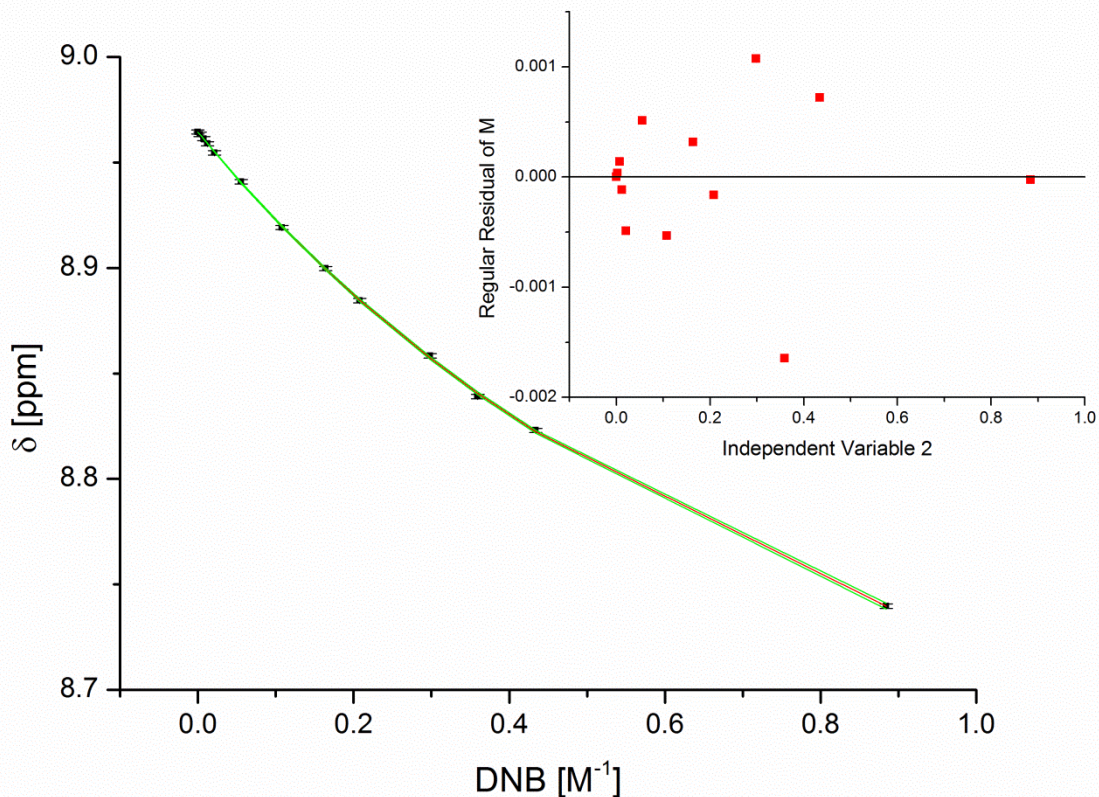
Picture 19. *Fitted curve (red) and corresponding 95% confidence intervals (green) of proton 5 in the titration with DNB. The error bars in the y-direction correspond to the measurement uncertainty of the spectrometer. The inset shows the residual plot of the fitted curve from which the runs test was performed.*

The uncertainties of the association constants from table 5 range between 2% and 71%, and the lower constants have the bigger uncertainties. Like before, for protons with the lowest sensing response measurement uncertainties become more dominant. All uncertainties are in a range where they still give a good idea of the size of the sensing effect perceived by the proton in question. Also, the results of the runs test do not show any significant systematic deviations between model and fit. χ^2_{red} values indicate small random error between model and fit, although it is slightly less small for proton 7. The fit for proton 7 also shows the lowest $\bar{R}^2$ value, but still over 98% of the variance of the fit values is accounted for. Hence, the fits can be considered good and overall the uncertainties are reasonable.

Apart from the fact that all the determined association constants are low, what is interesting about the values in table 5 is their distribution, ranging from 0.07±0.05 M^{-1} to

1.75 ± 0.46 M^{-1}. When comparing the association constants with the protons from which they were determined, the biggest association constant was measured for proton 6 which is located on the aryl clip, and so is the proton with the lowest K_a, proton 8. It was not possible to obtain values from proton 4 because its signal overlaps with one of the DNB signals. The second highest values stem from proton 5 (which is located in the gap) and, interestingly, proton 9. Protons 1 and 2 show bigger response than any proton in sensors **1c-1f**. Proton 7 shows the weakest effect apart from proton 8. It is concluded that DNB complexes, although weakly, in the "biphenylic" region of sensor **1h**. This conclusion is based on the fact that the protons showing the most favorable complexation behavior with DNB either help forming the gap (protons 5 and 6) or are structurally near (protons 9); the through space distance between protons 9 and 5 can come as close as 5.82 Å in the calculated structure (cf. picture 30). It is impossible to say in which manner this happens from association constants alone, but the arylic clips appear to have an influence. Of course the problem of the distance between the clips is not solved, but their influence is believed to be shown. The averaged association constant of sensor **1h** with DNB is $K_a = 0.74 \pm 0.15$ M^{-1}. But keeping in mind the range over which the single values are distributed the averaged value is probably too low.

2.6 Gap-Size Adjustable Styryl-Sensors

2.6.1 Design and Synthetic Strategy

The problem of inadequate gap size can also be approached from the perspective that the size of the gap could be dynamically adapted to the guest by increasing rotational freedom of and in the pincers. Replacing bendable acetylene moieties with twofold rotatable styryl moieties introduces two additional rotational axes per styryl unit, thereby reducing preorganization of the sensor but rendering it more flexible with its gap size adjustable over more than 5 Å (cf. picture 20). Not only would the sensor potentially be given the possibility to adjust the gap size as needed in the particular case through rotation of the styryl pincers, but the aryl groups in the styryl pincers themselves may rotate into two parallel planes, which should maximize their interaction with guests in the size-adapted gap (cf. picture 20).
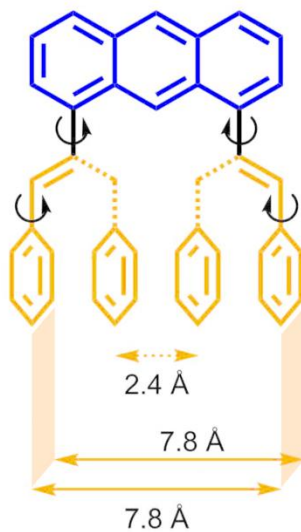
Picture 20. *Concept behind sensors* **1i** *and* **1j***: the styryl-linkers allow the structure adapting the gap size between the pincers to the guest. The aryl-moieties in the pincers are able to form parallel planes, which should maximize the interaction of the clips with a guest molecule.*

Scheme 21 shows a synthetic analysis of sensors **1i-1j**.
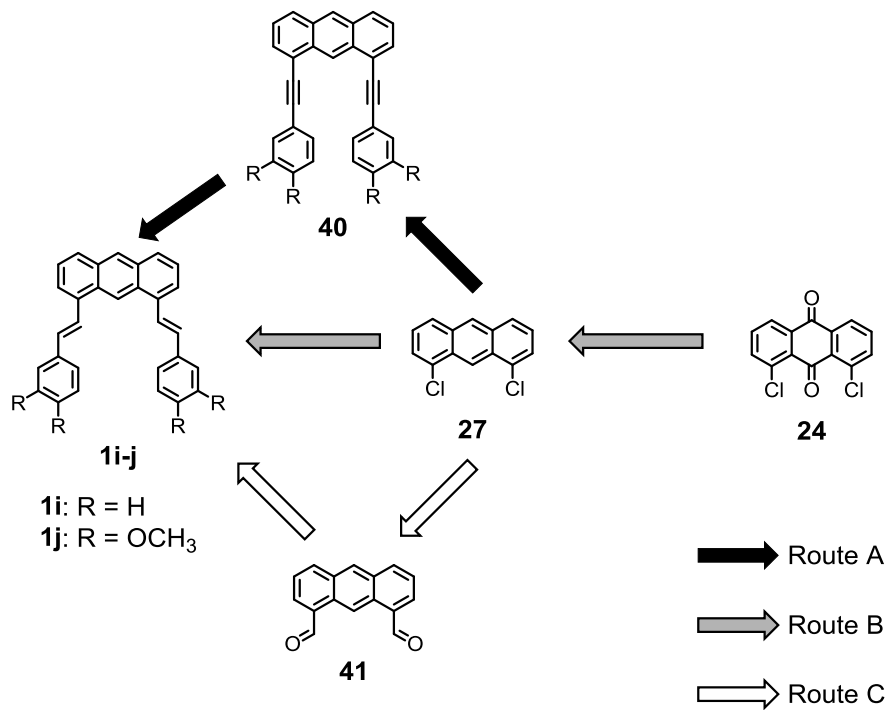
Scheme 21. *Synthetic analysis of sensors* **1i** *and* **1j***.*

97

All three pathways can be lead back to 1,8-dichloroanthracene **27** which is available from 1,8-dichloroanthraquinone **24** through reduction of the latter with Zn powder in aq. NH$_3$ as described above.[40] Three possibilities are considered here for the introduction of the styrene-tweezers. The first possibility is to introduce phenylacetylene in a Sonogashira cross coupling. 1,8-bis(phenylethynyl)anthracene **40** is then envisaged to be reduced into the corresponding styrene-analogue 1,8-distyrylanthracene **1i** or **1j** in a Pd-catalyzed reduction.[52]

In route B it is planned to directly introduce the styrene-moieties in a Pd-catalyzed Heck coupling. Because Pd-catalyzed couplings to aromatic chlorides can be difficult due to their low reactivity of the latter catalyst screening and general optimization of the reaction conditions may be necessary.[41, 42]

The main difference between route C and routes A and B is that for route C the introduction of the clips no cross coupling is intended. Instead it is planned to use a Horner-Wadsworth-Emmons (HWE) reaction to connect the phenyl groups to the anthracene. Anthracene-1,8-dicarbaldehyde **41** is targeted in two-step procedure starting from anthracene **27**. First, Rosenmund-von Braun-conditions with CuCN are proposed to yield in 1,8-dicyanoanthracene, and subsequent reduction with DIBAL-H is expected to result in dicarbaldehyde **41**; the proposed HWE reaction between carbaldehyde **41** the according phosphonates is intended to result in target molecules **1i-j**.[53]

2.6.2 Synthesis

Considering the three synthetic pathways presented above, the following factors are obvious: route A and route B have comparable key steps, a Sonogashira coupling in route A and a Suzuki coupling in route B. Route A consists of one more step, namely the reduction from the acetylene to the double bond. Concerning route C, although HWE reactions are a powerful method in the synthesis of double bond and routinely used in stilbene synthesis, route B is more straight forward, shorter and avoids toxic cyanides.

It was therefore decided to concentrate on route B, as it contains the least reaction steps.

Scheme 22 gives an overview of the synthesis of sensors **1i-j**.
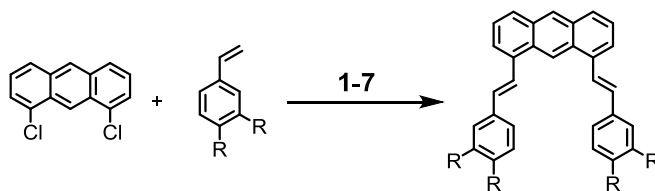
Entry	R	Base	Solvent	Catalyst	T [°C]	t [h]	yield [%]
1	-H	Cs_2CO_3	DMF	$Pd_2(dba)_3$/$P(^tBu)_3$	120	18	40
2	-OMe	Cs_2CO_3	DMF	$Pd_2(dba)_3$/$P(^tBu)_3$	120	18	------
3	-OMe	Cs_2CO_3	DMF	$Pd(amphos)Cl_2$	120	18	------
4	-OMe	Dicyclohexylmethylamine	Toluene	$Pd_2(dba)_3$/$P(^tBu)_3$	110	20	(55)
5	-OMe	Dicyclohexylmethylamine	Toluene	$Pd_2(dba)_3$/$P(^tBu)_3$	110	20	------
6	-OMe	Dicyclohexylmethylamine	Toluene	$Pd(amphos)Cl_2$	110	20	------
7	-OMe	Dicyclohexylmethylamine	Toluene	POPd	110	20	------
8	-OMe	Cs_2CO_3	DMSO	$Pd_2(dba)_3$/$P(^tBu)_3$	160	16	60

Scheme 22. *Overview of the synthesis of compounds 1i and 1j.*

Fu reported the utility of $P(^tBu)_3$ as ligand in Pd-catalyzed Heck couplings, especially in the case of hindered and/or electron-rich aryl chlorides.[54] Choice of base can affect the outcome of Heck couplings considerably. Cs_2CO_3 has been reported to deliver good results for similar systems.[55] DMF was chosen because it is considered the standard solvent in Heck couplings.[56] The reaction of anthracene **27** with styrene as described in entry 1 in scheme 22 yielded receptor **1i** in 40% yield. The product was purified by column chromatography. ^{1}H-NMR revealed the exclusive formation of the *E*-isomer, with the protons in the styryl-bridge exhibiting the coupling constant $J = 16.0$ Hz.[57, 58] For the more electron-rich 3,4-dimethoxystyrene **1j** the same conditions resulted in no reaction

at all. Using Pd(amphos)Cl$_2$ as catalyst which was used in the Suzuki coupling of anthracenes **1d** and **1e** with 3,4-dimethoxybenzeneboronic acid was equally fruitless. Next, two parameters were changed simultaneously. Since target sensor **1j** consists of a relatively rigid, pi-conjugated structure, using toluene as solvent might help the reaction to proceed by keeping anthracene **27** and the monosubstituted species in solution. Furthermore it was reported that using dicyclohexylmethylamine instead of Cs$_2$CO$_3$ can enhance the performance of the Pd$_2$(dba)$_3$/P(^{t}Bu)$_3$ system.[59] Employing the conditions given in entry 4 in scheme 22 gave the monocoupled product (E)-1-chloro-8-(3,4-dimethoxystyryl)anthracene in 55% yield. However, the compound did not undergo further reaction when subjected again to the same conditions. As can be seen in entries 6 and 7, neither Pd(amphos)Cl$_2$ nor POPd did result in product formation. Both these catalysts are known for the coupling of sterically demanding and/or electron-rich substrates.[23, 30] Although 3,4-dimethoxystyrene is electron-rich, sterically it is not a particularly demanding molecule, considering that the methoxy-substituents are located in the *meta-* and *para*-positions relative to the styrene moiety. 1,8-dichloroanthracene **27** may not be particularly reactive, but following the catalytic cycle of Heck reactions the first step is the oxidative addition of the anthracene to the Pd-catalyst. The same holds true for Suzuki couplings and rather electron rich species have been coupled to 1,8-dichloroanthracene under similar conditions earlier in this work.[24] Although it is daring to compare different coupling reactions with each other it still raises the question whether the challenge can be overcome through simple heating. It is possible that the second coupling in the formation of sensor **1j** has a rather big activation energy, which may be overcome through reaction temperature. Conditions in entry 8 are similar to entry 2, except that DMF is replaced with DMSO for higher reaction temperature. The conditions given in entry 8 resulted in 1,8-bis((E)-3,4-dimethoxystyryl)anthracene **1j** in 60% yield. Interestingly this yield is higher than for 1,8-di((E)-styryl)anthracene **1i**, where the reaction is electronically less demanding. The increased reaction temperature is a likely explanation.

2.6.3 Titration Experiments
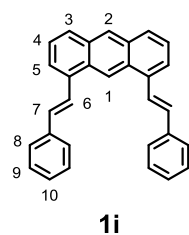
**Picture 21.** *Structure and numbering of sensor* **1i***.*
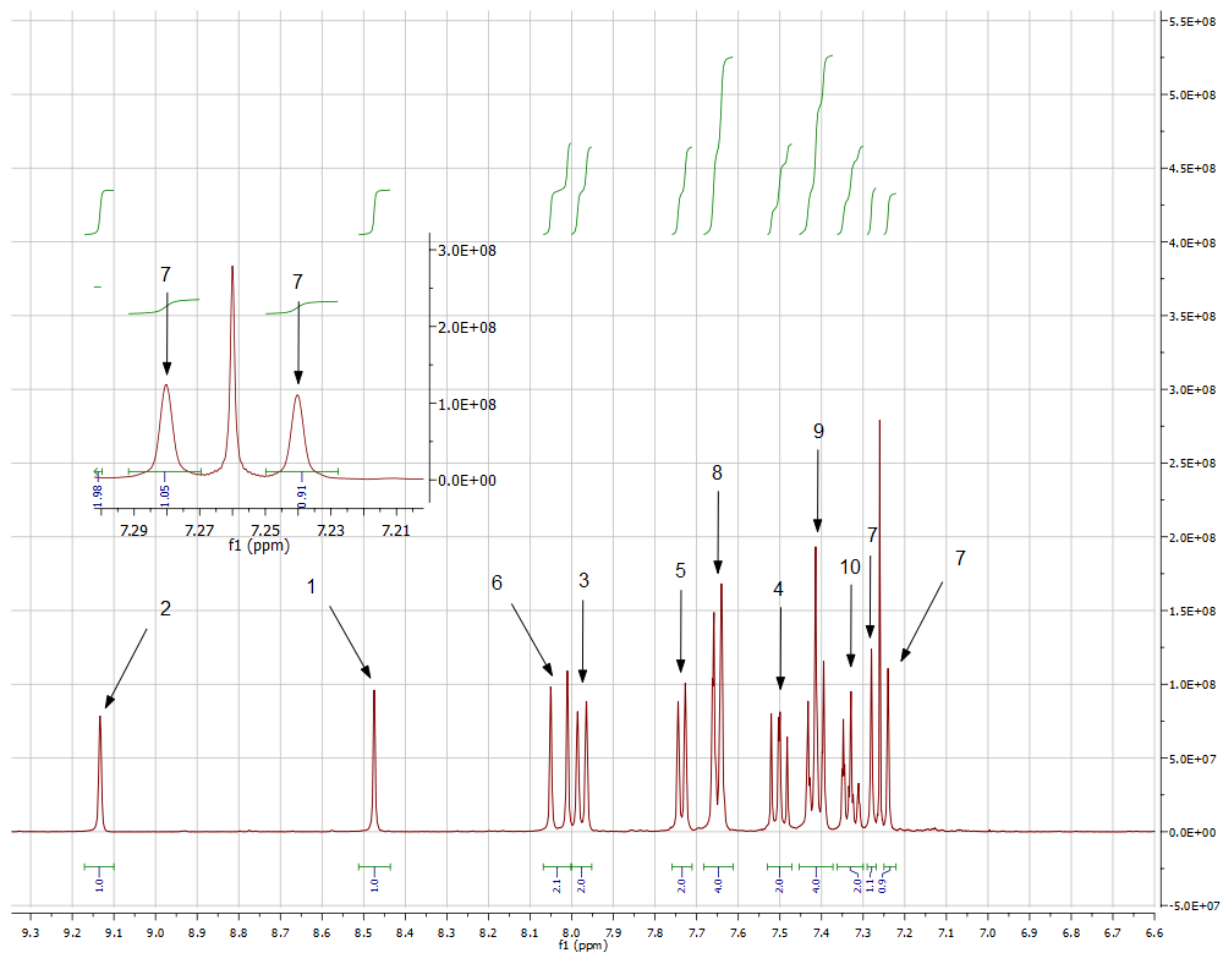
Picture 22. *^{1}H-NMR spectrum of sensor* **1i** *with proton assignments. The inlay on the left shows the assignment of proton 7 whose signal is disrupted by the solvent peak of CDCl$_3$ at 7.26 ppm.*

Proton	K_a [M^{-1}]	Observed runs	Upper and lower limit of runs	$\overline{R}^2$	χ^2_{red}
1	1.99±0.34	7	3,--	0.999	4.17*10^{-7}
2	1.76±0.36	6	2, 9	0.998	2.89*10^{-6}
3	0.94±0.13	8	3, --	0.995	1.50*10^{-6}
4	0.73±0.05	5	2, --	0.999	4.49*10^{-8}
5	0.80±0.04	6	4, 13	0.999	7.56*10^{-8}
6	1.16±0.12	5	4, 14	0.997	1.14*10^{-6}
7	0.74±0.05	11	4, 13	0.999	1.15*10^{-7}
8	0.83±0.31	6	4, 13	0.971	2.88*10^{-6}
9	0.70±0.07	4	4, 13	0.998	1.44*10^{-7}
10	0.47±0.05	6	4, 14	0.999	8.52*10^{-8}

Table 6. *Summary of the fitting procedures of sensor* **1i** *with DNB.*
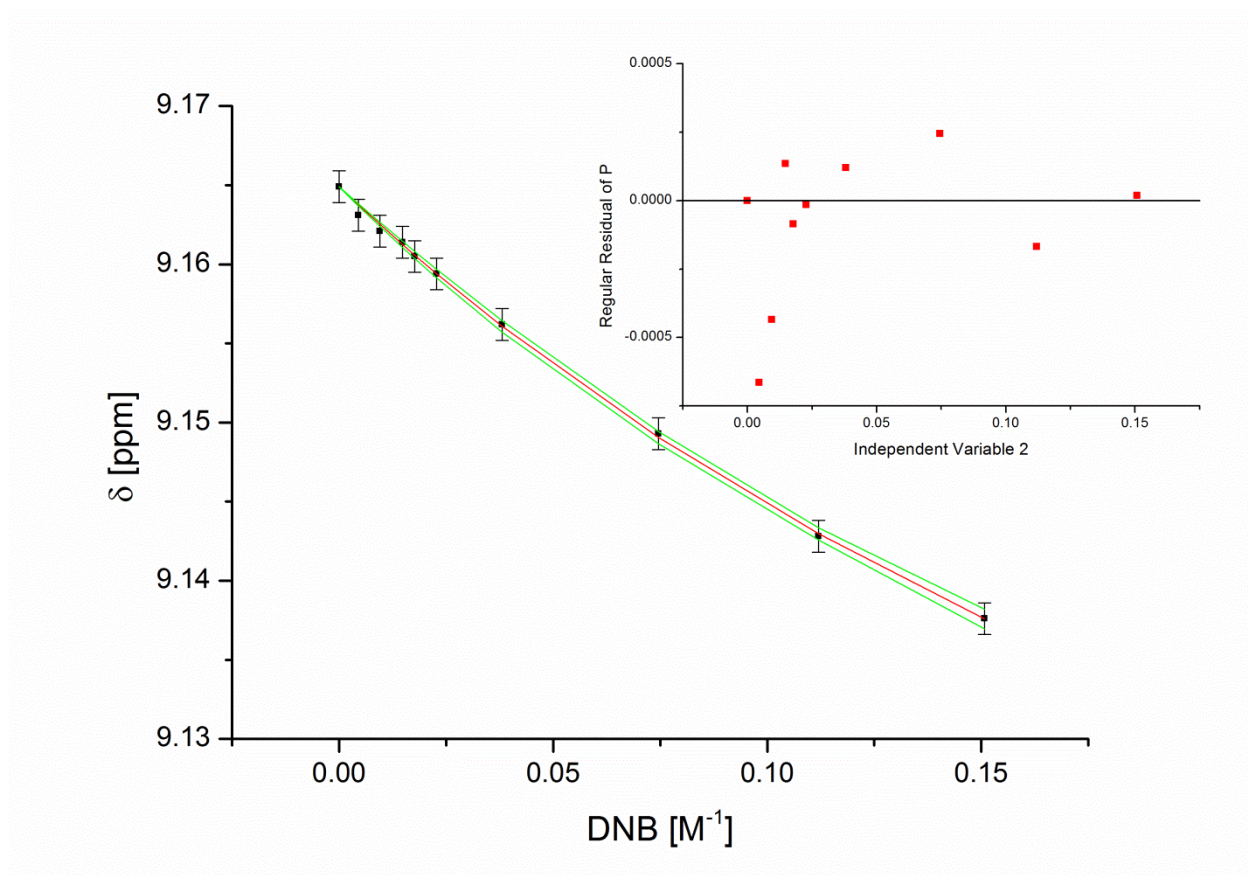
Picture 23. *Fitted curve (red) and corresponding 95% confidence intervals (green) of proton 2 in the titration with DNB. The error bars in the y-direction correspond to the measurement uncertainty of the spectrometer. The inset shows the residual plot of the fitted curve from which the runs test was performed.*

Runs test, $\overline{R}^2$ and χ^2_{red} hint at good fits throughout (table 6). $\overline{R}^2$ might be comparatively low for proton 8 but the runs test and $\overline{R}^2$ indicate the fit to be valid. The calculated uncertainties of the association constants allow defining them with sufficient precision, even under the assumption that the uncertainties are possibly too small.

The biggest effect towards titration with DNB was measured in protons 1 and 6, both of which are located at the inside of or on the rotatable clips. The association constants themselves are not high but the highest that were measured apart from xanthone-based sensor **1c** in this work. The rotatable clip moieties seem to help assembling the DNB-sensor complex, but as mentioned before association constants alone do not allow to precisely determining the precise mode of complex formation.

103

Comparing association constants of sensor **1i** with the results of the more electron-abundant analog sensor **1j** will be interesting in terms of the influence of the electron-density in the aryl clips. The measured association constants of sensor **1j** with DNB are shown in table 7.
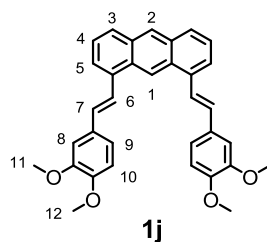
Picture 24. *Structure and numbering of sensor* **1j**.
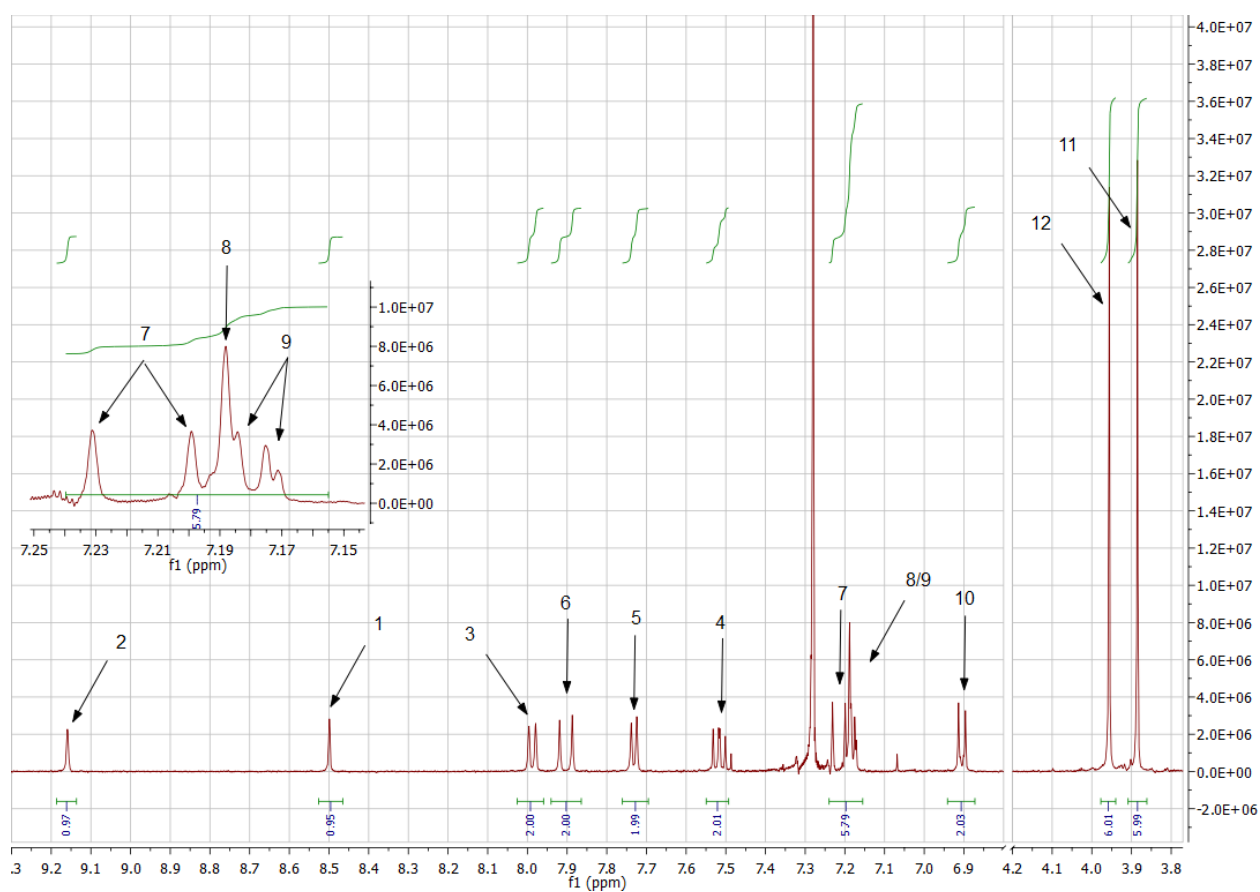
Picture 25. *^{1}H-NMR spectrum of sensor* **1j** *with proton assignments. The inlay on the left shows the assignment of protons 7-9 for clarity.*

Proton	K_a [M^{-1}]	Observed runs	Upper and lower limit of runs	$\overline{R}^2$	χ^2_{red}
1	1.14±0.03	8	2, 9	0.999	1.04*10^{-6}
3	0.64±0.11	6	2, 9	0.999	2.84*10^{-7}
4	0.85±0.03	8	2, --	0.999	2.00*10^{-7}
5	0.86±0.04	6	2, 9	0.999	5.86*10^{-7}
7	0.65±0.06	6	2, --	0.999	2.55*10^{-7}
8	0.18±0.07	4	2, 7	0.999	1.77*10^{-7}
10	0.39±0.03	4	2, --	0.999	3.66*10^{-7}
12	0.40±0.03	4	2, --	0.999	2.10*10^{-7}

Table 7. *Summary of the fitting procedures of sensor* **1j** *with DNB.*
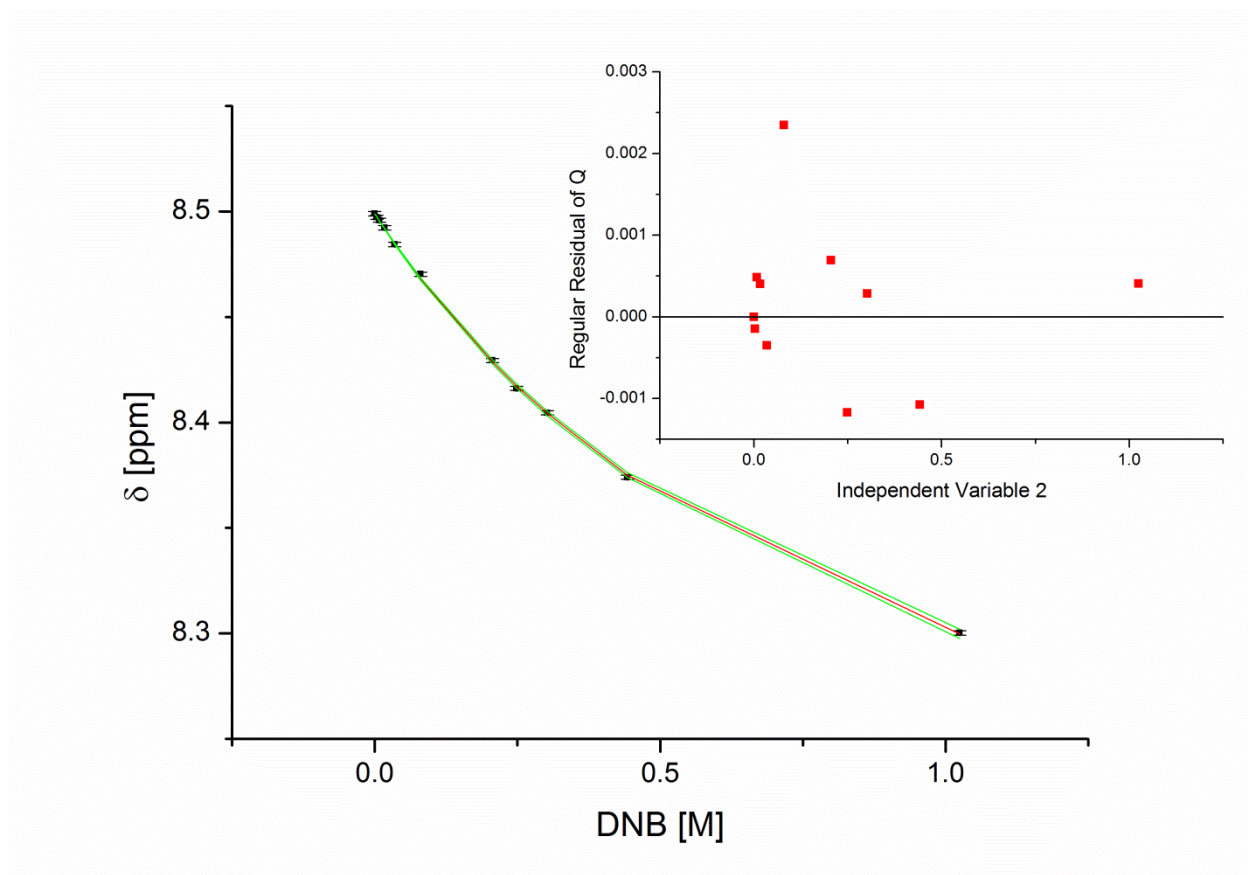
Picture 26. *Fitted curve (red) and corresponding 95% confidence intervals (green) of proton 1 in the titration with DNB. The error bars in the y-direction correspond to the measurement uncertainty of the spectrometer. The inset shows the residual plot of the fitted curve from which the runs test was performed.*

Compared to the unsubstituted clips in sensor **1i**, the clips in sensor **1j** have higher electron density because of the additional methoxy-substituents in the styryl-moieties. This was expected to be reflected in the complexation behavior of molecule **1j** towards DNB. Although the best-fit association constants are very similar between sensor **1i** and the more electron dense sensor **1j**, the determined association constants for the latter are rather lower in comparison to the former. It is concluded that the additional electron density in the clips of sensor **1j**, provided by the methoxy-substituents, does not show a positive measurable effect in the complexation of DNB.

2.7 Selected Self-Association Studies

2.7.1 Overview

The association constants for sensors **1c-1j** are generally low, ranging from 24 M^{-1} to 0.25 M^{-1}. A possible reason is self-association of the sensor molecules. If they preferred to assemble with themselves instead of the analytes, it would explain their reluctant complexation behavior towards DNB.[60] With regards to the general structure of the sensors they could not only self-associate via their chromophore spacers but they could also intercalate with one another (picture 27).[61]
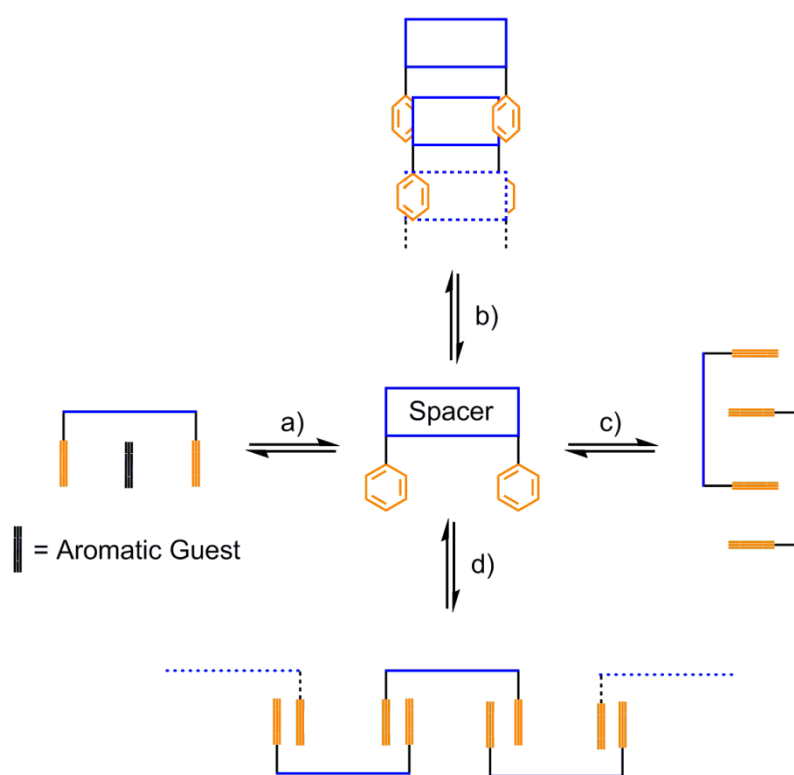
Picture 27. *a) Binding of aromatic guests and competing self-association processes, such as b) complexation of the spacer, c) dimerization and d) oligomerization.*

A number of formulas exist for this task.[62] Here, the equal K indefinite self-association model was used. In the equal K indefinite self-association model it is assumed that a sensor molecule A form stacks (dimers, trimers, etc.) with the equilibrium constant K_s being constant:[63]

$$A_j + A \overset{K_s}{\leftrightarrow} A_{j+1} \qquad (23)$$

It can also be shown that

$$[A_0] = \frac{[A]}{(1-K_s[A])^2} \qquad (24)$$

with $[A_0]$ being the total concentration of solute A and $[A]$ the monomer concentration in solution. Under the assumption that at the end of a stack the changes in proton shift for a solute molecule are half of what it experiences within a stack, the proton shift of the j-mer δ_j is expressed as

$$\delta_j = \frac{(j-1)\delta_i + \delta_m}{j} \qquad (25)$$

where δ_m is the proton shift of the monomer and δ_i is the maximum proton shift of the solute present in the stack. In the regime of rapid exchange, as is usually the case in self-association, the observed chemical shift covering all species in solution $\delta_{measured}$ is given by

$$\delta_{measured} = \frac{[A]}{[A_0]} \left\{ \frac{\delta_m}{1-K_s[A]} + \frac{\delta_i K_s[A]}{(1-K_s[A])^2} \right\} \qquad (26)$$

which by substitution with eq. (24) becomes

$$\delta_{measured} = \left(\frac{\sqrt{1+4K_s[A_0]}-1}{2K_s[A_0]} \right) \delta_m + \left(1 + \frac{1-\sqrt{1+4K_s[A_0]}}{2K_s[A_0]} \right) \delta_i \qquad (27)$$

δ_i and K_s were calculated in the fitting procedure, along with δ_m.[62, 63] The model does not differentiate between dimers and higher aggregates formally, but in this case the size of the stacks is of less interest than the equilibrium between monomers and aggregates in general.[63, 64]

2.7.2 Titration Experiments

Molecules **1d**, **1h** and **1j** were tested for self-association.

Sensor **1d** showed negligible proton shifts upon dilution in the measured concentration range (0.13 mM to 64 mM) and can be attributed to the measurement uncertainty of the NMR-spectrometer. For protons 1, 3 and 4 (figure 28) association constants could be determined albeit with large uncertainties (70%-90%, table 8). The small proton shifts and limitations in the instrument sensitivity are likely causes. The corresponding goodness of fit tests (table 8) further supports that statement as the $\overline{R}^2$ values are high (>0.92) but χ_{red}^2 indicates a considerable error component for all three protons.
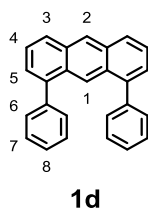
Picture 28. *Structure and numbering of sensor* **1d***.*

Proton	K_s [M^{-1}]	Observed runs	Upper and lower limit of runs	$\overline{R}^2$	χ_{red}^2
1	1.78±1.25	3	2,--	0.990	0.05
3	2.03±1.57	5	2, --	0.981	0.08
4	4.23±3.80	3	Not defined	0.928	0.48

Table 8. *Summary of the fitting procedures of the self-association with sensor* **1d***.*

Accordingly, these K_s values are weakly defined and no self-association was detectable for sensor **1d** over the range of the experiment. The diminished statistical basis of the determined K_s values mirrors the small proton shifts in the dilution experiments. Combining the observed absence of self-association in large parts of the molecule with

the observed absence of self-association in protons 1, 3 and 4 over most of the tested concentration range, it is concluded that the shifts observed in the remaining concentration range are unlikely to originate from dilution. The association constants in this case are therefore considered a mathematical artifact, because the concentration-dependent proton shifts scattered within the range of the measurement uncertainty of the instrument used.[65] Thus, self-association of sensor **1d** can be ruled out as competing factor in host-guest titrations between molecule **1d** and DNB.

In the case of sensor **1h**, no signs self-association was found; the shifts for every proton remained constant in the tested concentration range (0.04 mM to 5.5 mM). The highest concentration tested is not very high but it is five times higher than sensor concentrations in the complexation studies (cf. chapter 3.1). Either sensor **1h** does not measurably self-assemble in the concentration range of interest or it does it so readily that monomer formation is negligible at 0.04mM, which is unlikely. Even if self-association of sensor **1h** had a negative impact on its complexation performance with DNB, it is too small to be detected in the (constant) concentration used in complexation measurements and can be discarded as significant factor in guest-complexation.

A self-association effect was measured in the case of sensor **1j** (table 9 and picture 29).
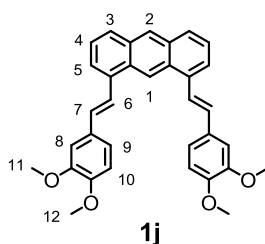

Picture 29. *Structure and numbering of sensor* **1j**.

110

Proton	K_s [M^{-1}]	Observed runs	Upper and lower limit of runs	$\overline{R}^2$	χ^2_{red}
1	1.25±0.31	4	2, 9	0.998	0.73
2	1.04±0.11	6	2, 9	0.999	0.13
3	0.98±0.11	4	2, 9	0.999	0.08
4	0.97±0.12	6	2, 9	0.999	0.07
5	1.15±0.39	6	2, --	0.997	0.40
6	0.91±0.13	6	2, 10	0.999	0.07
10	0.73±0.12	6	2, 10	0.999	0.07
11	1.00±0.50	5	2, --	0.995	0.20
12	0.22±0.19	6	2, 10	0.999	0.04

Table 9. *Summary of the fitting procedures of the self-association with sensor* **1j***.*

With the exception of protons 11 and 12 the uncertainties are reasonably small. χ^2_{red} is larger than in the host-guest titrations for all protons (cf. table 7) with proton 1 having the highest value of 0.73. Over the concentration range tested (0.25 mM to 13 mM) shifts changed with an average of about 0.05 ppm. The χ^2_{red} values for molecule **1j** can therefore be interpreted as an indication for reduced self-association.[65]

The determined self-association constants K_s are comparable to the measured association constants K_a of **1j** with DNB. Although the two processes (stacking of sensor **1j** with DNB and self-association of **1j**) show low K_a and K_s values respectively and are very similar, the processes they describe are in interplay with each other. Hence, the determined association constants K_a for sensor **1j** from section *2.6.3* are apparent association constants K_{app} rather than association constants K_a and describe more than the association between monomers of **1j** and DNB. Two scenarios are discussed here.
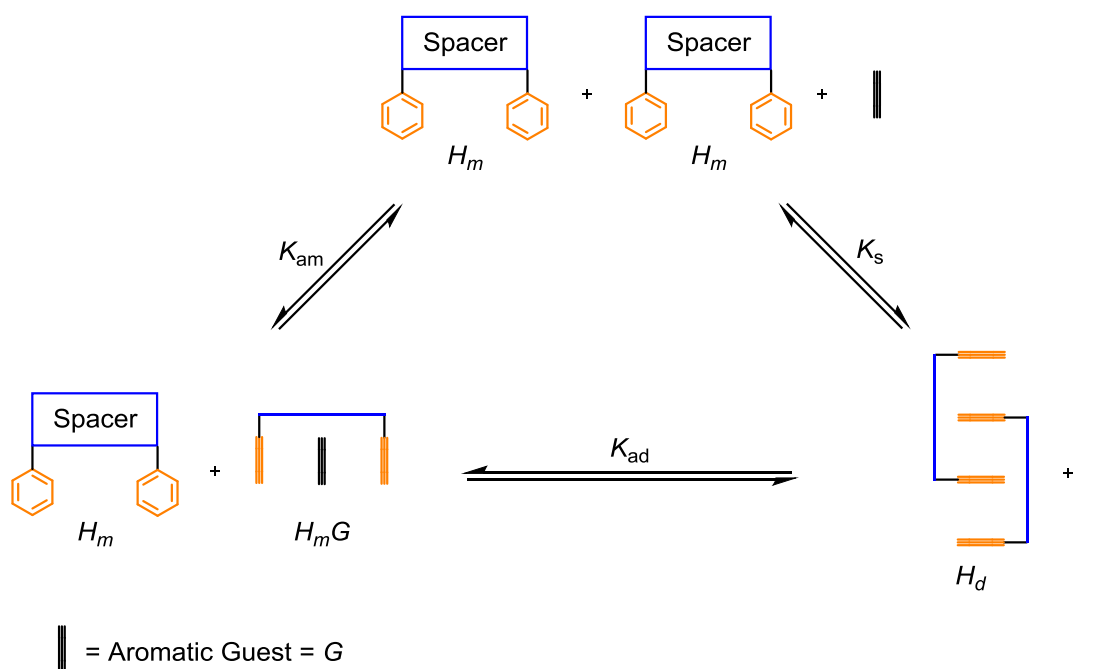
Picture 30. *Thermodynamic cycle of host-guest-titrations allowing monomer (*H_m*)- and dimer (*H_d*)-complexation of the host with an aromatic guest (*G*) to host-guest-complexes (*H_mG*).*

Picture 30 shows a schematic representation of the involved microscopic associations where it is assumed that a) K_s describes the dimerization of sensor **1j**, b) both dimer H_d and monomer H_m are able to form host-guest complexes H_mG with DNB and c) K_a values for **1j** in section *2.6.3* are apparent association constants K_{app} involving and describing all processes shown in picture 30 (and therefore are named K_{app} for the remainder of this section). The microscopic association constants K_{am}, K_{ad} and K_s in picture 30 are defined as follows:

$$K_{am} = \frac{[H_m G]}{[H_m][G]} \tag{28}$$

$$K_s = \frac{[H_d]}{[H_m]^2} \tag{29}$$

$$K_{ad} = \frac{[H_m G]^2}{[H_d][G]^2} \tag{30}$$

Formally, one molecule of monomer H_m binds one molecule of guest G, but two monomers H_m are needed to form one dimer H_d and one dimer H_d binds two guests G, which has been taken into account in equations (29) and (30) by the corresponding exponents.

Following the schematic cycle in picture 30 and equations (28)-(30), K_{am} can also be expressed as

$$K_{am} = \frac{[H_m G]}{[H_m][G]} = \sqrt{\frac{[H_d]}{[H_m]^2} * \frac{[H_m G]^2}{[H_d][G]^2}} = \sqrt{K_s * K_{ad}} \tag{31}$$

Because of fast-exchange, the monomer-, dimer- and host-guest-fractions of sensor **1j** cannot be distinguished spectroscopically and give an averaged signal; in other words, all three association processes are measured simultaneously, resulting in a macroscopic apparent association constant K_{app}. The apparent association constant K_{app} can be written as

$$K_{app} = K_{am} * K_s * K_{ad} = K_{am}^3 \tag{32}$$

Because K_{app} and K_s are known, equation (32) can be used to determine both K_{am} and K_{ad}. By first determining K_{am} with

$$K_{am} = \sqrt[3]{K_{app}} \tag{33}$$

the result can then be used in the determination of K_{ad}:

$$K_{ad} = \frac{K_{app}}{K_{am} * K_s} \tag{34}$$

The results of the described calculations are shown in table10.

Proton	K_{app} [M^{-3}]	K_s [M^{-1}]	K_{ad} [M^{-1}]	K_{am} [M^{-1}]
1	1.14±0.03	1.25±0.31	0.88±0.22	1.04±0.02
3	0.64±0.11	0.98±0.11	0.76±0.17	0.86±0.01
4	0.85±0.03	0.97±0.12	0.93±0.12	0.95±0.02
5	0.86±0.04	1.15±0.39	0.79±0.27	0.95±0.03
10	0.39±0.03	0.73±0.12	0.73±0.14	0.73±0.03
12	0.40±0.03	0.22±0.19	2.47±2.14	0.74±0.03

Table 10. *Determined values of K_{ad} and K_{am} according to the association model in picture 30.*

For protons 1-5, K_{ad} and K_{am} not only show similar values but the values of K_{am} fall into the range of uncertainty of the corresponding K_{ad} values. For the same protons, both K_{ad} and K_{am} differ from the determined K_{app} values by 10%-20% in both directions (positive and negative). K_{app} can be considered a good estimator for K_{ad} and K_{am} and self-association of the host **1j** does not appear to significantly affect the examined host-guest titration in the model shown in picture 30.

For proton 10, K_{ad} and K_{am} are in a similar range, but they both are about twice the determined value of K_{app}. Although all these values are within the same order of magnitude, self-association of **1j** shows a detectable influence on the binding of DNB by sensor **1j** for proton 10.

In the case of proton 12, the determined value of K_{ad} is twice the K_{am} value and six times the value of K_{app}. Although this could point at a substantial influence of K_s, the uncertainty of the latter (and hence the uncertainty of K_{ad}) is very large. When the frontier values K_s as determined by the uncertainty are used, it is found that $1.32 \leq K_{ad} \leq 18.02$. Therefore, while it can be said that in proton 12 dimerization of **1j** as shown in

picture 30 may interfere with the binding of guests, the exact extent is challenging to determine.

In summary, following the proposed model, the effect of self-association of sensor **1j** shows at best negligible effect on protons 1-5, a small effect on proton 10 and a potentially considerable effect (up to two orders of magnitude in association constant values) on proton 12. With protons 10 and 12 being located on the pincers of the molecule and protons 1-5 being located on the aromatic backbone, these findings might point at optimization potential concerning the exact structure of sensor **1j**, but more importantly, they validate the underlying adaptable- tweezers design concept.

2.7.2.2 Model II

In the second case discussed it is assumed that dimers H_d of **1j** cannot directly form host-guest complexes: intuitively, the guest-binding site of the first host-molecule H_m is already occupied by a second host molecule H_m (microscopic association constant K_s in picture 31) and thus, complexation of an aromatic guest G is more likely to occur with the host monomer (microscopic association constant K_{am} in picture 31). Hence, the system in picture 30 simplifies to the system in picture 31.
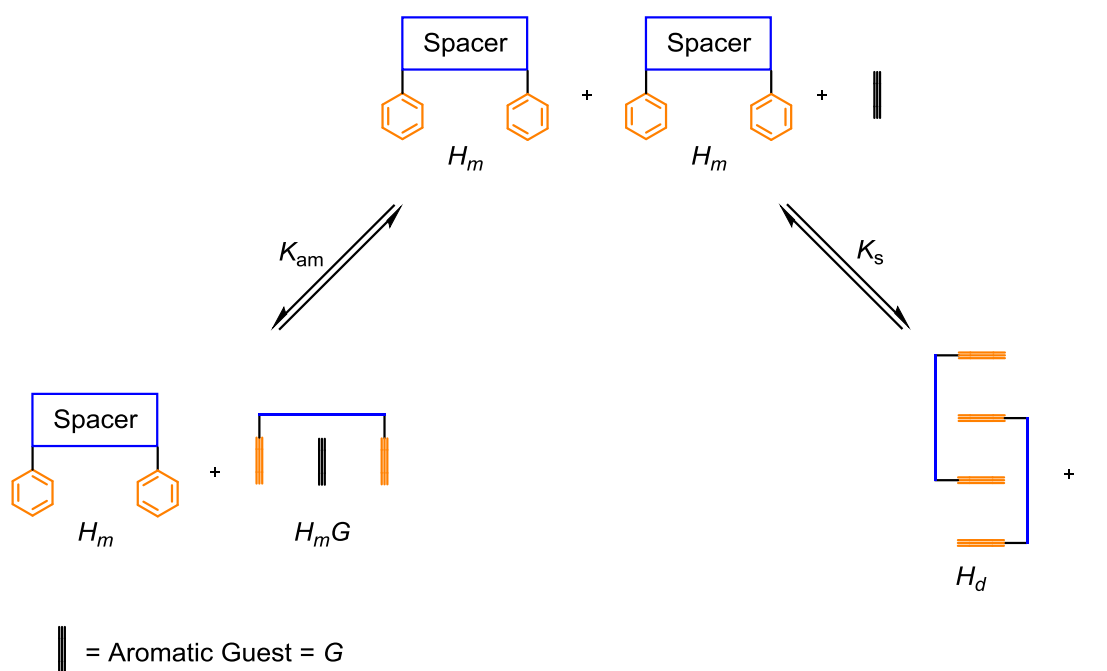
|| = Aromatic Guest = G

Picture 31. *System where only the monomer of the host (*Hm*) may undergo complexation with an aromatic guest (*G*) into host-guest-complexes (*HmG*). Monomer concentration [*Hm*] is also dependent on the self-association of* Hm *into host dimer* Hd*.*

Because equations (28) and (29) are also applicable this simpler case, K_{app} takes the following form:

$$K_{app} = K_{am} * K_s \tag{35}.$$

With K_{app} and K_s known, equation (35) gives direct access to K_{am} (cf. table 11).

Proton	K_{app} [M^{-2}]	K_s [M^{-1}]	K_{am} [M^{-1}]
1	1.14±0.03	1.25±0.31	0.91±0.23
3	0.64±0.11	0.98±0.11	0.65±0.13
4	0.85±0.03	0.97±0.12	0.88±0.11
5	0.86±0.04	1.15±0.39	0.75±0.26
10	0.39±0.03	0.73±0.12	0.53±0.10
12	0.40±0.03	0.22±0.19	1.82±1.57

Table 11. *Determined values of* K_{ad} *according to the association model in picture 31.*

The values from model II are comparable to model I. Again, K_{app} and K_{am} values for protons 1-5 are similar once their uncertainties are taken into account. Although the self-association constants K_s found for these protons are slightly larger than the associated K_{am} values, K_{am} values in protons 1-5 are represented well by K_{app}. For proton 10, K_{am} is about 40% larger than K_{app} and even when including their uncertainties the values are specifiable, albeit by a very thin margin. Host dimerization of **1j** shows a small but discernible negative influence on the complexation of DNB in proton 10, as seen in model I. Similarly, this negative influence is more pronounced or more visible in proton 12. As mentioned, in the case of proton 12 the determined K_s value shows a large uncertainty. Applying its boundary values (0.03 and 0.41) to equation (32), it is found that $0.98 \leq K_{am} \leq 13.3$. Again self-association of the host shows an influence on the association constants K_{am} determined for protons located on the pincers. The uncertainty of K_s for proton 12 makes it demanding to quantify the extent, but one order of magnitude is easily possible. Thus, the general findings using the association model II add to model I. In both models it was shown that the measured apparent association constants K_{app} of sensor **1j** differed from the determined association constants K_{am}/ K_{ad} (model I) and K_{am} (model II) to various degrees. These differences can be assigned to self-association of the host **1j**, which is described by the self-association constant K_s. In model I as well as in model II it was found that for protons 1-5 the effect of host self-association on the formation of host-guest complexes with DNB is negligible. For protons 10 and 12, which (unlike protons 1-5) are not located on the aromatic backbone

of molecule **1j** but on the adaptable styryl-pincers, self-association was found to have a more discernible impact. Starting with model I, K_{am}, K_{ad} and K_s for proton 10 displayed similar values, about twice the determined K_{app} value, which shows that in this case self-association is a measurable factor in host-guest complexation on proton 10. In model II, the situation is comparable and K_{app} does not describe K_{am} properly because of self-association of **1j**. While on proton 10, self-association has a negative effect on guest complexation according to both models and can be described, the determined values for both K_{am} and K_{app} are of the same order of magnitude. On proton 12 this is not necessarily the case. In model I, the determined K_{app} is half of K_{am} and one fifth of K_{ad}. Although these results have some ambiguity because of the large uncertainty of the K_s value, calculations with the boundary values of K_s indicate that self-association of **1j** lowers host-guest complexation by one order of magnitude easily. In model II the results are comparable. The K_{am} values based on the boundary values of K_s are not quite as much larger than K_{app} as in model I, particularly for the lower boundary, but they complement the findings from model I.

An interesting point is that according to model I, the determined K_{ad} and K_{am} values of protons 10 and 12 suggest that host-guest complex formation from the host dimer is, as a process, favored over complex formation of the monomer ($K_{ad} > K_{am}$).

In terms of molecular design, finding increased influence of host self-association on guest-binding on protons located on the styryl-pincers compared to protons of the backbone, it can be said that the exact structure of **1j** is not optimized, also in view of the determined association constant values K_{app}, K_{am} and K_{ad}. But it must also be emphasized that it validates the underlying molecular design concept of the molecule: rotatable pincers that, together with a backbone, form adaptable molecular tweezers able to host aromatic guests.

In short, it was found that for sensors **1c** and **1h** self-association does not measurably interfere with guest binding. In the case of sensor **1j** an effect was found in parts of the molecule. The effect is hard to quantify, but it is possible that host-aggregation lessens guest-complexation by a whole order of magnitude. But it is also found that the general molecular design behind sensor **1j** is validated by these results.

2.8 Interpretation

2.8.1 General

Table 12 gives a summary over the measured association constants and the gap sizes in molecular tweezers **1c** – **1j**.

Molecule	K_a [M^{-1}]	Gap Size [Å][a)]
1c	21.5±1.31	4.7-4.9
1d	0.35±0.09	5.0-5.5
1e	0.43±018	5.0-5.8
1f	0.25±0.02	5.1-6.5
1h	0.07±0.05 M^{-1} to 1.75±0.46	6.1-6.8
1i	0.47±0.05 to 2.7±0.31	2.5-7.3
1j	0.38±0.03 to 1.14±0.27	2.5-7.3

a) measured in the ground state equilibrium geometry calculated on the B3LYP/6-31G* level.

Table 12. K_a values towards DNB and gap sizes of sensors **1c-1j**.

Roughly, the association constants can be divided into three groups. Xanthone **1c** has the highest value, followed by **1h**-**1j** which show considerable distributions of values, and values of **1d**-**1f** are the lowest. Each of these three groups differs by roughly one order of magnitude for the averaged (**1c**-**1f**) or highest measured values (**1h**-**1j**). In terms of gap size, the data displayed in table 10 does not follow any clear trend. The molecules synthesized in this work possess different backbones/spacers but they are structurally similar because of their spacer-tweezer buildup. The smaller the gap the closer the clips are brought together and the more their rotation is restricted. If rotatable bonds are rigidified upon binding, the entropic cost associated with the conformational state selection of a binding event may lower binding strength. In more rigid structures the entropic cost of binding is minimized by conformational restrictions, because only a few conformations are allowed before binding.[66-69] In similar systems, Zimmerman *et al.* showed that for every frozen single-bond rotation (before association with a guest) the

association constant increases by a factor of 4.[70] According to Cram, preorganized hosts are structurally set for low solvation and binding prior to complexation.[71] High entropic loss is often associated with strong binding and vice versa.[72] It is safe to say that the distance between the clips largely determines the degree of their rotation and therefore the overall rigidity of molecules 1c-1j. Rigid molecules or molecules with high rotational barrier of the clips can be considered having paid a part of entropic cost of binding already during synthesis.[67] Therefore gap size not only determines whether binding in the cleft takes place but plays an integral part in sensor preorganization.

Picture 32 shows the optimized geometries of sensors **1c**-**1j** and their electrostatic potentials on the van der Waals surfaces on the B3LYP/6-31g[*] level. Because of their –I effect, alkoxy-substituents rather increase the electrostatic potential on the rings they are attached to.[73] Concerning gap size and preorganization, the qualitative comparison of the calculated surfaces of the sensors with the association constants found earlier allows for the observations in the following section.
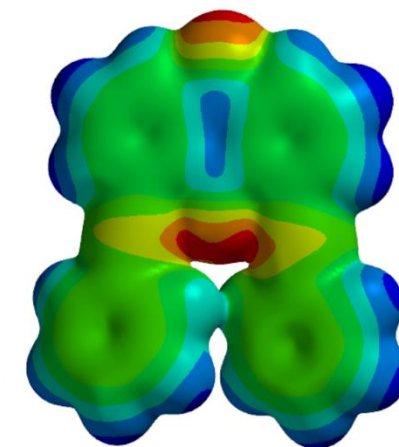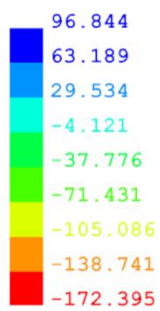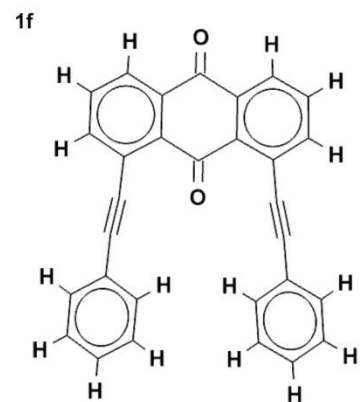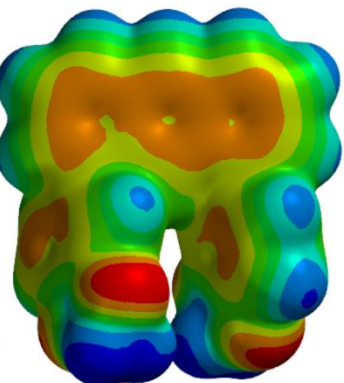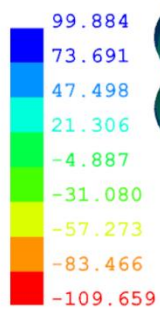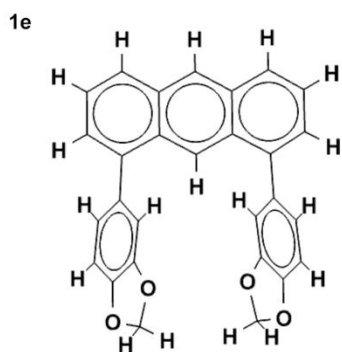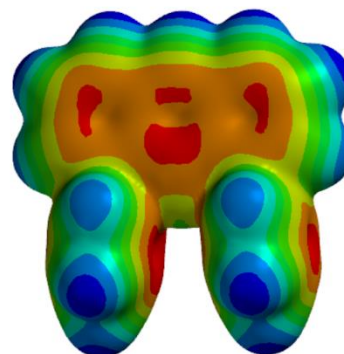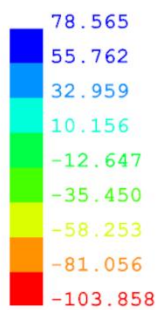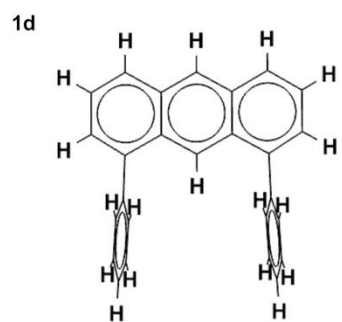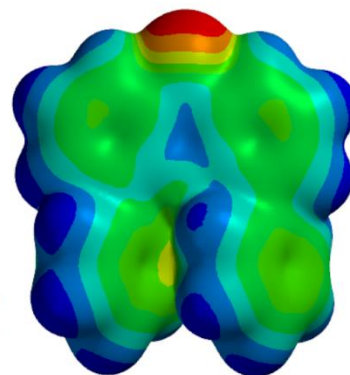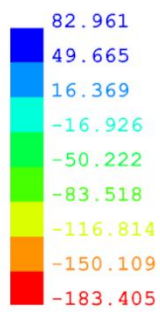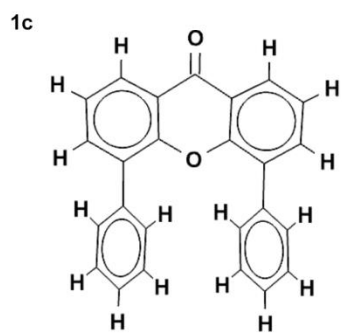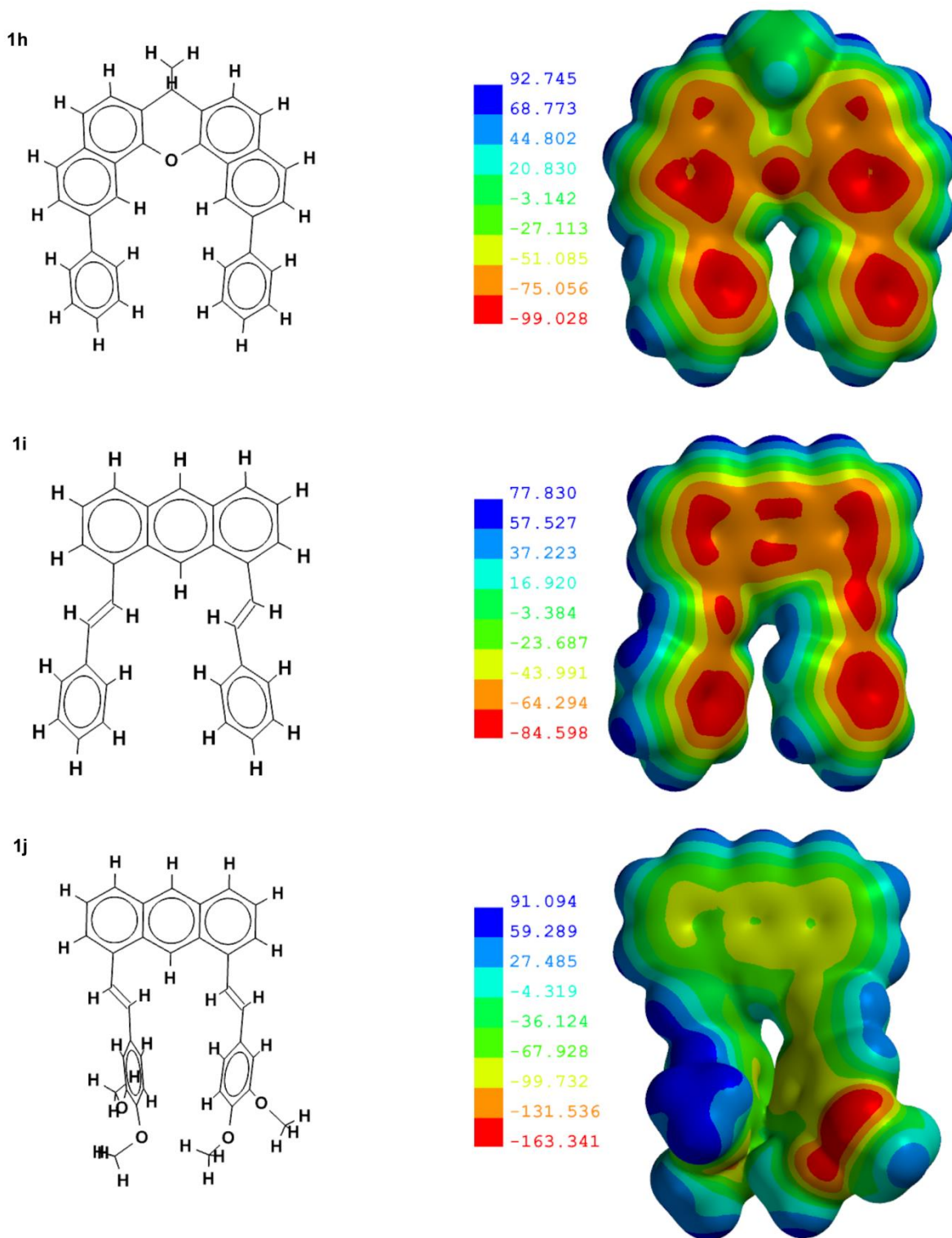
Picture 32. *Optimized geometries of sensors **1c**-**1j** (left) and their electrostatic potential laid on the van der Waals surfaces (right) on the B3LYP/6-31g* level. The legend in the middle shows the colour code of the electrostatic potential in [kJ/mol].*

122

The calculated ground-state structure of xanthone **1c** not only has the smallest gap size (between 4.7 Å and 4.9 Å) but also showed the most response towards DNB in the titrations. The van der Waals surface of xanthone **1c** shows that the clips are ordered in offset-parallel fashion to each other and their van der Waals clouds overlap, indicating interaction between the clips. This likely reduces free rotation of the clips and renders the whole structure more rigid.[69, 74] As a consequence, loss of entropy upon complexation is probably much smaller for xanthone **1c** than for molecules where no interaction between the clips is indicated in their equilibrium geometry in the ground state. Even if binding of DNB to xanthone **1c** is weak, enhanced rigidity of the molecule would result in more favorable binding between **1c**.[66-72] Direct interaction of the clips also indicates that binding does not occur in the gap. Also, the small range of the determined association constants for the single protons in xanthone **1c** suggest not enough gap width between the clips for the complexation of DNB between the tweezers.

The calculated gap size in sensor **1h** is between 6.1 Å and 6.8 Å, which in principle is large enough to host aromatic guests. No interaction between the clips is indicated which, due to the bigger gap size, may increase rotational freedom in sensor **1h**, thereby increasing entropic cost of conformational selection and decreasing binding strength.[66-72] The distribution of the association constants measured in **1h** suggests binding of DNB in the gap. Possible reasons are discussed below.

Gap sizes are difficult to determine in molecules **1i** and **1j**. Because of the styrene clips both **1i** and **1j** are more rotatable and less rigid than **1c**-**1h**; although loss of entropy upon bonding increases with the number of rotatable moieties, these losses in entropy might be made up for by better adaptivity/preorganization of the molecules.[75] In the calculated structure the gap size ranges from 5.0 Å to 6.5 Å in **1i** and 4.5 Å to 5.8 Å in **1j**. The conformational change to accommodate a guest should be small. In **1j** the calculated structure suggests interaction between the substituents on the clips which would pose an additional energetic barrier to overcome. As observed for **1h**, binding in the gap is suggested for both **1i** and **1j** by considering the association constants measured for different protons.

Sensors **1d** to **1f** showed the smallest association constants. As general observation these three sensors also showed very narrow distributions in the measured K_a values.

The gaps in **1d** and **1e** are rather small to host aromatic guests (5.0-5.5 Å in **1d**, 5.0-5.8 Å in **1e**). Compared to xanthone **1c**, anthracenes **1d** and **1e** might be slightly less rigid because of their larger gap sizes. The calculated structures do not indicate interaction between the aromatic clips. In terms of gap size and rigidity it can be said that molecules **1d** and **1e** are more similar to xanthone **1c** than the other molecules in this work. Nevertheless association constants in **1c** are two orders of magnitude higher. Possible reasons for this discrepancy are discussed in the following sections. But like in molecule **1c**, distribution of the association constants of **1d** and **1e** reflects the unfavorable gap size of both sensors.

The calculated structure of **1f** shows that the aromatic clips are not preferably ordered face-to-face to each other but in the same plane. But in solution it is likely all rotamers are populated in the ground state because in aryl-acetylene bond conjugation dependency between the angle of the two moieties and conjugation is negligible.[76] Also, the calculated HOMO frontier orbitals suggest that the molecule can be considered as two independent OPEs (picture 32). The binding of aromatic guests between the clips or even on one of the acetylenic arms would therefore greatly reduce internal rotation.

The main forces behind π-π interactions are introduced in chapter 1. With the basic structural features of molecules **1c**-**1j** laid out, in the following section it is discussed how these features might influence the forces behind π-π interactions in these molecules. The analysis in sections *2.8.2* and *2.8.3* refer to the measured association constants from the titrations of sensors **1c**-**1j**. Although self-association of sensor **1j** was found to have a measurable influence on its guest-binding behavior, its extent could not be put in numbers and the following analysis should not substantially suffer.

2.8.2 Electrostatics

Following the findings of Hunter and Sanders and the results of Siegel and Cozzi, if π-π interactions are governed mainly by electrostatics, they become more favorable with increasing electron-deficiency in both molecules. Decreasing electron density in both stacking partners has been shown to increase aromatic interactions because relative absence of electrons indicates higher electrostatic potential.[74, 77-79]

On the right side of picture 32 the electrostatic surface potentials of the geometry-optimized sensors are displayed. The values given for the electrostatic potentials in picture 32 alone do not allow drawing conclusions concerning the sensing performance of molecules **1c**-**1j** because topological features and the distribution of the potentials in the molecules are not accounted for. Additionally, the color codes are relative within a specific molecule and not applicable to other molecules.[80] If the electrostatic surface potentials are displayed in a way where the values are solely divided into positive/negative potential, the influence of the gap on electrostatic interactions may be discussed more conveniently. Picture 33 is similar to picture 32, with the difference that on the right side the electrostatic potential surfaces are standardized such that blue regions have an electrostatic potential bigger than 1 and red regions have an electrostatic potential smaller than -1.

1c
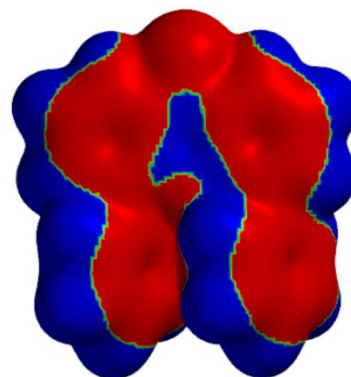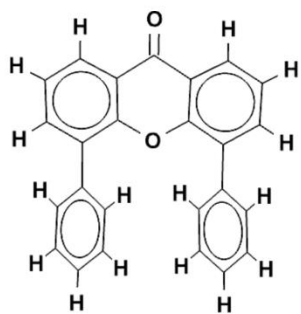
1d
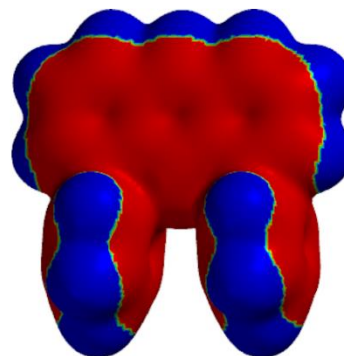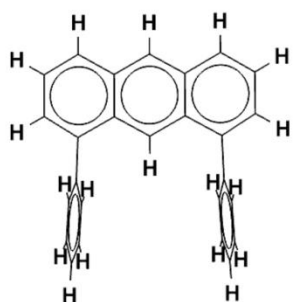
1e
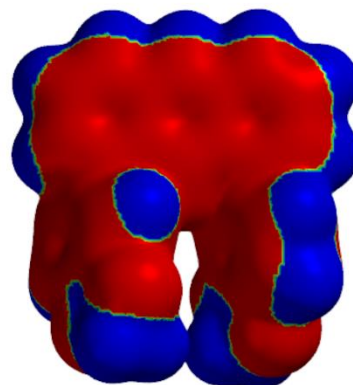
1f

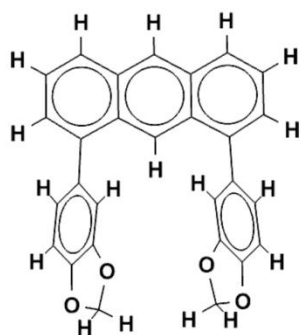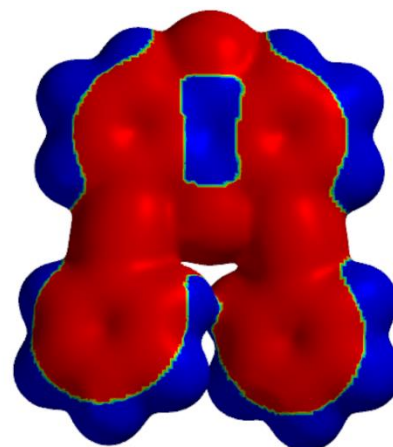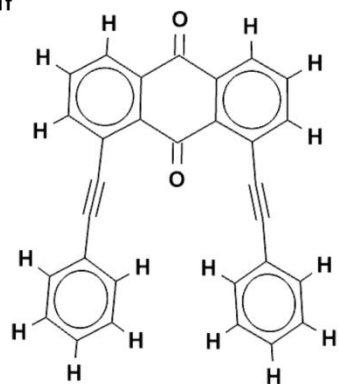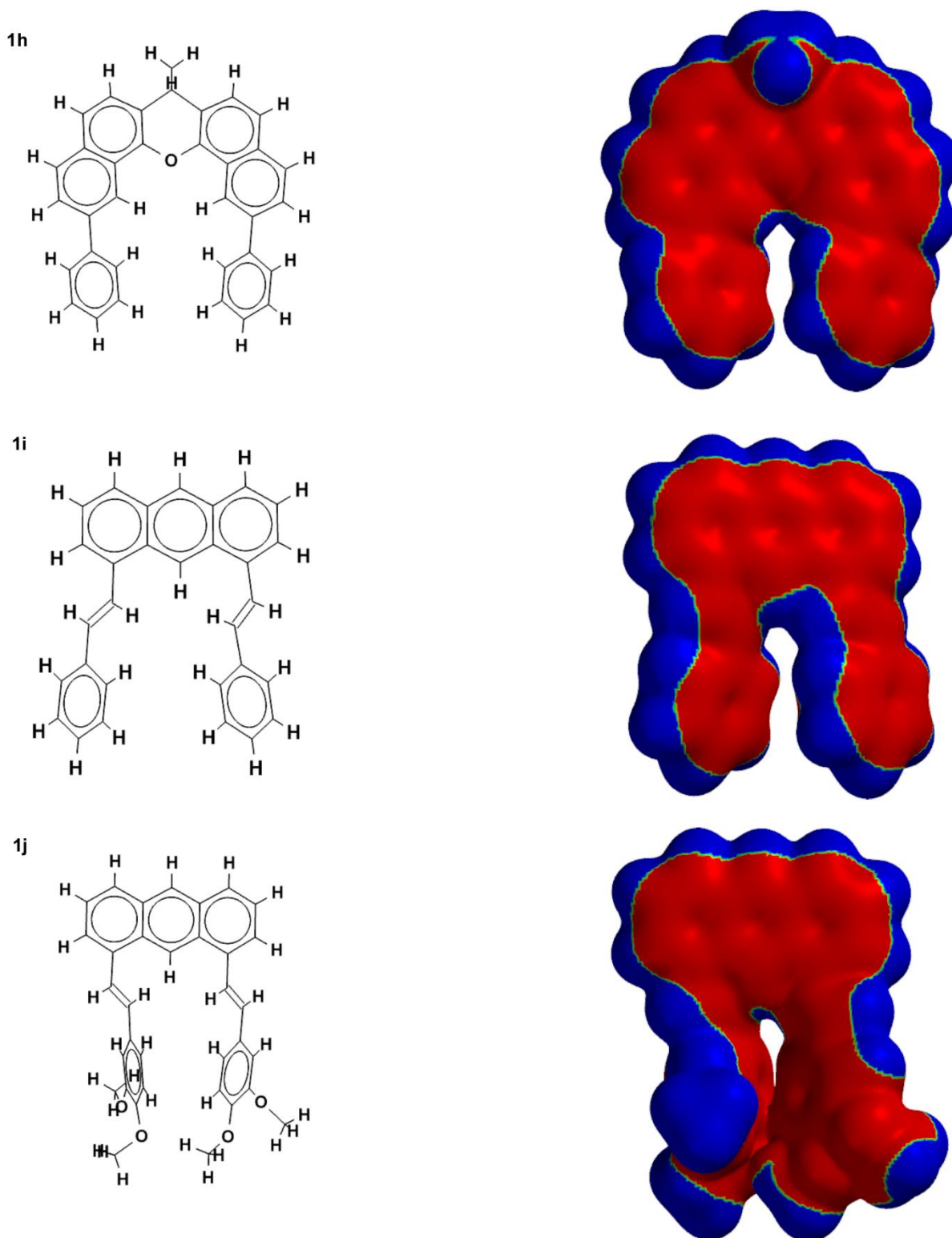**Picture 33.** *Optimized geometries of sensors **1c-1j** (left) and their electrostatic potential laid on the van der Waals surfaces (right) on the B3LYP/6-31g* level. In blue regions electrostatic potential ≥1 and in red regions electrostatic potential ≤-1.*

127

Table 13 shows the measured association constants of sensors **1c**-**1j** and the calculated van der Waals surfaces showing negative electrostatic potential in [%].

Molecule	K_a	negative potential surface [%]
1c	21.5±1.31	52
1d	0.35±0.09	58
1e	0.43±018	58
1f	0.25±0.02	58
1h	0.07±0.05 M^{-1} to 1.75±0.46	55
1i	0.47±0.05 to 2.7±0.31	55
1j	0.38±0.03 to 1.14±0.27	54

Table 13. *Association constants of sensors **1c**-**1j** and corresponding calculated van der Waals surface areas displaying negative potential in [%].*

According to table 13 (and by ignoring all other possible factors), a drop of one order of magnitude of the (highest) K_a values measured in this work is accompanied by an 2-3% increase of negative potential surface. It is possible that in solution the situation is different and it is also assumed that the potentials are equally distributed over the molecule and constant, but the correlation between molecular properties and association constant may allow for further insight.

Xanthone **1c** showed the largest response in the titrations with DNB and no measurable response towards benzonitrile. Apart from the carbonylic C=O bond in the xanthone spacer the electrostatic potential a largely uniform positive potential was calculated along the edges (pictures 32 and 33). Nitrile-substituents have a smaller inductive effect than nitro-groups, which delivers an electrostatic explanation for the low response of **1c** towards benzonitrile, which is in accord with the findings of Siegel and Cozzi; the offset-stacking configuration of the interacting clips is conforming to the Hunter-Sanders model.[74, 77] When partitioning the electrostatic surface potential into positive/negative

potential domains (picture 33), roughly 50% of the surface has a positive electrostatic potential. The rigidity of xanthone **1c** probably optimizes electrostatic interactions insofar as it minimizes entropic cost upon association with DNB.

In naphthaxanthone **1h** the largest association constant is one order of magnitude smaller than in xanthone **1c**. The electrostatic potential as calculated is half of **1c** on the negative end but about 10% higher on the positive maximum. Although this would point at a higher average value and therefore more favorable electrostatic binding features, when partitioning the potential surface into the same positive/negative domains like before it is seen that the surface area displaying negative potential is about 3% higher than in **1c**.[77] The enlarged gap size could render the entropic cost of association very high due to the enhanced rotation of the aromatic clips; electrostatic interactions could also be very dependent on available surface area. Such a dependency was shown for proteins but is hard to put in numbers. [81]

Concerning calculated electrostatic properties styryl **1i** is more comparable to **1h** than to **1c**. Not only are their upper and lower boundaries similar but more importantly also their ratios of surface area with negative electrostatic potentials. Because the linkers in **1h** are twofold rotatable, the gap size upon binding is not known at this point. In terms of preorganization the question arises how the interplay of the two styryl arms compensates the possible entropic disadvantage of 4 rotating bonds compared to only two in **1h**. It is possible that entropy losses are compensated through optimized geometry of association of DNB with the clips.[72, 82]

The calculated electrostatic potential surface in molecule **1j** suggests lower minimum and higher maximum values than in **1i** with the lowest potential located on the oxygen atoms of the methoxy-substituents. The effect of the indicated intramolecular interaction between the two adjacent clips on the overall electrostatic conditions is not quantifiable. The association constants determined for **1j** and DNB imply relative preference for association in the gap compared to the spacer. Under the assumption of complexation of DNB between the two clips the electrostatic potential distribution over molecule **1j** would probably become more evenly distributed (due to the breaking of the interaction between the clips and the subsequent geometric changes in the linker) and its values become more similar to **1i**. The negative potential surface area is comparable to **1i** and **1h**, but

because of the calculated intramolecular interaction this value may be subject to change upon complexation. But the additional methoxy-substituents did not enhance the association of **1j** with DNB compared to **1i**, although sensors **1i** and **1j** may be electrostatically different on the calculated level, attributable to the methoxy substitutents in **1j**. In the ground state Mulliken-like charge-transfer interactions do rarely contribute significant stabilization to π-π interactions, hence the methoxy substituents would exert their influence through the –I effect.[74] But the rotatable methoxy-moieties might impose additional steric constraints towards association and counteract possible electrostatic advantages **1j** holds over **1i**. For the molecules in this work, so far the size of negative or positive electrostatic potentials appear to be less important in numerical value than in relative surface area.

This last claim is supported by equivalent considerations for sensors **1d**-**1f**.

Topologically, anthracenes **1d** and **1e** are the closest to xanthone **1c** compared to the other sensors in this work. The association constants of the former two towards DNB can be deemed identical but they are two orders of magnitude smaller than the association constant of the latter. The gaps in **1d** and **1e** are slightly larger than the gap in **1c** but do not host aromatic guests, as indicated by the association constants for the observed protons in the titrations with DNB. The calculated electrostatic potentials (picture 32) propose widening of the range of the potential in both directions in substituted sensor **1e** compared to unsubstituted anthracene **1d**, as seen in styryls **1i** and **1j**. The range of the electrostatic potential in molecule **1d** is narrower in both directions compared to xanthone **1c** while anthracene **1e** shows both a higher maximum and a higher minimum value towards **1c**. The (theoretical) electrostatic differences between anthracenes **1d** and **1e** do not seem to have much influence in the titrations. Electrostatically, the link between anthracenes **1d** and **1e** also constitutes the main difference between these two molecules and xanthone **1c**- the ratio of the electrostatic potential surface possessing negative potential, which is 58% for both anthracenes **1d-e** and 52% for molecule **1c**.

According to the overall association constant, anthraquinone **1f** belongs to the same group as **1d** and **1e**. Its calculated electrostatic potential surface boundary values are best comparable with **1c**. The overlap of the clips indicated in the calculated structure is

very small and rotation of the benzene-acetylene bonds is assumed. Numerically, molecule **1f** showed the lowest K_a values but they essentially identical to **1d** and **1e**. No preference for complexation in the gap over the spacer or vice versa is discernible and association of DNB over the whole surface of sensor **1f** is probable. With the largest calculated electrostatic potential boundary value difference (followed by xanthone **1c**), 58% of the total surface possesses negative electrostatic potential. If loss of rotation of the clips in the presence of DNB was the main reason for the low K_a values, higher values would be expected for the protons in the backbone than in the clips. From an entropy-enthalpy compensation view, rotation of the clips in the presence of DNB might as well be considered as a sign of weak electrostatic preconditions between sensor and analyte rather than a major limiting factor.[68, 72]

Of course the different gap sizes, spacers and numbers of rotating moieties in all these molecules may result in different association modes and changes in entropies through association may not be equally important throughout; plus, these values are averaged over the whole molecules. But the correlation is interesting.

2.8.3 Van der Waals Dispersion Forces

The importance of dispersive van der Waals-interactions in stacking interactions is under discussion in the literature. Whereas calculations propose dispersion interactions as main interaction, in solution they are often considered minor.[74, 77, 83-89] However, several authors tried to quantify the gain in stability in aromatic interactions in relation to the number of interacting aromatic rings experimentally as well as theoretically.[90-95] In calculated and surface experiments, Wagner *et al.* showed that the degree to which the size of the aromatic molecule determines the strength of dispersive interactions depends at least linearly on the number of carbon atoms in each interacting molecule; this is attributed to the increasing deconfinement of the π-electrons in larger aromatic systems.[90] Thus, dispersive interactions are expected to become increasingly important in larger aromatic systems. In order to explore this dependence, the HOMOs of sensors **1c-1j** are calculated. Despite the fact that dispersion forces include all electrons and a HOMO contains only two electrons, the actual size of the aromatic system should be

reasonably approximated with the HOMO electrons, the decisive question being whether and to what extent the clips are in conjugation with the aromatic backbones. Therefore, in a fully conjugated sensor the contribution of dispersive interactions is expected to be higher than in a similar sensor with little or no conjugation between the moieties. With up to potential 20 additional interacting atoms in the clips dispersion could potentially greatly influence association strength.

The calculated HOMOs of molecules **1c**-**1j** are shown in picture 34.

1c

1d

1e

1f

1h

1i

1j
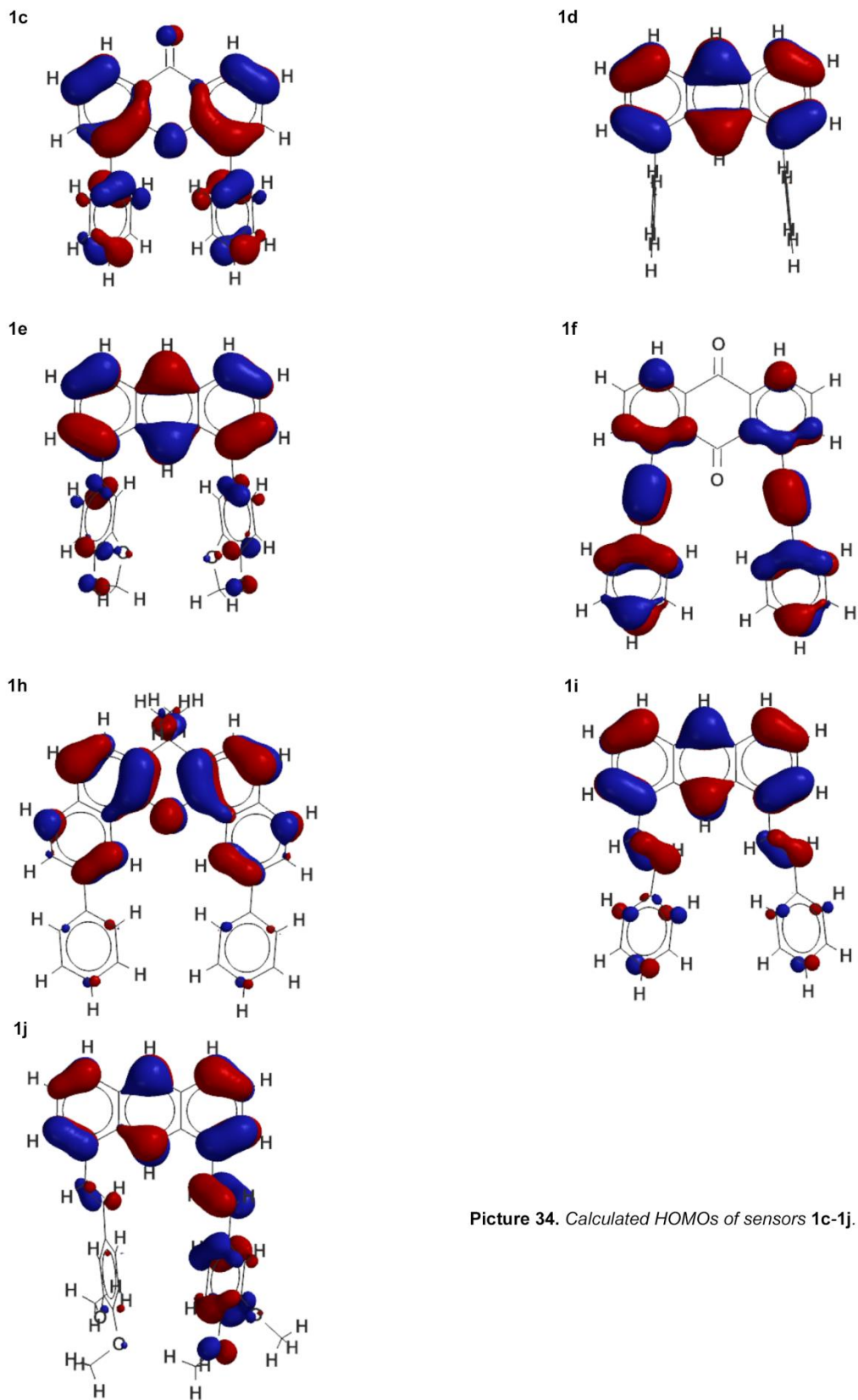
Picture 34. *Calculated HOMOs of sensors* **1c-1j**.

133

In xanthone **1c** the calculated HOMO indicates conjugation over the whole molecule, again pointing at the postulated rigidity of the molecule. The strength of dispersion forces between xanthone **1c** and DNB should therefore be bigger than in xanthone or benzene alone.[90, 95] Analogous to electrostatic interactions, the relative strength of the interactions would be dependent on inherent structural features of sensor **1c**. The strength of the dispersive interactions relative to electrostatics cannot be determined because **1c** also has the most favorable electrostatic predispositions for stacking with DNB and the association constants of protons 1-6 are very similar across xanthone **1c**. Apart from the fact that it probably does not sandwich DNB, xanthone **1c** shows the best preorganization towards association with DNB of the molecules in this series.[96, 97]

Contrary to **1d**, anthracene **1e** shows slight conjugation between the aromatic clips and the aromatic spacer in the HOMO, which may be due to the +M effect of the substituents on the clips.[98] This would point at stronger dispersive interactions with aromatic guests. However, it is not translated into notable differences between the association constants of **1d** and **1e**. Not only are the averaged association constants for the measured protons in both molecules largely identical, but in both cases the distribution of the measured single values does not allow to determine a preference of DNB for association to the spacer or to the aromatic clips, speaking against notable influence of dispersion forces in these systems. At this level of theory, electrostatic shortcomings in sensors **1d** and **1e** are far more suitable to explain their low response towards DNB than diminished dispersive interactions.

According to the calculated HOMOs, **1f** can be considered as two independent OPEs. The number of atoms per binding interaction is the lowest and accordingly to the model applied, dispersion interactions are expected to be the lowest for this molecule. No conclusions regarding the relative importance of dispersion towards eletrostatics are drawn because **1f** also displayed the most unfavorable electrostatic preconditions and the lowest association constants of the molecules in this work.[74, 77]

In napththaxanthone **1h** the calculated HOMO is mainly located on the spacer and conjugation extends only slightly into the benzene clips in the equilibrium conformation. Upon association with DNB, the torsion angle between the spacer and the clips and hence conjugation between the two would at best stay the same. The association

constants of the protons suggest preference of complexation of DNB on/between the benzene clips over the spacer. As was the case for anthracenes **1d** and **1e**, the role of dispersion forces in the system examined seems to be very small.

Apart from being dependent on the exact conformation of the free and bound sensors, in styryls **1i** and **1j** dispersive interactions alone between the sensors and DNB likely cannot account for differences in association constants. In **1i** the HOMO extends over the backbone and the styryl linker moieties as well as over the benzene clips, but conjugation with the latter is diminished. In **1j** the HOMO is located on the backbone, one of the linkers and the attached clip while on the other linker and clip the HOMO is only partially present. This may be due to the mentioned interaction of the second clip with the first one. If it is assumed that upon binding between the clips the HOMO extends to both clips equally, higher K_a values would be expected for molecule **1j** than for **1i**. But because they are at the best the same, if not higher in **1i**, it is concluded that dispersion forces are of less influence than electrostatics in **1i** and **1j** as well.

The conclusion that π-π interactions in molecules **1c-1j** are mainly governed by electrostatic factors is in accordance with the models proposed by Hunter and Sanders and Siegel and Cozzi.[74, 77]

However, it has also been shown that the size of aromatic systems can greatly influence the strength of π-π interactions.[83, 84, 87, 99-101] In order to exert this influence a minimal size would be required as this size effect is additive with the number of involved atoms. This could offer the possibility to build optimized structures where clip size and clip electronics not only yield favorable electrostatic and dispersive preconditions but also promote rigidity and suitable preorganizational features.

The role of solvent was explicitly left out. Because the nature of the solvent influences association greatly, some aspects are nonetheless described here.[66, 69, 102-105] It was reported that bulky solvents such as chloroform can favor association in molecular tweezers because the solvent molecules may be too large to fit into the cleft, leaving parts of the sensor molecule undissolved. The binding of aromatic guests in the cleft would amount to solvation of these parts, thereby promoting association.[96] Also, poor solubility of the guest results in the solvent would result in the same effect, although for

the exactly reverse reasons, as long as association of guest with the host is more favored than self-association of the guest.[74] The polarity of the solvent employed also can change the order of magnitude not only of the association constant of interest but also of the degree to which electrostatic and dispersive forces contribute to the binding event.

2.9 Synthesis towards other Sensing Principles

2.9.1 Watersoluble Sensor

Titrations of sensors **1c**-**1i** revealed low K_a for the complexation of 3,5-DNB or PhCN indifferently of the gap size between the arylic clips and their substitution. Compounds such as TNT and DNB are slightly water-soluble. 4,4'-(anthracene-1,8-diyl)dibenzoic acid **44** should be watersoluble under alkaline conditions through the formation of its dibenzoate. The gap between the clips is thought to provide a hydrophobic pocket. Upon deprotonation, the resulting negative charge between the carbonylic oxygen atoms should render the aryl-clips slightly electron-abundant.[106]
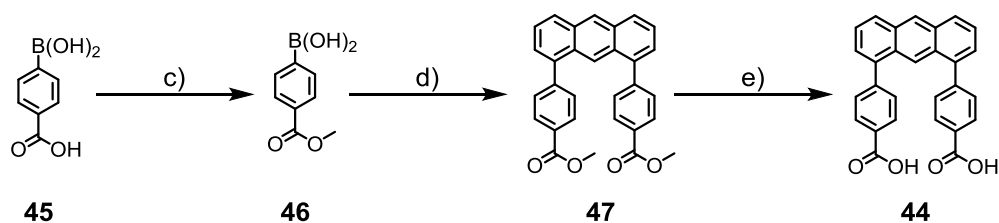
2.9.2 Synthesis

The synthetic strategy is identical to the strategy used in the synthesis of compounds **1d** and **1e** (scheme 23).
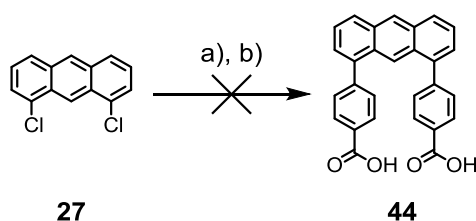
a) 4-carboxyphenylboronic acid, Pd(PPh$_3$)$_4$, Cs$_2$CO$_3$, Toluene, 110°, overnight
b) 4-carboxyphenylboronic acid, Pd(Amphos)Cl$_2$, Cs$_2$CO$_3$, Toluene, 110°C, overnight

Scheme 23. *Attempted synthesis of sensor* **44***.*

First it was tried to couple 4-carboxyphenylboronic acid **45** directly with 1,8-dichloroanthracene in a double Suzuki-reaction. Both Pd(PPh$_3$)$_4$ as well as Pd(amphos)Cl$_2$, which is a more suited catalyst in the Suzuki-reaction with aromatic chlorides, were tried in the Suzuki- coupling of 4-carboxyphenylboronic acid **45** to dichloroanthracene **27**.[41] No reaction was observed in both cases. The carboxylic acid moiety in 4-carboxyphenylboronic acid is easily deprotonated and the resulting carboxylate might interact with the Pd(0) catalyst in the reaction.[107] Also, carboxylic acids and boronic acids are known to interact with each other;[108] and arylboronic acids with electron-withdrawing groups can be prone to deboronation.[109] Therefore boronic acid **45** was converted into its methyl ester **46**. The subsequent Suzuki-reaction with 1,8-dichloroanthracene **27** yielded dimethyl 4,4'-(anthracene-1,8-diyl)dibenzoate **47** in 60% yield. Treatment of benzoate **47** with KOH yielded 4,4'-(anthracene-1,8-diyl)dibenzoic acid **44** quantitatively (scheme 24). However, compound **44** was insoluble in D$_2$O and NaOD in the measurable concentration range of ^{1}H NMR spectroscopy. Insolubility of sensor **44** was also observed in H$_2$O, 1M aq. NaOH and 1M aq. KOH solutions. Aggregate formation is likely, given that molecule **44** consists of two hydrophilic clips and a hydrophobic backbone.


c) SOCl$_2$, MeOH, 50°C, 3h, quant. d) 1,8-dichloroanthracene, Pd(Amphos)Cl$_2$, Cs$_2$CO$_3$, toluene, 110°C, overnight, 60% e) KOH, THF/H$_2$O (5:1), rt, 5h, quant.

Scheme 24. *Synthesis of sensor* **44**.

2.9.3 Synthesis towards a Sensor-Functionalized Surface

In the absence of an electromagnetic field, electric dipole moments in a material or sample of polar molecules are randomly oriented and the apparent electric dipole of the system is zero. When irradiated with microwaves, the dipoles align in the direction of the field and an oscillating electric dipole polarization is induced in the molecular ensemble.[110],[111] Because they are rotating in phase with the applied field, the dipoles (and hence the molecules) have to rotate faster when the frequency of the field is increased. Ultimately, reorientation of the dipoles will stay behind the frequency of the applied field and molecular rotation cannot keep up with the field's frequency.[112] Similarly, if the field is turned off the molecules do not fall back in random orientations straight away but only after a certain time (usually in the picosecond range). This time is called relaxation time τ.[113] Relaxation times are influenced by several factors, notably molecular structure and the ability of the compounds to interact intermolecularly and/or intramolecularly (such as hydrogen bonding). It has been shown that phenols and substituted phenols undergo intermolecular and intramolecular association and are able to form clusters. This can elongate relaxation times by a factor of 2-4.[114] Thus, when phenols align to an external field and their electric dipoles are polarized, the apparent dipole of the phenol cluster still exists for a certain, concentration-dependent amount of time even if the external field is removed. Until relaxation, the apparent electric dipole resulting from the aligned polar(ized) molecular cluster should favor interactions of the latter with other polar moieties. Like this, it should be possible to temporarily concentrate polar analytes, such as nitroaromatic compounds, in a controlled way. Most nitroaromatic compounds of interest have very low vapor pressures and for instrumental detection of such analytes, preconcentration is usually required. When molecules such as **55** or **67** form a monolayer on a surface (for example functionalized glass), the polarization of such tweezers in a microwave field should allow the resulting clusters to interact (or be temporarily "charged") with (potentially airborne) nitroaromatic analytes. Relaxation of the aggregates into molecules **55** or **67** would amount to the controlled release of the analytes to allow their detection with mass spectrometry in a suitable instrumental setup. This project aims at the synthesis of molecules like **55** or **67** that, upon attachment on a surface and polarization in a microwave field, are able to catch

and release nitroaromatic molecules in sufficient amounts to be detected by mass spectrometry.
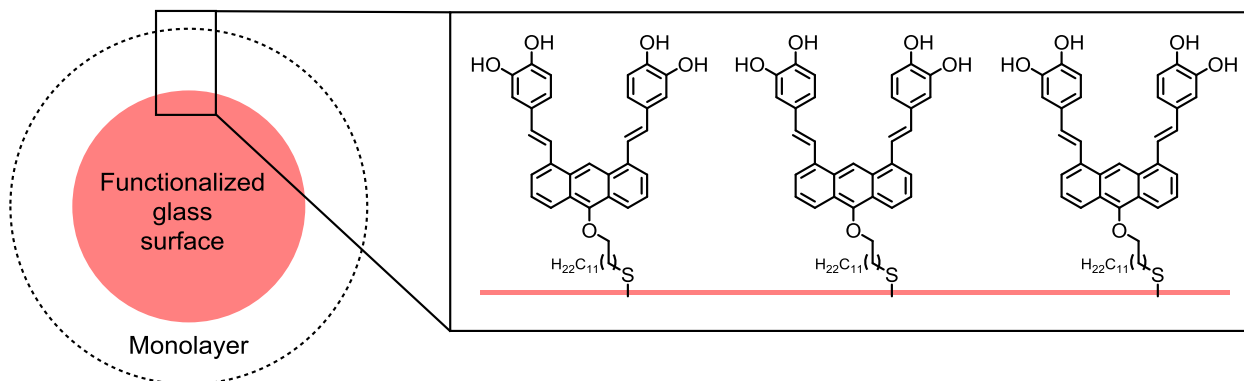

Picture 35. *Model of a surface functionalized with molecule **55**.*

2.9.4 Design and Synthetic Strategy

The design of target compounds **55** and **67** is based on sensors **1i** and **1j**, but two additional features are introduced. The two styryl-clips contain catechol substituents and the aromatic spacer is linked to an alkyl-linker chain with an S-acetyl anchor group. The catechol substituents are introduced for two reasons: a) as mentioned, phenols and their derivatives usually display elongated relaxation times because of hydrogen bonding (thereby sustaining the net polarization of the cluster), and b) their elevated dielectric constants due to the –OH groups should allow them to ultimately generate a stronger polarization in the applied field, which may further enhance their interaction with nitroaromatic guests.[114],[115] The alkyl-linker serves to attach the target compounds to the gold surface(cf picture 33). S-acetyl groups can be used to form stable S-Au bonds and are therefore chosen as end group in the alkyl-linker.[116],[117] The remaining linker consists of a C_{12} alkyl-chain, which was chosen to sufficiently "insulate" the gold surface from both the sensor molecules and the nitroaromatic guests.[118] In contrast to molecule **67**, the attachment of the linker to the sensing part of molecule **55** is determined through ease of synthesis, but this point will be accessed in more detail later in the chapter.

Scheme 25 shows the synthetic strategies towards molecules **55** and **67**.
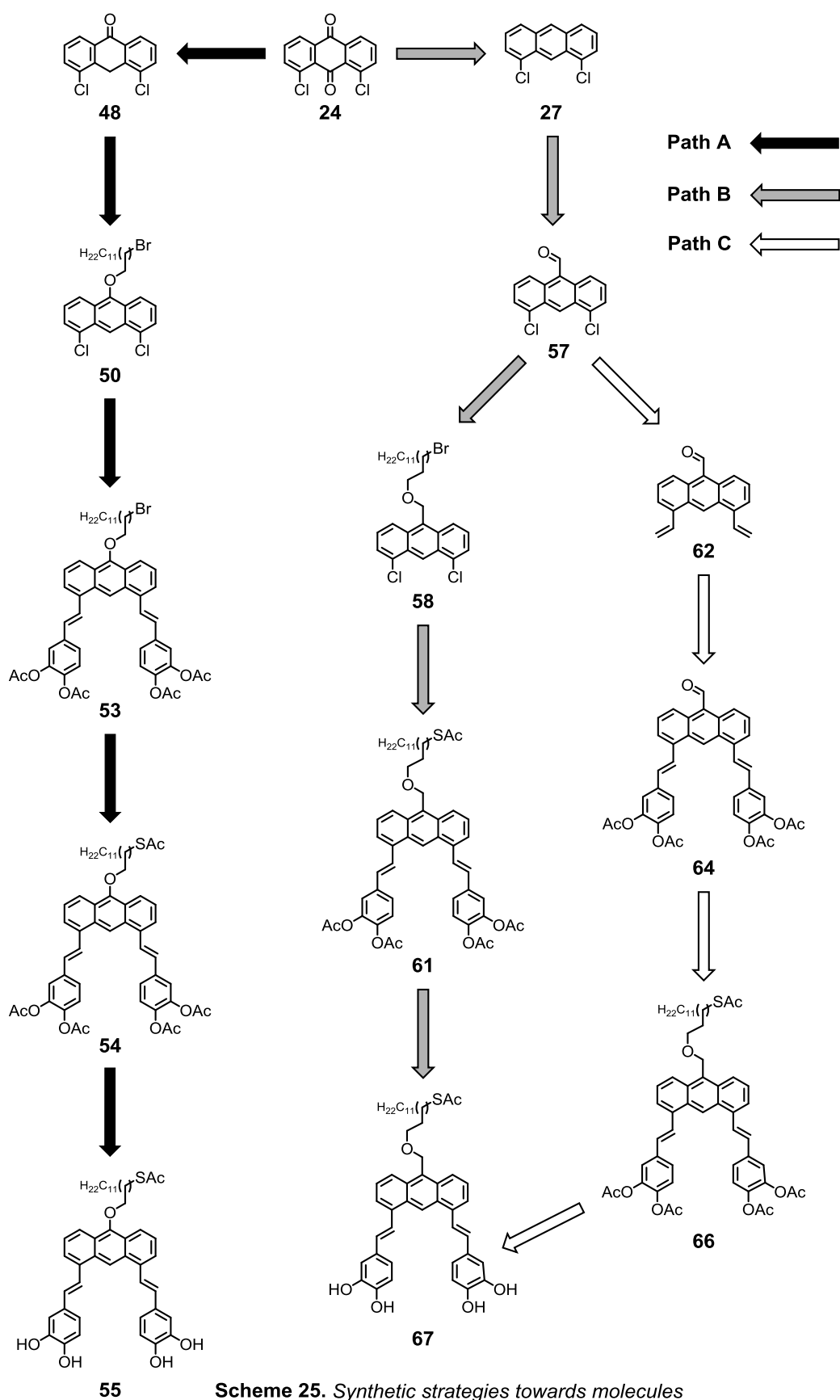
Scheme 25. *Synthetic strategies towards molecules* **55** *and* **67**.

In path A the aliphatic linker is planned to be introduced in a two-step procedure. After reduction of 1,8-dichloroanthraquinone **24** to 1,8-dichloroanthrone **48** the base-induced enol of the latter is thought to react with 1,12-dibromododecane in a substitution reaction to deliver anthracene **50**.[119]-[121] A Pd-catalyzed Heck cross-coupling followed by a S_N2 reaction with potassium thioacetate are envisaged to result in compound **54**. The cross coupling is decided to be carried out after the introduction of the dodecane-linker because the base-labile acetyl-protection groups in the aromatic pincers would probably be cleaved during the substitution reaction and the resulting phenolate(s) would undergo further nucleophilic attack on the bromide of the linker chain. The S_N2 reaction between anthracene **53** and potassium thioacetate is expected to introduce the protected sulfur moiety (molecule **54**) to prevent uncontrolled oxidative disulfide formation. Alkaline O-acetyl deprotection of molecule **54** is intended to obtain target structure **55**. Conditions have to be chosen such that either the S-acetyl moiety on the aliphatic linker is preserved or that disulfide-formation is favored in case of deprotection.[122]

Path B leads to a different final compound **67**, where the alkyl linker is attached to a benzylic oxygen atom instead of a phenolic one like in molecule **55**. The first step planned is the reduction of anthraquinone **24** to anthracene **27** that was used in the synthesis of the anthracene based sensors **1d** and **1e**.[40] Vilsmeyer-Haack formylation is envisaged to turn molecule **27** into anthraldehyde **57**. Reduction of molecule **57** with NaBH$_4$ to the corresponding alcohol and subsequent S_N2 reaction with 1,12-dibromododecane are intended for the transformation of aldehyde **57** into anthracene **58**. The subsequent steps are analogous to path A. The acetyl-protected pincers are intended to be introduced in a Heck coupling between anthracene **58** and 3,4-diacetoxystyrene, subsequently establishing molecule **61** through a S_N2 reaction with potassium thioacetate. Alkaline deprotection of styryl **61** is envisaged to yield target structure **67**.[122]

The first two steps in path C are identical to path B. But instead of the alkyl linker the vinyl moieties are introduced first. Therefore it is planned to assemble anthraldehyde **64** from molecule **57** in two consecutive Pd-catalyzed reactions. The first of these two reactions is a Stille coupling with tributylvinyl stannane, followed by a Heck reaction of

distyryl **62** with 3,4-diacetoxystyrene.[123] After the reduction of anthraldehyde **64** with NaBH$_4$ and a substitution reaction of the resulting alcohol with 1,12-dibromododecane, a similar S$_N$2 reaction with potassium thioacetate is expected to result in anthracene **66**. The last step towards target compound **67** is identical to route B.

2.9.5 Synthesis

Path A

Reduction of anthraquinones to anthrones can be challenging because many procedures lead directly to anthracenes or provide mixtures of partially reduced products. Both conditions shown in scheme 26 are literature-known and known to reduce 1,8-dichloroanthraquinone **24** to 4,5-dichloroanthrone **48**.[119],[120]
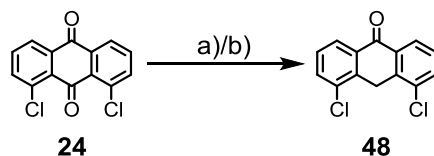

a) SnCl$_2$, HCl , AcOH, 120°C, 5h, 40%
b) Na$_2$(S$_2$O$_4$), DMF/H$_2$O (1:1), 90°C, 4h, 60%

Scheme 26. *Reduction of molecule **24** to anthrone **48**.*

The reduction of **24** with stannous chloride in acetic acid provided anthrone **48** in 40% yield whereas reduction with Na$_2$(S$_2$O$_4$) in DMF and H$_2$O resulted in 60% anthrone **48**. The reaction with stannous chloride is less selective and reduction on both ketones can occur. This is reduced through the use of conditions b) in scheme 26, where the carbonyl between the *peri* substituents is reduced selectively.[120]

Initially, the alkyl linker was planned to be introduced in two steps, the first being the base-promoted aromatization of anthrone **48** to hydroxyxanthracene **49** (cf. Scheme 27).
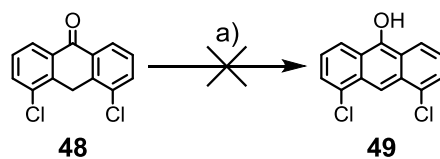
a) NaOH, MeCN, rt, 2h

**Scheme 27**. *Intended formation of 4,5-dichloroanthracene-9-ol.*

Instead of anthracene **49**, almost quantitative formation of 1,8-dichloroanthraquinone was observed. Apparently, after deprotonation of the sp^3 carbon on anthrone **48** oxidation is preferred over aromatization; due to the limited resonance-stabilization in the middle ring, oxidation of anthracene cores to the corresponding anthraquinone is often observed, depending on substituents and chemical environment.[124] However, under similar conditions and in the presence of 1,12-dibromododecane, anthracene **50** was obtained in 85% yield via base-induced enolisation of anthrone **48** (cf. Scheme 28).[121]
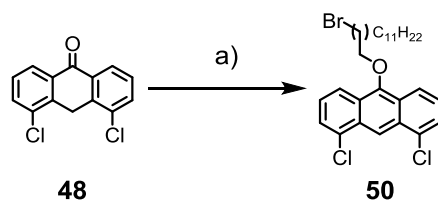
a) 1,12-dibromododecane, K$_2$CO$_3$, DMF, 55°C, overnight, 85%

**Scheme 28**. *Alkylation of anthrone 48 to anthracene 50.*

After successful alklylation of anthrone **48** the next step was the introduction of the aryl rods in a Heck coupling. First, it was tried to couple anthracene **50** with styrene in order to obtain have a reference substance (cf. scheme 29).
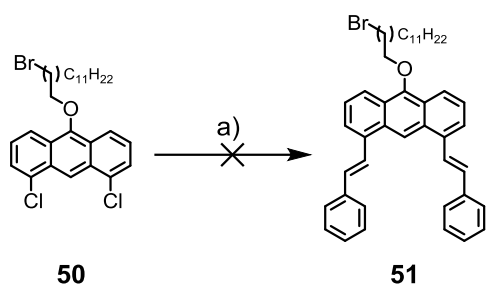
a) Styrene, Pd(P^{t}Bu$_3$)$_2$, Cs$_2$CO$_3$, DMSO, 160°C, 5h

Scheme 29. *Attempted synthesis of styryl* **51***.*

However, although TLC indicated full conversion of educt **50** and formation of a new product, no product could be isolated because the product decomposed during chromatographic purification. It was reported previously that similar compounds are neither light- nor air-stable.[124]-[134] In order to determine whether this was an inherent problem of the reaction conditions chosen or a more general property of potential target structures a Sonogashira reaction was performed (cf. scheme 30).
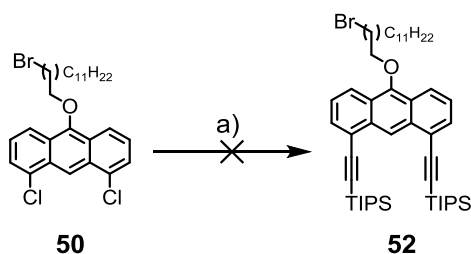
a) TIPS-Acetylene, PdCl$_2$(CH$_3$CN)$_2$, ^{t}BuXPhos Cs$_2$CO$_3$, Acetonitrile, 90°C, 5h

Scheme 30. *Attempted Sonogashira reaction towards structure* **52***.*

Like before, formation of a product was observed but it decomposed during flash chromatography. A number of possible explanations exist. First, as mentioned, the 9-position of the anthracene to which the linker is attached and the 10-position between the chlorine atoms are more reactive than the other positions because they are less stabilized through resonance.[128] The nature of the substituent at these positions

therefore has a big influence on the formation of side- and degradation products. For example, endoperoxide formation in anthracenes increases with electron density in the substrates.[135] The photochemistry of anthracenes is largely governed by lone pair electrons in the substituents.[128] Additionally, the degradation of substituted anthracenes on various solid supports has been reported, including silica and aluminium oxide.[136]

In order to not only reduce electron density in the anthracene spacer but also to further reduce the influence of the oxygen lone pairs from it, it was decided to redesign the molecule: repositioning the oxygen atom in benzylic (compound **67** in scheme 25) instead of phenolic position (compound **55** in scheme 25) might increase the stability of the target molecule and its precursors towards numerous side reactions.

Path B

Starting from anthracene **27**, two ways of formylation were tested for its transformation into 4,5-dichloroanthracene-9-carbaldehyde **57** (cf. scheme 31).[137], [138]
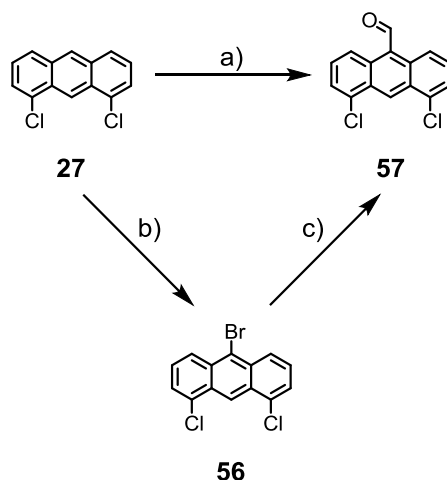
a) dichloro(methoxy)methane, AlCl$_3$, CH$_2$Cl$_2$, 0°C to rt, 1h, 45%
b)Br2, CH$_2$Cl$_2$, 0°C to rt; overnight, quant.
c) DMF, *n*-BuLi, THF, -78°C to rt, 1h, 75%

Scheme 31. *Evaluation of the reaction conditions tried in the synthesis of aldehyde **57**.*

First, a Rieche-formylation (conditions a) in scheme 31) was tried.[137] The 45% yield of the reaction was not very high; in Rieche formylations side products such as multiple

formylation or even cross-linked products are plausible and have been reported.[139] In contrast, the two step procedure shown in scheme 31 (conditions b) and c)) delivered anthraldehyde **57** in a much better yield. The reaction of anthracene **27** with elemental bromine was quantitative and quenching a solution of anthracene **56** with DMF after halogen-lithium exchange in THF gave molecule **57** 75% yield.[138] Additionally, anthracene **56** is an interesting building block on its own, potentially offering useful possibilities in the synthesis of similar molecules like the ones targeted in this project.

After establishing the promising precursor **57**, the introduction of the alkyl linker was approached in two consecutive steps. After reducing carbaldehyde **57** with NaBH$_4$, the resulting alcohol was alkylated as shown in scheme 32 to alkoxyanthracene **58** (scheme 32).
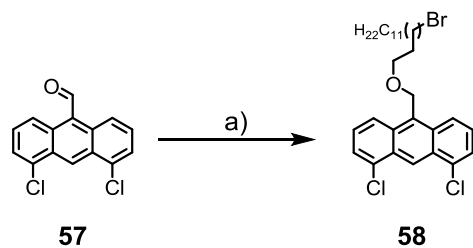
a) 1. NaBH$_4$, THF, 0°C to rt, 1h
    2. 1,12-dibromododecane, K$_2$CO$_3$, MeCN, 85°C, overnight, quant. (2 steps)

Scheme 32. *Conditions employed in the synthesis of anthracene* **58** *from aldehyde* **57***.

With functionalized anthracene **58** in hand, the approach towards the following coupling reactions was identical to path A (cf. schemes 29 and 30). Again, in both reactions no product, including anthracene or anthraquinone derivatives, could be isolate, despite full conversion of the starting material **58**. It is concluded that replacing the phenolic linker with a benzylic linker did not sufficiently stabilize the anthracene spacer in the projected synthesis.
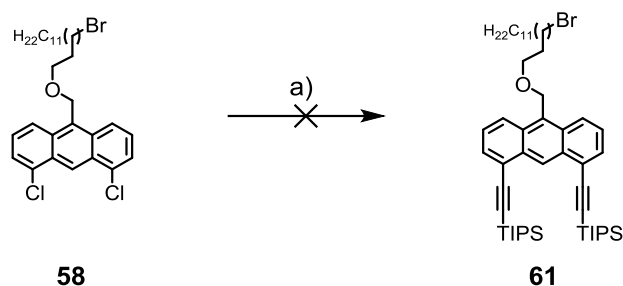
a) TIPS-acetylene, PdCl$_2$(CH$_3$CN)$_2$, XPhos, Cs$_2$CO$_3$, Acetonitrile, 90 °C, 7h

Scheme 34. *Attempted Sonogashira reaction towards molecule* **61**.

When the same Sonogashira test-reaction conditions were applied as in path A, no product could be isolated. Although extending the π-system through addition of conjugated units has been shown to stabilize acenes, oxidative stability of (substituted) anthracene(s) is also determined greatly by the nature of substituents. Especially in the less resonance-stabilized 9- and 10- positions, electron withdrawing substituents can hinder oxidation.[140] Therefore, if the aromatic pincers are introduced before the linker moiety as proposed in path C, the electron-accepting aldehyde in the 9-position might not only help to facilitate couplings but may also reduce anthracene degradation as coupling conditions on aromatic chlorines are generally rather harsh.

Path C

The conditions for the Stille cross-coupling depicted in scheme 35 were developed by Fu and co-workers specifically for aryl chlorides, which can be reluctant in coupling reactions.[123] The conditions in scheme 35 delivered anthraldehyde **61** in almost 60% yield.
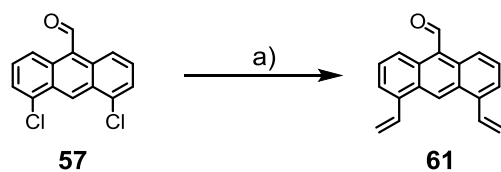

a)Tributyl(vinyl)tin, Pd(P^{t}Bu$_3$)$_2$, CsF, dioxane, 100 °C, 72h, 58%

Scheme 35. *Stille coupling of aldehyde* **57**.

The reaction proceeded slowly and 3 days reaction time was needed. After 48 h, mainly monocoupled product was present in GC-MS spectra. Molecule **61** could be subjected to flash chromatography under laboratory atmosphere without noticeably polymerizing and could even be regained after the attempted Heck coupling with 4-bromo-1,2-phenylene diacetate **62** (cf. scheme 36).

From anthraldehyde **61** the synthesis can go two directions. The aldehyde-moiety can be reduced to the benzylic alcohol and then alkylated before introducing the catechol units, but the reduction of the aldehyde would rather slow down the intended coupling and a similar strategy provided poor results in synthetic pathway B. Therefore it was decided to try to introduce the acetyl-protected catechol moieties first.

When subjected to the Heck conditions shown in scheme 36, anthracene **61** did not react.

a) Pd(amphos)Cl$_2$, K$_2$CO$_3$, DMF, 150 °C, overnight
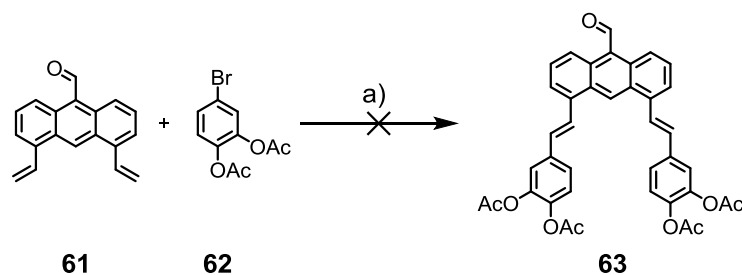
Scheme 36. *Attempted Heck coupling between aldehyde* **61** *and aryl* **62**.

The aryl halide **62** is rather electron-deficient to to the acetoxy-substituents in the 3- and 4-positions, which should facilitate oxidative addition to the catalyst in the reaction. However, in Heck coupling the insertion of the alkene to the catalyst during the catalytic cycle may be very dependent on steric factors. In Heck couplings of 9-10-divynilanthracene the *peri*-hydrogens in the 1/4 and 5/8 positions make the reaction centers sterically demanding and impede addition of the organometallic intermediate to the olefinic double bond.[141] The situation might be comparable in 1,8-divinylanthracene.

148

This drawback might be overcome through elevated heating (microwave or change of solvent) or through choice of a different ligand.

The aldehyde moiety in anthracene **61** is electron-withdrawing and the reaction under the applied conditions is slow; in anthracene **58** the alkyl linker is already inserted and the system more electron abundant than is case for anthracene **61**. It is possible that at increased temperatures in a high-boiling solvent such as DMSO the reaction would proceed. In Heck couplings of 9-10-divynilanthracene the *peri*-hydrogens in the 1/4 and 5/8 positions make the reaction centers sterically demanding and impede addition of the organometallic intermediate to the olefinic double bond. The situation might be comparable in 1,8-divinylanthracene **61**. This drawback might be overcome through elevated heating (microwave or change of solvent) or through choice of a different ligand.

3 Conclusion and Outlook

The goal of this project was the synthesis and evaluation of molecular tweezers able to detect nitroaromatic guests. While not all projected sensing principles were achievable, molecules **1c-1j** were successfully synthesized. Their sensing performances were determined in 1H-NMR titrations, where 1,3-dinitrobenzene (1,3-DNB) was used as nitroaromatic model compound. In some cases benzonitrile was used as guest as well, but the binding towards the host molecules was too weak to be detected. Association constants between the molecular tweezers and 1,3-DNB were generally low, ranging between 20 M^{-1} and 0.1 M^{-1}. The results were obtained by nonlinear regression and interpreted in terms of molecular structure of the tweezers and their structural features. The interpretations were based on calculated properties of the sensors. The following points are suggested:

a) The influence of the gap size in the formation of host-guest complexes (i.e. the distance between the aromatic pincers) cannot be reduced to distances and bond

lengths, but the whole molecular structure of tweezers **1c**-**1j** has to be taken into account, including the interplay between the moieties (the backbone and the aromatic pincers): not only can favorable enthalpy in a binding event be punished or compensated with unfavorable entropy, but since both the aromatic spacers and the clips in molecules **1c**-**1j** are aromatic they may be conjugated with each other to variable degrees which may significantly change the chemical properties of the single components as well as the overall molecule.

b) Based on the conducted calculations the interactions between host and guest appear to be largely governed by electrostatic interactions in molecules **1c**-**1j**, as proposed by Hunter and Sanders and Cozzi and Siegel.[74],[77]

c) Also in accordance with Hunter/Sanders and Cozzi/Siegel, the strong electrostatic component of association suggests that electron-withdrawing substituents on the aromatic clips allow for stronger binding than electron-donating ones, at least in the ground-state.[74],[77]

d) Apart from showing the most favorable electrostatic preconditions for π-stacking interactions, xanthone **1c** may also the be most suited molecule of the series to undergo significant dispersive interactions with aromatic guests, which leads to the question whether bigger pincers than (substituted) benzenes such as anthracene- or pyrene-derivatives may significantly enhance the "sandwiching" of aromatic guests in comparable molecules.

e) As far as determined, self-association of the host is not a general problem inherent in molecular tweezers, but if it occurs, such as in sensor **1j**, it may lower the association constant between host and guest by one order of magnitude or more and has therefore to be considered in the design of similar compounds.

In terms of molecular structure and following points a) – e), apart from the criteria introduced in chapter *1.4.3* the following conclusions can be drawn (picture 36):

- molecular tweezers should be rigid enough and/or show enough preorganization to minimize entropy-enthalpy compensation but still be flexible enough to accommodate a range of potential guest molecules; the required limitation in conformational restriction of

the molecules could be addressed not only through rigid backbones and suitable linkers between backbone and the pincers (such as –C=C- double bonds or ether bonds as seen in molecule **39** in chapter *1.4.3*) but also through the size of the pincers in relation to the gap size between the pincers;

- the tweezers should be optimized to favor electrostatic interactions with potential guests; therefore electron-deficient aromatic pincers are desirable;

- although dispersive interactions in π-stacking interactions are less important a priori, they might become more important in larger pincers; therefore, larger pincers might additionally improve host-guest complexations; picture 36 shows several proposed molecular tweezers displaying these criteria to various degrees.
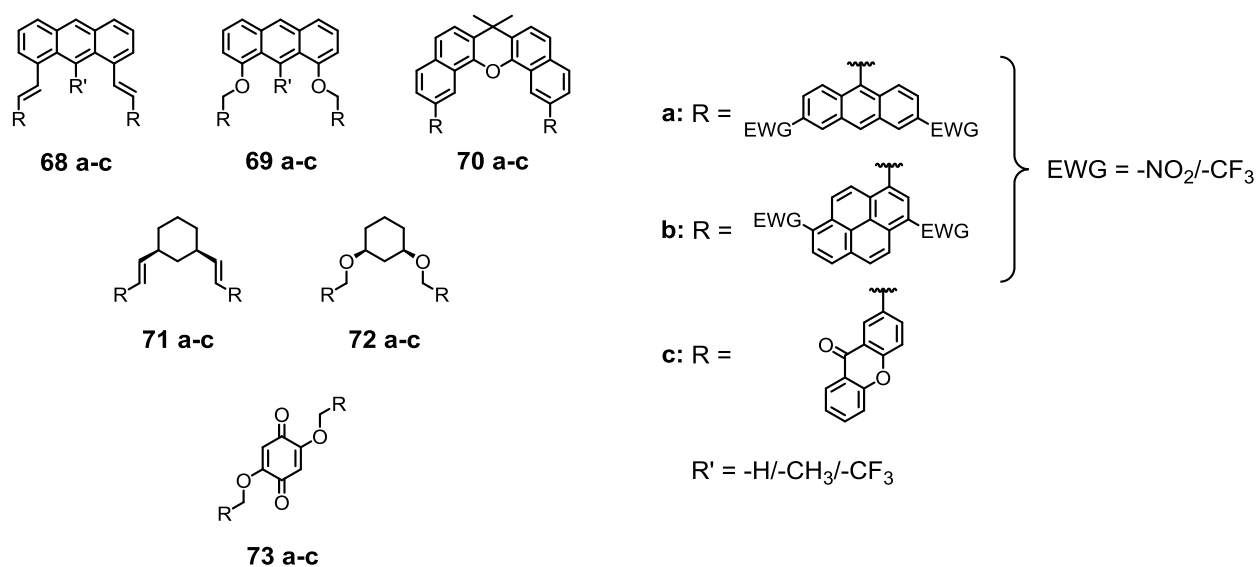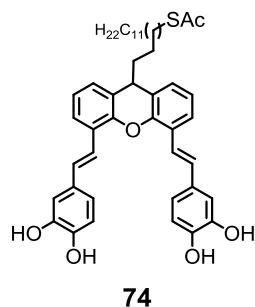

Picture 36. *Structures of proposed molecular tweezers **68 - 73**, based on the findings of this work (as proposed in points a) - e) in this section).*

Sensors **68** to **70** are direct derivatives from sensors **1h**-**1j**. Irrespective of the different linkers between molecules **68** and **69**, the main focus in these structures lies in their pincers **a-c**, which are not only larger than the pincers used in this work but also carry electron-withdrawing substituents (**a** and **b**). Xanthone **c** would make interesting clips insofar as it would be fascinating to observe its guest-binding properties in cooperative fashion, considering the results from sensor **1c**. The gap size in sensor **70** is already relatively big and it is possible that a less adaptable linker (here: a single =C-C= bond) would be enough to accommodate a variety of guests: provided the pincers are large

151

enough (for example pincer **b**), and if the planes described by each pincer are sufficiently extended, it is possible that the pincers form a cone which could harbor guest molecules. In all the proposed molecules **68**-**70**, the increased size of the pincers **a-c** and their relative electron-deficiency are proposed to maximize both dispersive and electrostatic interactions, respectively, but also to further restrict conformational freedom of the molecules. Structures **71** and **72** both use a *cis*-1,3-substituted cyclohexane spacer, as MM2-based calculations indicated that in the depicted structures the gap size may be in a favorable range. Also, molecules **71** and **72** may be accessible in modular fashion and the aliphatic backbone removes at least one potential pathway of self-association of the molecules. More general, the removal of possible conjugation between backbone and pincers should minimize the influence of the backbone on the pincers and consequently should facilitate controlling electron-density in the clips. Structure **73** is proposed because the oxidative stability of the dihydroxyquinone backbone, which could be of importance in the repeated use of possible hand-held devices.

Because with larger and substituted (and therefore probably generally more efficient) aromatic pincers, self-association of the host could become more prevalent than in this study; prevention of self-association could be achieved through either choice of the backbone, functionalization of the backbone aiming at reduction of cavity depth (thereby reducing accessibility for larger guests, i.e. the pincers) or through bulky substituents on the aromatic pincers. One possibility could be to replace the NO_2-substituents in pincers **a-c** with bulkier $-CF_3$ groups which could hinder self-association: it is likely that host-host-associations would include pincer-pincer interactions from neighboring sensors, and the (compared to $-NO_2$) relatively large $-CF_3$ moieties could sterically impede neighboring pincers from stacking but still allow the comparably small and flat nitroaromatic guests to enter the cavity/gap formed by the pincers. Alternatively, substituents such as $-CF_3$ or $-CH_3$ could also be attached to the backbone, limiting rotational freedom of the linkers and the pincers and reducing the depth of the gap towards larger guests.

Synthesis of surface-functionalizing molecules **55** and **67** suffered from chemical instability of the anthracene-backbone in several of the key-reactions. Nevertheless, anthraldehyde **61** exhibited considerable stability. Although molecule **61** did not react to target-precursor **63** under Heck conditions, it is possible that elevated temperature or a different ligand may result in the desired transformation. Alternatively, a different backbone may remove or lessen the encountered stability issues while still retaining the functional features of the molecule, for example xanthene in proposed structure **74**, as shown in picture 37.

74

Picture 37. *Structure of proposed molecular tweezers **74** with potential enhanced stability in the backbone, based on the findings of this work.*

153

Bibliography

(1) Wen, R.; Yan, C.-J.; Yan, H.-J.; Pan, G.-B.; Wan, L.-J. *Chemical Communications* **2011**, *47* (24), 6915.

(2) Czarnik, A. W. *Nature* **1998**, *394* (6692), 417.

(3) Vijayakumar, C.; Tobin, G.; Schmitt, W.; Kim, M.-J.; Takeuchi, M. *Chemical Communications* **2010**, *46* (6), 874.

(4) Hunter, C. A.; Sanders, J. K. M. *Journal of the American Chemical Society* **1990**, *112* (14), 5525.

(5) Yoshizawa, M.; Klosterman, J. K. *Chem. Soc. Rev.* **2014**, *43* (6), 1885.

(6) Zhang, Z.; Li, X.; Song, T.; Zhao, Y.; Feng, Y. *Journal of Medicinal Chemistry* **2012**, *55* (23), 10735.

(7) Wilson, A. J. *Annual Reports Section "B" (Organic Chemistry)* **2007**, *103*, 174.

(8) Cockroft, S. L.; Perkins, J.; Zonta, C.; Adams, H.; Spey, S. E.; Low, C. M. R.; Vinter, J. G.; Lawson, K. R.; Urch, C. J.; Hunter, C. A. *Organic & Biomolecular Chemistry* **2007**, *5* (7), 1062.

(9) Nkansah, M. A.; Christy, A. A.; Barth, T. *Chemosphere* **2011**, *84* (4), 403.

(10) Odrowaz-Sypniewski, M. R.; Tsoungas, P. G.; Varvounis, G.; Cordopatis, P. *Tetrahedron Letters* **2009**, *50* (44), 5981.

(11) Lennox, A. J. J.; Lloyd-Jones, G. C. *Chem. Soc. Rev.* **2014**, *43* (1), 412.

(12) Correia-da-Silva, M.; Sousa, E.; Duarte, B.; Marques, F.; Carvalho, F.; Cunha-Ribeiro, L. M.; Pinto, M. M. M. *Journal of Medicinal Chemistry* **2011**, *54* (15), 5373.

(13) Gaekwad, Y. G. *Journal of the Indian Chemical Society* **1978**, *55* (8), 794.

(14) Zhang, H.; Shi, R.; Gan, P.; Liu, C.; Ding, A.; Wang, Q.; Lei, A. *Angewandte Chemie International Edition* **2012**, *51* (21), 5204.

(15) Shibuya, I.; Katoh, E.; Gama, Y.; Oishi, A.; Taguchi, Y.; Tsuchiya, T. *HETEROCYCLES* **1996**, *43* (4), 851.

(16) Ozturk, T.; Ertas, E.; Mert, O. *Chemical Reviews* **2007**, *107* (11), 5210.

(17) Rausis, T.; Schlosser, M. *European Journal of Organic Chemistry* **2002**, *2002* (19), 3351.

(18) Shi, J.; Zhang, X.; Neckers, D. C. *The Journal of Organic Chemistry* **1992**, *57* (16), 4418.

(19) Irie, M.; Sakemura, K.; Okinaka, M.; Uchida, K. *The Journal of Organic Chemistry* **1995**, *60* (25), 8305.

(20) Rehm, D.; Weller, A. *Israel Journal of Chemistry* **1970**, *8* (2), 259.

(21) Cross, W.; Hawkes, G. E.; Kroemer, R. T.; Liedl, K. R.; Loerting, T.; Nasser, R.; Pritchard, R. G.; Steele, M.; Watkinson, M.; Whiting, A. *Journal of the Chemical Society, Perkin Transactions 2* **2001**, No. 4, 459.

(22) Batsanov, S.S. *Inorg. Mat.* **2001**, *37* (9), 871.

(23) Littke, A. F.; Dai, C.; Fu, G. C. *Journal of the American Chemical Society* **2000**, *122* (17), 4020.

(24) Meijere, A. de; Diederich, F. *Metal-catalyzed cross-coupling reactions*, 2nd, completely rev. and enl. ed.; Wiley-VCH: Weinheim, 2004.

(25) Van Leeuwen, P. W. N. M.; Kamer, P. C. J.; Reek, J. N. H.; Dierkes, P. *Chemical Reviews* **2000**, *100* (8), 2741.

(26) Ishiyama, T. *Organic Syntheses* **1993**, *71*, 89.

(27) Wallow, T. I.; Novak, B. M. *The Journal of Organic Chemistry* **1994**, *59* (17), 5034.

(28) Wallow, T. I. *Organic Syntheses* **1998**, *75*, 61.

(29) Smith, G. B.; Dezeny, G. C.; Hughes, D. L.; King, A. O.; Verhoeven, T. R. *The Journal of Organic Chemistry* **1994**, *59* (26), 8151.

(30) Li, G. Y. *Angewandte Chemie International Edition* **2001**, *40* (8), 1513.

(31) Spivey, A. C.; Fekner, T.; Spey, S. E. *The Journal of Organic Chemistry* **2000**, *65* (10), 3154.

(32) Widenhoefer, R. A.; Zhong, H. A.; Buchwald, S. L. *Journal of the American Chemical Society* **1997**, *119* (29), 6787.

(33) Sagrera, G.; Bertucci, A.; Vazquez, A.; Seoane, G. *Bioorganic & Medicinal Chemistry* **2011**, *19* (10), 3060.

(34) Dai, M.; Yuan, X.; Kang, J.; Zhu, Z.-J.; Yue, R.-C.; Yuan, H.; Chen, B.-Y.; Zhang, W.-D.; Liu, R.-H.; Sun, Q.-Y. *European Journal of Medicinal Chemistry* **2013**, *69*, 159.

(35) Thordarson, P. *Chem. Soc. Rev.* **2011**, *40* (3), 1305.

(36) H.J. Motulsky, A. C. *Fitting models to biological data using linear and nonlinear regression. A practical guide to curve fitting.*; GraphPad Software Inc., San Diego CA, www.graphpad.com ., 2003.

(37) Wendy Rotz. *ASA Section on Survey Research Methods* **2006**, 3615.

(38) Yamashita, M.; Yamamoto, Y.; Akiba, K.; Hashizume, D.; Iwasaki, F.; Takagi, N.; Nagase, S. *Journal of the American Chemical Society* **2005**, *127* (12), 4354.

(39) Filatov, M. A.; Guilard, R.; Harvey, P. D. *Organic Letters* **2010**, *12* (1), 196.

(40) House, H. O.; Hrabie, J. A.; VanDerveer, D. *The Journal of Organic Chemistry* **1986**, *51* (6), 921.

(41) Guram, A. S.; King, A. O.; Allen, J. G.; Wang, X.; Schenkel, L. B.; Chan, J.; Bunel, E. E.; Faul, M. M.; Larsen, R. D.; Martinelli, M. J.; Reider, P. J. *Organic Letters* **2006**, *8* (9), 1787.

(42) Harzmann, G. D.; Neuburger, M.; Mayor, M. *European Journal of Inorganic Chemistry* **2013**, *2013* (19), 3334.

(43) Hoffman, D. M.; Hoffmann, R.; Fisel, C. R. *Journal of the American Chemical Society* **1982**, *104* (14), 3858.

(44) Bürkle, M.; Viljas, J. K.; Vonlanthen, D.; Mishchenko, A.; Schön, G.; Mayor, M.; Wandlowski, T.; Pauly, F. *Physical Review B* **2012**, *85* (7).

(45) Haworth, R. D. *Journal of the Chemical Society (Resumed)* **1932**, 1125.

(46) Crosby, I. T.; Shin, J. K.; Capuano, B. *Australian Journal of Chemistry* **2010**, *63* (2), 211.

(47) Furukawa, A.; Arita, T.; Fukuzaki, T.; Mori, M.; Honda, T.; Satoh, S.; Matsui, Y.; Wakabayashi, K.; Hayashi, S.; Nakamura, K.; Araki, K.; Kuroha, M.; Tanaka, J.; Wakimoto, S.; Suzuki, O.; Ohsumi, J. *European Journal of Medicinal Chemistry* **2012**, *54*, 522.

(48) Carroll, F. I.; Blough, B. E.; Abraham, P.; Mills, A. C.; Holleman, J. A.; Wolckenhauer, S. A.; Decker, A. M.; Landavazo, A.; McElroy, K. T.; Navarro, H. A.; Gatch, M. B.; Forster, M. J. *Journal of Medicinal Chemistry* **2009**, *52* (21), 6768.

(49) Niculescu-Duvaz, D.; Niculescu-Duvaz, I.; Suijkerbuijk, B. M. J. M.; Ménard, D.; Zambon, A.; Davies, L.; Pons, J.-F.; Whittaker, S.; Marais, R.; Springer, C. J. *Bioorganic & Medicinal Chemistry* **2013**, *21* (5), 1284.

(50) Furukawa, A.; Arita, T.; Fukuzaki, T.; Mori, M.; Honda, T.; Satoh, S.; Matsui, Y.; Wakabayashi, K.; Hayashi, S.; Nakamura, K.; Araki, K.; Kuroha, M.; Tanaka, J.; Wakimoto, S.; Suzuki, O.; Ohsumi, J. *European Journal of Medicinal Chemistry* **2012**, *54*, 522.

(51) Menezes, J. C. J. M. D. S.; Srinivasan, B. R.; Raghavaiah, P.; Paknikar, S. K.; Kamat, S. P. *Journal of Heterocyclic Chemistry* **2011**, *48* (4), 952.

(52) Luo, F.; Pan, C.; Wang, W.; Ye, Z.; Cheng, J. *Tetrahedron* **2010**, *66* (6), 1399.

(53) Rogers, M. E.; Averill, B. A. *The Journal of Organic Chemistry* **1986**, *51* (17), 3308.

(54) Fu, G. C. *Accounts of Chemical Research* **2008**, *41* (11), 1555.

(55) Littke, A. F.; Fu, G. C. *The Journal of Organic Chemistry* **1999**, *64* (1), 10.

(56) De Meijere, A.; Bräse, S. *Journal of Organometallic Chemistry* **1999**, *576* (1-2), 88.

(57) Hesse, M. *Spektroskopische Methoden in der organischen Chemie*; Thieme: Stuttgart, 1979.

(58) Li, J.; Hua, R.; Liu, T. *The Journal of Organic Chemistry* **2010**, *75* (9), 2966.

(59) Hills, I. D.; Fu, G. C. *Journal of the American Chemical Society* **2004**, *126* (41), 13178.

(60) Fokkens, M.; Schrader, T.; Klärner, F.-G. *Journal of the American Chemical Society* **2005**, *127* (41), 14415.

(61) Rowan, A. E.; Elemans, J. A. A. W.; Nolte, R. J. M. *Accounts of Chemical Research* **1999**, *32* (12), 995.

(62) Branchi, B.; Balzani, V.; Ceroni, P.; Kuchenbrandt, M. C.; Klärner, F.-G.; Bläser, D.; Boese, R. *The Journal of Organic Chemistry* **2008**, *73* (15), 5839.

(63) Martin, R. B. *Chemical Reviews* **1996**, *96* (8), 3043.

(64) Bogdan, M.; Floare, C. G.; Pîrnau, A. *Journal of Physics: Conference Series* **2009**, *182*, 012002.

(65) Wallach, D., S., C. D. In *Psychologie der Kognition: Reden and Vorträge anlässlich der Emeritierung von Werner Tack*; University of Saarland Press: Saarbrueken, Germany, 2005; pp 115–154.

(66) Karplus, M. *Journal of Molecular Recognition* **2010**, *23* (2), 102.

(67) Zimmerman, S. C. In *Bioorganic Chemistry Frontiers*; Dugas, H., Ed.; Springer Berlin Heidelberg: Berlin, Heidelberg, 1991; Vol. 2, pp 33–71.

(68) Fenley, A. T.; Muddana, H. S.; Gilson, M. K. *Proceedings of the National Academy of Sciences* **2012**, *109* (49), 20006.

(69) Williams, D. H.; Stephens, E.; O'Brien, D. P.; Zhou, M. *Angewandte Chemie International Edition* **2004**, *43* (48), 6596.

(70) Zimmerman, S. C.; Mrksich, M.; Baloga, M. *Journal of the American Chemical Society* **1989**, *111* (22), 8528.

(71) Cram, D. J. *Angewandte Chemie International Edition in English* **1986**, *25* (12), 1039.

(72) Searle, M. S.; Williams, D. H. *Journal of the American Chemical Society* **1992**, *114* (27), 10690.

(73) Suresh, C. H.; Alexander, P.; Vijayalakshmi, K. P.; Sajith, P. K.; Gadre, S. R. *Physical Chemistry Chemical Physics* **2008**, *10* (43), 6492.

(74) Hunter, C. A.; Lawson, K. R.; Perkins, J.; Urch, C. J. *Journal of the Chemical Society, Perkin Transactions 2* **2001**, No. 5, 651.

(75) Chodera, J. D.; Mobley, D. L. *Annual Review of Biophysics* **2013**, *42* (1), 121.

(76) Schmieder, K.; Levitus, M.; Dang, H.; Garcia-Garibay, M. A. *The Journal of Physical Chemistry A* **2002**, *106* (8), 1551.

(77) Cozzi, F.; Cinquini, M.; Annuziata, R.; Siegel, J. S. *Journal of the American Chemical Society* **1993**, *115* (12), 5330.

(78) Gung, B. W.; Patel, M.; Xue, X. *The Journal of Organic Chemistry* **2005**, *70* (25), 10532.

(79) Gung, B. W.; Xue, X.; Reich, H. J. *The Journal of Organic Chemistry* **2005**, *70* (9), 3641.

(80) http://downloads.wavefun.com/Spartan10Manual.pdf.

(81) Sheinerman, F. B.; Honig, B. *Journal of Molecular Biology* **2002**, *318* (1), 161.

(82) Sun, H.; Hunter, C. A.; Llamas, E. M. *Chem. Sci.* **2015**, *6* (2), 1444.

(83) Hwang, J.; Dial, B. E.; Li, P.; Kozik, M. E.; Smith, M. D.; Shimizu, K. D. *Chem. Sci.* **2015**, *6* (7), 4358.

(84) Zeinalipour-Yazdi, C. D.; Pullman, D. P. *The Journal of Physical Chemistry B* **2006**, *110* (47), 24260.

(85) Šponer, J.; Riley, K. E.; Hobza, P. *Physical Chemistry Chemical Physics* **2008**, *10* (19), 2595.

(86) Moreira da Costa, L.; Stoyanov, S. R.; Gusarov, S.; Seidl, P. R.; Walkimar de M. Carneiro, J.; Kovalenko, A. *The Journal of Physical Chemistry A* **2014**, *118* (5), 896.

(87) Doxtader, M. M.; Mangle, E. A.; Bhattacharya, A. K.; Cohen, S. M.; Topp, M. R. *Chemical Physics* **1986**, *101* (3), 413.

(88) Foster, E. J.; Jones, R. B.; Lavigueur, C.; Williams, V. E. *Journal of the American Chemical Society* **2006**, *128* (26), 8569.

(89) Liu, T.; Schneider, H.-J. *Angewandte Chemie International Edition* **2002**, *41* (8), 1368.

(90) Wagner, C.; Fournier, N.; Ruiz, V. G.; Li, C.; Müllen, K.; Rohlfing, M.; Tkatchenko, A.; Temirov, R.; Tautz, F. S. *Nature Communications* **2014**, *5*, 5568.

(91) Björk, J.; Hanke, F.; Palma, C.-A.; Samori, P.; Cecchini, M.; Persson, M. *The Journal of Physical Chemistry Letters* **2010**, *1* (23), 3407.

(92) Debnath, S.; Cheng, Q.; Hedderman, T. G.; Byrne, H. J. *physica status solidi (b)* **2008**, *245* (10), 1961.

(93) Zacharia, R.; Ulbricht, H.; Hertel, T. *Physical Review B* **2004**, *69* (15).

(94) Debnath, S.; Cheng, Q.; Hedderman, T. G.; Byrne, H. J. *The Journal of Physical Chemistry C* **2008**, *112* (28), 10418.

(95) Lima, C. F. R. A. C.; Rocha, M. A. A.; Schröder, B.; Gomes, L. R.; Low, J. N.; Santos, L. M. N. B. F. *The Journal of Physical Chemistry B* **2012**, *116* (11), 3557.

(96) Zimmerman, S. C. In *Bioorganic Chemistry Frontiers*; Dugas, H., Ed.; Springer Berlin Heidelberg: Berlin, Heidelberg, 1991; Vol. 2, pp 33–71.

(97) Hardouin–Lerouge, M.; Hudhomme, P.; Sallé, M. *Chem. Soc. Rev.* **2011**, *40* (1), 30.

(98) Ding, X. B.; Zheng, J. G.; Jin, Y. D.; Aerts, G.; Peng, B. X.; Heremans, P. L.; Borghs, G.; Geise, H. J. *Synthetic Metals* **2004**, *142* (1-3), 267.

(99) Gardner, R. R.; Christianson, L. A.; Gellman, S. H. *Journal of the American Chemical Society* **1997**, *119* (21), 5041.

(100) Huc, I.; Rebek, J. *Tetrahedron Letters* **1994**, *35* (7), 1035.

(101) Branchi, B.; Balzani, V.; Ceroni, P.; Kuchenbrandt, M. C.; Klärner, F.-G.; Bläser, D.; Boese, R. *The Journal of Organic Chemistry* **2008**, *73* (15), 5839.

(102) Waters, M. L. *Current Opinion in Chemical Biology* **2002**, *6* (6), 736.

(103) Das, A.; Ghosh, S. *Angewandte Chemie International Edition* **2014**, *53* (8), 2038.

(104) Shanmugaraju, S.; Mukherjee, P. S. *Chem. Commun.* **2015**, *51* (89), 16014.

(105) Kim, S. K.; Lim, J. M.; Pradhan, T.; Jung, H. S.; Lynch, V. M.; Kim, J. S.; Kim, D.; Sessler, J. L. *Journal of the American Chemical Society* **2014**, *136* (1), 495.

(106) Broxton, T. J.; Chung, R. P. T. *The Journal of Organic Chemistry* **1990**, *55* (12), 3886.

(107) Narahashi, H.; Shimizu, I.; Yamamoto, A. *Journal of Organometallic Chemistry* **2008**, *693* (2), 283.

(108) Pareek, A.; Rani, P.; Kumar, N.; Sharma, P.; Kishore, D. *ChemInform* **2015**, *46* (10), no.

(109) Lei, X.; Obregon, K. A.; Alla, J. *Applied Organometallic Chemistry* **2013**, *27* (7), 419.

(110) Thostenson, E. T.; Chou, T.-W. *Composites Part A: Applied Science and Manufacturing* **1999**, *30* (9), 1055.

(111) Patterson, D.; Schnell, M.; Doyle, J. M. *Nature* **2013**, *497* (7450), 475.

(112) Crossley, J. *Royal Institute of Chemistry, Reviews* **1971**, *4* (1), 69.

(113) Gabriel, C.; Gabriel, S.; H. Grant, E.; H. Grant, E.; S. J. Halstead, B.; Michael P. Mingos, D. *Chemical Society Reviews* **1998**, *27* (3), 213.

(114) Magee, M. D.; Walker, S. *Canadian Journal of Chemistry* **1971**, *49* (7), 1106.

(115) Min, Y.; Akbulut, M.; Kristiansen, K.; Golan, Y.; Israelachvili, J. *Nature Materials* **2008**, *7* (7), 527.

(116) Tour, J. M.; Jones, L.; Pearson, D. L.; Lamba, J. J. S.; Burgin, T. P.; Whitesides, G. M.; Allara, D. L.; Parikh, A. N.; Atre, S. *Journal of the American Chemical Society* **1995**, *117* (37), 9529.

(117) Love, J. C.; Estroff, L. A.; Kriebel, J. K.; Nuzzo, R. G.; Whitesides, G. M. *Chemical Reviews* **2005**, *105* (4), 1103.

(118) Shein, J. B.; Lai, L. M. H.; Eggers, P. K.; Paddon-Row, M. N.; Gooding, J. J. *Langmuir* **2009**, *25* (18), 11121.

(119) House, H. O.; Ghali, N. I.; Haack, J. L.; VanDerveer, D. *The Journal of Organic Chemistry* **1980**, *45* (10), 1807.

(120) Prinz, H.; Wiegrebe, W.; Müller, K. *The Journal of Organic Chemistry* **1996**, *61* (8), 2853.

(121) Zhao, W.; Tang, Q.; Chan, H. S.; Xu, J.; Lo, K. Y.; Miao, Q. *Chemical Communications* **2008**, No. 36, 4324.

(122) Sepporta, M. V.; López-García, M. Á.; Fabiani, R.; Maya, I.; Fernández-Bolaños, J. G. *European Journal of Pharmaceutical Sciences* **2013**, *48* (4-5), 790.

(123) Littke, A. F.; Schwarz, L.; Fu, G. C. *Journal of the American Chemical Society* **2002**, *124* (22), 6343.

(124) Behrens, T. Darstellung von tricyclischen, benzoiden Kohlenwasserstoffen mit elektronenziehenden Substituenten und EPR-spektroskopische Untersuchung ihrer Radikalanionen, University of Hamburg: Hamburg, 1999.

(125) Debestani, R.; Ellis, K. J.; Sigman, M. E. *Journal of Photochemistry and Photobiology A: Chemistry* **1995**, *86* (1-3), 231.

(126) Chae, Kyu Ho, K., Yong Woon. *Journal of Photoscience* **2002**, *9* (3), 57.

(127) Greene, F. D.; Misrock, S. L.; Wolfe, J. R. *Journal of the American Chemical Society* **1955**, *77* (14), 3852.

(128) Huang, J.; Su, J.-H.; Tian, H. *Journal of Materials Chemistry* **2012**, *22* (22), 10977.

(129) Becker, H. D.; Langer, V.; Becker, H. C. *The Journal of Organic Chemistry* **1993**, *58* (23), 6394.

(130) Parker, V. D.; Nilsson, A.-M.; Wikander, G.; Karrer, P.; Shimizu, A. *Acta Chemica Scandinavica* **1970**, *24*, 2775.

(131) Becker, H. D. *Chemical Reviews* **1993**, *93* (1), 145.

(132) Meador, M. A.; Hart, H. *The Journal of Organic Chemistry* **1989**, *54* (10), 2336.

(133) Hargreaves, J. S.; Webber, S. E. *Macromolecules* **1984**, *17* (2), 235.

(134) Hou, Y.; Wan, P. *Photochemical & Photobiological Sciences* **2008**, *7* (5), 588.

(135) Münzenberg, C. Synthesis of Compounds Presenting Three and Four Anthracene Units as Potential Connectors to Mediate Infinite Lateral Growth at the Air/Water Interface, ETH Zürich: Zürich, 2009.

(136) Teinemaa, E.; Kirso, U. *Polycyclic Aromatic Compounds* **1999**, *14* (1-4), 275.

(137) Stogryn, E. L. *Journal of Medicinal Chemistry* **1974**, *17* (5), 563.

(138) Lamm, J.-H.; Vishnevskiy, Y. V.; Ziemann, E.; Kinder, T. A.; Neumann, B.; Stammler, H.-G.; Mitzel, N. W. *European Journal of Inorganic Chemistry* **2014**, *2014* (5), 941.

(139) Cox, O., Chemical Modification of Polysulfone, University of Bath: Bath, 2012.

(140) Zweig, A.; Maurer, A. H.; Roberts, B. G. *The Journal of Organic Chemistry* **1967**, *32* (5), 1322.

(141) Weitzel, H.-P., M., K. *Makromol. Chem.* **1990**, *191* (11), 2837.

4 Experimental Section

4.1 General Remarks

^{1}H NMR Titrations

All ^{1}H NMR Titrations were performed on a Bruker Avance III 500 Ultrashield (500 MHz) spectrometer at room temperature. In all cases the host concentration was kept at 1mM concentration in $CDCl_3$. For better precision, the amount of $CDCl_3$ used in all host concentrations was determined not by volume but by weight on a Mettler Toledo AX205 and a Mettler AE200 balance. In order to keep the host concentration constant throughout the whole titration process, all guest solutions were prepared in 1mM host solution with a guest concentration of 1 M. All solutions were prepared prior to use and stored in closed volumetric flasks during measurements in order to minimize exposure to moisture. The amount of guest present in the single measurements was determined through integration of suitable peaks in the ^{1}H NMR spectra. The chemical shifts were determined relative to trimethylsilane TMS (0.000 ppm).

The nonlinear fitting procedures were executed in OriginPro 8.5.1 (OriginLab, 2011), using formula (15) as described in section 1.5. To account for measurement uncertainties of the spectrometer, all chemical shifts were attributed an uncertainty of ±0.001 ppm prior to fitting. The 95% confidence intervals were determined by the corresponding algorithm in Origin 8.5.1.

Analytical Instruments

Nuclear magnetic resonance (NMR)

Proton NMR (^{1}H NMR) spectra were recorded on Bruker Avance III 250 (250 MHz), Bruker Avance III 400 (400 MHz) and Bruker Avance III 500 Ultrashield (500 MHz) spectrometers at room temperature. The chemical shifts are shown in ppm (parts per million) relative to trimethylsilane TMS (0.000 ppm) or a residual solvent peak and *J* values are given in Hz (Hertz).

Carbon NMR (^{13}C NMR) spectra were recorded on Bruker Avance III 250 (63 MHz), Bruker Avance III 400 (101 MHz) and Bruker Avance III 500 Ultrashield (126 MHz) spectrometers at room temperature. Chemical shifts are given in ppm (parts per million) relative to the residual solvent peak.

Mass Spectrometry (MS)

MALDI-TOF-MS (Matrix Assisted Laser Desorption/Ionisation-Time of Flight-Mass Spectrometry) spectra were recorded with a Bruker Microflex. No matrices were used except were indicated otherwise. DART-MS was performed on a IonSense DART-SVP100 (He, 450 °C) connected to a Shimadzu LC--2020.

Gas-Chromatography (GC-MS)

GC-MS was performed on a Shimadzu GCMS-2020 SE equipped with a Zebron 5 MS Inferno column, allowing achieving temperatures up to 350 °C.

Gel Permeation Chromatography (GPC)

Gel Permeation Chromatography was performed on a Shimadzu LC-8A with CHCl$_3$ as elution solvent.

Solvents and Reagents

Unless stated otherwise, all solvents and reagents were used without further purification. Dry solvents were purchased from Acros AG, Merck, Sigma-Aldrich and Fluka AG. Technical grade solvents were used for column chromatography, HPLC grade solvents for recrystallizations, dry solvents (stored under inert gas) solvents for air and/or moisture sensitive reactions. For column chromatography silica gel 60 from Fluka (40–63 µm) and Siliaflash® p60 (40–63 µm) from Silicycle were used; basic aluminium oxide

(Brockmann activity I, 0.05-0.15 mm) and neutral aluminium oxide (details) were obtained from Fluka AG. Precoated silica gel TLC plates (20x20 cm on aluminium sheets) were used from Merck KGaA; precoated basic aluminium oxide and neutral aluminium oxide TLC plates also from Merck KGaA were used. For detection UV lamps at 254 nm or 366 nm were employed. Argon 4.8 from PanGas AG was employed.

4.2 Synthetic Procedures

9H-xanthene-9-thione

3
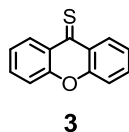
Xanthone (1.98 g, 10.0 mmol, 1.00 eq.) and Lawesson's reagent (4.09 g, 10.1 mmol, 1.01 eq.) were refluxed in 20 ml toluene (dry, Ar) for 1h. After cooling, silica was added into the reaction mixture and the solvent was removed under reduced pressure. The dried powder was added on top of a column and the product was purified by column chromatography (SiO$_2$; toluene) (75%).

^{1}H NMR (400 MHz, CDCl$_3$): δ = 8.75 (ddd, J = 8.2, 1.7, 0.5 Hz, 2H), 7.76 (td, J = 8.6, 7.0, 1.7 Hz, 2H), 7.56 – 7.45 (ddd, 2H), 7.38 (td, J = 8.2, 7.0, 1.2 Hz, 2H) ppm.

^{13}C NMR (101 MHz, CDCl$_3$): δ = 150.54, 134.88, 129.91, 129.09, 124.76, 118.28 ppm.

GC-MS (EI+, 70 eV): m/z (%) = 214 (6) [M$^+$], 213 (16) [M$^+$], 212 (100) [M$^+$], 211 (13) [M$^+$], 168 (38), 139 (31), 106 (11).

spiro[xanthene-9,2'-[1,3]dioxolane]
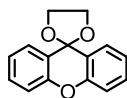
4a

To a solution of thioxanthone **3** (424 mg, 2.00 mmol, 1.00 eq.), ethylene glycol (149 mg, 2.40 mmol, 0.13 ml, 1.20 eq.) and silver trifluoroacetate AgOCOCF$_3$ (1.10 g, 5.00 mmol, 2.50 eq.) in acetonitrile (10 ml), trimethylamine (809 mg, 8.00 mmol, 1.11 ml, 4.00 eq.) was added dropwise and the reaction mixture was stirred at room temperature for 15 min. After removal of the solvent under reduced pressure, ethyl acetate was added and the mixture was filtered to remove Ag$_2$S. The organic phase was concentrated and the solvent removed under reduced pressure and the product purified by column chromatography (SiO$_2$; hexane/ethyl acetate 1:1) (65 %).

^{1}H NMR (400 MHz, CDCl$_3$): δ = 7.62 (dd, *J* = 7.8, 1.7, 0.5 Hz, 1H), 7.43 – 7.35 (m, 1H), 7.24 – 7.15 (m, 2H), 4.37 (s, 4H).

^{13}C NMR (101 MHz, CDCl$_3$): δ = 151.97, 149.12, 130.03, 126.05, 123.32, 116.93, 66.47 ppm.

GC-MS (EI+, 70 eV): m/z (%) = 240 (43) [M$^+$], 209 (100), 196 (19), 180 (49), 168 (24), 152 (29), 139 (39), 76 (23), 63 (17).

2-fluoro-3-iodobenzoic acid

6
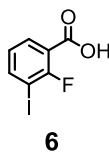
To a solution of *n*-buthllithium in tetrahydrofurane at -78°C, diisopropylamine and 1-fluoro-2-iodobenzene were added consecutively and stirred at the same temperature for 2 h, after which the reaction mixture was poured over an excess of freshly crushed carbon dioxide pellets. After neutralization, the target compound was recrystallized from ethyl acetate (60 %).

¹H NMR (250 MHz, DMSO-d_6): δ = 8.04 (ddd, *J* = 7.6, 5.7, 1.7 Hz, 1H), 7.81 (ddd, *J* = 7.7, 7.0, 1.7 Hz, 1H), 7.15 – 7.04 (m, 1H) ppm.

¹³C NMR (63 MHz, DMSO-d_6): δ = 164.45 (d, *J* = 3.6 Hz), 161.45 , 157.42 , 142.91 , 131.85 , 126.14 (d, *J* = 4.4 Hz), 121.13 ppm.

3,6-dihydroxy-9H-xanthen-9-one
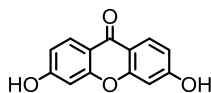
14

2, 2, 4, 4'-tetrahydroxybenzophenone (10.0 g, 40.6 mmol, 1.00 eq.) was heated for 24 h at 220°C in a furnace. The crude was suspended in 500 ml H_2O at 60°C and filtered. The residue was collected and dried under vacuum (85%).

^{1}**H NMR** (500 MHz, DMSO-d_6): δ = 10.81 (s, 2H), 7.98 (dt, J = 8.8, 1.4 Hz, 2H), 6.86 (dd, J = 8.8, 2.5 Hz, 2H), 6.82 (d, J = 2.3 Hz, 2H) ppm.

^{13}**C NMR** (126 MHz, DMSO-d_6): δ = 173.90, 163.35, 157.46, 127.76, 113.99, 113.65, 102.08 ppm.

3,6-dihydroxy-4,5-diiodo-9H-xanthen-9-one
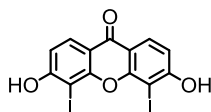
15

3,3'-dihydroxyxanthone (1.14 g, 5.00 mmol, 1.00 eq.) was dissolved in ethanol (75 ml) and I_2 (1.02 g) dissolved in 30 ml ethanol was added, followed by iodic acid HIO_3 (0.35 g) in H_2O (5 ml). After stirring the solution at reflux temperature for 2 h, the reaction was cooled to room temperature and quenched with aq. $Na_2S_2O_3$ and extracted with ethyl acetate. The combined organic phases were washed with brine and H_2O. After removal of the solvent under reduced pressure, the product was purified by flash chromatography (SiO_2; cyclohexane/ethyl acetate 20:1) (63%).

^{1}H NMR (500 MHz, DMSO-d_6): δ = 11.72 (s, 2H), 8.00 (d, J = 8.7 Hz, 2H), 7.02 (d, J = 8.7 Hz, 2H) ppm.

^{13}C NMR (126 MHz, DMSO-d_6): δ = 173.29, 163.40, 157.12, 127.53, 114.27, 112.59, 73.73 ppm.

4,5-diiodo-9-oxo-9H-xanthene-3,6-diyl bis(trifluoromethanesulfonate)

16
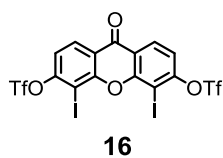
3,6-dihydroxy-4,5-diiodo-9H-xanthen-9-one **15** (480.0 mg, 1.00 mmol, 1.00 eq.) and N-phenyl bis(trifluoromethanesulfonamide) (715 mg, 2.00 mmol, 2.00 eq.) were dissolved in 20 mL of CH_2Cl_2 (dry, Ar). After the adding ethyldiisopropylamine (323.1 mg, 2.50 mmol, 0.43 ml, 2.50 eq.), the solution was stirred at room temperature for 6 h. The solvent was removed under reduced pressure and the product purified by column chromatography (SiO_2, CH_2Cl_2 with 5% methanol) (73 %).

^{1}H NMR (250 MHz, DMSO-d_6): δ = 8.35 (d, J = 8.8 Hz, 2H), 7.56 (d, J = 8.8 Hz, 2H) ppm.

EI-MS (70 eV): m/z (%) = 746 (11), 745 (17) 744 (100) [M$^+$], 611 (36), 583 (19), 484 (10), 450 (27), 422 (14).

4,5-diiodo-3,6-dimethoxy-9H-xanthen-9-one
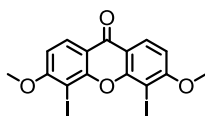
17

3,3'-dihydroxy-4, 4'diiodo-9H-xanthone **15** (750 mg, 1.56 mmol, 1.00 eq.) was suspended in 75 ml acetone (dry, Ar) and K_2CO_3 (6.00 eq.) was added. After the dropwise addition of dimethyl sulfate (16 eq.), the reaction was slowly heated to 60°C and stirred overnight. The solution was cooled to room temperature, 1M aq. NaOH (20 ml) was added slowly and the reaction was stirred for 1 h. After filtration, the residue was repeatedly washed with H_2O and recrystallized from acetic acid (90%).
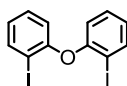
^{1}H NMR (250 MHz, DMSO-d_6): δ = 8.08 (d, J = 8.8 Hz, 2H), 7.15 – 6.99 (m, 2H), 3.94 (s, 6H) ppm.

^{13}C NMR (63 MHz, DMSO-d_6): δ = 164.54, 157.48, 127.47, 114.96, 113.24, 100.57, 56.07 ppm.

MS (MALDI-ToF, positive ion reflector mode): m/z (a.u.) = 403 [M-I+Na$^+$], 402 [M-I+Na$^+$], 401 [M-I+Na$^+$], 388, 374, 333, 296, 279, 268, 257.

R_f (SiO$_2$, ethyl acetate) = 0.38
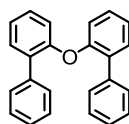
2,2'-oxybis(iodobenzene)

19

2,2'-oxydianiline (190 mg, 0.95 mmol, 1.00 eq.) was given at RT into a stirred solution of p-TsOH·H$_2$O (542 mg, 2.85 mmol, 3.00 eq.) in MeCN (10 ml) and the suspension was cooled to 0°C. A solution of NaNO$_2$ (131 mg, 1.90 mmol, 2.00 eq.) and KI (394 mg, 2.40 mmol, 2.50 eq.) in water (3 ml) was added slowly. After stirring for 30 min. at 0°C, the solution was heated to 90°C and stirred for additional 3h. The reaction was quenched with H$_2$O, sat. aq. NaHCO$_3$ and 20% aq. Na$_2$S$_2$O$_3$. After extraction of the organic phases with tBMe the solvent was removed under reduced pressure and the crude was purified by column chromatography (SiO$_2$, cyclohexane/CH$_2$Cl$_2$ 2:1) (55%).

^{1}H-NMR (400 mHz, CD$_2$Cl$_2$): δ = 7.94 (dd, *J* = 7.9 Hz, *J* = 1.6 Hz, 2H), 7.65 (m, 2H), 6.96 (m, 2H), 6.82 (dd, *J* = 8.2 Hz, *J*= 1.5 Hz, 2H) ppm.

^{13}C NMR (101 MHz, CD$_2$Cl$_2$): δ = 155.99, 140.08, 129.64, 125.50, 118.72, 88.41 ppm

GC-MS (EI+, 70 eV): m/z (%)= 422 (50) [M$^+$], 168 (100), 139 (52), 76 (39), 50 (21).
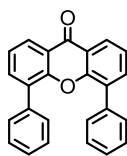
2,2'-oxydibiphenyl

20

2,2'-oxybis(iodobenzene) **19** (114 mg, 0.27 mmol, 1.00 eq.), phenylboronic acid pinacol ester (242 mg, 1.19 mmol, 4.40 eq.), K_2CO_3 (164 mg, 1.19 mmol, 4.40 eq.) and $Pd(PPh_3)_4$ (15 mol%) were given in a Schlenktube (dry, Ar) and dissolved in 10 ml of a methanol/H_2O (3:1) mixture. The solution was stirred at 89°C overnight. The reaction was diluted with water und extracted with toluene. After removal of the solvent the residue was purified by column chromatography (SiO_2, cyclohexane) (67%).

^{1}H-NMR (400 mHz, $CDCl_3$): δ = 7.42 (m, 4H), 7.37 (dd, J = 7.6 Hz, J = 1.7 Hz, 2H), 7.31 (m, 6H), 7.21 (m, 2H), 7.11 (td, J = 7.5 Hz, J = 1.1 Hz, 2H), 6.90 (dd, J= 8.2 Hz, ^4J(H,H) = 1.0 Hz, 2H) ppm.

^{13}C-NMR (63 mHz, $CDCl_3$): δ = 118.8, 123.4, 127.1, 127.9, 128.5, 129.4, 131.2, 133.2, 137.9, 154.0 ppm.

**R_f** (SiO_2, cyclohexane) = 0.28

4,4'-diphenyl-9*H*-xanthene-9-one

1c

2,2'-oxydiphenyl **20** (20.0 mg, 0.06 mmol, 1.00 eq.), Pd(OAc)$_2$ (0.68 mg, 5.00 mol%) and K$_2$S$_2$O$_8$ (34.0 mg, 0.12 mmol, 2.00 eq.) were given into a Schlenk tube (dry, Ar). The tube was evacuated and purged with CO three times. Afterwards TFA (1 ml) was added with a syringe. The mixture was heated to 50°C for 4h. After the release of CO the reaction was quenched with H$_2$O and extracted with CH$_2$Cl$_2$. The combined organic layers were dried with Na$_2$SO$_4$ and the solvent removed. The product was purified by column chromatography (SiO$_2$, cyclohexane/ethyl Acetate 1:1) (41%).

^{1}H-NMR (400 mHz, CDCl$_3$): δ = 8.38 (dd, *J* = 8.0 Hz, *J* =1.7 Hz, 2H), 7.71 (dd, *J* = 7.4 Hz, *J* =1.7 Hz, 2H), 7.45 (t, *J* = 7.8 Hz, 2H), 7.31 (m, 6H), 7.19 (t, *J* = 7.5 Hz, 4H) ppm;

MS (MALDI-ToF, positive ion reflector mode): m/z (a.u.) = 351, 350, 349 [M+H$^+$], 321.

5,5'-(oxybis(2,1-phenylene))bis(benzo[d][1,3]dioxole)

23
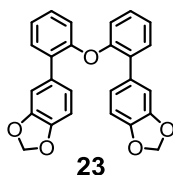
2,2'-oxybis(iodobenzene) **19** (100 mg, 0.24 mmol, 1.00 eq.), 3,4-(methylenedioxy)phenyl boronic acid pinacol ester (259 mg, 1.04 mmol, 4.40 eq.), K_2CO_3 (143 mg, 1.04 mmol, 4.40 eq.) and $Pd(PPh_3)_4$ (15 mol%) were given in a Schlenktube (dry, Ar) and dissolved in 10 ml of a methanol/H_2O (3:1) mixture. The solution was stirred at 90°C overnight. The reaction was diluted with water und extracted with toluene. After removal of the solvent the residue was purified by column chromatography (SiO_2, cyclohexane/ethyl acetate, 1:1) (50%).
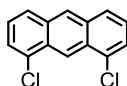
^{1}H NMR (400 MHz, Acetone-d_6): δ = 7.36 (dd, J = 7.6, 1.8 Hz, 2H), 7.23 (ddd, J = 8.2, 7.4, 1.8 Hz, 2H), 7.11 (td, J = 7.5, 1.2 Hz, 2H), 6.95 – 6.89 (m, 4H), 6.84 (dd, J = 8.2, 1.2 Hz, 2H), 6.82 – 6.77 (m, 2H), 5.95 (s, 4H)

^{13}C NMR (101 MHz, Acetone-d_6): δ = 154.75, 148.36, 147.87, 133.59, 132.55, 131.93, 129.45, 124.53, 123.58, 119.66, 110.47, 108.76, 102.06 ppm.

GC-MS (EI +, 70 eV): m/z (%) = 412 (5) [M$^+$], 411 (28) [M$^+$], 410 (100) [M$^+$], 155 (11), 139 (35), 127 (12).

R_f (SiO_2, cyclohexane/ ethyl acetate 1:1) = 0.73
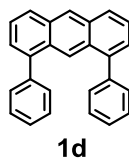
1,8-dichloroanthracene

27

1,8-dichloroanthraquinone (10.0 g, 36.1 mmol, 1.00 eq.) was suspended in aq. 28% NH_3 (120 ml) and H_2O (90 ml) and cooled in an ice-bath to 0°C. Zn dust (22.0 eq.) was added in portions over 15 min. The slurry was warmed to room temperature, stirred for 20 min, heated slowly and stirred for 4 h at 80°C. The mixture was allowed to reach room temperature and the mixture was filtered. The filtrate was extracted with CH_2Cl_2 (3x50ml) and the residue in the filter was bloated/suspended repeatedly with boiling CH_2Cl_2. The combined organic phases were concentrated and the crude product was recrystallized from a mixture of aq. 12M HCl (40 ml) and *i*-PrOH (440 ml) (55%).

^{1}H NMR (400 MHz, CDCl$_3$): δ = 9.26 (q, *J* = 0.9 Hz, 1H), 8.48 (d, *J* = 0.9 Hz, 1H), 7.95 (dq, *J* = 8.6, 0.9 Hz, 2H), 7.63 (dd, *J* = 7.2, 1.0 Hz, 2H), 7.42 (dd, *J* = 8.5, 7.2 Hz, 2H) ppm.

^{13}C NMR (101 MHz, CDCl$_3$): δ = 132.83, 132.65, 129.71, 127.77, 127.44, 126.190, 125.84, 121.22 ppm.

GC-MS (EI +, 70 eV): m/z (%) = 250 (11) [M$^+$], 249 (10) [M$^+$], 248 (65) [M$^+$], 247 (15) [M+], 246 (100) [M$^+$], 176 (39), 124 (13), 88 (25).

1,8-diphenylanthracene

1d

A mixture of 1,8-dichloroanthracene **27** (200.00 mg, 0.81 mmol, 1.00 eq), 4-phenylboronic acid (296.3 mg, 2.43 mmol, 3.00 eq.), Pd(amphos)Cl$_2$ (6 mol%) and Cs$_2$CO$_3$ (1.85 g, 5.67 mmol, 7.00 eq.) in 15 ml toluene/H$_2$O (10:1) (Ar) was stirred at reflux for 2 h. After cooling to room temperature, the reaction mixture was washed with H$_2$O. After removal of the solvent under reduced pressure, the crude was purified through flash chromatography (SiO$_2$; cyclohexane/ ethyl acetate 5:1), followed by GPC (63%).
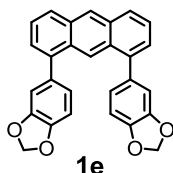
^{1}H NMR (400 MHz, CDCl$_3$): δ = 8.67 – 8.58 (m, 1H), 8.55 (s, 1H), 8.04 (dt, J = 8.7, 1.2 Hz, 2H), 7.59 – 7.46 (m, 6H), 7.45 – 7.38 (m, 6H), 7.38 – 7.32 (m, 2H) ppm.

^{13}C NMR (101 MHz, CDCl$_3$): δ = 140.57, 140.45, 131.86, 130.08, 129.98, 128.11, 127.64, 127.21, 126.73, 126.12, 125.29, 124.01 ppm.

MS (MALDI-ToF, positive ion reflector mode): m/z (a.u.) = 330 [M+H$^+$].

***R*$_f$** (SiO$_2$, cyclohexane/ ethyl acetate 5:1) = 0.80

1,8-bis(3,4-(methylenedioxy)phenyl)anthracene

1e

A mixture of 1,8-dichloroanthracene **27** (200.00 mg, 0.81 mmol, 1.00 eq), 3,4-(methylenedioxy)phenyl boronic acid (403.0 mg, 2.43 mmol, 3.00 eq.), Pd(amphos)Cl$_2$ (6 mol%) and Cs$_2$CO$_3$ (1.85 g, 5.67 mmol, 7.00 eq.) in 15 ml toluene/H$_2$O (10:1) (Ar) was stirred overnight at reflux temperature. After cooling to room temperature, the reaction mixture was washed with H$_2$O. After removal of the solvent under reduced pressure, the crude was purified through flash chromatography (SiO$_2$; Cyclohexane/ ethyl acetate 3:1), followed by GPC (40%).

^{1}H NMR (400 MHz, CDCl$_3$): δ = 8.66 (d, J = 1.2 Hz, 1H), 8.51 (s, 1H), 8.10 − 7.91 (m, 2H), 7.50 (dd, J = 8.5, 6.7 Hz, 2H), 7.38 (dd, J = 6.8, 1.2 Hz, 2H), 7.07 − 6.94 (m, 4H), 6.91 (d, J = 8.5 Hz, 2H), 6.03 (s, 4H) ppm.

^{13}C NMR (101 MHz, CDCl$_3$): δ = 147.51, 146.86, 140.11, 134.42, 131.87, 130.17, 127.48, 126.67, 125.87, 125.28, 124.04, 123.54, 110.60, 108.08, 101.06 ppm.

MS (MALDI-ToF, positive ion linear mode): m/z (a.u.) = 833, 466, 433, 418 [M$^+$].

R_f (SiO$_2$, cyclohexane/ ethyl acetate 3:1) = 0.47

1,8-bis(phenylethynyl)anthraquinone
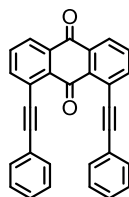
1f

1,8-dichloroanthraquinone **27** (277 mg, 1.00 mmol, 1.00 eq.), phenylacetylene (225 mg, 2.20 mmol, 0.24 ml, 2.20 eq.), 5mol% copper(I) iodide (5mol%, 10.0 mg) and Pd(Amphos)Cl$_2$ (5mol%, 35.0 mg) were mixed in toluene (dry, Ar) (10 ml) and freshly distilled trimethylamine (3 ml). The solution was heated at 110°C for 4h. After cooling to room temperature, the reaction mixture was passed through a silica plug and the target molecule was isolated by GPC (30%).

^{1}H NMR (400 MHz, CDCl$_3$): δ = 7.61 – 7.49 (m, 6H), 7.41 – 7.31 (m, 10H) ppm.

^{13}C NMR (101 MHz, CDCl$_3$): δ = 178.83, 143.50, 132.51, 129.21, 128.44, 121.80, 99.98, 98.17, 81.55, 73.90 ppm.

R_f (SiO$_2$, cyclohexane/ ethyl acetate 1:1) = 0.64
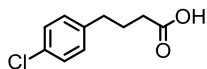
4-(4-chlorophenyl)-4-oxobutanoic acid
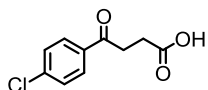
29

A mixture of succinic anhydride (2.00 g, 2.00 mmol, 1.00 eq.), chlorobenzene (10 mL) and anhydrous aluminum chloride (301.3 mg, 2.26 mmol, 1.13 eq.) was heated at reflux temperature overnight. The reaction was quenched with 6 M aq. HCl at 0°C. After extraction of the mixture with ethyl acetate, the product was purified by extracting the organic phases with 2 M aq. NaOH, filtering the combined aqueous phases and acidic precipitation through 12 M HCl. The precipitate was filtered, washed with H_2O, dried under reduced pressure and recrystallized from methanol (74 %).

^{1}H NMR (400 MHz, CDCl$_3$) δ 7.93 (d, J = 8.3 Hz, 2H), 7.48 – 7.43 (m, 2H), 3.33 – 3.25 (m, 2H), 2.85 – 2.76 (m, 2H).
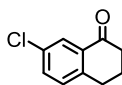
4-(4-chlorophenyl)butanoic acid

30

A round-bottom flask with a condenser and a Dean-Stark trap was charged with 4-(4-chlorophenyl)-4-oxobutanoic acid **29** (5.00 g, 23.5 mmol, 1.00 eq.), potassium hydroxide (2.93 g, 52.2 mmol, 2.22 eq.), hydrazine monohydrate (2.57 g, 51.4 mmol, 2.50 ml, 2.19 eq.), and triethylene glycol (25 mL). The heterogeneous mixture was stirred at 125°C for 1.5 h (during which the the mixture became homogenous) and then at 180°C during 3.5 h. After cooling the reaction mixture to room temperature, it was diluted with H_2O (25 mL) and given into 30 ml of 2.5 M aq. hydrochloric acid. The crude product formed overnight and was filtered off, dissolved in sat. aq. potassium carbonate (50 mL), diluted with H_2O (100 mL) and poured into 2.5 M aq. hydrochloric acid. Upon full precipitation, the product was collected, washed on a filter with H_2O und dried under reduced pressure (67 %).

^{1}H NMR (400 MHz, CDCl$_3$): δ = 7.25 (m, 2H), 7.17 – 7.07 (m, 2H), 2.65 (dd, *J* = 8.3, 6.9 Hz, 2H), 2.37 (t, *J* = 7.4 Hz, 2H), 2.05 – 1.87 (m, 2H) ppm.

^{13}C NMR (101 MHz, CDCl$_3$): δ = 178.47, 139.60, 131.84, 129.83, 128.54, 34.31, 32.95, 26.09 ppm.
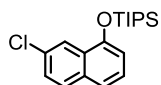
7-chloro-1-tetralone

31

Polyphosphoric acid (10 g, used as solvent) was place in a beaker and heated to 90 °C on a steam bath and 4-(4-chlorophenyl)butanoic acid **30** (1.50 g, 7.55 mmol, 1.00 eq)) was added portionwise. After stirring the mixture for 5 min, an additional 20 g excess of polyphosphoric acid was added. After another 5 min of heating, the thick, homogeneous viscous orange oil was cooled to 60 °C and H_2O (100 mL) was added. The end of the reaction was indicated through the absence of the orange oil, after which the mixture was cooled to room temperature and extracted with methyl tert-butyl ether. The combined organic phases were washed with H_2O, 1 M aq. NaOH solution, H_2O, 3% (v/v) aq. acetic acid, sat. aq. sodium bicarbonate and finally with H_2O. The combined organic phases were dried over Na_2SO_4 and the solvent removed under reduced pressure (95%).

¹H NMR (400 MHz, $CDCl_3$): δ = 8.00 (d, *J* = 2.3 Hz, 1H), 7.42 (dd, *J* = 8.2, 2.4 Hz, 1H), 7.21 (d, *J* = 8.2 Hz, 1H), 2.93 (t, *J* = 6.1 Hz, 2H), 2.65 (dd, *J* = 7.3, 5.8 Hz, 2H), 2.14 (p, *J* = 6.5 Hz, 2H) ppm.

¹³C NMR (101 MHz, $CDCl_3$): δ = 197.13, 142.65, 133.82, 133.27, 132.87, 130.36, 126.97, 38.82, 29.12, 23.05 ppm.

((7-chloronaphthalen-1-yl)oxy)triisopropylsilane

32

7-chloro-1-tetralone **31** (360.0 mg, 2.00 mmol, 1.00 eq.) was dissolved in CH_2Cl_2 (dry, Ar) (8 ml). After the addition of triethylamine (303.6 mg, 3.00 mmol, 0.42 ml, 1.50 eq.), triisopropylsilyl triflate (2.40 mmol, 735.41 mg, 0.65 ml, 1.20 eq.,) was given into the reaction mixture. The reaction was stirred at room temperature for 2 h. The reaction mixture was washed with aq. sodium bicarbonate, dried over Na2SO4 and the solvent removed under reduced pressure. Without further purification, the crude was dissolved in dioxane (10 ml) and 2,3-dichloro-5,6-dicyanobenzoquinone (DDQ) (1.36 g, 6.00 mmol, 3.00 eq. relative to starting material **31**) and heated at 80°C for 1 h. The solution was cooled to room temperature and filtered. The filtered solid was washed with hexane. The combined organic phases were concentrated and the product purified by column chromatography (SiO_2; hexane) (80% over two steps).

^{1}H NMR (400 MHz, CDCl$_3$): δ = 8.23 (d, J = 2.2 Hz, 1H), 7.73 (d, J = 8.7 Hz, 1H), 7.40 (dd, J = 8.7, 2.1 Hz, 2H), 7.30 (t, J = 7.9 Hz, 1H), 6.93 – 6.86 (m, 1H), 1.17 (d, J = 7.5 Hz, 21H) ppm.

^{13}C NMR (101 MHz, CDCl$_3$): δ = 151.31, 133.18, 130.99, 129.27, 128.34, 127.01, 126.22, 121.88, 120.33, 112.77, 18.10, 13.05 ppm.

1-bromo-7-chloro-3,4-dihydronaphthalene-2-carbaldehyde
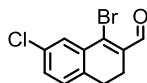
33

A solution of dimethylformamide (486 mg, 6.64 mmol, 0.51 ml, 4.00 eq.) in CH_2Cl_2 (dry, Ar) (10 ml) was cooled to 0°C. PBr_3 (1.12 g, 4.15 mmol, 0.39 ml, 2.50 eq.) was added. After stirring for 1.5 h, 7-chlorotetralone **31** (300 mg, 1.67 mmol, 1.00 eq.) in CH_2Cl_2 (dry, Ar) (5 ml) was added; then the solution was warmed to room temperature for 1 h and then stirred at reflux temperature for 2.5 h. After cooling to room temperature, the reaction mixture was carefully given into a solution of 1:1 sat. aq. $NaHCO_3/H_2O$ at 0°C and neutralized with solid $NaHCO_3$. The mixture was extracted with CH_2Cl_2. Following the removal of the solvent of the combined organic phases, the product was purified by column chromatography (SiO_2; cyclohexane/ethyl acetate, 40:1) (40%).

GC-MS (EI+, 70 eV): m/z (%) = 272 (18) [M$^+$], 270 (13) [M$^+$], 237 (15), 162 (50), 128 (100), 77 (10), 63 (14).
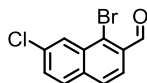
7-chloronaphthalen-1-ol
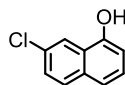
34

A mixture of ((7-chloronaphthalen-1-yl)oxy)triisopropylsilane **32** (400.0 mg, 1.14 mmol, 1.00 eq.), *N*-methyl-2-pyrrolidone (5.0 mL), NaOH (500.0 mg, 12.5 mmol, 11.0 eq.), H_2O (0.5 mL) and MeOH (2.0 mL) was stirred for 3 h at 60°C. After cooling to room temperature, the reaction mixture was diluted with H_2O and washed with cyclohexane. Subsequent to acidification with 6M aq. HCl, the aqueous phase was extracted ethyl acetate. The combined organic phases were washed with H_2O, dried over Na_sSO_4, the solvent removed under reduced pressure and the product was purified by column chromatography (SiO_2; cyclohexane/ethyl acetate 4:1).

^{1}H NMR (400 MHz, $CDCl_3$): δ = 8.19 (d, *J* = 2.1 Hz, 1H), 7.74 (d, *J* = 8.8 Hz, 1H), 7.46 – 7.38 (m, 2H), 7.30 (t, *J* = 7.9 Hz, 1H), 6.87 – 6.79 (m, 1H) ppm.

^{13}C NMR (101 MHz, $CDCl_3$): δ = 129.24, 127.41, 126.09, 121.05, 120.51, 109.48 ppm.

1-bromo-7-chloro-2-naphthaldehyde

35

A mixture of 1-bromo-7-chloro-3,4-dihydronaphthalene-2-carbaldehyde 33 (518.0 mg, 1.89 mmol, 1.00 eq.) and 2,3-dichloro-5,6-dicyano-*p*-benzoquinone (1.40 g, 5.67 mmol, 3.00 eq.) in toluene (15 ml) was refluxed for 3 days. After filtering through Celite and repeated washing of the residue on the Celite with hot toluene, the solvent was removed under reduced pressure and the crude was purified by column chromatography (SiO$_2$, cyclohexane/toluene 10:1).

^{1}H NMR (400 MHz, CDCl$_3$): δ = 10.65 (t, *J* = 1.1 Hz, 1H), 8.51 (dt, *J* = 2.1, 0.7 Hz, 1H), 7.94 (d, *J* = 8.5 Hz, 1H), 7.86 – 7.77 (m, 2H), 7.68 – 7.58 (m, 1H).

^{13}C NMR (101 MHz, CDCl$_3$): δ = 192.47, 135.37, 134.63, 133.01, 132.06, 131.13, 130.56, 130.05, 128.13, 127.11, 124.50.

GC-MS (EI+, 70 eV): m/z (%) = 272 (24) [M$^+$], 271 (33) [M$^+$], 270 (99) [M$^+$], 269 (100) [M$^+$], 268 (75) [M$^+$], 267 (75) [M$^+$], 241 (33), 160 (78), 126 (68), 99 (26), 80 (19), 75 (34), 62 (19), 51 (11).

2,12-dichloro-7,7-dimethyl-7H-dibenzo[c,h]xanthene
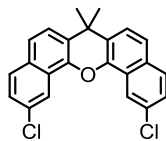
39

A mixture 7-chloronaphthalen-1-ol **34** (50.0 mg, 0.28 mmol, 1.00 eq), acetone (28.0 mg, 0.56 mmol, 35.0 µl, 2.00 eq.) and *p*-toluenesulfonic acid (2g) was slowly heated to 125°C and stirred for 1.5h. After cooling the reaction was diluted with H_2O and extracted with CH_2Cl_2. The combined organic phases were washed with 1M aq. NaOH and dried with Na_2SO_4. After removal of the solvent the product was purified through column chromatography twice (1. SiO_2, cyclohexane/ ethyl acetate 10:1; 2. Basic Alox, cyclohexane/CH_2Cl_2 10:1) (45%).

^{1}H NMR (400 MHz, $CDCl_3$): δ = 8.22 (d, *J* = 2.2 Hz, 2H), 7.72 (d, *J* = 8.8 Hz, 2H), 7.40 (dd, *J* = 8.7, 2.0 Hz, 2H), 7.34 – 7.27 (m, 2H), 6.89 (dd, *J* = 7.5, 1.0 Hz, 2H), 1.83 (s, 6H) ppm.

^{13}C NMR (101 MHz, $CDCl_3$): δ = 151.29, 133.16, 130.97, 129.25, 128.32, 127.00, 126.20, 121.86, 120.31, 112.76, 18.09, 13.04 ppm.

MS (MALDI-ToF, positive ion reflector mode): m/z (a.u.) = 723, 706, 686, 672, 476, 377 [M$^+$], 363, 329, 299.

R_f (Basic Alox, cyclohexane/ ethyl acetate 10:1) = 0.37

7,7-dimethyl-2,12-diphenyl-7H-dibenzo[c,h]xanthene

1h
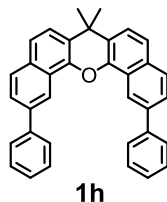
A mixture of 2,12-dichloro-7,7-dimethyl-7H-dibenzo[c,h]xanthene **39** (35.0 mg, 0.10 mmol, 1.00 eq.), phenylboronic acid (45.0 mg, 0.37 mmol, 2.00 eq.), Cs_2CO_3 (241.0 mg, 0.74 mmol, 4.00 eq.) and Pd(Amphos)Cl$_2$ (4.00 mg, 6 mol%) in toluene/H$_2$O (10:1) (11 ml) was stirred at reflux temperature for 6 h under an argon atmosphere. The solvent was removed under reduced pressure and the compound was purified by column chromatography (SiO$_2$; cyclohexane/ethyl acetate 2:1) (30%).

^{1}H NMR (400 MHz, CDCl$_3$): δ = 8.95 (dt, *J* = 1.8, 0.7 Hz, 2H), 7.99 – 7.88 (m, 6H), 7.86 (dd, *J* = 8.5, 1.9 Hz, 2H), 7.71 – 7.52 (m, 8H), 7.51 – 7.43 (m, 2H), 1.83 (s, 6H) ppm.

^{13}C NMR (101 MHz, CDCl$_3$): δ = 144.37, 141.13, 138.34, 132.22, 128.99, 128.05, 127.53, 127.22, 125.55, 124.50, 124.29, 123.55, 122.43, 119.80, 34.29, 33.04 ppm.

MS (MALDI-ToF, positive ion reflector mode): m/z (a.u.) = 463 [M+H$^+$], 449.

1,8-di((E)-styryl)anthracene
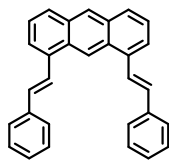
1i

Under an Ar atmosphere, 1,8-dichloroanthracene **27** (100mg, 0.41mmol, 1.00 eq.), styrene (92.9 mg, 0.10 ml, 0.89mmol, 2.20 eq), Cs_2CO_3 (290 mg, 0.89mmol, 2.20 eq.), $Pd_2(dba)_3$ (11.1 mg, 3mol%,) and $^tBu_3P$ (10.0 mg, 12 mol%) were dissolved in DMF (10 ml). The reaction solution was stirred at 120°C for 18 h. After cooling, the reaction was diluted with toluene (20 ml). After extracting 4 times with 3% (v/v) aq. HCl, the organic phases were dried with Na_2SO_4, the solvent removed and the product isolated through flash chromatography (SiO_2; cyclohexane/ ethyl acetate 10:1) (40%).

^{1}H NMR (400 MHz, $CDCl_3$): δ = 9.15 – 9.11 (m, 1H), 8.48 (s, 1H), 8.03 (d, J = 16.0 Hz, 2H), 7.98 (d, J = 8.5 Hz, 2H), 7.74 (dt, J = 6.9, 1.0 Hz, 2H), 7.68 – 7.62 (m, 4H), 7.50 (dd, J = 8.5, 6.9 Hz, 2H), 7.46 – 7.38 (m, 4H), 7.38 – 7.29 (m, 2H), 7.26 (d, J = 16.0 Hz, 2H) ppm.

^{13}C NMR (101 MHz, $CDCl_3$): δ = 137.65, 135.55, 132.18, 131.81, 129.92, 128.83, 128.11, 127.88, 127.57, 126.77, 126.00, 125.45, 123.48, 118.92 ppm.

MS (DART-EI): m/z (%) = 383 (100) [M+H$^+$], 365 (40), 268 (12), 261 (10), 255 (30), 201 (61), 183 (34).

R_f (SiO_2, cyclohexane/ ethyl acetate 10:1) = 0.35

1,8-bis((E)-3,4-dimethoxystyryl)anthracene

1j
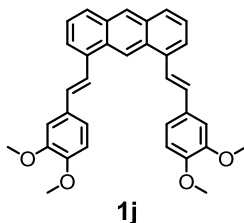
Under an Ar atmosphere, 1,8-dichloroanthracene **27** (100 mg, 0.41 mmol, 1.00 eq.), 3,4-dimethoxystyrol (146.2 mg, 0.13 ml, 0.89 mmol, 2.20 eq), Cs_2CO_3 (290 mg, 0.89 mmol, 2.20 eq.), $Pd_2(dba)_3$ (11.1 mg, 3mol%) and $^tBu_3P$ (10.0 mg, 0.012 ml, 12 mol%) were dissolved in DMSO (10 ml). The reaction solution was stirred at 160°C for 16 h. After cooling, the reaction was diluted with toluene (20 ml). After extracting 4 times with 3% (v/v) aq. HCl, the organic phases were dried with Na_2SO_4, the solvent removed and the product isolated through flash chromatography (SiO_2; toluene/pentane 1:1) (60%).

^{1}H NMR (400 MHz, $CDCl_3$): δ = 9.14 (s, 1H), 8.47 (s, 1H), 7.96 (d, J = 8.5 Hz, 2H), 7.88 (d, J = 15.9 Hz, 2H), 7.71 (d, J = 6.9 Hz, 2H), 7.55 – 7.44 (m, 2H), 7.19 (d, J = 16.4 Hz, 2H), 7.16 (d, J = 7.1 Hz, 4H), 6.92 – 6.84 (m, 2H), 3.93 (s, 6H), 3.86 (s, 6H) ppm.

^{13}C NMR (101 MHz, $CDCl_3$): δ = 149.27, 149.18, 135.67, 131.92, 131.84, 130.84, 129.87, 127.84, 127.52, 125.45, 124.16, 123.16, 119.90, 118.95, 111.32, 109.09, 56.02, 55.79 ppm.

MS (DART-EI): m/z (%) = 520 (100) [M+NH$_4^+$], 503 (80) [M+H$^+$], 430 (10), 414 (52), 400 (10), 382 (16), 378 (19), 365 (18), 335 (13), 218 (61), 200 (57), 196 (19), 183 (22).

R_f (SiO_2, pentane/toluene 1:1) = 0.55
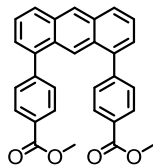
(4-(methoxycarbonyl)phenyl)boronic acid
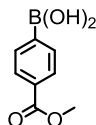
46

SOCl$_2$ (24.0 mmol, 2.86 g, 1.74 ml, 6.00 eq.) was slowly added to a solution of 4-Boronobenzoic acid (664 mg, 4.00 mmol, 1.00 eq) in 15 mL MeOH (dry, Ar) under heavy stirring. The reaction mixture was stirred at 50°C for 3 h. After removing the solvent under reduced pressure, the crude was dissolved in brine and extracted with ethyl acetate. The combined organic phases were dried over Na$_2$SO$_4$ and the solvent evaporated (quant.).

^{1}H NMR (400 MHz, CDCl$_3$): δ = 8.31 (d, *J* = 7.7 Hz, 2H), 8.17 (d, *J* = 7.7 Hz, 2H), 3.98 (s, 3H) ppm.

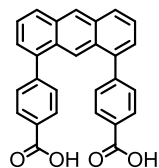Dimethyl-4,4'-(anthracene-1,8-diyl)dibenzoate

47

1,8-dichloroanthracene **27** (200 mg, 0.81 mmol, 1.00 eq.), 4-(methoxycarbonyl)-phenylboronic acid (437 mg, 2.43 mmol, 3.00 eq.) and Cs_2CO_3 (1.85 g, 5.67 mmol, 7.00 eq.) were dissolved in toluene/H_2O (1:1) (Ar) (15ml) under an argon atmosphere and the solution was stirred at 110°C overnight. After cooling the reaction mixture to room temperature, the solvent was remove under reduced pressure and the product was purified by column chromatography (SiO_2; CH_2Cl_2) (60 %).

^{1}H NMR (400 MHz, CDCl$_3$): δ = 8.57 (s, 1H), 8.42 (s, 1H), 8.07 (dd, J = 8.3, 4.4 Hz, 6H), 7.70 – 7.46 (m, 6H), 7.46 – 7.38 (m, 2H), 3.98 (s, 6H) ppm.

^{13}C NMR (101 MHz, CDCl$_3$): δ = 166.88, 145.12, 139.44, 131.81, 129.95, 129.82, 129.47, 129.10, 128.33, 127.06, 126.45, 125.33, 123.32, 52.14.

4,4'-(anthracene-1,8-diyl)dibenzoic acid

44

Dimethyl-4,4'-(anthracene-1,8-diyl)dibenzoate **47** (9.20 mg, 0.021 mmol, 1.00 eq.) was stirred in THF/H_2O (5:1) (6 ml) with potassium hydroxide (0.12 mmol, 7.00 mg, 6.00 eq.) at room temperature for 5 h. The reaction mixture was diluted with ethyl acetate and extracted with 1 M aq. NaOH solution. The product was isolated through acidic precipitation with 12 M HCl and filtration of the combined aqueous phases. The product was washed on the filter with cold H_2O and dried under reduced pressure (quant.).

^{1}H NMR (400 MHz, DMSO-d_6): δ = 12.96 (s, 2H), 8.82 (s, 1H), 8.50 (s, 1H), 8.22 (d, J = 8.6 Hz, 2H), 8.04 (d, J = 8.1 Hz, 2H), 7.67 (dd, J = 27.2, 8.0 Hz, 3H), 7.52 (d, J = 6.7 Hz, 1H) ppm.

4,5-dichloroanthrone
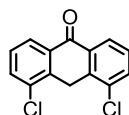

48

A mixture of 1,8-dichloroanthraquinone **24** (750 mg, 2.69 mmol, 1.00 eq.) and $Na_2S_2O_4$ (4.21 g, 24.2 mmol, 9.00 eq.) in DMF/H_2O (1:1, v/v) (60 ml) was heated slowly heated to 90°C and stirred for 4h. After cooling to room temperature and diluting with H_2O (300 ml), the solution was extracted with CH_2Cl_2. After removing the solvent from the combined organic phases under reduced pressure, the compound was purified by column chromatography (SiO_2, toluene/pentane 3:1) (60%).

^{1}H NMR (400 MHz, $CDCl_3$): δ = 8.32 (dd, *J* = 7.9, 1.3 Hz, 2H), 7.73 (dd, *J* = 7.9, 1.3 Hz, 2H), 7.48 (tt, *J* = 7.8, 0.7 Hz, 2H), 4.29 (s, 2H) ppm.

^{13}C NMR (101 MHz, $CDCl_3$): δ = 137.36, 134.21, 133.78, 133.75, 132.89, 128.11, 126.40, 29.49 ppm.

MS (MALDI-ToF, positive ion reflector mode): m/z (a.u.) = 514, 472, 412, 376, 263 [M+H$^+$], 239, 141.

10-(12-bromododecoxy)-1,8-dichloroanthracene

50
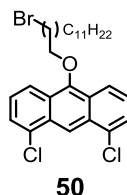
A mixture of 4,5-dichloroanthrone **48** (121 mg, 0.46 mmol, 1.00 eq.), 1,12-dibromododecane (604 mg, 1.84 mmol, 4.00 eq) and K_2CO_3 (95.0 mg, 0.69 mmol, 1.50 eq.) was stirred in 10 ml dimethylformamide (dry, Ar) at 55°C overnight. After cooling to room temperature, the reaction mixture was diluted with CH_2Cl_2 and washed with 3% (v/v) aq. HCl. The organic phase was concentrated and the product purified by column chromatography (SiO_2; cyclohexane/CH_2Cl_2 10:1) (85%).

^{1}H NMR (400 MHz, CDCl$_3$): δ = 9.05 (d, J = 1.1 Hz, 1H), 8.21 (dt, J = 8.8, 1.1 Hz, 2H), 7.62 (dd, J = 7.1, 1.0 Hz, 2H), 7.40 (dd, J = 8.8, 7.1 Hz, 2H), 4.15 (t, J = 6.6 Hz, 2H), 3.41 (t, J = 6.9 Hz, 2H), 2.11 – 1.95 (m, 2H), 1.86 (dt, J = 14.4, 6.9 Hz, 2H), 1.72 – 1.59 (m, 2H), 1.50 – 1.23 (m, 14H) ppm.

^{13}C NMR (101 MHz, CDCl$_3$): δ = 152.55, 132.93, 130.09, 126.22, 126.05, 125.20, 121.77, 116.40, 34.06, 32.86, 30.61, 29.62, 29.59, 29.55, 29.46, 28.80, 28.20, 26.95, 26.21 ppm.
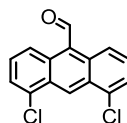
10-bromo-1,8-dichloroanthracene
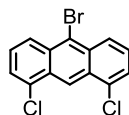
56

1,8-dichloroanthracene **27** (700 mg, 2.83 mmol, 1.00 eq.) was dissolved under Ar atmosphere in CH_2Cl_2 (dry, Ar) (30 ml) and bromine (467 mg, 2.92 mmol, 1.03 eq., 0.15 ml) dissolved in CH_2Cl_2 (dry, Ar) (15 ml) was added dropwise at 0°C. The reaction was warmed to room temperature and stirred overnight. After removing all volatile components from the reaction mixture under reduced pressure the target compound was obtained in quantitative yield without further purification.

^{1}H NMR (400 MHz, CDCl$_3$): δ = 9.39 (d, *J* = 1.0 Hz, 1H), 8.49 (dt, *J* = 8.9, 1.0 Hz, 2H), 7.69 (dd, *J* = 7.2, 1.0 Hz, 2H), 7.54 (dd, *J* = 8.9, 7.2 Hz, 2H) ppm.

4,5-dichloroanthracene-9-carbaldehyde

57

Method 1

In a 10 ml two-neck flask (dry, Ar), 10-bromo-1-8-dichloroanthracene **56** (64.0 mg, 0.20 mmol, 1.00 eq.) was dissolved in degassed THF (5 ml). After cooling the solution to -78°C, *n*-butyllithium (14.1 mg, 0.22 mmol, 2.20 eq., 0.14 ml of a 1.6 M solution in hexane) was added. After stirring for 20 min., the reaction was quenched by adding DMF (1 ml). After removal of the solvents under reduced pressure the crude was purified by column chromatography (SiO$_2$, pentane) (75%).

Method 2

To a solution 1,8-dichloroanthracene **27** (124 mg, 0.50 mmol, 1.00 eq.) and AlCl$_3$ (120 mg, 0.90 mmol, 1.80 eq.) in CH$_2$Cl$_2$ (dry, Ar) (10 ml), dichloromethyl-methylether (69.0 mg, 0.60 mmol, 0.06 ml, 1.2 eq.) was added dropwise at 0°C. The reaction was stirred at room temperature for 1h and poured into 6M aq. HCl. After extraction with Toluene (2x100ml), the combined organic phases were dried with Na$_2$SO$_4$, the solvent was removed and the product was purified with column chromatography (SiO$_2$, toluene) (45%).

^{1}H NMR (400 MHz, CDCl$_3$): δ = 9.27 (q, *J* = 0.9 Hz, 1H), 8.48 (d, *J* = 0.9 Hz, 1H), 7.95 (dq, *J* = 8.6, 0.9 Hz, 2H), 7.64 (dd, *J* = 7.2, 0.9 Hz, 2H), 7.42 (dd, *J* = 8.5, 7.2 Hz, 2H) ppm.

^{13}C NMR (101 MHz, CDCl$_3$): δ = 162.99, 129.58, 127.64, 127.31, 126.05, 125.70, 121.08, 115.00, 109.86 ppm.

GC-MS (EI+, 70 eV): m/z (%) = 277 (10) [M$^+$], 276 (45) [M$^+$], 275 (22) [M$^+$], 274 (70) [M$^+$], 273 (14) [M$^+$], 246 (50), 239 (100), 210 (46), 176 (95), 149 (22), 123 (24), 110 (11), 105 (39), 98 (21), 87 (55), 74 (30), 63 (12), 50 (10).

R_f (SiO$_2$, pentane) = 0.64

10-((12-bromododecoxy)methyl)-1,8-dichloroanthracene
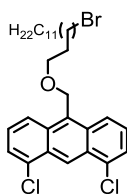
58

4,5-dichloroanthracene-9-carbaldehyde (10.0 mg, 0.04 mmol, 1.00 eq.) was dissolved in THF (dry, Ar) (5 ml). After cooling the solution to 0°C in an ice-bath, $NaBH_4$ was added, the ice-bath removed and the reaction stirred for 1h. The reaction was quenched with H_2O (15 ml). The aqueous reaction solution was extracted with ethyl acetate. The combined organic phases were dried with Na_2SO_4, the solvent was removed under reduced pressure and the crude product was used in the next step without further purification.

The crude was dissolved in 8 ml Acetonitrile (dry, Ar), together with 1,12-dibromododecane (17.8 mg, 0.54 mmol, 1.50 eq.) and K_2CO_3 (7.50 mg, 0.54 mmol, 1.50 eq.). The mixture was heated overnight at 85°C. After removal of the solvent, the crude was directly subjected to column chromatography (SiO_2; Cyclohexane/Ethyl acetate 10:1) (quant.).

¹H NMR (400 MHz, $CDCl_3$): δ = 9.37 (s, 1H), 8.32 (dt, J = 8.9, 1.1 Hz, 2H), 7.64 (dd, J = 7.2, 0.9 Hz, 2H), 7.48 (dd, J = 8.9, 7.2 Hz, 2H), 5.61 (s, 2H), 2.12 – 1.91 (m, 2H), 1.83 – 1.50 (m, 4H), 1.44 – 1.01 (m, 6H), 0.92 – 0.74 (m, 10H).

¹³C NMR (101 MHz, $CDCl_3$): δ = 133.35, 132.52, 131.36, 129.24, 126.51, 125.85, 123.20, 122.62, 57.73, 31.94, 29.72, 29.38, 22.71, 14.14 ppm.

R$_f$ (SiO_2, Cyclohexane/ CH_2Cl_2 10:1) = 0.31

4,5-divinylanthracene-9-carbaldehyde
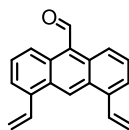
61

In dioxane (dry, Ar) (10 ml), 4,5-dichlroanthracene-9-carbaldehyde (70.0 mg, 0.25 mmol, 1.00 eq.), tributylvinyltin (178 mg, 0.56 mmol, 0.16 ml, 2.20 eq.), CsF (170 mg, 1.12 mmol, 4.40 eq.) and bis(tri-tert-butylphosphine)palladium (3 mol%, 3.90 mg) were dissolved. After heating the reaction mixture at 85°C for 72h, the reaction was quenched with H_2O (50 ml) and the extracted with toluene (100 ml). After removal of the solvent the desired compound was purified by column chromatography (SiO_2, pentane) (58%).

^{1}H NMR (400 MHz, CDCl$_3$): δ = 8.91 (d, *J* = 1.3 Hz, 1H), 8.44 (s, 1H), 7.99 – 7.92 (m, 2H), 7.69 – 7.57 (m, 4H), 7.46 (dd, *J* = 8.5, 6.9 Hz, 2H), 5.88 (dd, *J* = 17.3, 1.6 Hz, 2H), 5.57 (dd, *J* = 11.0, 1.6 Hz, 2H) ppm.

^{13}C NMR (101 MHz, CDCl$_3$): δ = 207.55, 136.15, 134.69, 131.60, 129.65, 128.19, 127.33, 125.32, 123.31, 118.80, 117.39 ppm.

GC-MS (EI+, 70 eV): m/z (%) = 261 (24) [M+H$^+$], 260 (9) [M+H$^+$], 259 (19) [M+H$^+$], 258 (7) [M+H$^+$], 257 (12) [M+H$^+$], 205 (56), 149 (90), 147 (100), 121 (36), 57 (10).

Name:	Lukas Jundt
Address:	Colmarerstrasse 3, 4055 Basel
Birthday/Place:	05.10.1981, Aarau, Schweiz
Telephone:	+41 (0)79 751 37 53
E-Mail:	jundt.lukas@gmail.com

Education

05/2010 – 05/2016	**PhD** in Chemistry, Department of Chemistry, University of Basel, Switzerland PhD thesis: *Molecular Tweezers in Nitroaromatic Sensing.* Supervisor: **Prof. Dr. Marcel Mayor** Referee: **Prof. Dr. Oliver Wenger**
09/2008 – 03/2010	**M.Sc.** in Chemistry, Department of Chemistry, University of Basel, Switzerland Master thesis: *NLO-active push - pull molecules for applications on resonant antennas*. Supervisor: **Prof. Dr. Marcel Mayor** Referee: **Prof. Dr. Helma Wennemers**
02/2006 – 08/2008	**B.Sc.** in Chemistry, Department of Chemistry, University of Basel, Switzerland
10/2002 – 09/2005	Studies in Forensic Sciences, University of Lausanne, Switzerland
08/2001 – 10/2002	Gap year: trip around the world (SGP, HK, AUS, USA, JA), language stay in Aix-en-Provence (FR)
08/1997 – 07/2001	Matura (Typus B) at Kantonsschule Zofingen (AG), Switzerland

Experience

2010 - 2013	Teaching assistant in the organic undergraduate laboratory course for pharmacy students, University of Basel
2010 - 2013	Teaching assistant in the organic undergraduate laboratory course for biology students, University of Basel
2011, 2013	Supervision of visiting students and their projects on the occasion of "Schweizer Jugend forscht""
02/2009 – 08/2009	Research on Ruthenium 2,2':6'2''-terpyridine complexes Supervisor: **Prof. Dr. Edwin Constable/Prof. Dr. Catherine Housecroft**
09/2008 – 01/2009	Research on light-switchable azo-biphenyls Supervisor: **Prof. Dr. Marcel Mayor**

Languages

- German (native)
- English (fluent)
- French (fluent)
- Latin (intermediate)

Oral Presentations

- Statusworkshop Baden Württemberg Stiftung, Bad Herrenalb, 2015, Germany
- Rigi Workshop, Rigi-Kulm, 2013, Switzerland
- 32nd REGIO-Symposium, 2012, Rheinfelden, Baden, Germany

Poster Presentations

- Clariant Chemistry Day, 2014, Basel, Switzerland
- Swiss Chemical Society Fall Meeting, 2013, Lausanne, Switzerland
- 33rd REGIO-Symposium, 2013, Mittelwihr, France
- Swiss NanoConvention, 2013, Basel, Schweiz
- Rigi Workshop, Rigi-Kulm, 2013, Switzerland (competitive)
- 32nd REGIO-Symposium, 2012, Rheinfelden, Baden, Germany
- 31st REGIO-Symposium, 2011, Sornetan, Switzerland
- 30th REGIO-Symposium, 2010, Mittelwihr, France

Publications

- *Determining Inversion Barriers in Atropisomers – A Tutorial for Organic Chemists*, Michel Rickhaus, Lukas Jundt, Marcel Mayor, *Chimia*, **2016**, *70*, 192.